

DEVELOPMENT OF POLYIMINE-BASED DYNAMIC COVALENT
NETWORKS: FROM MALLEABLE POLYMERS TO HIGH-
PERFORMANCE COMPOSITES

by

Philip Taynton

B.S., University of California, Santa Cruz, Santa Cruz, California, 2008

A thesis submitted to the
Faculty of the Graduate School of the
University of Colorado in partial fulfillment
of the requirement for the degree of
Doctor of Philosophy
Department of Chemistry & Biochemistry

2015

This thesis entitled:

“Development of Polyimine-Based Dynamic Covalent Network: From Malleable Polymers to
High-Performance Composites”

written by Philip Taynton

has been approved for the Department of Chemistry & Biochemistry

David Walba, Ph. D.

Wei Zhang, Ph. D.

Date:___

The final copy of this thesis has been examined by the signatories, and we
Find that both the content and the form meet acceptable presentation standards
Of scholarly work in the above mentioned discipline.

Thesis Abstract

Taynton, Philip

(Department of Chemistry & Biochemistry)

Development of Polyimine-Based Dynamic Covalent Network: From Malleable Polymers to High-Performance Composites

Thesis directed by Dr. Wei Zhang

Since the advent of synthetic polymers over a century ago, polymer science and technology development has transformed and enhanced our way of life from clothing to food storage to electronics and automobiles. To suit different applications, two broad categories of synthetic polymers have been developed: linear polymers, or thermoplastics, which can be melted, or solubilized, and reprocessed into a new shape or form; and network polymers, or thermosets, which are usually unable to be melted or reshaped once cured. The irreversible and permanent nature of thermosets was initially desirable for enabling high strength and long service lifetimes, but also makes thermosets inherently unrecyclable. Recently, dynamic covalent chemistry has been employed to form malleable thermosets, a new class of network polymers which can be reprocessed, and recycled like thermoplastics. The focus of this dissertation is the development of robust, catalyst-free malleable thermosets using exchangeable imine (a.k.a. Schiff-base) chemical links, and exploration of their great potential in fabricating high-performance composite materials.

Our work in this field began with a collaborative effort to explore the recyclability of catalyst-containing epoxy-acid networks, which were one of the first malleable thermoset materials identified. Our work with epoxies resulted in the discovery of a linear relationship between the glass transition temperature of a material, and the temperature at which the material becomes malleable due to bond exchange reactions.

Next we turned our attention to development of malleable thermosets using dynamic imine chemistry. Polyimine networks were developed which exhibit excellent mechanical strength and malleability under mild conditions without an added catalyst. The polymers were found to be completely hydrolytically stable, yet water could be used to catalyze the bond exchange reactions, leading to room temperature malleability. Further development led to both hydrophilic and hydrophobic network polyimines that exhibit a broad range of mechanical properties from elastomers with room temperature malleability, to semi-crystalline polymers with high tensile strength and thermal stability.

We found that the reversibility of imine-linked malleable thermosets could enable uniquely efficient recycling processes. This method was used to develop carbon fiber reinforced composites (CFRC's) in which the fiber and resin materials could be recovered and recycled in their original form. These thermoset composites are also moldable, weld-able and repairable due to crosslink exchange of the polymer binder. In another application, powders of such imine-linked malleable thermosets were combined with ion-conductive sulfide powders to form electrolyte membranes for solid-state lithium ion batteries exhibiting record-setting stability for FeS₂ solid state batteries, and a four-fold improvement in energy density over previously-reported solid state rechargeable lithium ion batteries. This work has brought to light a method for fabricating environmentally stable, yet highly functional Schiff-base thermosets, which have the potential to enable a large number of transformative applications particularly regarding composite materials.

In Chapter 1, an overview is given of the current (state-of-art) development and applications of vitrimeric networks. The advantages of the polyimine networks are highlighted.

In Chapter 2 our investigations of the fundamental behavior of catalyst-containing malleable thermoset materials will be discussed. In this work we synthesized various iterations of the malleable epoxy-acid thermosets pioneered by Liebler's group. Key results included development of a simple grind-and-press recycling methodology with optimized processing conditions, and fundamental study of the relationship between the glass transition temperature (T_g) of the vitrimer and the activation energy (E_a) of the crosslink exchange reactions which enable the malleability.

Chapter 3 details our development of catalyst-free malleable polyimine networks. These Schiff-base networks behave as traditional thermosets under ambient conditions, yet exhibit malleable flow, and very efficient recyclability under mild heating. These materials demonstrate an extremely low molding temperature for their mechanical strength when compared with traditional thermoplastic materials. The networks are perfectly resistant to hydrolysis, yet the presence of water catalyzes the bond exchange reaction, enabling room temperature malleability and recycling.

In Chapter 4, the structure-function relationship of polyimines is investigated. Polyimine is formulated to give a range of both hydrophilic and hydrophobic varieties with mechanical properties ranging from semicrystalline to elastomeric. The concentration-dependent effect of metal centered additives such as Sc^{III} and Cu^{II} are investigated with interesting results. Importantly, a wide range of mechanical and chemical properties are achievable by simple substitution of the diamine monomer from a library of commercially available species.

Chapter 5 discusses the development of polyimine carbon fiber reinforced composite (CFRC) materials. These materials combine the excellent mechanical properties of CFRC's with unique processability and reprocessability enabled by Schiff-base chemistry. Significantly, an excess of diamine monomer is used to solubilize the polymer network, leading to energy neutral closed-loop recycling of both the composite fibers, and the binder material. The recyclant binder material is directly reused to make polyimine networks with no loss of mechanical performance. The composites are weldable, moldable and repairable by simple and quick (~1 minute) application of heat and pressure.

In Chapter 6, polyimines are used as binder materials in the separator materials of solid-state lithium ion batteries. As a binder for the separator layer in all solid state lithium ion batteries, polyimines provide an extremely simple and efficient solid-state process for battery production, as well as record-setting stability for a solid-state FeS_2 lithium ion battery which exhibits a four-fold improvement in energy density over cells prepared without malleable thermoset binders.

Chapter 7 concludes and summarizes the present work, and provides an outlook on future developments and potential impacts of this work.

Acknowledgement

First and foremost, I would like to thank the people who have supported me during my pursuit of a Ph.D. Most importantly I thank my wife, Preethi Mathew, who has been a constant support and encouragement, even while she was earning her own graduate degree. She helped me keep going especially during the first year and a half, when nothing worked for me in the lab. She also helps me maintain a life outside of work, which is critical for sanity. Special thanks also should go to my parents-in-law: Babu & Lalitha Mathew. They graciously hosted us for two years while Preethi and I were both graduate students.

It has been a true pleasure to be a part of the doctoral program in University of Colorado at Boulder, under Professor Wei Zhang. I would like to express my gratitude to Wei, for his guidance, support and encouragement throughout my graduate school career. His commitment and enthusiasm for chemistry, along with his dedication to excellence were a motivation, and continue to be an inspiration for me. His open mind and willingness to try new things has led us into an interesting adventure together which will continue in the form of Mallinda LLC. It has been an honor to work with and learn from him. Special thanks also to David Walba for being willing to step in as my official advisor when that was needed due to a conflict of interest. I would also like to thank my thesis committee—Steven George, SeHee Lee and Yifu Ding—for their helpful suggestions and valuable insight.

I am extremely grateful to all past and current members of the Zhang Group for their friendship and camaraderie over the past four years. We shared a lot of good laughs which made the monotony and daily disappointments and setbacks of synthetic lab work much more enjoyable. I thank Dr. Alice Jin, Dr. Haishen Yang, Chao Yu, Ryan McCaffrey, Kenji Okochi, Dr. Ya Du, Dr. Chenxi Zhang, Dr. Qi Wang, Dr. Huagang Li, Youlong Zhu, Guolong Lu, Setareh Azarnoush, Dr. Jyothish Kuthanapillil, Ryan Denman, Michael Ortiz, Lili Tan, Xinyu Hu, and my undergraduate helpers Sam Loob, James Pritchard, and Chengpu Zhu.

I would also like to acknowledge the contributions of my collaborators. My collaborators not only helped introduce me to the field of malleable thermosets, but also helped with identifying applications, designing projects, and provided a high level of interaction which allowed for truly interdisciplinary developments. I would like to thank Professor H. Jerry Qi and

Professor SeHee Lee, and particularly their students: Dr. Kai Yu and Justin Whiteley. Thanks also to Dr. Danielle Molina-Piper.

Financial support was provided by National Science Foundation through the Innovation-CORPS fellowship, the Membrane Science, Engineering and Technology (MAST) Center, the State of Colorado's Advanced Industries Accelerator program, and the University of Colorado at Boulder. I would also like to thank our Department of Chemistry and Biochemistry, as well as the school of Engineering for providing such a collaborative rather than competitive research atmosphere. Special thanks also to Professor Brad Bernthal, and all who are involved in the New Venture Challenge and the entrepreneurial community of CU Boulder.

Contents

Chapter 1

Overview of the Recent Progress in Malleable Thermosets (Vitrimers)-1-

1.1 Introduction.....	-1-
1.2 Epoxy-Acid Malleable Thermosets.....	-2-
1.3 Malleable Thermosets through Olefin Metathesis.....	-5-
1.4 Disulfide-containing Malleable Thermosets.....	-6-
1.5 Malleable Polylactide Thermosets.....	-9-
1.6 Malleable Polyurea and Vinylogous Urethane Thermosets.....	-10-
1.7 Other Chemically Linked Malleable Thermosets.....	-12-
1.8 Imine Chemistry, and malleable Schiff-base thermosets.....	-14-
1.9 Conclusions.....	-14-
1.10 References.....	-15-

Chapter 2

Efficient reprocessing and recycling of epoxy-acid malleable thermosets and the influence of stoichiometry on the glass transition and bond exchange reactions.....-20-

2.1 Abstract.....	-20-
2.2 Introduction.....	-21-
2.3 Polymer Synthesis.....	-24-
2.4 Recycling and Reprocessing of Epoxy-Acid Malleable Thermosets.....	-26-
2.5 Influence of Stoichiometry on T_g and Malleability.....	-40-
2.6 Conclusions.....	-48-
2.7 Experimental Data.....	-49-
2.8 References.....	-55-

Chapter 3

Heat- or water-driven malleability in a highly-recyclable covalent network polymer...-59-

3.1 Abstract.....	-59-
3.2 Introduction.....	-60-
3.3 Results and Discussion.....	-61-
3.4 Conclusion.....	-67-
3.5 Experimental Details.....	-68-
3.6 References.....	-81-

Chapter 4

Imine-linked malleable thermosets: Influence of formulation and moisture on the bond exchange reaction.....-85-

4.1 Abstract.....	-85-
4.2 Introduction.....	-85-
4.3 Formulating with commercially available diamines.....	-88-
4.4 Formulating with trialdehyde monomers.....	-94-
4.5 Conclusions.....	-98-
4.6 Experimental section.....	-98-
4.7 References.....	-116-

Chapter 5

Repairable woven carbon fiber composites with full recyclability enabled by malleable thermosets.....-119-

5.1 Abstract.....	-119-
-------------------	-------

5.2 Introduction.....	-119-
5.3 Results and Discussion.....	-121-
5.4 Conclusion.....	-128-
5.5 Experimental Details.....	-129-
5.6 References.....	-145-
Chapter 6	
Ultrathin solid-state Li-ion electrolyte membrane facilitated by a self-healing polymer matrix.....	-148-
6.1 Abstract.....	-148-
6.2 Introduction.....	-148-
6.3 Results and Discussion.....	-150-
6.4 Conclusion.....	-157-
6.5 Experimental Details.....	-158-
6.6 References.....	-167-
Chapter 7	
Conclusions and Future Work.....	-170-
7.1 Overview of objectives.....	-170-
7.2 Advanced composite materials.....	-171-
7.3 Lithium metal batteries.....	-172-
7.4 Mixed matrix membranes.....	-173-
7.5 References.....	-173-
Bibliography.....	-175-
Vita.....	-185-

CHAPTER 1

Overview of the Recent Progress in Malleable Thermosets (Vitrimers)

1.1 Introduction

Covalent network polymers (commonly called thermosets) have traditionally maintained whatever shape they were initially formed in¹⁻² and upon failure, cannot be reprocessed or recycled.³ Furthermore, any shape change that occurs due to reversible bond exchange reactions (e.g. disulfide crosslinks) has been known as ‘creep’ and has been considered a drawback of the polymeric material.⁴ Therefore, it is by design that thermoset networks are irreversible and essentially unrecyclable. Theoretically, then, by design covalent network polymers can be made reprocessable and fully recyclable, and that is the subject of the present work.

One very well-known approach to introducing reversibility to network polymers is the introduction of thermodynamically-reversible bonds into the polymer backbone. This approach is largely achieved through cyclization reactions such as the Diels Alder (DA) reaction. In these systems, the Diels Alder adduct is stable under ambient conditions, but at higher temperatures, the reverse DA reaction dominates, and the network is largely depolymerized, but when cooled back down, the crosslink density of the network can be restored. This approach is well studied,⁵ and has been shown to enable mending and self-healing of network polymers,⁶ and even repairable fiber-reinforced composite materials.⁷

More recently, covalent network polymers have been developed which incorporate dynamic bonds which can undergo bond-breaking and bond-forming reactions at essentially

equal rates, meaning that they can remain insoluble during processing. This is advantageous as the gel-sol (de-polymerization) transition which takes place in many DA polymers is largely undesirable for structural applications. In 2005, Scott and coworkers showed that stress relaxation can be achieved in a network polymer in the solid state (with minimal loss of crosslink density during processing) by activating imbedded photoinitiators followed by a reversible addition-fragmentation (RAFT) radical exchange process which effectively scrambles the covalent bonds leading to effective relaxation of mechanical stresses in the network.⁸ Alternatively, catalysts can be used to achieve reversibility and exchange of thermally stable covalent bonds. Montarnal and coworkers showed in 2011 that an epoxy-acid network polymer can undergo transesterification reactions at elevated temperatures when the appropriate (zinc acetate) catalyst is incorporated.⁹ The rate of these reactions at room temperature is extremely slow, which enables standard network polymer performance with minimal creep under normal operating conditions. Critically, the authors studied the rheological behavior of these new intrinsically malleable thermoset materials, showing them to be malleable while maintaining their crosslink density, and exhibit an Arrhenius-like temperature-dependent stress relaxation behavior, just like silica glass. This malleable thermoset concept has since been realized through a number of dynamic covalent chemical systems including epoxy-acids, poly-olefins, disulfides, siloxanes, polyureas, and polyimines. A brief review of the development and applications of each of these classes of malleable polymers is given below.

1.2 Epoxy-Acid Malleable thermosets

As mentioned above, Montarnal *et al.* made use of a zinc acetate catalyst to enable transesterification at elevated temperatures as a means of cross-link exchange in an epoxy-acid network formed from by the combination of the diglycidyl ether of bisphenol A (DGEBA) with

a mixture of fatty acids (containing triacids and diacids in an approximate 7:3 ratio respectively).⁹ A conceptual drawing of transesterification within the network is reproduced below in Figure 1.1.

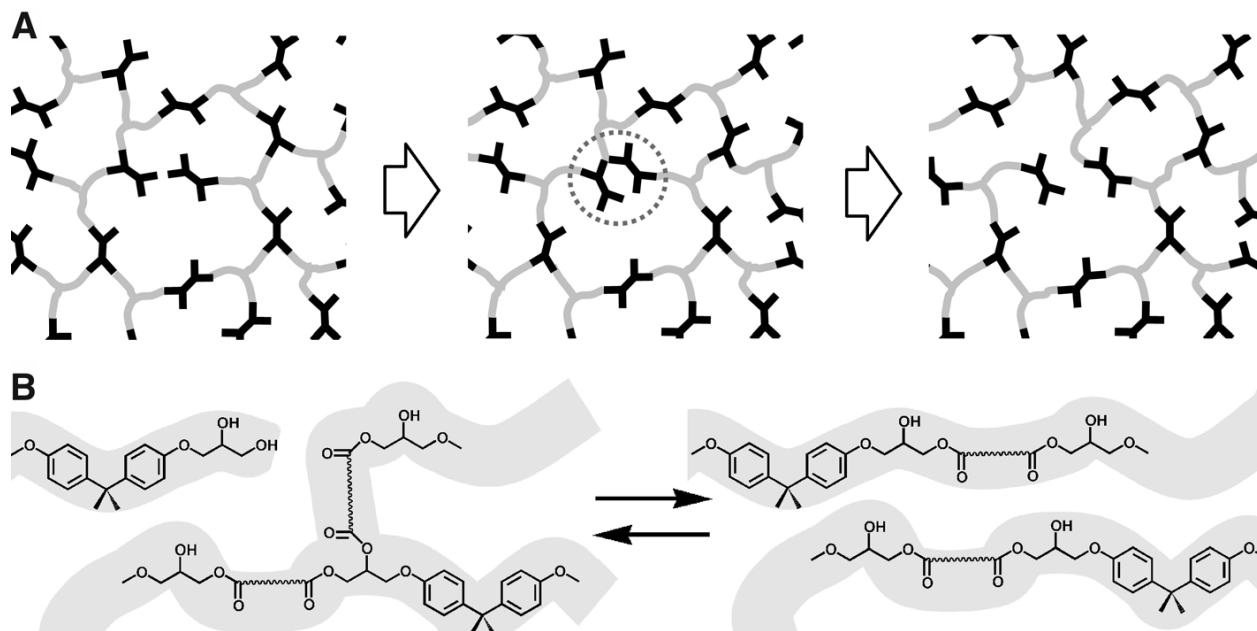


Figure 1.1 **A.** An illustration conceptually representing a bond exchange reaction in the network. **B.** Detail of the proposed transesterification reaction. *Reproduced from*[9].

The malleable character of the epoxy-acid network was characterized by stress-relaxation experiments over a range of temperatures as reproduced in Figure 1.2. The rate of bond exchange reaction can be greatly influenced by catalyst choice and concentration,¹⁰ and the glass transition temperature (T_g) of the polymer matrix.¹¹ Conceptually, at higher temperatures, the transesterification reaction takes place at higher rates, enabling a temperature-dependent relaxation of stresses in the polymer matrix. This stress-relaxation was demonstrated visually by twisting a ribbon of the material, and holding the turns in place. Since the stressed material rotates polarized light, the stresses could be visualized when viewed through crossed polarizers.

Upon application of heat via a heat gun for a few minutes, all of the stresses were relaxed, and the material no longer rotated polarized light.

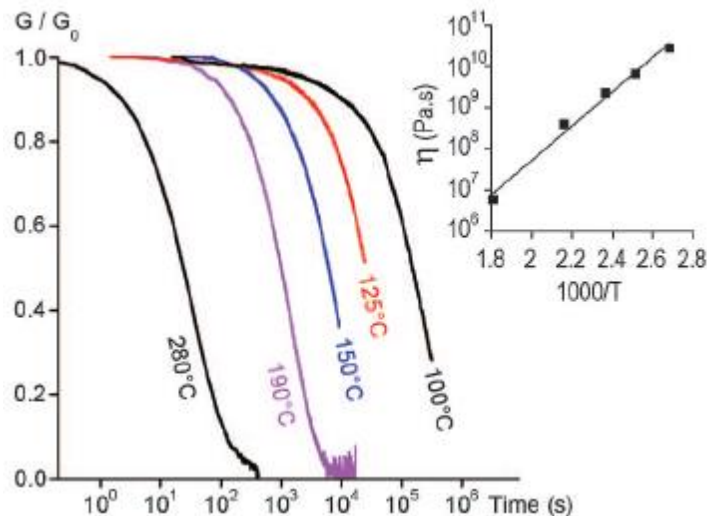


Figure 1.2 Stress-relaxation within the polymer matrix is faster at higher temperatures; a behavior which fits an Arrhenius plot (upper right), from which the activation energy (E_a) of the crosslink exchange reaction can be inferred. *Reproduced from* [9].

The recyclability of the polymer matrix was also demonstrated by grinding the polymer into a powder, and subsequently injection molding to reform a dog bone-type tensile testing sample. The recycled samples exhibited a moderate loss in elastic modulus, yet maintained essentially the same tensile strength as the fresh material. Better results can be obtained when the recycling conditions are optimized in a compression-molding rather than injection molding process.¹²



Figure 1.3 Exchangeable liquid crystal elastomers enable monodomains resulting in effective thermal actuators. The dome-shaped elastomer becomes flat upon heating to the isotropic phase. *Reproduced from* [13].

Impressively, Altuna et. al. reported catalyst-free “green” epoxy-acid vitrimers which were completely derived from plant-based monomers.¹⁴ The authors combined epoxidized soybean oil with an aqueous citric acid solution. The resulting material exhibited stress-relaxation, moldability, and weldability at 160 °C. While the catalyst-free functionality, and use of plant-based monomers was impressive, the tensile strength of the network (less than 1 MPa) was nearly 2 orders of magnitude lower than other reported vitrimers. Yang and co-workers added carbon nanotubes to a catalyst-containing epoxy-acid vitrimer, which enabled light-activated welding of the material.¹⁵ Thus the photothermal effect of carbon nanotubes enabled a light trigger of the vitrimeric welding.

One of the most impressive applications for malleable epoxy networks demonstrated to date is Pei et al.’s use of exchangeable ester links to form moldable liquid crystalline elastomers.¹⁶ Liquid crystalline elastomers have great potential for transforming external stimuli into mechanical reactions (e.g. synthetic muscles), yet it is very difficult to achieve macroscale alignment of the liquid crystals across multiple crystalline domains.¹⁷ Inclusion of exchangeable bonds allowed for the long-range orientation of the liquid crystalline elastomers into monodomains, as confirmed by X-ray diffraction. This enabled a triple shape-memory effect, and dome-shaped actuators which could reversibly be made flat upon heating to the isotropic phase, as reproduced in Figure 1.3.

1.3 Malleable Thermosets through Olefin Metathesis

Olefin metathesis is a very popular and useful chemical transformation enabled by efficient catalysts, such as those developed by the Grubbs group.¹⁸ The mechanism of olefin metathesis is illustrated in Figure 1.4 below, and involves binding of the olefin to the catalyst

prior to the metathesis reaction. This means that much like the catalyst-enabled transesterification reaction, the new bonds are formed at the same rate as bond cleavage. This leads to stable malleability and stress-relaxation without compromising the mechanical robustness of the polymer network. Lu and coworkers showed that by simply adding Grubbs 2nd generation catalyst to cross-linked polybutadiene rubber (an olefin containing polymer), malleable behaviors such as reparability, and weldability were observed. Interestingly, the catalyst-containing rubbers could be easily welded to butadiene rubbers containing no catalyst. Also, the high activity Grubbs 2nd generation catalyst at room temperature led to self-healing behavior under ambient conditions. Taking it a step further, the authors showed that damage in butadiene rubber could be healed by simply sprinkling catalyst (in powder form) over the surface of the damaged area- leading to healing of cracks. This represents a very simple and convenient, albeit expensive, route to malleable thermosets. The group later demonstrated the effect of catalyst concentration on the malleable behavior of the insoluble network.¹⁹ It was also found that the healing efficiency of Grubbs catalyst-containing polyolefins could be further improved by inclusion of H-bonding moieties within the network.²⁰

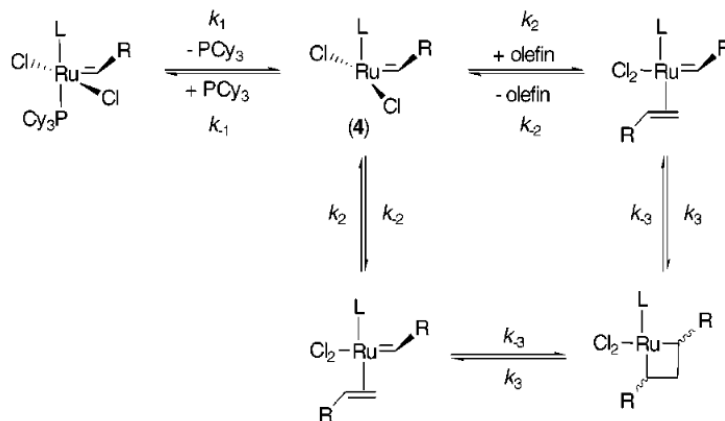


Figure 1.4 Catalytic cycle of Grubbs' Ruthenium olefin metathesis catalyst. *Reproduced from [21].*

1.4 Disulfide-containing Malleable Thermosets

The disulfide linkage is a dynamically exchangeable, labile chemical bond which has long been used to provide cross-links in natural rubbers, such as vulcanized rubber for tires.²² Disulfide metathesis is primarily responsible for the creep, or change in shape over time of natural rubbers (as mentioned above), and represents a logical chemical bond to use in intentionally malleable thermosets. Pepels and coworkers created malleable thiol-containing thermosets with disulfide links, yet contended that the malleable behavior was due to pH-dependent thiol-disulfide exchange.²³ The authors observed stress-relaxation behavior and room temperature self-healing, but reported that the malleable behavior decreased over time, possibly owing to oxidation of the thiol moieties.

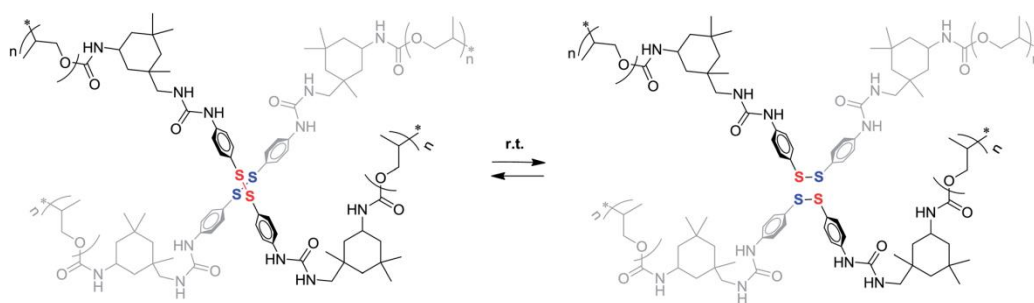


Figure 1.5 Aromatic disulfides used as exchangeable crosslinks. *Reproduced from* [24].

Rekondo et al. took advantage of the room-temperature activity of disulfide metathesis to form self-healing elastomers utilizing bis(4-aminophenyl)disulfide as a dynamic crosslinker. This led to self-healing with quantitative recovery of mechanical properties.²⁴ Later the same group demonstrated the reprocessability and recyclability of aromatic disulfide cross-linked poly(urea-urethane) polymers (Figure 1.5).²⁵ The material exhibited 3000% elongation at break and a tensile strength less than 1 MPa. Interestingly, in spite of the well-known room-temperature activity of the disulfide metathesis reaction, the PUU network did not exhibit significant stress-relaxation behavior at temperatures below 90 °C. The authors proposed that this could be due to quadruple H-bonding of the urethane groups. The hypothesis was corroborated by FTIR

spectroscopy experiments, which revealed shifts in the peaks attributed to the urea, urethane, and amide groups from 90 °C to 110 °C. This data is reproduced in Figure 1.6 below. These results are significant since they reveal that thermally stable dynamic polymers can be prepared using room-temperature active links. Essentially the principle is similar to other studies where the T_v is dependent on the T_g of the material.

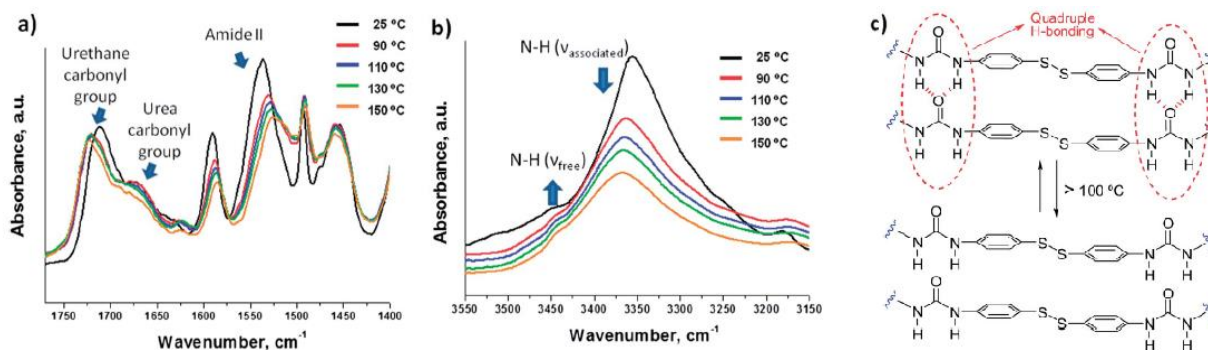


Figure 1.6 a. & b.: FTIR spectra of polyureaurethane polymer with exchangeable aromatic disulfide crosslinks. FTIR shift from 90 °C to 110 °C corresponds to quadruple H-bonding of the urethane groups as illustrated in **c**. *Reproduced from [25].*

In contrast, Lei and coworkers utilized an aliphatic disulfide-linked network, to which a tri-n-butylphosphene catalyst was added to enable malleable behavior.²⁶ The authors demonstrated the temperature-dependent stress relaxation, recyclability, and room temperature self-healing of the material. Imbernon et al. prepared epoxidized natural rubber which was made reprocessable by exchangeable disulfide crosslinks.²⁷ Up to 100 °C, the material's properties were similar to a permanently crosslinked rubber control material. At elevated temperatures the material became recyclable, but did not achieve complete recovery of its virgin properties.

One of the simplest approaches to disulfide vitrimers was Griebel and coworkers' combination of elemental sulfur (S_8) with 1,3-diisopropenyl benzene.²⁸ By varying the ratio of the feed stocks, a variety of thermal and mechanical properties were achieved, with 80% sulfur

content resulting in the most dynamic behavior, as determined by viscosity measurements. The authors attributed the tunability to the lower dissociation energies of S-S bonds in longer sulfur chains. The work was interesting since the dissociation energy of the dynamic bonds involved could be controlled by simple stoichiometry, but the mechanical properties and malleable properties were not fully characterized.

Overall, it is rare to find vitrimers with tensile strengths above a few MPa which contain disulfide links as a critical chemical link in the polymer backbone. It is questionable whether some of these “network polymers” have higher molecular weights than commercial thermoplastic materials. Overall, the utility of the disulfide link may continue to be its use as a crosslinking agent, though its dynamic nature can certainly be used to a much greater advantage, as the presently reviewed work has shown.

1.5 Malleable Polylactide Thermosets

Polylactones are chemically similar to epoxy acid polymers as both achieve malleability through the transesterification reactions (Figure 1.7). Brutman et al. developed a polylactone vitrimer which contained a Sn(II) catalyst, and exhibited stress-relaxation behavior, and repairability of broken tensile samples resulting in 102% recovery of tensile strength.²⁹ By varying catalyst content and the hydroxyl functionality, the authors were able to achieve a range of mechanical properties and T_g values. It was found that for polylactone vitrimers, the T_v was always within a few degrees of the T_g , and thus lower temperature processing was accessible for the polylactones reported than for other ester-linked vitrimers. For example, epoxy-acid vitrimers catalyzed by zinc acetate exhibit $T_v \sim 50$ °C above the T_g of a given formulation.¹¹ It makes sense that if the chemical energy barrier to the bond exchange reaction is low enough,

then the malleability of the polymer will largely be a function of T_g . Catalyst-containing malleable epoxy materials represent a very versatile system since Leibler's group has shown that low T_g elastomers can have high processing temperatures, and presently Brutman et al. have shown in principle that high T_g semi-crystalline polymers could have access to malleability just above their glass transition, and it all seemingly depends simply on catalyst choice and concentration.

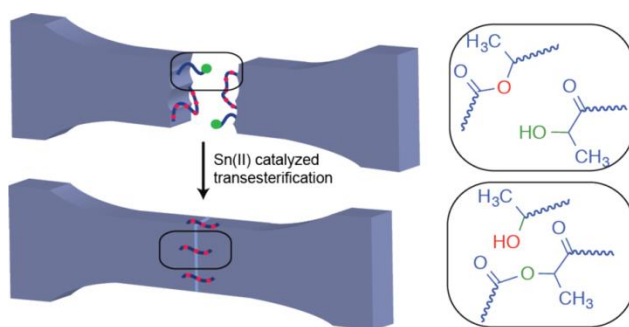


Figure 1.7 Malleable polylactide vitrimers are chemically similar to epoxy-acid networks. *Reproduced from [29].*

1.6 Malleable Polyurea and Vinylogous Urethane thermosets

Polyurethanes represent a very versatile polymer system, which have a wide variety of commercial applications from impact-absorbing foams to structural materials and composites. Ying and coworkers report that by introducing bulky, sterically hindered amines (Figure 1.8), the typically stable urethane and urea-urethane bonds were made reversible.³⁰ The authors combined a small library of hindered amines with isocyanates, and measured the binding constants of each by monitoring using $^1\text{H-NMR}$ spectroscopy. While the resulting polymers exhibited room temperature self-healing, and catalyst free malleability, they were not very strong. Though the elastomers exhibited $>200\%$ elongation at break, they had a tensile strength of <1 MPa. It is possible that the sterically hindered amines are not able to react efficiently enough to form network polymers with high molecular weight.

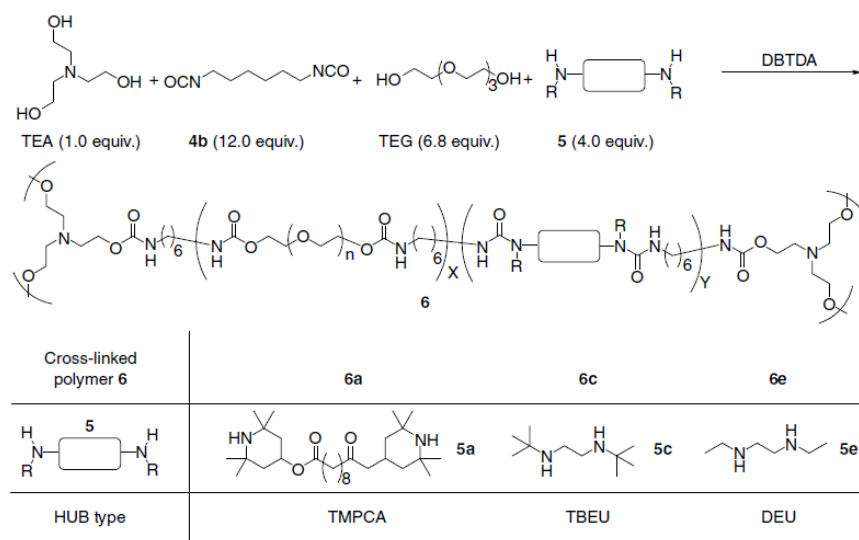


Figure 1.8 Bulky diamine monomers enable malleable polyurethanes. *Reproduced from [30].*

Vinylogous urethane vitrimers were prepared by Denissen and co-workers, and like polyimines, exhibit a combination of catalyst-free malleability, room temperature stability and robust mechanical properties.³¹ The authors first conducted a series of kinetic experiments on model compounds to identify vinylogous urethane linkages which exhibited dynamic transamination reactions at elevated temperatures. Then cyclohexane dimethanol bisacetoacetate was synthesized in two steps, and combined with commercially available diamines and triamines (Figure 1.9). The resulting polymer networks exhibited excellent mechanical properties (Young's modulus ~ 2.4 GPa, and tensile strength ~ 90 MPa), and catalyst-free stress-relaxation in under 2 minutes at 160 °C. The recyclability of the polymer was also demonstrated. The similar behavior to polyimine networks (discussed below) could be due to the fact that vinylogous urethanes have an imine-containing resonance structure, which may play a role in the bond exchange mechanism.

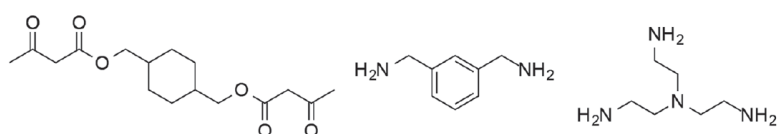


Figure 1.9 Monomers used to prepare vinylogous urethane vitrimers. *Reproduced from* [31].

1.7 Other Chemically Linked Malleable Thermosets

The popular click chemistry has also been utilized to prepare malleable thermoset materials. Formation of poly(1,2,3-triazoles) followed by crosslinking with difunctional alkyl halides results in ionic liquid (polytriazolium) network polymers, as reported by Obadia et al.³² The polymers were found to exhibit catalyst-free malleability due to the trans-alkylation of C-N bonds within the network (Figure 1.10), which is not a commonly used dynamic covalent reaction. An excess of alkyl halide dangling chains enabled the reprocessability and recyclability of the material as direct exchange of alkyl groups would involve considerable steric interactions. The dynamic ionic liquid networks were found to exhibit ionic conductivity typical of non-doped, highly crosslinked ionic liquid polymers, with a maximum conductivity of $2 \times 10^{-8} \text{ Scm}^{-1}$ for the bromide ion. The malleable behavior of the polymers was investigated by molding experiments and recycling studies. Interestingly, the choice of alkyl halide had a strong effect on the T_g of the polymers as the alkyl iodides resulted in much higher T_g 's than did the alkyl bromides. Such functional vitrimers could find application in batteries, and membranes for fuel cells or CO_2 recovery.

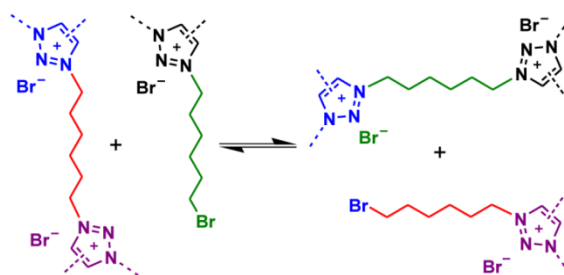


Figure 1.10 Transalkylation mechanism enables malleable ionic liquid thermosets. *Reproduced from* [32].

Guan's research group, which reported the first catalyst-containing polyolefin vitrimers, also developed a small library of malleable thermosets based on the well-known dynamic boronic ester linkage (Figure 1.11).³³ The authors claim rational tunability of the transesterification rate, and thus the stress relaxation rate and healing efficiency of the malleable boronic esters developed. This was achieved through selection of sterically-hindered diols for fast-exchange of boronic ester linkages, or unhindered diols for slow-exchange of boronic ester linkages, with correspondingly fast/slow stress relaxation and self-healing efficiency. The authors intelligently chose to use the dynamic ester linkage as an exchangeable crosslinker, rather than incorporating the labile dynamic bond into the polymer backbone. In this way, the mechanical properties were acceptable (elastomers with up to 500% elongation at break, and up to 3 MPa tensile strength). Even though the polymers which contained less of the crosslinker were more robust in this case, it seems better mechanical performance can be attained from vitrimers with labile dynamic bonds when such labile linkages are used as crosslinkers rather than when they constitute the main linkage in the polymer backbone.

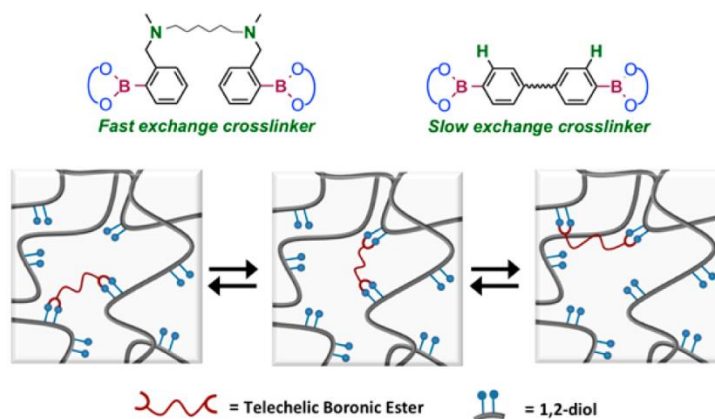


Figure 1.11 Dynamic boronic ester crosslinks enabled catalyst-free tunable malleability in a crosslinked polymer. *Reproduced from [33].*

1.8 Imine chemistry, and malleable Schiff-base thermosets

Imine linkages, also known as Schiff bases, represent a very well-explored dynamic covalent bond.³⁴ They are one of the most common linkages used to form well-defined molecular cages, and macrocycles,³⁵ and they were the functional group at the core of Jean Marie Lehn's polyhydrozone "dynamers" which were linear polymers shown to swap functionality when exposed to various monomers, which could then be infused into the polymer backbone.³⁶⁻³⁷ In many iterations, Schiff bases are highly labile dynamic bonds, prone to hydrolysis when exposed to moisture. While others have explored the hydrolytic stability of various imine linkages,³⁸ our group was the first to develop polyimine networks which are stable against hydrolysis and characterize their malleability, which can be induced by either heat or water.³⁹ The imine-linked networks are quite versatile, and can be made to be functionally moisture-resistant, and have been shown to exhibit mechanical properties ranging from elastomeric (>200% elongation with tensile strengths ~10 MPa) to semicrystalline (<5% elongation, tensile strength up to 65 MPa), and T_g 's ranging from 10 °C to 110 °C.⁴⁰ From this breadth of formulations has already come applications of the material from binder materials for solid state lithium ion batteries⁴¹ to recyclable carbon fiber composite materials.⁴²

1.9 Conclusion

While the field of malleable thermosets/vitrimers holds much promise for providing a new generation of recyclable, and easily processable thermoset materials, the science is very much in its infancy. New chemical and synthetic approaches are being published each month, and very few practical applications of these materials have been published to date. A good variety of dynamic bonds have been explored, and it seems appropriate to make a distinction between robust and labile dynamic covalent bonds when evaluating how to design a robust

vitrimeric material. Generally robust linkages will form irreversibly in high conversion during the polymerization reaction. They will be moderately stable against environmental exposure: oxygen, moisture, UV light, and will involve a bond exchange mechanism which involves new bond formation prior to or concurrent with bond-breaking- often beginning with a nucleophilic attack. These systems often require addition of catalysts to lower the activation energy of the bond exchange reaction. More labile dynamic covalent links can enable catalyst-free malleability, and highly active room temperature self-healing. These linkages are more appropriately employed as crosslinkers for linear polymers of moderate molecular weight, have not yet been shown to enable robust mechanical properties when incorporated into the backbone of the polymer.

1.10 References

- [1] J. J. Alkonis and W. J. MacKnight, Introduction to polymer viscoelasticity 2nd Ed., New York: Wiley, 1983.
- [2] M. Doi, Introduction to polymer physics, Oxford: Oxford University Press, 1996.
- [3] G. G. Odian, Principles of polymerization 4th Ed., Hoboken, NJ: Wiley, 2003.
- [4] A. N. Gent, "Relaxation processes in vulcanized rubber II: Secondary relaxation due to network breakdown," *Journal of Applied Polymer Science*, vol. 6, pp. 442-448, 1962.
- [5] M. Q. Zhang and M. Z. Rong, "Intrinsic self-healing of covalent polymers through bond reconnection towards strength restoration," *Polymer Chemistry*, vol. 4, pp. 4878-4884, 2013.
- [6] X. X. Chen, M. A. Dam, K. Ono, H. B. Shen, S. R. Nutt, K. Sheran and F. Wudl, "A Thermally Re-mendable Cross-Linked Polymeric Material," *Science*, vol. 295, pp. 1698-1702, 2002.
- [7] J. S. Park, T. Darlington, A. F. Starr, K. Takahashi, J. Riendeau and H. T. Hahn, "Multiple healing effect of thermally activated self-healing composites based on Diels-Alder

- reaction," *Composites Science and Technology*, vol. 70, no. 15, pp. 2154-2159, 2010.
- [8] T. F. Scott, A. D. Schneider, W. D. Cook and C. N. Bowman, "Photoinduced Plasticity in Cross-Linked Polymers," *Science*, vol. 308, pp. 1615-1617, 2005.
- [9] D. Montarnal, M. Capelot, F. Tournilhac and L. Leibler, "Silica-Like Malleable Materials from Permanent Organic Networks," *Science*, vol. 334, no. November, pp. 965-968, 2011.
- [10] M. Capelot, M. Unterlass, F. Tournilhac and L. Leibler, "Catalytic Control of the Vitrimer Glass Transition," *ACS Macro Lett.*, vol. 1, pp. 789-792, 2012.
- [11] K. Yu, P. Taynton, W. Zhang, M. Dunn and H. J. Qi, "Influence of Stoichiometry on the Glass Transition and Bond Exchange Reactions in Epoxy Thermoset Polymers," *RSC Advance*, vol. 4, pp. 48682-48690, 2014.
- [12] K. Yu, P. Taynton, W. Zhang, M. Dunn and H. J. Qi, "Reprocessing and recycling of thermosetting polymers based on bond exchange reactions," *RSC Advances*, vol. 4, no. 20, pp. 10108-10117, 2014.
- [13] Z. Pei, Y. Yang, Q. Chen, E. M. Terentjev, Y. Wei and Y. Ji, "Mouldable liquid-crystalline elastomer actuators with exchangeable covalent bonds," *Nature Materials*, vol. 13, p. 36, 2014.
- [14] F. I. Altuna, V. Pettarin and R. J. Williams, "Self-healable polymer networks based on the cross-linking of epoxidised soybean oil by an aqueous citric acid solution," *Green Chemistry*, vol. 15, pp. 3360-3366, 2013.
- [15] Y. Yang, Z. Pei, X. Zhang, L. Tao, Y. Wei and Y. Ji, "Carbon nanotube-vitrimer composite for facile and efficient photo-welding of epoxy," *Chemical Science*, vol. 5, pp. 3486-3492, 2014.
- [16] Y. Yang, Z. Pei, Q. Chen, E. M. Terentjev, Y. Wei and Y. Ji, "Mouldable liquid-crystalline elastomer actuators with exchangeable covalent bonds," *Nature Materials*, vol. 13, pp. 26-31, 2014.
- [17] C. Ohm, M. Brehmer and R. Zentel, "Liquid crystalline elastomers as actuators and sensors," *Advanced Materials*, vol. 22, pp. 3366-3387, 2010.
- [18] G. C. Vougioukalakis and R. H. Grubbs, "Ruthenium-Based Heterocyclic Carbene-Coordinated Olefin Metathesis Catalysts," *Chemical Reviews*, vol. 110, no. 3, pp. 1746-1787, 2009.

- [19] Y.-X. Lu, F. Tournilhac, L. Leibler and Z. Guan, "Making Insoluble Polymer Networks Malleable via Olefin Metathesis," *Journal of the American Chemical Society*, vol. 134, no. 20, pp. 8424-8427, 2012.
- [20] J. A. Neal, D. Mozhdghi and Z. Guan, "Enhancing Mechanical Performance of a Covalent Self-Healing Material by Sacrificial Noncovalent Bonds," *Journal of the American Chemical Society*, vol. 137, no. 14, pp. 4846-4850, 2015.
- [21] M. S. Sanford, M. Ulman and R. H. Grubbs, "New insights into the mechanism of ruthenium-catalyzed olefin metathesis reactions," *Journal of the American Chemical Society*, vol. 123, no. 4, pp. 749-750, 2001.
- [22] F. R. Eirich, in *Science and technology of rubber 3rd edition*, Amsterdam, Elsevier, 2005, p. 768.
- [23] M. Pepels, I. Filot, B. Klumperman and H. Goossens, "Self-healing systems based on disulfide-thiol exchange reactions," *Polymer Chemistry*, vol. 4, no. 18, pp. 4955-4965, 2013.
- [24] A. Rekondo, R. Martin, A. Ruiz de Luzuriaga, G. Cabanero, H. J. Grande and I. Odriozola, "Catalyst-free room-temperature self-healing elastomers based on aromatic disulfide metathesis," *Materials Horizons*, p. DOI: 10.1039/C3MH00061C, 2014.
- [25] R. Martin, A. Rekondo, A. Ruiz De Luzuriaga, G. Cabanero, H. Grande and I. Odriozola, "The processability of a poly (urea-urethane) elastomer reversibly crosslinked with aromatic disulfide bridges," *Journal of Materials Chemistry A*, vol. 2, no. 16, pp. 5710-5715, 2014.
- [26] Z. Q. Lei, H. P. Xiang, Y. J. Yuan, M. Z. Rong and M. Q. Zhang, "Room-temperature self-healable and remoldable cross-linked polymer based on the dynamic exchange of disulfide bonds.," *Chemistry of Materials*, vol. 26, no. 6, pp. 2038-2046, 2014.
- [27] L. Imbernon, E. K. Oikonomou, S. Norvez and L. Leibler, "Chemically crosslinked yet reprocessable epoxidized natural rubber via thermo-activated disulfide rearrangements," *Polymer Chemistry*, vol. 6, pp. 4271-4278, 2015.
- [28] J. J. Griebel, N. A. Nguyen, A. V. Astashkin, R. S. Glass, M. E. Mackay, K. Char and J. Pyun, "Preparation of Dynamic Covalent polymers via Inverse Vulcanization of Elemental Sulfur," *ACS Macro Letters*, vol. 3, pp. 1258-1261, 2014.
- [29] J. P. Brutman, P. A. Delgado and M. A. Hillmyer, "Polylactide Vitrimers," *ACS Macro*

- Letters*, vol. 3, pp. 607-610, 2014.
- [30] H. Ying, Y. Zhang and J. Cheng, "Dynamic urea bond for the design of reversible and self-healing polymers," *Nature Communications*, vol. doi:10.1038/ncomms4218, p. 3218, 2014.
- [31] W. Denissen, G. Rivero, R. Nicolay, L. Leibler, J. M. Winne and F. E. Du Prez, "Vinylogous Urethane Vitrimers," *Advanced Functional Materials*, vol. 25, no. 16, pp. 2451-2457, 2015.
- [32] M. M. Obadia, B. P. Mudraboyina, A. Serghei, D. Montarnal and E. Drockenmuller, "Reprocessing and Recycling of Highly Cross-linked Ion-Conducting Networks through Transalkylation Exchanges of C-N Bonds," *Journal of the American Chemical Society*, vol. 137, no. 18, pp. 6078-6083, 2015.
- [33] O. R. Cromwell, J. CHung and Z. Guan, "Malleable and self-healing covalent polymer networks through tunable dynamic boronic ester bonds," *Journal of the American Chemical Society*, vol. 137, pp. 6492-6495, 2015.
- [34] M. E. Belowich and J. F. Stoddart, "Dynamic imine chemistry," *Chemical Society Reviews*, vol. 41, no. 6, pp. 2003-2024, 2012.
- [35] Y. Jin, Q. Wang, P. Taynton and W. Zhang, "Dynamic Covalent Chemistry Approaches Towards Macrocycles, Molecular Cages, and Polymers," *Accounts of Chemical Research*, vol. 47, pp. 1575-1586, 2014.
- [36] G. Godin, B. Legrand, A. Trachsel, J.-M. Lehn and A. Herrmann, "Dynamic polymer blends-- component recombination between neat dynamic covalent polymers at room temperature," *Chemical Communications*, vol. 46, pp. 3125-3127, 2010.
- [37] W. G. Skene and J.-M. Lehn, "Dynamers: Polyhydrazone reversible covalent polymers, component exchange, and constitutional diversity," *Proceedings of the National Academy of Science*, vol. 101, pp. 827-8275, 2004.
- [38] C. Godoy-Alcantar, A. K. Yatsimirsky and J.-M. Lehn, "Structure-stability correlations for imine formation in aqueous solution," *Journal of Physical Organic Chemistry*, vol. 18, pp. 979-985, 2005.
- [39] P. J. Taynton, K. Yu, R. K. Shoemaker, Y. Jin, H. J. Qi and W. Zhang, "Heat- or Water-Driven Malleability in a Highly Recyclable Covalent Network Polymer," *Adv. Mater.*, vol. 26, pp. 3938-3942, 2014.
- [40] P. Taynton, S. Loob, H. Ni, Li, R. Shoemaker, K. Yu, H. J. Qi and W. Zhang, "polyimine

vitrimers," *under preparation*.

- [41] J. M. Whiteley, P. J. Taynton, W. Zhang and S.-H. Lee, "Ultrathin solid-state Li-ion electrolyte membrane facilitated by a self-healing polymer matrix," *Advanced Materials*, Under Review.
- [42] P. Taynton, H. Ni, S. Loob, H. Li, H. J. Qi and W. Zhang, "Fully Recyclable & Repairable Woven Carbon Fiber Composites enabled by Malleable Thermosets," *Advanced Materials*, Submitted.

CHAPTER 2

Efficient reprocessing and recycling of epoxy-acid malleable thermosets and the influence of stoichiometry on the glass transition and bond exchange reactions

(Manuscripts published under the titles “Reprocessing and Recycling of Thermoset Polymers based on Bond Exchange reaction” in *RSC Advance* **2014**, *4*, 10108-10117, and “Influence of Stoichiometry on the Glass Transition and Bond Exchange Reactions in Epoxy Thermoset Polymers” in *RSC Advance* **2014**, *4*, 48682-48690, each coauthored with Yu, K.; Zhang, W.; Dunn, M. L.; and Qi, H. J.)

2.1 Abstract

It was recently reported that thermally malleable polymers with bond exchange reactions (BERs) can rearrange their microscopic network topology without impairing the network integrity. This opens an avenue to recycle thermoset polymers that traditionally are very difficult to recycle. Presently, the reprocessing and recycling ability of a thermoset polymer (an epoxy thermosetting network) with exchangeable bonds in a pulverous state is studied. A detailed investigation was performed to study the effect of reprocessing conditions (such as time and pressure) on the material mechanical performance and is presently reported. We also presently demonstrate that the temperature dependent BER rate could be tuned by adjusting the stoichiometry of monomers. As the ratio of hard segments in the epoxy thermoset network is increased, the material's glass

transition temperature (T_g) is increased, with a corresponding increase in the temperature required to achieve a given stress relaxation rate. From the experimental stress relaxation curves, we determined the energy barrier for the BERs in different networks. With the T_g being elevated from 30.3 °C to 63.0 °C, the BER energy barrier is linearly increased from 68.2 kJ mol⁻¹ to 97.3 kJ mol⁻¹. Such a correlation between these two thermomechanical behaviors provides an additional design parameter (beyond catalyst choice) which can aid in achieving highly tunable service conditions for practical engineering applications of thermally malleable thermosets.

2.2 Introduction

Reprocessing and recycling of thermosetting polymers is inherently difficult for traditional technology because of the irreversible nature of their chemical cross-links. Disposal of such polymer waste typically requires landfills, high temperature, or toxic chemicals, which lead to significant environmental concerns. While thermoplastic polymers can flow and be easily reprocessed by heat, their solvent resistance, thermal and mechanical properties at high temperature are unsatisfactory, and hence cannot replace thermosets in many engineering applications, especially those requiring high-performance such as the aircraft and automotive industry.¹

In view of the increasing amount of thermosetting polymer waste generated, new reprocessing and recycling routes have been successively proposed. One approach consists of reutilizing finely ground thermoset scrap as reinforcements for other elastomers,²⁻⁴ ceramics⁵ and concrete⁶⁻⁹ to improve the related properties or extend their service lifetime. However, such operation on polymer wastes usually involves surface chemical modifications before usage to facilitate their combination with the matrix,² which is costly and less viable for large scale

production. From both environmental and economic points of view, a preferable technology would enable us to simply weld thermosets and repair their components in service to improve the sustainability, or reprocess and recycle the thermoset into valuable resources without environmental impact. Tremendous efforts were made in the past to this end, such as surface interlocking,¹⁰⁻¹¹ inter-diffusion of network defects¹² and adding linear thermoplastic chains at the interface.¹³⁻¹⁵ For a more robust and efficient welding effect, thermally reversible reactions based on covalent chemistry¹⁶⁻²³ were developed where networks with bonds capable of breaking and reforming²¹⁻²² or exchanging pairs of atoms²³ can as a result flow when heated. Another method consists of using radicals to initiate exchange reactions and create plasticity in thermosets.²⁴⁻²⁸ Although these two strategies offer possibilities to combine the reprocessability, reparability and excellent welding performance of thermoset polymers, their immediate widespread application is limited either because of the abrupt viscosity drop of the thermoset network during the operation²⁹⁻³⁰, or the unavoidable termination reactions.

In contrast, recently reported thermally malleable thermosetting epoxy polymers using bond exchange reactions (BER) by Leibler and co-workers¹ are based on a different molecular mechanism. The network topology can be rearranged due to the internal transesterification at high temperature, and frozen upon cooling. The polymer viscosity is gradually changed versus temperature following an Arrhenius law during the operation,¹ and hence the network integrity is maintained. In addition, since no additional monomers or termination reactions are introduced into the system, the numbers of links and average functionality of polymer chains are unchanged. Leibler and co-workers have experimentally demonstrated that the thermally induced BER can release the internal stress of a thermoset polymer, and allow the material to be reshaped, welded

together, and reprocessed,¹ which has drawn significant interests in the study of this type of polymers.³¹

In the present chapter, we experimentally study the reprocessing and recycling ability of such epoxy with exchangeable bonds in a pulverous state. Due to the large surface area and small size of polymer particles, their handling, transportation, and storage can offer convenience in comparison with traditional polymer scrap in bulk form, which can promote their incorporation into industrial applications in thermoset recycling, structure rehabilitations and component rework. Leibler and co-workers demonstrated that the epoxy glassy polymer (hard networks) essentially maintains its stress–strain behavior after being ground to a fine powder and injection molded back into a cohesive solid.¹ But in the present work, we begin with further investigating the effect of reprocessing conditions (such as temperature, time, and pressure), as well conducting an investigation of the mechanical performance of the material through multiple generations of recycling. In addition, the effect of formulation on T_g was investigated.

Since T_g plays a unique role in determining a polymer's mechanical properties, it is intriguing to investigate how it will affect the BER kinetics. Existing experimental results show that the BERs become active only when the temperature is significantly higher than the associated T_g , but the relationship between them is unclear. A connection between the glass transition and BERs would be desirable to engineers when estimating the reprocessing time³² required for such malleable thermosets or selecting suitable thermal conditions during practical operations.

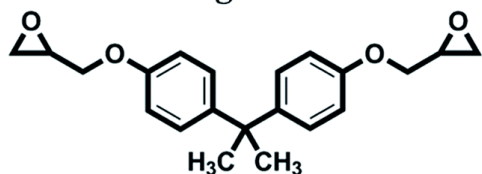
We report that by simply mixing the monomer fatty acids and glutaric anhydride in different ratios, the T_g of the epoxy network is tunable due to the alternation of network structure

and chain mobility. The stress relaxation behavior in the resulting thermoset polymers was then investigated. The temperature dependency of each epoxy sample is shown to follow the Arrhenius type time–temperature superposition (TTSP), and the measured energy barrier for BERs exhibits an approximately linear relationship with the associated T_g . This enables us to predict the relaxation times of the epoxy thermoset polymers under different temperatures.

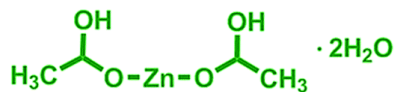
2.3 Polymer Synthesis

The thermoset polymer network with exchangeable bonds used in this study was prepared following the method used by Leibler and coworkers.¹ The monomers diglycidyl ether of bisphenol A (DGEBA), glutaric anhydride and the metal catalyst ($Zn(Ac)_2$) were ordered from Sigma Aldrich (St. Louis, MO, USA) and used as received without further purification. The Epoxide Equivalent Weight (EEW) of DGEBA is 172–176 g eq⁻¹. The mixture of fatty acid monomers (Pripol 1040) was kindly provided by Uniqema Inc (Paterson, NJ, USA). Detailed chemical structures of each used reagent are shown in Figure 2.1. Five groups of epoxy polymer were prepared in this study and the stoichiometry of each composition is listed in Table 2.1. The ratio of epoxy group and metal catalyst is unchanged in each epoxy network (1 : 0.05), while the fatty acid and glutaric anhydride are mixed with different ratios. The total amount of the carboxylic acid and acyl groups in these two monomers is equal to the stoichiometry of epoxy group. We note here that the Epoxy 1 and Epoxy 5 polymers are the same epoxy soft and hard networks which have been previously studied by Montarnal et al..¹

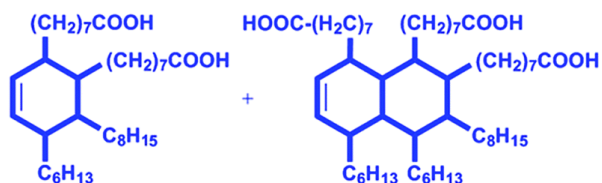
Chemical Reagents



DGEBA



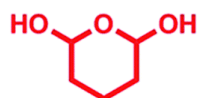
Catalyst



23wt%

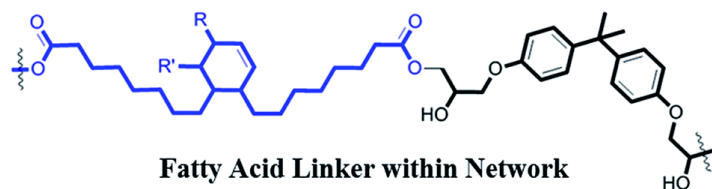
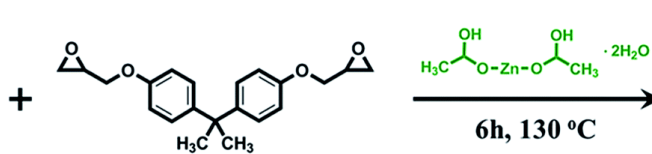
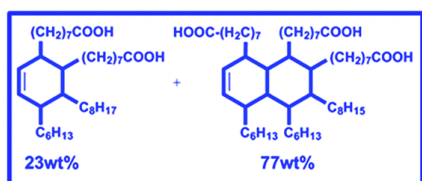
77wt%

Fatty acid mixture

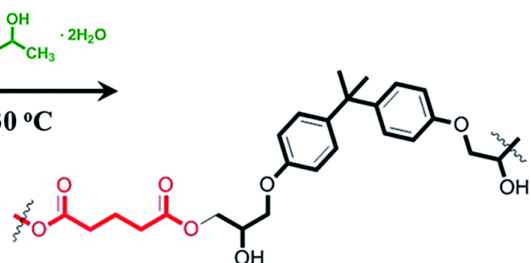
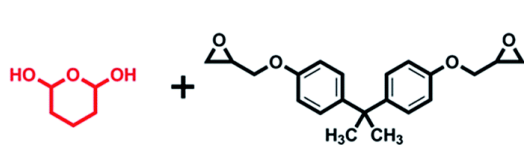


Glutaric anhydride

Polymer Synthesis:



Fatty Acid Linker within Network



Anhydride Linker within Network

Figure 2.1 Schematic view of the chemical reagents used in this study, as well as the formation of anhydride and fatty acid linkers within the thermoset network.

Table 2.1 Stoichiometry (normalized molar content) of each formulation

polymer	Epoxy Group (in DGEBA)	Catalyst (Zn(Ac) ₂)	Acid group (in fatty acid)	Acyl group (in glutaric anhydride)
Epoxy 1	1	0.05	1	0
Epoxy 2	1	0.05	0.5	0.5
Epoxy 3	1	0.05	0.4	0.6
Epoxy 4	1	0.05	0.2	0.8
Epoxy 5	1	0.05	0	1

For polymer synthesis, all the epoxy materials with different composition were prepared following the same procedure. In Step 1, the catalyst was mixed with fatty acids and/or glutaric anhydride with in a round-bottom flask and stirred at 130 °C until homogeneous mixing was achieved. In Step 2, solid DGEBA was heated up to 130 °C until totally melted, and then manually stirred with the acid–anhydride mixture in Step 1 at 130 °C until the mixture became homogeneous and translucent. In Step 3 the mixture in Step 2 was poured into a PTFE mold, and covered with a PTFE lid, and placed in an oven under a 500 g weight for 6 h at 130 °C. Figure 2.1 also depicts the anhydride and fatty acid linkers within the thermoset network.

2.4 Recycling and Reprocessing of Epoxy-Acid Malleable Thermosets

Figure 2.2 shows schematically the overall procedure of recycling and reprocessing. The bulk polymer is first pulverized into powder, which is then compacted into a mold by applying pressure. The compacted powders are then heated to weld them into a bulk polymer. This process is repeated several times and the bulk polymer is evaluated for its mechanical properties after each generation of recycling. The details are described below. The recycling and reprocessing experiments were performed using Epoxy 1.

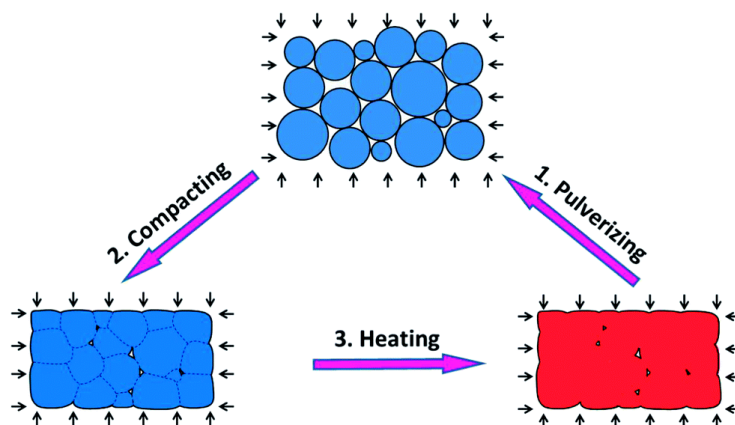


Figure 2.2 The schematic graphs for a typical reprocessing and recycling routine. (1) Bulk polymer is pulverized into powder. (2) The powders were then compacted by applying pressure. (3) The compacted powder is heated under pressure. Due to the internal bond exchange reaction (BER), the polymer particles are welded and interfaces disappear. This process is repeated several times.

2.4.1 DMA and stress relaxation tests

The glass transition behavior of the prepared epoxy-acid thermoset network was tested by dynamic mechanical analysis (DMA). A bulk polymer sample, with the dimensions of 10 mm × 5 mm × 1.0 mm was tested by a DMA tester (Model Q800, TA Instruments, New Castle, DE, USA) on the tensile mode. The sample was first heated to 100 °C and stabilized for 20 minutes to reach thermal equilibrium, and then a preload of 1 kPa and an initial strain with a magnitude of 0.1% were applied. During the experiment, the strain was oscillated at a frequency of 1 Hz with a peak-to-peak amplitude of 0.1% while the temperature was decreased from 100 °C to -50 °C at a rate of 1 °C min⁻¹. The temperature in the chamber was held at -50 °C for 30 minutes and then increased to 100 °C at the same rate. This procedure was repeated multiple times and the data from the last cooling step was reported. Figure 2.2a shows the experimental results of the DMA experiments. The temperature corresponding to the peak of the tan δ curve (30.1 °C) was taken to be the glass transition temperature T_g . It should be noted that these experimental results are slightly different from the work of Leibler et al.³³ where a different heating rate was adopted

during the tests. The storage modulus of each sample was also plotted as a function of temperature.

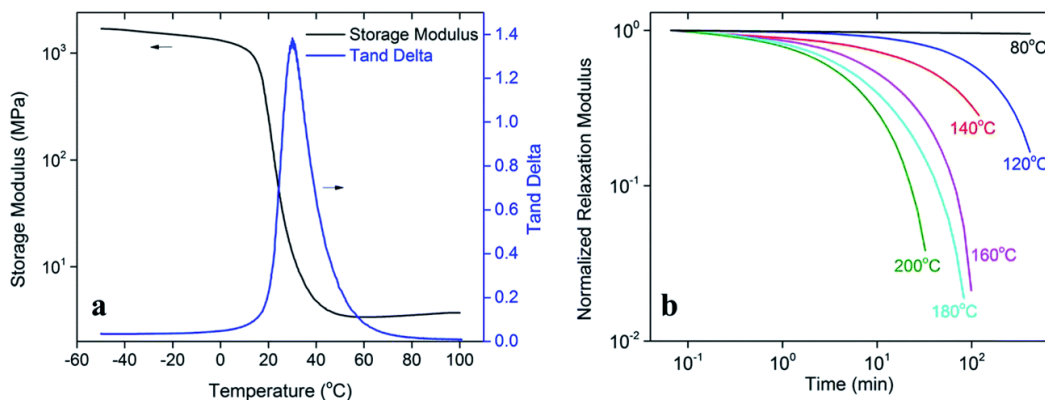


Figure 2.3 Thermomechanical characterization of the epoxy-acid thermosetting polymer. **a.** Glass transition behavior of the prepared thermoset polymer. **b.** The stress relaxation behavior of the thermoset polymer at different temperatures.

The time and temperature dependent relaxation modulus of the epoxy-acid thermoset network was also tested on the DMA tester. During the test, the polymer sample with the same dimension mentioned above was initially preloaded by 1×10^{-3} N force to maintain the straightness. After reaching the testing temperature, it was allowed 30 min to reach thermal equilibrium. The specimen was stretched by 1% on the DMA tester and the deformation was maintained during the subsequent tests. The decrease of stress was recorded and the stress relaxation modulus was calculated. Figure 2.3b depicts the results of relaxation tests at 6 different temperatures (80 °C, 120 °C, 140 °C, 160 °C, 180 °C and 200 °C) on a double logarithmic plot. Specially, at 180 °C, the bond exchange reaction (BER) is initiated and the normalized relaxation modulus is decreased from 1 to 0.15 within 30 min, indicating an 85% release of the internal stress within the thermoset polymer.

The stress relaxation behavior shown in Figure 2.3 is attributed to the BERs.^{1,19} In an exchange reaction, an active group connected to a dangling polymer chain moves around and

adds to an existing bond. This will form an intermediate structure, and form a new bond and a new active group upon completion of the reaction. The collective effect of such exchange reactions is to rearrange the topology of the network structure while preserving the bond density. When mechanical stress is exerted on the network, the network topology rearrangement allows gradual relaxation of the stress. During this process, because the bond density is preserved, this material is insoluble and maintains macroscopic structural integrity even at high temperatures. In addition, when two pieces of this material are brought into contact, molecular bonds can be established across the contacting surfaces due to the exchange reactions, which is utilized in this study to achieve self-healing and interface welding among the polymer particles.

2.4.2 Tension Tests

The DMA tester was used to carry out tension tests at room temperature (23 °C). The loading rate was chosen to be a small value (5% per min for all tests) to minimize viscoelastic effects. The samples were trimmed uniformly into the size of 12 mm × 3 mm × 1.1 mm for testing. For each tension test, at least four samples were tested and the average values are reported.

2.4.3 Pulverous Sample Preparation

The bulk sample was manually abraded by a sandpaper to render the pulverous state. The isolated polymer particles were observed by using an optical microscope and shown in Figure 2.4a. From the microscopic morphology, it is seen the particles are irregularly shaped in profile. The particle size and the distribution were analyzed using Imagine J software. As shown in Figure 2.4b, the outline of each polymer particle was extracted. The particle diameter is taken to be the diameter of the circle with equal area of each corresponding particle profile. The result of

the analysis is shown in the inset view of Figure 2.4b. It is seen that the diameter of most particles (over 77%) are distributed within 25–120 μm .

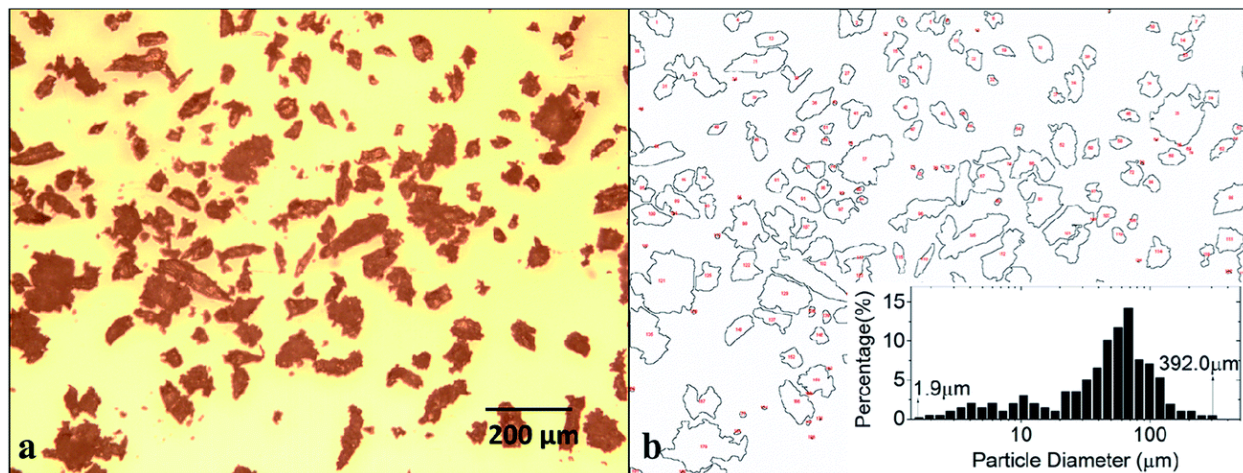


Figure 2.4 Analysis of particle sizes. **a.** Microscopic observation of the isolated polymer particles. **b.** Particle size and distribution analysis in Imagine J.

2.4.4 Experimental setup for processing

An aluminum punch mold was machined. Since the rate of BER is thermally sensitive, it is important to precisely control the sample temperature during the tests. In the present work, we adopt the method that was previously developed by the authors.³⁴ The specially designed aluminum punch mold is shown in Figure 2.5a, where three hollow slots were machined in the platen to improve the thermal convective properties and temperature distribution during the heating. After filling the polymer powders into the mold (Figure 2.5b), it was then transferred into a customized thermal chamber for heating, while the applied pressure was controlled by a universal material testing machine (MTS, Model Insight 10, Eden Prairie, MN, USA). The temperature in the thermal chamber manufactured by Thermcraft (Model LBO, Winston Salem, NC, USA) was controlled with a Eurotherm controller (Model Euro 2404, N. Chesterfield, VA, USA) where a built-in electrical heater with a fan and an externally attached tank of liquid

nitrogen provided the heat and cooling. In the work of Leibler et al.,³³ 1 MPa in pressure was introduced to promote the surface welding effect. Indeed, for a polymer in the elastic state, such a pressure would not noticeably affect the thermodynamics and reactions of polymer chains until it reaches to an extremely high value (in GPa ranges) when the free volume of single polymer chain is collapsed.³⁵⁻³⁷ In this paper, the applied pressure was also chosen to be small enough (90 kPa in maximum) to avoid affecting the transesterification reactions.

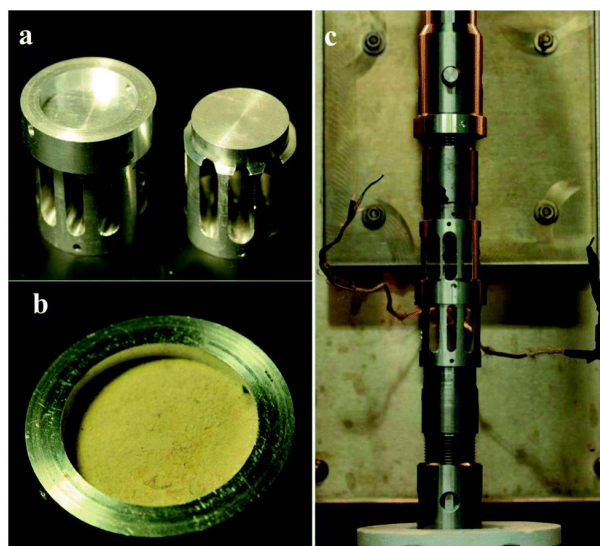


Figure 2.5 Experimental setup for the reprocessing and recycling test of thermoset polymer. **a.** Aluminum punch mold. **b.** Polymer powder is placed into the mold. **c.** The heating is conducted in a customized thermal chamber with pressure applied via the MTS machine.

2.4.5 Time and pressure dependent reprocessing quality of the thermoset polymer

The reprocessing ability of the thermoset polymers is demonstrated in this section, with considerations on the influence of reprocessing time and pressure. A fresh bulk thermoset sample is shown in Figure 2.6a for comparison. Figure 2.6b shows the appearance of the polymer from the pulverous state to the finished bulk state in a typical case with a 45 kPa pressure. We limit ourselves in this paper to a constant temperature (180 °C) during the operation, and record the

heating time immediately after the sample is placed in an oven at 180 °C. Due to the BER, the polymer powder starts surface welding and self-assembly. At 10 min (middle figure of figure 2.6b), isolated pulverous polymer tends to be in a compacted and consolidated form. Further heating of the sample under pressure for 30 min renders an essentially complete welding effect where the sample appears transparent and resembles the fresh sample (shown in the right figure of figure 2.6b), indicating that the interfaces among particles have disappeared.

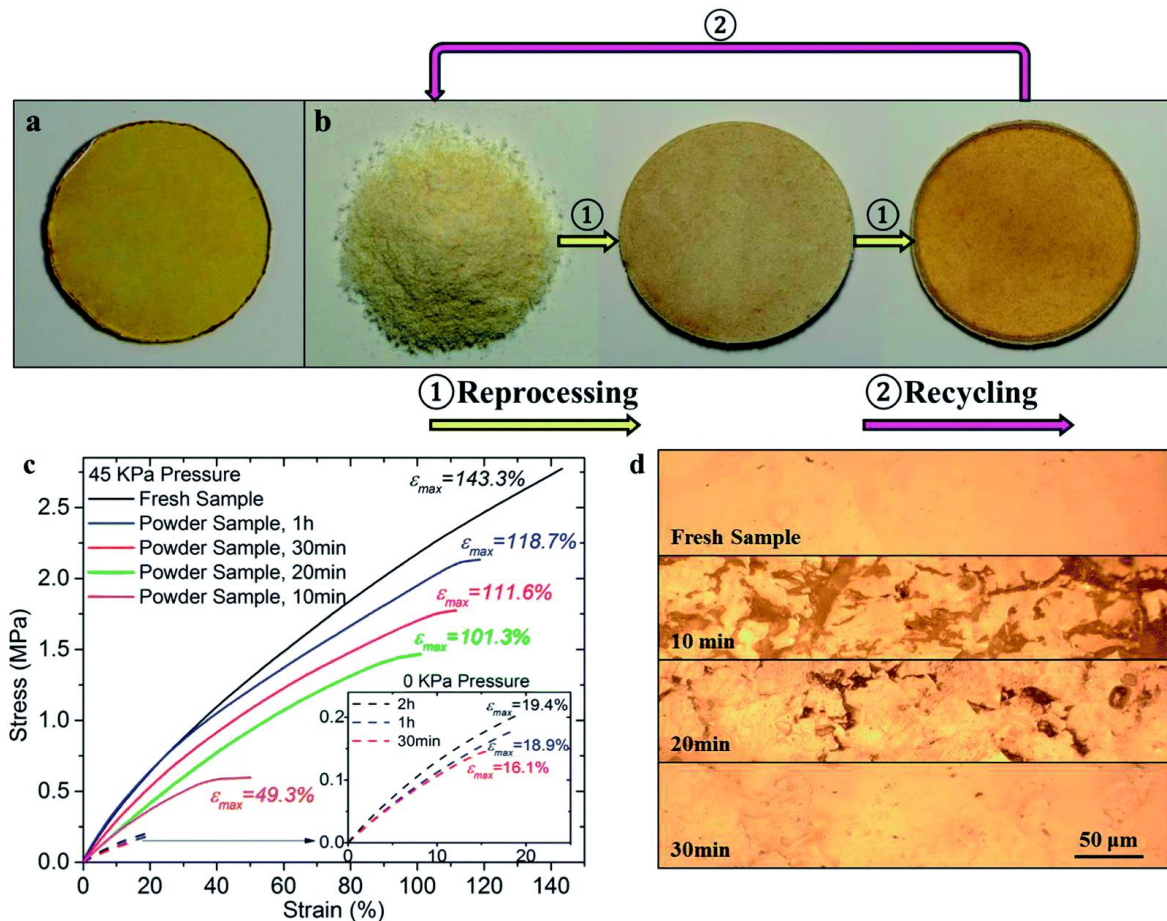


Figure 2.6 The typical reprocessing and recycling routine for the thermoset polymer and the stress–strain behavior after different reprocessing times. **a.** A fresh bulk thermoset polymer. **b.** The typical reprocessing and recycling routine (180 °C in temperature and 45 kPa in pressure). From left to right: pulverous polymer after milling, polymer powder after being heated for 10 min and 30 min respectively. **c.** Stress–strain curves of the reprocessed sample after being heated for different time and with 45 kPa pressure applied. Note: the fresh sample is also heated at 180 °C for 1 h to normalize the comparison. Inset view: stress–strain curves of powder sample

without pressure applied. **d.** Surface morphology of both fresh sample and powder samples at different heating time.

The time and pressure dependent welding effect of the pulverous thermoset polymer was quantified by the ultimate stretch (the stretch at the break) and initial elastic modulus (measured over the initial 15% stretch) of the reprocessed samples. The bulk thermoset polymer was reprocessed with different pressures (0 kPa, 2 kPa, 10 kPa, 45 kPa and 90 kPa, respectively) applied during the heating process. The stress–strain behavior of the thermoset samples reprocessed at 45 kPa is shown in Figure 2.6c. A fresh polymer sample was also tested after being heated at 180 °C for 1 h to normalize the comparison¹. For the pulverous sample heated for 10 min at 180 °C, we observed a relatively low initial elastic modulus of 2.2 MPa. The sample fails quickly with an ultimate stretch of 49.3%. With an increase of heating time, both the elastic modulus and ultimate stretch are improved in the reprocessed thermoset samples. With 30 min heating, the initial modulus and the ultimate stretch are 2.9 MPa and 111.6%, respectively (or 76.7% and 77.9% of those in the referential fresh sample, respectively). Such an increase in the material stretch ability is due to the gradually welded interfaces and increased connections among the polymer particles, as shown in the microscopic observations in Figure 2.6d. Before the pulverous thermoset is completely welded, numerous voids (the dark regions in Figure 2.6d with 10 min and 20 min of heating) exist within the matrix, which can propagate cracks under external loads and compromise stretch ability. At 30 min, the polymer powder is seen to be remolded into a coherent solid essentially resembling the fresh sample. The stress–strain curves in Figure 2.6c also reveal that the welding process is largely completed within 30 min when 45

¹ After being heated for 1 h at 180 °C, which is ~150 °C above the glass transition temperature of the thermoset polymer, a slight thermal induced hardening was observed in the material. The stretch ability was decreased by 3.8% (from 149.0% to 143.3%) and the initial modulus within the 15% stretch was increased by 5.7% (3.5 MPa to 3.7 MPa). Both of them are presented as reference values in figure 4.6a–d.

kPa pressure is applied. From 30 min to 1 h, the ultimate stretch of the reprocessed sample is increased by 7%. The inset in Figure 2.6c also shows the case when there is no pressured applied. The incompact polymer powder can only be partially welded, as evidenced by the very limited stretchability of less than 20% with an initial modulus around 1 MPa, even after being heated for 2 h.

The ultimate stretch and elastic modulus of the reprocessed samples under different reprocessing pressure and time are summarized in Figure 2.7a–d, respectively. Generally, both increasing pressure and increasing heating time can improve the final properties of the reprocessed samples. First, for the cases studied in this paper, both ultimate stretch and elastic modulus of the reprocessed samples can achieve the levels of fresh samples, with a clear trend where increasing either heating time or pressure can accelerate this process. Second, increasing pressure is more effective in recovering the elastic modulus than in recovering the ultimate stretch. For example, at 90 kPa, the elastic modulus reaches the fresh sample level within 20–30 min (Figure 2.7b and d); but within the same time period, the ultimate stretch only reaches 120% stretch, which is 80% of that of the fresh samples (Figure 2.7a and c). Third, the increased heating time can recover both the ultimate stretch and the elastic modulus to the fresh sample levels, as long as the pressure is larger than a critical value. For example, even with 2 kPa pressure, both ultimate stretch and elastic modulus almost achieve the fresh sample levels if heated for 720 min (6 h). Certainly, from the manufacturing point of view, heating for 720 min is not energy efficient; increasing the pressure can shorten the heating time and thus help the design of an optimized reprocessing procedure, which deserves future studies.

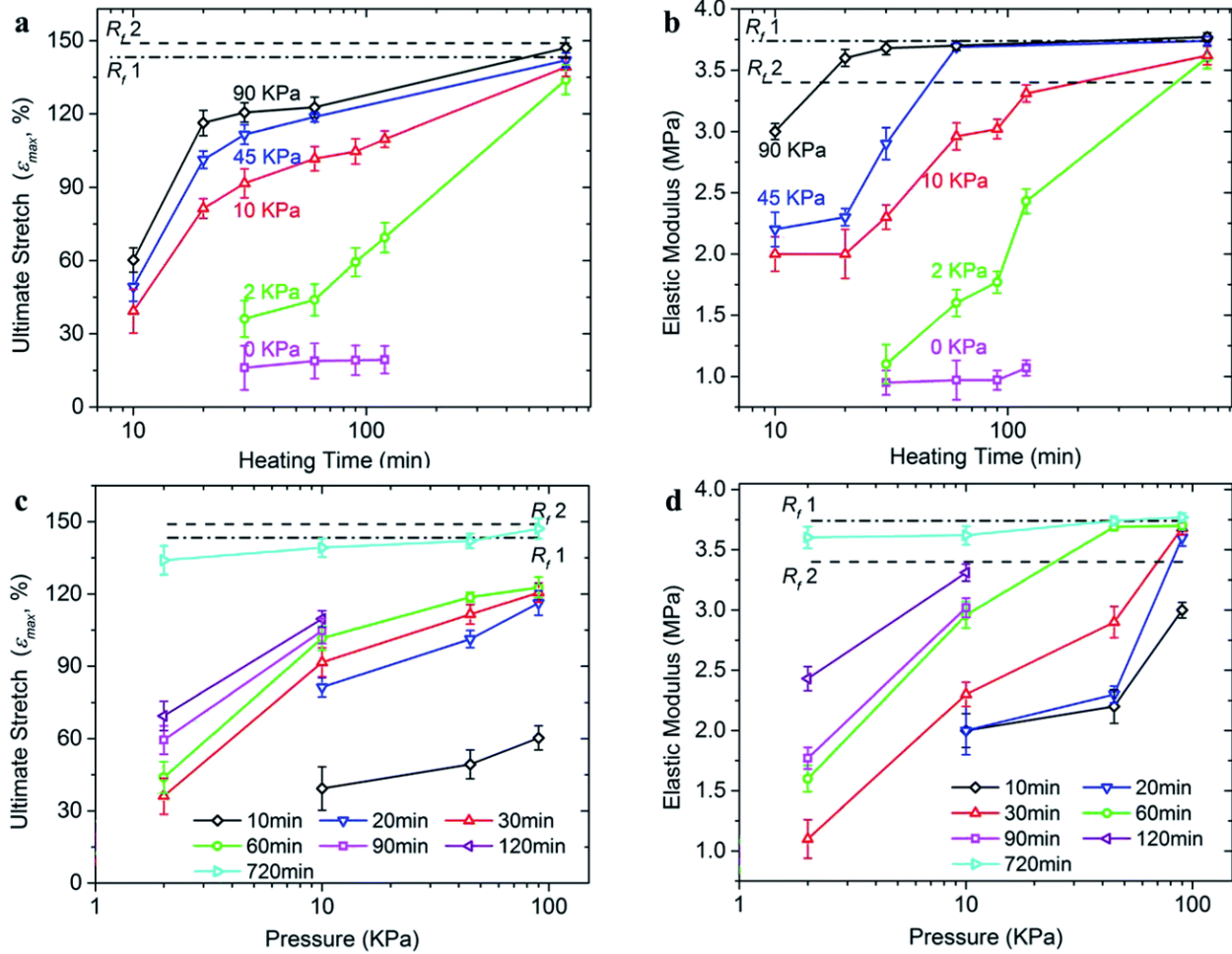


Figure 2.7 The time and pressure dependent ultimate stretch and initial modulus of the reprocessed thermoset polymer. **a.** Ultimate stretch (maximum strain before fracture) plot of the reprocessed sample as a function of heating time. **b.** Initial elastic modulus (within the first 15% stretch) as a function of heating time. **c.** Ultimate stretch as a function of applied pressure. **d.** Initial elastic modulus as a function of applied pressure. Note: R_{f1} denotes the referential property of a fresh bulk sample after being heating at 180 °C, while R_{f2} denotes that of the fresh sample without any heat treatment.

2.4.7 Recycling ability of the Epoxy-acid Malleable Thermoset

Since the polymer chains in the thermoset are only exchanged but not consumed during the recycling operation, several cycles might be achieved. A set of aluminum molds with digital-shape grooves was designed to test the recycling ability of the thermoset polymer. During the

experiments, each reprocessed sample was pulverized into powder by using the same grade of sandpaper, and then recycled to the next generation of the object. During each reprocessing cycle, the applied pressure is set to be 45 kPa. It should be noted that the influence of pressure on the healing efficiency of the pulverous polymer is related to the particle size. When compact the polymer powder at high temperatures, small-sized particles have larger contact surfaces and can quickly close the voids when a small pressure is applied. While for the large-sized particles, the applied pressure should be high enough to squeeze them together. Particles may also deform their shapes accordingly to close the voids before healing on the interfaces, which requires additional reprocessing time. Therefore, it is necessary to examine the possible alternation in particle size and distribution after the powder samples being reprocessed.

Figure 2.8a shows the microscopic observation of the isolated polymer particles after being reprocessed four times. The particle size distribution is summarized in Figure 2.8b and compared with that used in the first reprocessing routine (shown in Figure 2.4). It is seen that after 4 cycles, the particles size is slightly decreased. For the freshly abraded polymer powder, most particles (over 77%) are distributed within 25–120 μm , while this range is changed to 16–87 μm after the 4th cycle. This is because when we abrade a polymer sample with reprocessing history, in addition to the newly formed crack surfaces, some of the previously healed surfaces with lower strength may also break, which leads a smaller particle size distribution. However, since the change is not significant, we assume in the following study that the particle size does not vary during the recycling processes, and hence the interplay between particle size and pressure is negligible.

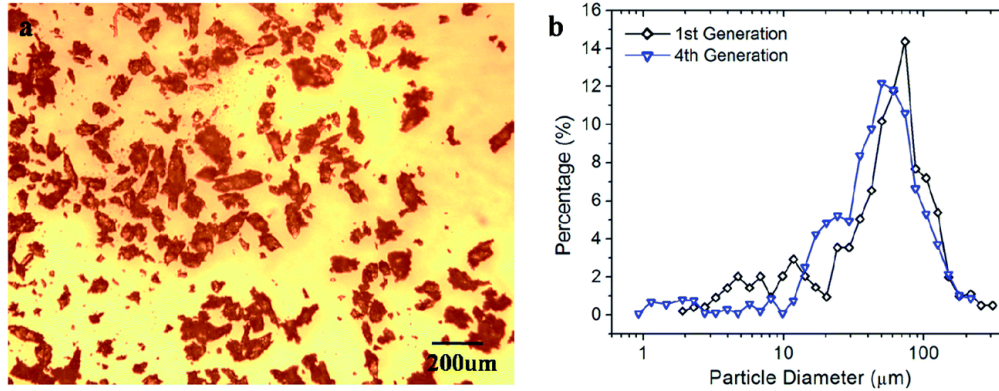


Figure 2.8 Analysis of particle sizes after being reprocessed for four times. **a.** Microscopic observation of the isolated polymer particles. **b.** Particle size and distribution analysis. Note: the black line indicates the particle size distribution shown in Figure 2.4.

With the same temperature (180 °C) and pressure (45 kPa) applied, all the pulverous thermosets were heated for 30 min. The manufactured sample in each cycle is shown in Figure 2.9a, where the digit numbers indicate recycling generation. It is seen that pulverous thermoset polymer possesses a good recycling ability in exhibiting transparent samples in different shapes. The glass transition temperature becomes slightly higher at 35.7 °C after the 4th generation of reprocessing, as compared to 30.1 °C of the fresh sample. Besides, the rubber modulus (as seen in the storage modulus curve after 60 °C) is decreased after the 4th reprocessing. This is because during the pulverization of the polymer material, some permanently cross-linked strands of the polymer network are broken on the fracture surfaces³⁸ and cannot be recovered during the subsequent healing process, which leads to a decreased crosslinking density and modulus in the rubber state. The stress–strain curves are shown in Figure 2.9c. It is remarkable to note that even after four times of reprocessing that sample still can achieve an ultimate stretch of 91.8% stretch. Figure 2.9d shows the evolution of the ultimate stretch and elastic modulus as a function of the number of recycling generations. Another set of recycling tests are also presented in the figure where the heating time in each cycle is 2 h. It is clear that although the properties of recycled

material decay over the number of recycling, they stay in a reasonably good range. Also, the amount of decay decreases as the number of recycling increases, suggesting that more cycles of recycling is possible. In addition, the elongated heating time will improve the properties of recycled material significantly. As shown in Figure 2.9c, a 6 hour heating of the 4th generation sample leads to the ultimate stretch of 137.7%, which is comparable to that of the fresh sample without recycling history.

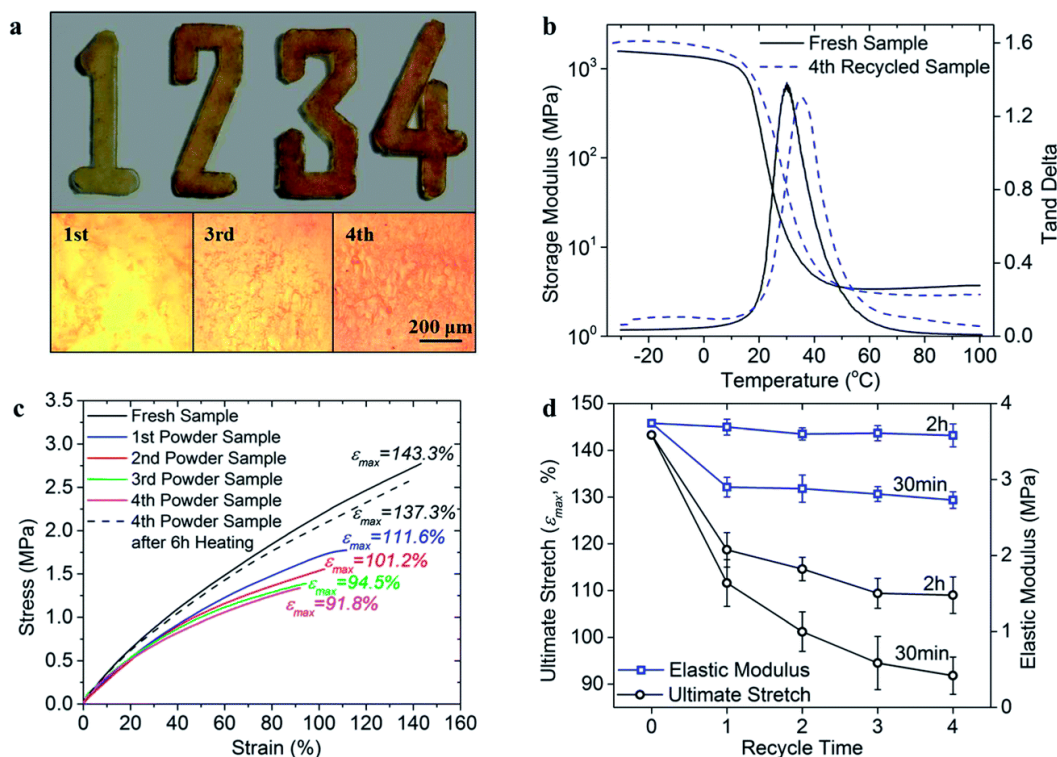


Figure 2.9 The recycling ability of the thermoset polymer. **a.** Top view: sample manufactured by using polymer powder after being recycled for multiple times. Digit numbers indicate the recycle generation. Bottom view: the surface roughness observation on the 1st, 3rd and 4th recycled samples **b.** Stress–strain behavior of the polymer powder sample after being recycled for different times. The heating time is 30 min in each cycle. **c.** Glass transition behavior of the fresh sample and sample recycled for four times. **d.** Ultimate stretch and initial elastic modulus plots as a function of recycle generations. Two sets of experiment are presented in the figure where the heating time in each reprocessing cycle is 30 min and 2 h respectively.

2.4.8 Repairing Bulk Polymers Using the Powder

In most engineering applications, the structural thermoset polymers are susceptible to damage in the form of cracks, fractures and abrasions. Isolated interfaces might not be easily brought into contact again for welding. Structural patching using a bulk polymer is also not practical as it will potentially change the dimensions of polymer components. In view of these facts, the use of a pulverous thermoset as a repair medium is potentially a better choice. We therefore extended our study on the reprocessing and recycling ability of thermoset polymers to this particular engineering application, namely utilizing polymer powder to reconnect the bulk material. As shown in Figure 2.10a, two strips of the bulk thermoset polymer were placed on a glass slide, with a large gap in between. Then the gap was filled with the polymer powder and sandwiched between two glass slides (Figure 2.10b). Utilizing the standard heating condition (30 min at 180 °C with a pressure of 45 kPa), the two polymer pieces were reconnected as shown in Figure 2.10c. The sample was further trimmed into a rectangular shape (Figure 2.10d) for tension tests.

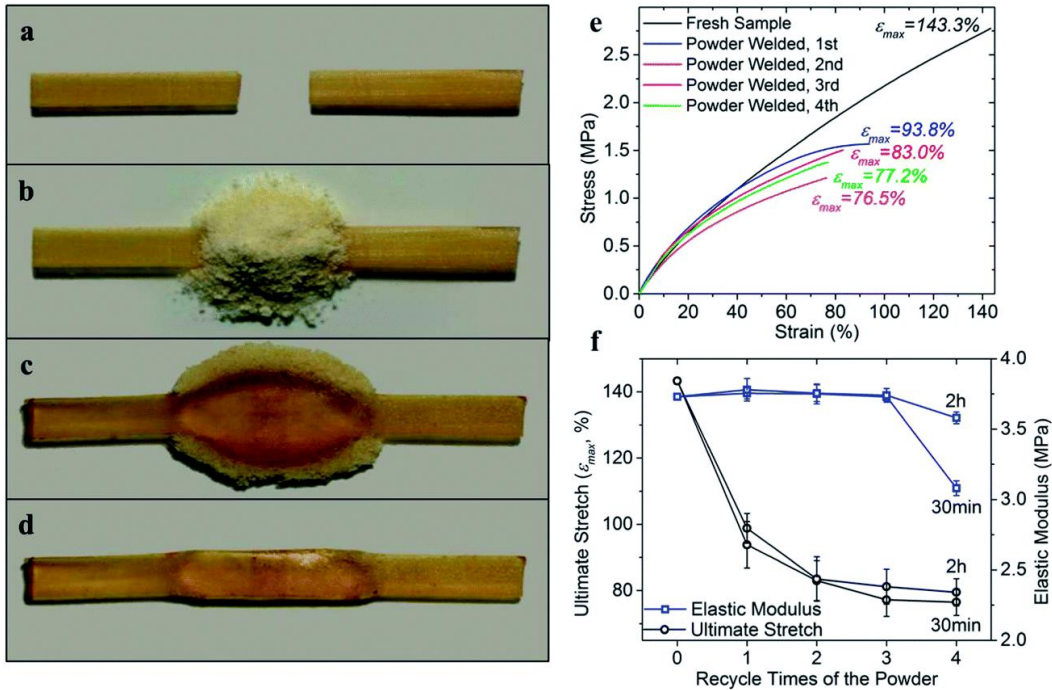


Figure 2.10 Welding isolated bulk thermoset strip by using the pulverous polymer. **a.** Two separated pieces of the thermoset polymer are placed on a glass slide. **b.** The gap is filled with the polymer powder. **c.** The separated thermoset polymer is healed and assembled together after being heated at 180 °C for 30 min (45 kPa in pressure). **d.** The sample is further trimmed into rectangular shape for tension test. **e.** The stress–strain curves of the welded sample by using polymer powder recycled for different times. The heating time is 30 min in each test. **f.** Ultimate stretch and initial elastic modulus plots as a function of recycle times of the applied polymer powder. Two sets of experiment are presented in the figure where the heating time in each test is 30 min and 2 h respectively.

The welding procedure mentioned above was also repeated with thermoset powder with recycling history (up to four generations), while the bulk polymer strips were always fresh samples. The stress–strain curves are then plotted in Figure 2.10e. It is seen that except for the 4th recycled powder healed sample, the initial elastic moduli of the other three samples are typically close to the fresh sample, while the ultimate stretch is lower than that of the reprocessed samples studied above. All the failures in the tested samples are located on the welded interface between the bulk polymer and the powder assembles. By using the powder that has been reprocessed four times, the ultimate stretch is decreased to 76.5% stretch. We conducted another set of experiments with 2 h of heating time in each operation, and the mechanical properties are summarized in Figure 2.10f for comparison. Since the polymer materials were sandwiched between glass slides with pressure, increasing heating time would not significantly improve the material's stress-bearing ability, which is limited by in-plane pressure during the operation, and subsequently the interface strength between the bulk polymer and powder assembly.

2.5 Influence of Stoichiometry on T_g and Malleability

2.5.1 Dynamic Mechanical Analysis

The glass transition of the prepared epoxy thermoset networks was tested by using a dynamic mechanical analysis (DMA) tester (Model Q800, TA Instruments, New Castle, DE,

USA). During the DMA test, when a sinusoidal strain boundary condition is applied, there is a phase lag (δ) in the measured sinusoidal stress if the tested material is viscous. In this manner, we can express the modulus as an in-phase storage modulus to quantify the polymer's elastic behavior, and an out of phase loss modulus to measure the energy dissipation within the polymer. The ratio of the loss to the storage modulus (i.e. $\tan \delta$) is referred as polymer damping, and the temperature corresponding to the maximum damping is typically used to characterize polymer T_g .³⁹⁻⁴⁰ The DMA T_g and stress relaxation measurements were conducted in the manner described above.

2.5.2 Glass Transition and BER induced Stress Relaxation

Figure 2.11 compares the DMA testing results and the glass transition behavior of the five epoxy thermosets. Figure 2.11a shows that as the ratio of anhydride hard linkers increases from 0 to 1, the T_g increases from 30.3 °C to 63.0 °C. Additionally, the $\tan \delta$ curve becomes wider but decreases in height. Figure 2.11b plots the storage modulus curves of each sample as a function of temperature. The material glassy modulus (initial modulus on each curve) and rubbery modulus (final modulus on each curve) are observed to increase as more glutaric anhydride linkers incorporated. These material properties, together with the tested T_g , are summarized in Figure 2.11c.

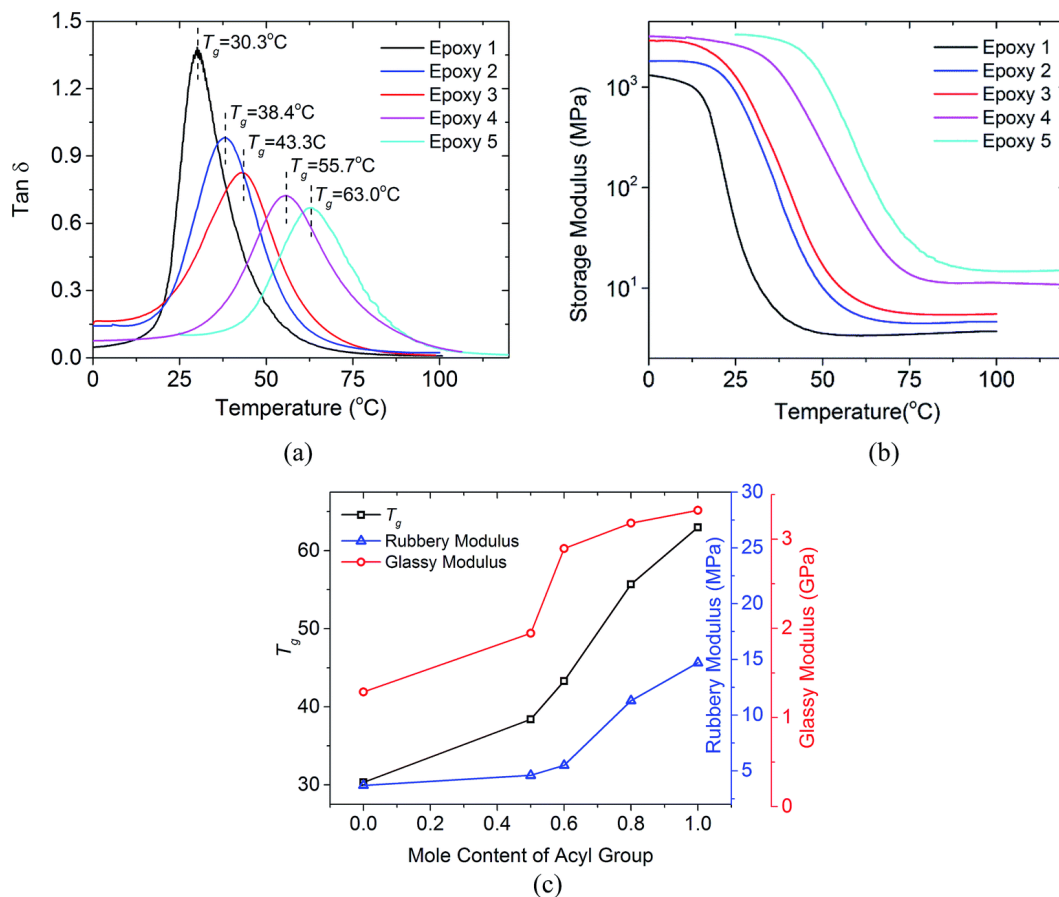


Figure 2.11 Comparisons of glass transition behavior of the five epoxy samples. **a.** $\text{Tan } \delta$ curves as a function of temperature. The T_g is taken to be the temperature corresponding to the peak value. **b.** Storage modulus curves as a function of temperature. **c.** Comparison of T_g , rubbery modulus and glassy modulus as a function of mole content of glutaric anhydride linkers. Note: the glassy modulus is taken to be the initial value on the storage modulus curves as shown in **b.**

The experimental results shown in Figure 2.11c indicate that the epoxy thermosets tend to become harder as we increase the proportion of anhydride linkers in the network. The change in glass transition and temperature dependent mechanical properties can be attributed to the alternation of network structure. As shown in Figure 2.1, compared with the anhydride hard linker, the fatty acid linker possesses longer backbone chains of carbon atoms, and hence has more freedom of motion and flexibility at a given temperature. When we include more hard linkers, the average flexibility and mobility of polymer chains is reduced and the crosslinking

density is increased, which is responsible for the elevated material modulus and T_g in most thermoset polymers.⁴¹⁻⁴² By properly choosing the ratio between fatty acid and glutaric anhydride, we can effectively tune the material glass transition and mechanical properties, which would offer a wider range of properties to best meet specific service conditions that require hard thermoset polymers as structural materials.

Figure 2.3b depicts the relaxation test results of Epoxy 1 at 6 different temperatures (80 °C, 120 °C, 140 °C, 160 °C, 180 °C and 200 °C). The relaxation modulus is normalized and plotted on a double logarithmic scale. It is seen that the BERs release the internal stress at a faster rate when the temperature is higher. For example, at 180 °C, the BER rate is sufficiently increased and the normalized relaxation modulus decreases from 1 to 0.15 within 30 min, indicating an 85% drop of the internal stress. Comparison between Figures 2.11a and 2.3b also reveals that the typical temperature required for BERs is significantly higher than glass transition temperature. As shown in Figure 2.11a, the glass transition is essentially complete at 80 °C, while the BERs are so sluggish (black line in Figure 2.3b) that the material essentially behaves like elastomer without much stress relaxation. By using the same stress relaxation tests, the time and temperature dependent relaxation curves of Epoxy 2–5 are shown in the experimental section of this chapter. It is observed that the BERs could render all the thermoset polymers malleable at different temperatures.

2.5.4 Characterization of the Temperature Dependent Stress Relaxation

The temperature dependent relaxation time τ is initially measured from the experimental relaxation curves (solid lines in Figure 2.12a) when normalized relaxation modulus declines to $1/e$ (~36.8%), which is showing a linear relationship with $1/(T + 273)$ in a semi-log scale (see

the inset view of Figure 2.12a). By using the determined relaxation times, we can effectively capture the time and temperature dependent relaxation behavior of the epoxy polymer (dash lines in Figure 2.12a).

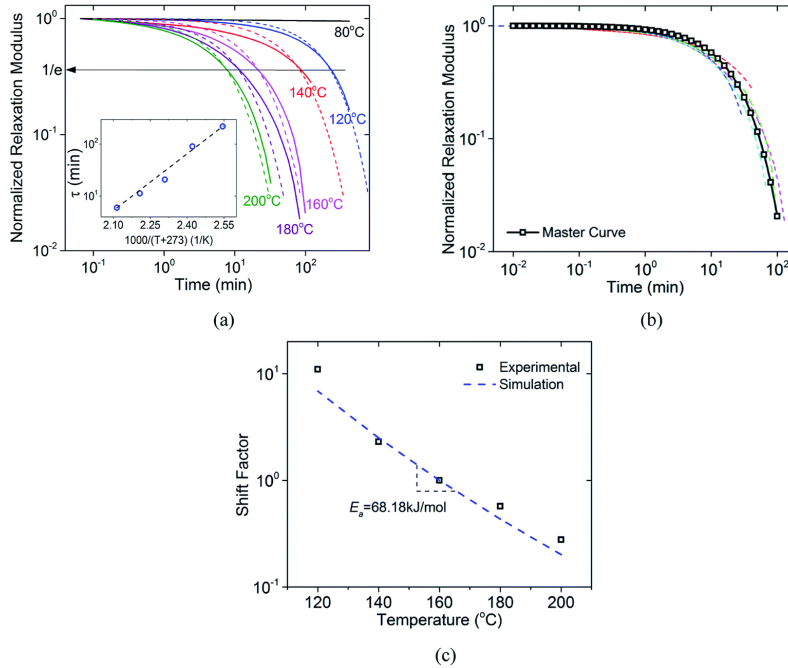


Figure 2.12 The temperature dependent stress relaxation behavior of the epoxy soft network. **a.** The stress relaxation behavior at different temperatures. Solid lines denote experimental results and dash lines show the expected Arrhenius behavior. The inset view shows the linear relationship between τ and $1000/T$. **b.** A master curve is constructed at the reference temperature of 160 °C. **c.** Shift factors plotted as a function of temperature.

Subsequently, by shifting the stress relaxation curves in Figure 2.12a horizontally to a reference temperature T_r (160 °C), we found that the curves can be superimposed and a master curve was constructed (see Figure 2.12b) with an extended timing scale, which also reflects the relaxation behavior of the epoxy thermoset at the reference temperature (160 °C). The existence of the master relaxation curve confirms that the kinetics of the BER induced stress relaxation follows the well-known TTSP.

The shift factors α_T during the timing scale transformation are plotted in Figure 2.12c as a function of temperature. The energy barrier could be determined by fitting the shift factor curve to predicted Arrhenius behavior. As shown in Figure 2.12c, the energy barrier E_a is determined to be $68.18 \text{ kJ mol}^{-1}$, and the pre-exponential factor k equals $2.17 \times 10^5 \text{ s}^{-1}$ at the reference temperature of $160 \text{ }^\circ\text{C}$.

2.5.5 Stress Relaxation of Epoxy-acid Networks with Different T_g

In addition to the epoxy soft network (Epoxy 1), we characterized the temperature dependent relaxation behavior of the rest epoxy samples (Epoxy 2–5) to investigate how the BER induced stress relaxation ability can be affected due to the alternation of material composition. By using the same relaxation tests and characterization procedure, the time and temperature dependent relaxation curves of Epoxy 2–5 are shown in the experimental section of this chapter. For these relaxation tests, since the temperature is set to be highly above the corresponding T_g , we further examined the material's thermal stability by using the thermogravimetric analysis (TGA) tester (Model, STA 6000, PerkinElmer, Waltham, MA, USA). The result (see experimental) shows that the decomposition onset temperatures of Epoxy 1–5 are between $\sim 350 \text{ }^\circ\text{C}$ and $390 \text{ }^\circ\text{C}$, which are much higher than the temperature used for stress relaxation tests, and therefore no thermally induced degradation will occur. Besides, uniaxial tension tests on Epoxy 1–5 after being heated for 30 min were also conducted, where temperatures are set to be the highest one in the corresponding stress relaxation test. It is seen that all of the epoxy samples after heat treatment exhibit thermally induced hardening effect with increased elastic modulus and decreased stretch ability. But the material strength is seen to be

stable without significant changes, which also indicates no obvious heat decomposition or network damage occurred within the epoxy samples during the stress relaxation tests.

Similar to the sample Epoxy 1, the Arrhenius type stress relaxation behavior enables us to construct master curves for each epoxy sample. To facilitate the comparisons, the reference temperature was uniformly set to 160 °C, and the predicted master curves are plotted in Figure 2.13a, which shows that as we increase the glutaric anhydride linker in the epoxy network, the characteristic relaxation time at the reference temperature is increased. For example, compared with the sample Epoxy 1 with a relaxation time of 20.9 min at 160 °C, the relaxation time of Epoxy 5 is predicted to be 3,456 min (~2.5 day). The increased relaxation times also indicate increased activation temperatures for BERs in the epoxy samples.

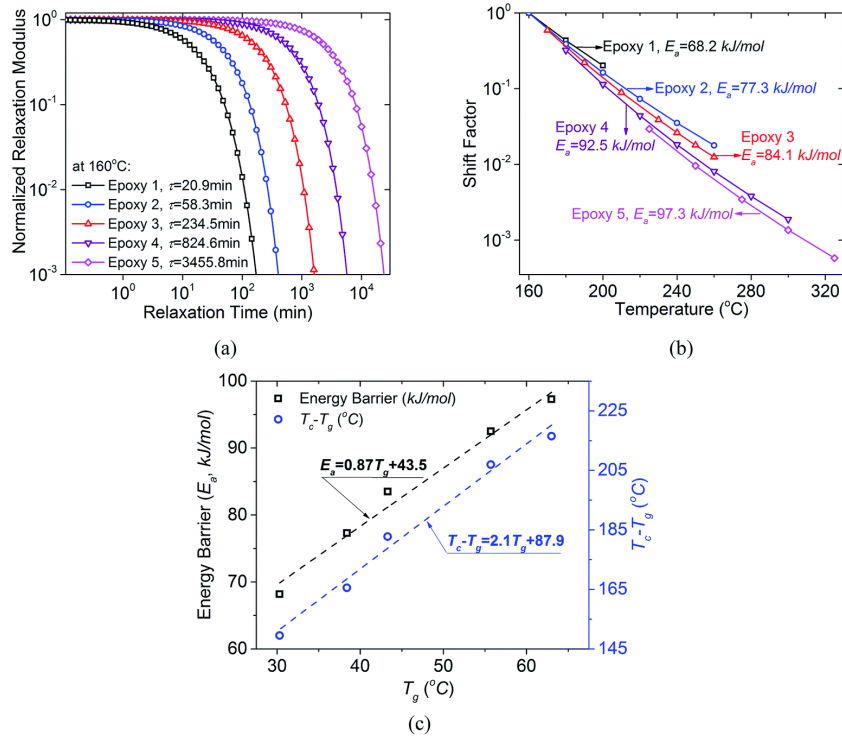


Figure 2.13 a. The master relaxation curves in each epoxy sample. The reference temperature is uniformly chosen to be 160 °C. **b.** The Arrhenius type shift factors plotted as a function of temperature. The energy barriers for the BERs in each epoxy sample are determined by fitting

curve slopes. **c.** Plot of the energy barrier for BERs and the difference between T_c and T_g as a function T_g .

The Arrhenius type temperature dependence of the shift factors in each epoxy sample is plotted in Figure 2.13b. Since the curve's slope tells the activation energy barrier for BERs, the gradual increase in the slopes of the curves indicates that the energy barrier for BERs also increases. This is because at a given temperature, the polymer chain mobility of epoxy with higher content of hard anhydride segments is lower, which reduces the possibility of polymer chains moving around to seek available site for bond exchanges. Based on the calculated energy barriers, together with the relaxation times at the reference temperature as shown in Figure 2.13a, one can calculate the extrapolated relaxation time of each sample at different temperatures.

For the convenience of comparison between the stress relaxation abilities of each sample, we further define a characteristic temperature T_c where the internal BER induced relaxation time is 10 min. Since the required temperature for BERs is typically higher than the glass transition temperature, the difference between them, namely $T_c - T_g$ actually quantifies how much additional energy is needed for the BERs after the glass transition is finished. This difference, along with the measured energy barrier for each epoxy sample, is plotted in Figure 2.13c as a function of the associated T_g . A linear relationship is found for both the energy barrier and $T_c - T_g$. The least square method generalized the following empirical formula, with 95% confidence bound for the fitting factors:

$$T_a = 0.87T_g + 43.5, \quad (2.1a)$$

$$T_c - T_g = 2.1T_g + 87.9. \quad (2.1b)$$

Note in the above two equations, the unit for temperatures is °C. The result in equation (2.1) qualitatively correlates the glass transition behavior and internal BERs of the epoxy thermosets, and indicates that if the epoxy polymer possesses a higher T_g , the difference between the T_g and the temperature to achieve comparable BER rate is larger.

2.6 Conclusions

First, we demonstrated that after being ground into a pulverous state of micrometer size particles and recycled multiple times, the thermoset polymer with exchangeable bonds could be assembled again into a coherent solid with mechanical properties comparable to the fresh bulk polymer. Considering the efficient and robust welding effect among polymer particles, as well as the maintained merits of thermoset polymer as stress-bearing materials during the healing operation, this strategy is suitable for repair of polymer structures in service, as well as reprocessing and recycling of thermoset waste in engineering applications. Although the material studied in this paper is limited to an epoxy-acid network, one can extend the concept of bond exchange and particle recycling to other thermoset polymers via the incorporation of an appropriate catalytic bond exchange system.

We further synthesized epoxy thermoset polymers with different glass transition temperatures (T_g) by changing the stoichiometric ratios among monomers. The tunable T_g can be attributed to the alternation in polymer chain mobility and network flexibility. By using the standard stress relaxation tests, all the epoxy samples were shown to be able to effectively release the internal stress and rendered the thermoset polymers to be malleable, but the rate of stress relaxation is affected by the material composition. Based on the kinetics of BERs, we

derived the detailed expression of the temperature dependent stress relaxation time. It is shown that the material relaxation behavior is following the Arrhenius type time–temperature superposition (TTSP). A master relaxation curve was consequently constructed, which further revealed the energy barrier for the BERs and enabled us to predict the relaxation time of each epoxy polymer at different temperatures. Finally, we experimentally correlated the glass transition behavior and internal BERs of the epoxy thermoset polymers. That is, when we gradually elevate T_g , the thermal energy required to achieve the same stress relaxation rate is linearly ramped. Such a correlation between these two thermomechanical behaviors provides an additional design parameter of thermally malleable thermosets and helps to achieve highly tunable service conditions for practical engineering applications.

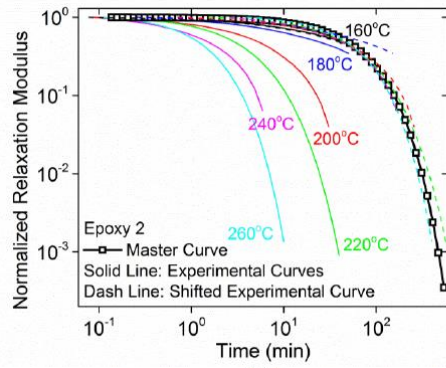
2.7 Experimental Details

2.7.1 Time and temperature dependent stress relaxation of Epoxy 2-5

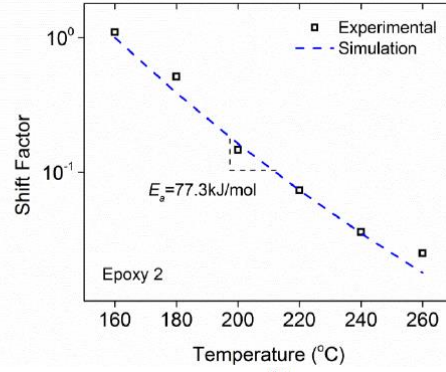
The time and temperature dependent stress relaxation behavior of Epoxy 2-5 is shown in Figure 2.14. The experimental procedure is the same as mentioned in the main text: all the epoxy samples with the same dimensions (10mm × 5mm × 1mm) were first preloaded by 1×10^{-3} N force to ensure straightness. After reaching the testing temperature, it was allowed 30 min for the thermal equilibrium. The specimen was then stretched by 1% on the DMA machine and the deformation was maintained during the test. The decrease of stress was recorded and the stress relaxation modulus was calculated.

Figure 2.14a, c, e and g firstly show the normalized relaxation modulus of Epoxy 2-5 at different temperatures. Then by shifting each curves horizontally into the reference temperature

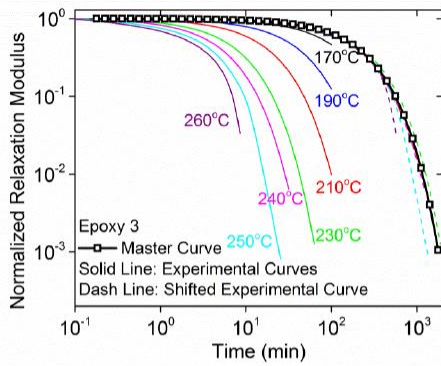
(160 °C), a master relaxation curve was constructed for each epoxy sample, which can be further captured by using an exponentially decay function. Both the simulation and the estimated relaxation times are presented in Figure 2.11a. During shifting the relaxation curves, the associated shift factors are then plotted in Figure 2.14b, d, f and h. It is seen the stress relaxation behavior of all the epoxy samples is following the Arrhenius type temperature-time superposition (TTSP). The different curve slopes of each sample indicate different energy barrier for the bond exchange reactions.



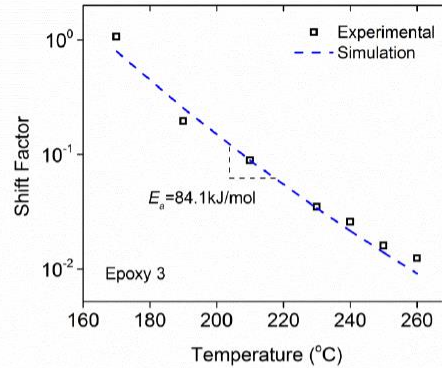
(a)



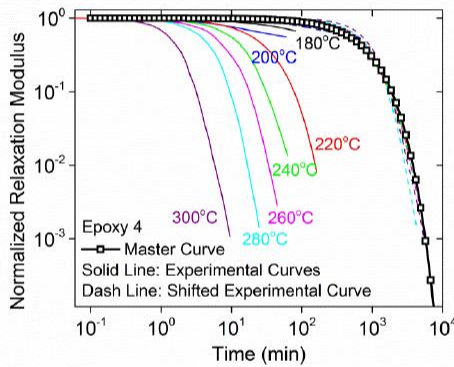
(b)



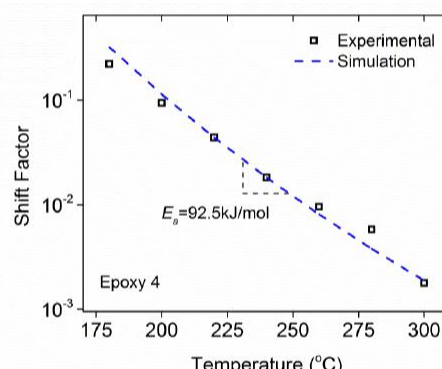
(c)



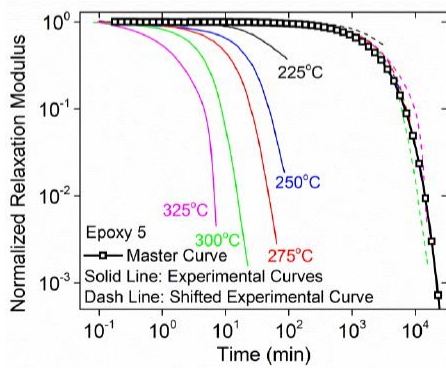
(d)



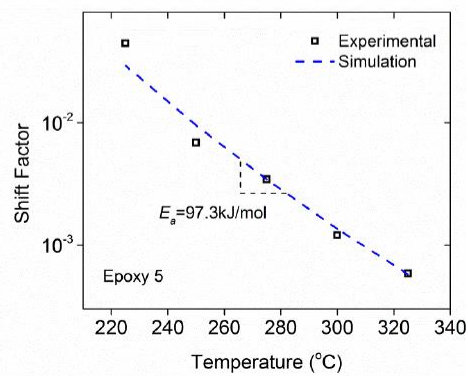
(e)



(f)



(g)



(h)

Figure 2.14 The stress relaxation curves, master relaxation curves and associated shift factors plots of **a.** Epoxy 2, **b.** Epoxy 3, **c.** Epoxy 4, **d.** Epoxy 5. The stress relaxation behavior of Epoxy 1 is shown in figure 2.2b.

2.7.2 Thermal stability of Epoxy 1-5

The thermal stability of epoxy materials was tested by using the thermogravimetric analysis (TGA) tester (Model, STA 6000, Perkin Elmer, Waltham, MA, USA). The samples weighing 20–25 mg were heated from 35 °C at a constant rate of 10 °C min⁻¹ in the presence of air. Weight loss due to the thermal degradation of Epoxy 1-5 was shown in Figure 2.15. It is shown that with the increment of crosslinking density of epoxy sample, the onset of decomposition temperature increases slightly. But these onset temperatures (~350 °C - ~390 °C) are much higher than the temperature used for stress relaxation, which suggest that no thermally induced degradation occurred during the relaxation tests.

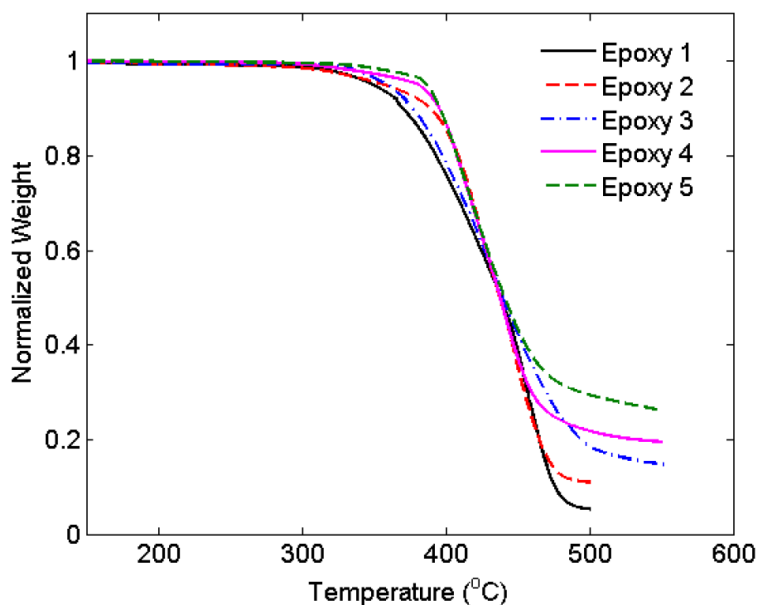


Figure 2.15 Normalized weight as a function of temperature during the TGA test.

In addition to the TGA tests, we further conducted uniaxial tension tests on Epoxy 1-5 after being heated for 30min. The temperatures are taken to be the highest one in the

corresponding stress relaxation test (i.e. 200 °C for Epoxy 1, 260 °C for Epoxy 2, 260 °C for Epoxy 3, 300 °C for Epoxy 4 and 325 °C for Epoxy 5). Meanwhile, fresh epoxy samples without heat treatment were also tested and their stress-strain curves are shown in figure 2.16.

All the tension tests were carried out on the DMA machine at room temperature (23 °C). The loading stress rate was chosen to be 3MPa/min, and at least three samples were tested for each epoxy material. Then the average modulus (measured over the initial 10% stretch), stretch ability (maximum strain before break) and strength (maximum stress before break) are summarized in Table 2.2.

As shown in Figure 2.16, after being heated for 30min, all the epoxy materials exhibit thermally induced hardening effect⁴³ with increased elastic modulus and decreased stretch ability. Such hardening effect is more obvious in epoxy material with higher T_g (see the relative change of mechanical property in Table 2.2). However, the material strength is seen to be stable without significant changes, which also indicates no obvious heat decomposition or network damage occurred within the epoxy samples at high temperature. Since in this study, we are focusing on the revealing of relationship between glass transition and BERs, this difference in mechanical properties after heat treatment can be ignored.

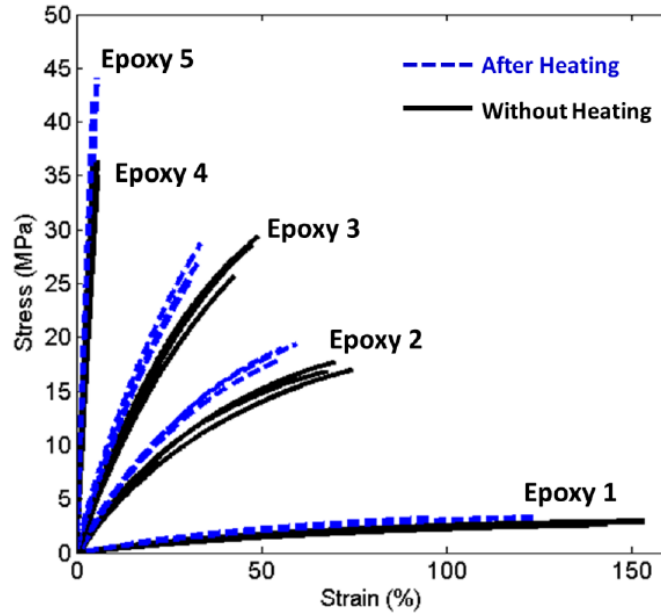


Figure 2.16 Stress-strain curves of Epoxy 1-5 before and after heat treatment.

Table 2.2 Summary of mechanical properties of Epoxy 1-5 before and after heat treatment

Elastic Modulus (MPa)	Before Heating	After Heating	Relative Charge
Epoxy 1	3.8	3.9	2.6%
Epoxy 2	59.1	66.2	11.9%
Epoxy 3	150.8	172.6	14.5%
Epoxy 4	659	745.1	13.1%
Epoxy 5	728.3	862.7	18.5%
Stretch Ability	Before Heating	After Heating	Relative Charge
Epoxy 1	144.9%	124.6%	-14.0%
Epoxy 2	70.8%	59.6%	-15.8%
Epoxy 3	46.5%	32.4%	-30.3%
Epoxy 4	5.8%	5.0%	-16.0%
Epoxy 5	4.6%	4.3%	-6.5%
Strength (MPa)	Before Heating	After Heating	Relative Charge
Epoxy 1	3	3.1	3.3%
Epoxy 2	17.5	17.9	2.3%
Epoxy 3	28.7	27	-5.9%
Epoxy 4	35.4	34.4	-2.8%
Epoxy 5	37.7	41.3	5.2%

2.8 References

- [1] D. Montarnal, M. Capelot, F. Tournilhac and L. Leibler, "Silica-Like Malleable Materials from Permanent Organic Networks," *Science*, vol. 334, no. November, pp. 965-968, 2011.
- [2] J. I. Kim, S. H. Ryu and Y. W. Chang, "Mechanical and dynamic mechanical properties of waste rubber powder/HDPE composite," *Journal of Applied Polymer Science*, vol. 77, no. 12, pp. 2595-2602, 2000.
- [3] A. M. Shanmugaraj, J. K. Kim and S. H. Ryu, "UV surface modification of waste tire powder: Characterization and its influence on the properties of polypropylene/waste powder composites," *Polymer Testing*, vol. 24, no. 6, pp. 739-745, 2005.
- [4] A. M. Shanmugaraj, J. K. Kim and S. H. Ryu, "Modification of rubber powder with peroxide and properties of polypropylene/rubber composites," *Journal of Applied Polymer Science*, vol. 104, no. 4, pp. 2237-2243, 2007.
- [5] A. A. Barber, V. A. Bhagavati, L. Ukkonen, A. Z. Elsherbeni, P. Kallio and L. Sydanheimo, "Performance of high-permittivity ceramic-polymer composite as a substrate for UHF RFID tag antennas," *International Journal of Antennas and Propagation*, pp. 1-8, 2012.
- [6] F. Hernandez-Olivares, G. Barluenga, M. Bollati and B. Witoszek, "Static and dynamic behaviour of recycled tyre rubber-filled concrete," *Cement and concrete research*, vol. 32, no. 10, pp. 1578-1596, 2002.
- [7] C. N. Albano, N. Camacho, J. Reyes, J. L. Feliu and M. Hernandez, "Influence of scrap rubber addition to Portland I concrete composites: destructive and non-destructive testing," *Composite Structures*, vol. 71, no. 3, pp. 439-446, 2005.
- [8] R. Siddique and T. R. Naik, "Properties of concrete containing scrap-tire rubber - an overview," *Waste Management*, vol. 24, no. 6, pp. 563-569, 2004.
- [9] G. Li, M. A. Stubblefield, G. Garrick, J. Eggers, C. Abadie and B. Huang, "Development of waste tire modified concrete," *Cement and Concrete Research*, vol. 34, no. 12, pp. 2283-2289, 2004.
- [10] J. O. Outwater and D. J. Gerry, "On Fracture Energy, Rehealing Velocity and Refracture Energy of Cast Epoxy Resin," *Journal of Adhesion*, vol. 1, pp. 290-298, 1969.

- [11] M. A. Rahmathullah and G. R. Palmese, "Crack-Healing Behavior of Epoxy-Amine Thermosets," *Journal of Applied Polymer Science*, vol. 113, no. 4, pp. 2191-2201, 2009.
- [12] M. Yamaguchi, S. Ono and M. Terano, "Self-repairing property of polymer network with dangling chains," *Materials Letters*, vol. 61, no. 6, pp. 1396-1399, 2007.
- [13] S. A. Hayes, F. R. Jones, K. Marshiya and W. Zhang, "A self-healing thermosetting composite material," *Composites Part A: Applied Science and Manufacturing*, vol. 38, no. 4, pp. 1116-1120, 2007.
- [14] X. Luo, R. Ou, D. E. Eberly, A. Singhal, W. Viratyaporn and P. T. Mather, "A Thermoplastic/Thermoset Blend Exhibiting Thermal Mending and Reversible Adhesion," *ACS applied materials & interfaces*, vol. 1, no. 3, pp. 612-620, 2009.
- [15] A. M. Peterson, H. Kotthapalli, M. A. M. Rahmathullah and G. R. Palmese, "Investigation of interpenetrating polymer networks for self-healing applications," *Composites Science and Technology*, vol. 72, no. 2, pp. 330-336, 2012.
- [16] S. J. Rowan, S. J. Cantrill, G. R. Cousins, J. K. Sanders and J. F. Stoddart, "Dynamic covalent chemistry," *Angewandte Chemie International Edition*, vol. 41, no. 6, pp. 898-952, 2002.
- [17] J. Lehn, "Dynamers: dynamic molecular and supraolecular polymers," *Prog. Polym. Sci.*, vol. 30, no. 8-9, pp. 814-831, 2005.
- [18] T. Maeda, H. Otsuka and A. Takahara, "Dynamic covalent polymers: Reorganizable polymers with dynamic covalent bonds," *Progress in Polymer Science*, vol. 34, no. 7, pp. 581-604, 2009.
- [19] C. Kloxin, T. Scott, B. Adzima and C. Bowman, "Covalent Adaptable Networks (CANs): A Unique Paradigm in Cross-Linked Polymers," *Macromolecules*, vol. 43, pp. 2643-2653, 2010.
- [20] R. J. Wojtecki, M. A. Meador and S. J. Rowan, "Using the dynamic bond to access macroscopically responsive structurally dynamic polymers," *Nature Materials*, vol. 10, no. 1, pp. 14-27, 2011.
- [21] M. S. Green and A. V. Tobolsky, "A New Approach to the Theory of Relaxing Polymeric Media," *Journal of Applied Physics*, vol. 17, no. 5, p. 407, 1946.
- [22] M. Rubinstein and A. N. Semenov, "Thermoreversible gelation in solutions of associating polymers. 2. Linear dynamics," *Macromolecules*, vol. 31, no. 4, pp. 1386-1397, 1998.

- [23] L. Leibler, M. Rubinstein and R. H. Colby, "Dynamics of Telechelic Ionomers - Can Polymers Diffuse Large Distances without Relaxing Stress," *Journal of Physics II*, vol. 3, no. 10, pp. 1581-1590, 1993.
- [24] H. Otsuka, K. Aotani, Y. Higaki and A. Takahara, "Polymer scrambling: Macromolecular radical crossover reaction between the main chains of alkoxyamine-based dynamic covalent polymers," *Journal of the American Chemical Society*, vol. 125, no. 14, pp. 4064-4065, 2003.
- [25] T. F. Scott, A. D. Schneider, W. D. Cook and C. N. Bowman, "Photoinduced Plasticity in Cross-Linked Polymers," *Science*, vol. 308, pp. 1615-1617, 2005.
- [26] R. Nicolay, J. Kamada, A. Van Wassen and K. Matyjaszewski, "Responsive Gels Based on a Dynamic Covalent Trithiocarbonate Cross-Linker," *Macromolecules*, vol. 43, no. 9, pp. 4355-4361, 2010.
- [27] G. Ghosh and M. W. Urban, "Self-Repairing Oxetane-Substituted Chitosan Polyurethane Networks," *Science*, vol. 323, no. 5920, pp. 1458-1460, 2009.
- [28] K. Imato, M. Nishihara, T. Kanehara, Y. Amamoto, A. Takahara and H. Otsuka, "Self-Healing of Chemical Gels Cross-Linked by Diarylbibenzofuranone-Based Trigger-Free Dynamic Covalent Bonds at Room Temperature," *Angewandte Chemie International Edition*, vol. 51, no. 5, pp. 1138-1142, 2012.
- [29] B. J. Adzima, H. A. Aguirre, C. J. Kloxin, T. F. Scott and C. N. Bowman, "Rheological and Chemical Analysis of Reverse Gelation in a Covalently Cross-Linked Diels-Alder Polymer Network," *Macromolecules*, vol. 41, no. 23, pp. 9112-9117, 2008.
- [30] Y. Zhang, A. A. Broekhuis and F. Picchioni, "Thermally Self-Healing Polymeric Materials: The Next Step to Recycling Thermoset Polymers?," *Macromolecules*, vol. 42, no. 6, pp. 1906-1912, 2009.
- [31] R. H. Long, H. Qi and M. L. Dunn, "Modeling the mechanics of covalently-adaptable polymer networks with temperature-dependent bond exchange reactions," *Soft Matter*, vol. 9, no. 15, pp. 4083-4096, 2013.
- [32] K. Yu, P. Taynton, W. Zhang, M. Dunn and H. J. Qi, "Reprocessing and recycling of thermosetting polymers based on bond exchange reactions," *RSC Advances*, vol. 4, no. 20, pp. 10108-10117, 2014.
- [33] M. Capelot, D. Montarnal, F. Tournilhac and L. Leibler, "Metal-Catalyzed Transesterification for Healing and Assembling of Thermosets," *J. Am. Chem. Soc.*, vol. 134,

pp. 7664-7667, 2012.

- [34] K. K. Westbrook, F. Castro, K. N. Long, A. J. Slifka and H. J. Qi, "Improved testing system for thermomechanical experiments on polymers using uniaxial compression equipment," *Polymer Testing*, vol. 29, no. 4, pp. 503-512, 2010.
- [35] A. S. Benjamin, M. Ahart, S. A. Gramsch, L. L. Stevens, E. B. Orler, D. M. Dattelbaum and R. J. Hemley, "Acoustic properties of Kel F-800 copolymer up to 85 GPa," *The Journal of Chemical Physics*, vol. 137, no. 1, p. 014514, 2012.
- [36] L. L. Stevens, E. B. Orler, D. M. Dattelbaum, M. Ahart and R. J. Hemley, "Brillouin-scattering determination of the acoustic properties and their pressure dependence for three polymeric elastomers," *The Journal of Chemical Physics*, vol. 127, no. 10, p. 104906, 2007.
- [37] Z. A. Dreger, J. Zhou, N. C. Dang and Y. M. Gupta, "Effect of high pressure on acoustic properties of several polymers: Use of impulsive stimulated light scattering method," *Journal of Applied Physics*, vol. 109, no. 8, p. 083507, 2011.
- [38] E. B. Stukalin, L.-H. Cai, N. A. Kumar, L. Leibler and M. Rubinstein, "Self-Healing of Unentangled Polymer Networks with Reversible Bonds," *Macromolecules*, vol. 46, no. 18, pp. 7525-7541, 2013.
- [39] D. M. Joseph and R. B. Prime, *Thermal Analysis of Polymers: Fundamentals and Applications*, John Wiley & Sons, 2009.
- [40] H. F. Brinson and C. L. Brinson, *Polymer engineering science and viscoelasticity: an introduction*, Springer, 2007.
- [41] J. C. Salamone, *Polymeric Materials Encyclopedia*, Boca Raton: CRC Press, 1996.
- [42] A. A. Askadskii, "Influence of crosslinking density on the properties of polymer networks," *Polymer Science U.S.S.R.*, vol. 32, no. 10, pp. 2061-2069, 1990.
- [43] C. L. Beyler and M. M. Hirschler, "Thermal Decomposition of Polymers," in *SFPE Handbook of Fire Protection Engineering, 3rd ed.*, Quincy, NFPA, 2001.

CHAPTER 3

Heat or water driven malleability in a highly-recyclable covalent network polymer *Development and characterization of polyimine network polymers*

(Manuscript published under the same title in *Advanced Materials* **2014**, **26**, 3938-3942, coauthored with Yu, K.; Shoemaker, R.; Jin, Y.; Qi, H.J.; Zhang, W.)

3.1 Abstract

Covalent network polymers, which offer robust mechanical properties, generally lack the ability to be recycled.¹ There has been a great deal of research effort to incorporate reversible cross-links into network polymers in order to obtain mechanically tough materials with malleable properties.²⁻¹² Many have employed non-covalent cross-links to achieve this goal. Ionic and hydrogen bonds are readily reversible and have been known to achieve efficient self-healing performances.¹³⁻¹⁶ However, these systems are generally vulnerable to heat as well as water and other polar solvents, and are not as resilient as covalent network polymers. Leibler and coworkers introduced the concept of incorporating a certain type of dynamic covalent interaction (*i.e.* reversible ester linkages) in a covalent network polymer, and demonstrated the malleability of epoxy-acid network polymers at elevated temperatures.² Recently, Guan and coworkers demonstrated that a cross-linked polybutadiene network becomes malleable when the olefin exchange reaction is enabled by introducing Grubbs' Ru complex.³ These polymers can be reshaped, healed, and molded together because of efficient cross-link exchange reactions

wherein new cross-links are formed at the same time as the original cross-links are cleaved. This enables the polymer to maintain a constant cross-link density throughout the process.¹⁷ However, these polymers' reprocessing requires very high temperatures (~180 °C) or relies on catalyst additives which add cost and complexity, and potentially limit the polymer lifetime due to catalyst quenching. Some catalyst-free malleable polymers have been developed,^{4,12} but these exhibit highly active cross-link exchange at ambient temperatures which leads to undesirable polymer creep in any load-bearing application.

3.2 Introduction

Imine chemistry, also known as Schiff base chemistry, is the most often employed reversible covalent interaction, and includes two distinct processes: imine condensation/hydrolysis, and imine exchange.¹⁸ The wide variety of commercially available diamines and dialdehydes makes polyimines highly accessible functional polymers, with many well-demonstrated unique functionalities.¹⁹⁻²³ Polyimines, which are described as dynamers by Lehn,²⁴⁻²⁵ are stimuli-responsive polymers, most notably exhibiting macroscopic responses to changes in pH.²⁶⁻²⁷ Several imine-containing polymers have been demonstrated, including pH-responsive hydrogels¹⁹ and a working organic light emitting diode (OLED).²² However, the potential of polyimines as malleable, mechanically resilient polymeric materials, as well as their processability, have remained largely unexplored. We envision that imine-linked polymers can take malleability in covalent network polymers to the next level of simplicity, affordability and practicality. Herein we present the first catalyst-free malleable polyimine which fundamentally behaves like a classic thermoset at ambient conditions yet can be reprocessed by application of either heat or water. This means that green, room temperature processing conditions are accessible for this important class of functional polymers.

3.3 Results and discussion

A cross-linked polyimine network was prepared from commercially available monomers: terephthalaldehyde, diethylene triamine, and tris(2-aminoethyl)amine (Figure 3.1a). A polyimine film was obtained by simply mixing the three above components in a 3:0.9:1.4 stoichiometry in the absence of any catalyst in a mixture of organic solvents (1:1:8, v/v/v, CH₂Cl₂/EtOAc/EtOH,), then allowing the volatiles to evaporate slowly. Alternatively, the polymer can be obtained as a powder by using pure ethylacetate as a solvent. The polymerization reaction was confirmed by infrared spectroscopy, which revealed that aldehyde end groups were consumed while imine linkages were formed (Figure 3.6). The resulting translucent polymer is hard and glassy at room temperature (T_g is 56 °C) (Figure 3.5) and has a modulus of near 1 GPa with stress at break of 40 MPa (Figure 3.7).

The time and temperature dependent relaxation modulus of the polyimine film was tested to characterize the heat-induced malleability. Figure 3.1b depicts the results of a series of relaxation tests over a wide range of temperatures (50 °C→127.5 °C) on a double logarithmic plot. Specifically, at 80 °C, the bond exchange reaction is initiated and the normalized relaxation modulus is decreased from 1 to 0.11 within 30 min, indicating an 89% release of the internal stress within the thermoset polymer. By shifting each relaxation curve horizontally with respect to a reference temperature at 80 °C, a master relaxation curve was constructed (Figure 3.1c), which indicates the stress relaxation of the polyimine follows the classic time-temperature superposition (TTSP) behavior. The plot of time-temperature shift factors as a function of temperature (Figure 3.1d) shows that the polyimine's stress-relaxation behavior exhibits Arrhenius-like temperature dependence. Using the extrapolation, we calculated that while it takes 30 min for the stress to be relaxed by ~90% at 80 °C, the same process would take ~480

days at room temperature. The polyimine is thus the first reported catalyst-free malleable polymer that mimics a classic thermoset at ambient temperatures and could be used for load bearing applications. The temperature (80 °C) required for fast bond exchange in the polyimine is easily obtainable, yet beyond the operating conditions encountered in most applications.

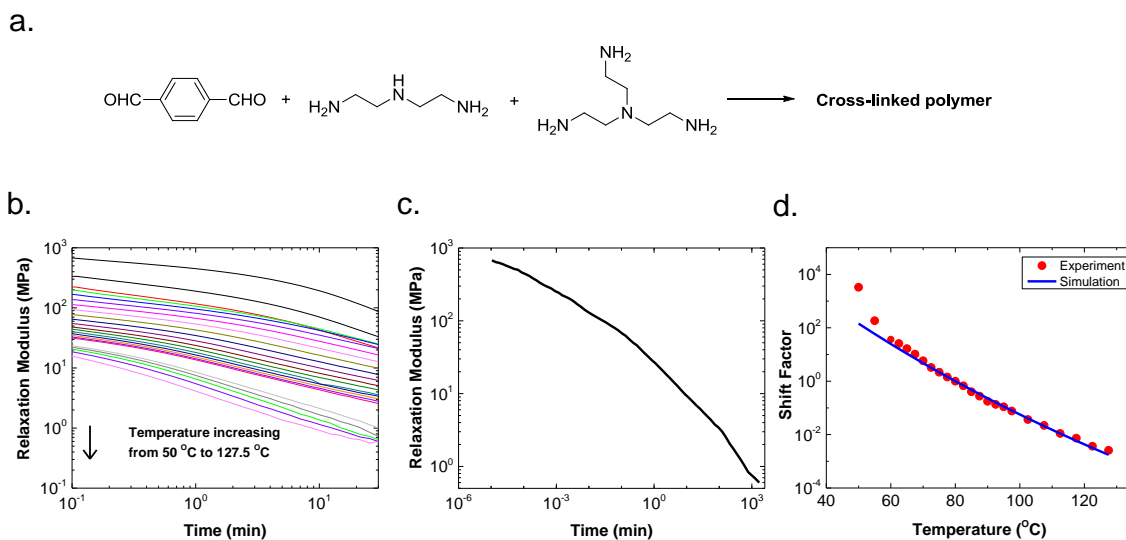


Figure 3.1 Polymer synthesis and stress-relaxation studies. **a.** Synthesis of cross-linked polyimine. **b.** Stress relaxation curves at various temperatures over a time period of 30 min. This data was used for the temperature-time superposition calculations. **c.** Temperature-time superposition master curve derived from data in Figure 3.1b. **d.** Shift factor vs. temperature plot for temperature-time superposition experiment. Blue line is derived from 80 °C reference temperature data from Figure 3.1c.

After the malleable behavior of the polyimine was confirmed, the recyclability of the material was explored. We investigated the durability of the imine-linked polymer toward complete reprocessing from powder to solid. It should be noted that this is a very demanding test as the transition from powder to coherent solid requires perfect healing across many thousands of interfaces between particles. Molding a batch of as-synthesized polymer powder under a pressure of 90 kPa for 45 min at 80 °C (Figure 3.2a) formed a solid polymer disc (Figure 3.2b). The disc was subsequently ground into a fine powder (Figure 3.2c) and the recycling process was repeated 3 times. Our study shows that the recycled materials exhibit no degradation in

mechanical strength through 4 generations of recycling. A slight decrease in elastic modulus through the first few recycling generations was observed (Figure 3.2d), indicating that the polymer becomes more flexible as it is recycled. Notably, there is no loss in the tensile strength of the polymer, but rather a slight increase is observed from the 1st through the 4th generation (Figure 3.2d). Overall, this catalyst-free polyimine exhibits impressive recyclability, indicating that the imine bond is resilient against recycling fatigue.

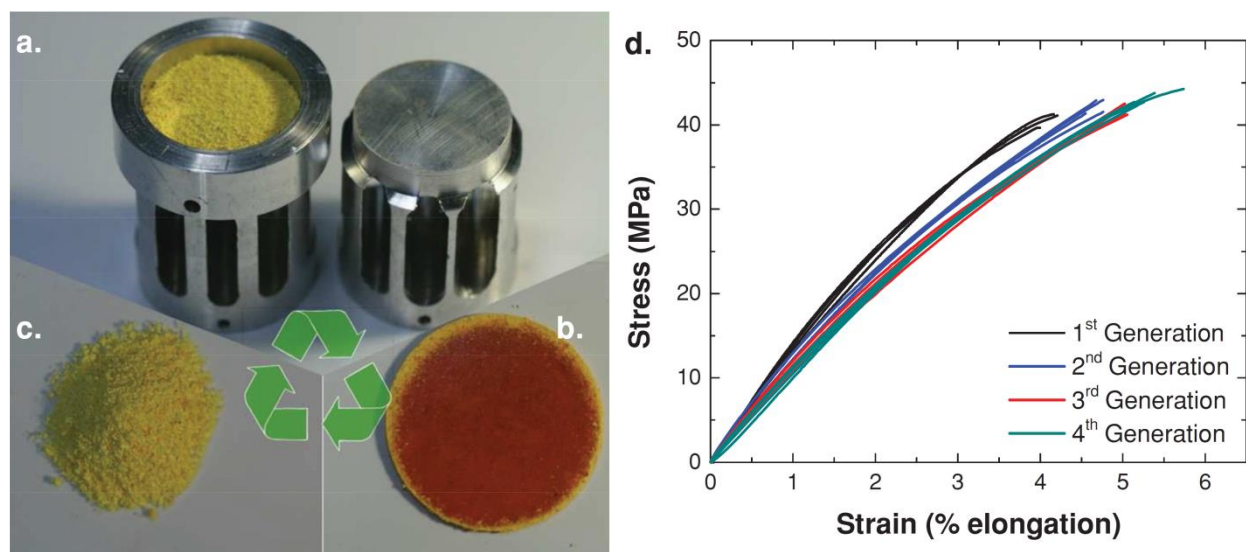


Figure 3.2 Recycling study. **a.** Aluminum mold used to heat press polyimine powder into solid disc. **b.** Solid polyimine disc formed from powder by pressing at 80 °C. This is the material used for stress strain testing in Figure 3.2d. **c.** Polyimine powder obtained by grinding the solid disc in Figure 3.2b with sandpaper. **d.** Stress strain curves for the solid shown in Figure 3.2b through four generations of recycling from powder to solid. For each generation, four separate stress-strain experiments are displayed. Black curves: 1st generation solid formed by heat-pressing the fresh as-synthesized polymer powder into a solid disc. Blue curves: 2nd generation solid formed by heat pressing the powder obtained by grinding the first generation solid. Red curves: 3rd generation solid formed by heat pressing the powder obtained by grinding the 2nd generation solid. Green curves: 4th generation solid formed by heat pressing the powder obtained by grinding the 3rd generation solid.

Imine linkages are often considered susceptible to cleavage by hydrolysis. However, the extent of hydrolysis is a simple matter of chemical equilibrium.²⁸ It has previously been shown that certain crystalline organic molecular cages containing multiple imine bonds have greatly improved resistance to hydrolysis.²⁹ We examined the characteristic stress-strain behavior for

polyimines at various levels of atmospheric humidity (Figure 3.10). Like wood, the polyimine material becomes more pliable with increasing atmospheric humidity, but even at very high atmospheric humidity levels (90% RH), the polymer's mechanical properties are drastically different than when it is saturated with water. When the polymer disc is immersed in water, the hard glassy polymer becomes soft and flexible as it swells. The sample reaches saturation and the swelling remains constant after 12 h (Figure 3.9). Importantly, the polymer retains its mechanical integrity even after 1 week under water at 96 °C. This combination of pliability and insolubility suggests that the malleability of the polyimine could also be activated by water. To characterize the malleability caused by water, a stress-relaxation experiment was performed under water at 25 °C on a polymer film sample that was initially saturated in water for 24 h. It reveals that the stress relaxation of the polyimine in water is comparable to the behavior observed at elevated temperatures. More importantly, the underwater condition allows more expedient stress relaxation than heating the polymer to 127.5 °C (Figure 3.3g). Such water-induced stress-relaxation behavior offers the remarkable opportunity of green and energy neutral reprocessing and reshaping of the polyimine thermoset. For instance, as-synthesized polyimine powder was reprocessed into a translucent polymer disc by simple molding in water for 24 h at room temperature under 90 kPa (Figure 3.3b & 3.3e). After drying under vacuum, the resulting polymer disc showed typical hard polymer behavior: high elastic modulus, and relatively small elongation at break. The water-healed polymer is more elastomeric compared to the heat-pressed powder (Figure 3.3f). In sharp contrast, when dry powder was reprocessed under the same conditions, a brittle disc of compacted powder was obtained (Figure 3.3d). There was thus no macro-scale evidence of bond exchange reactions in the absence of water at room temperature. These results clearly show that water can turn on the malleability of the polymer.

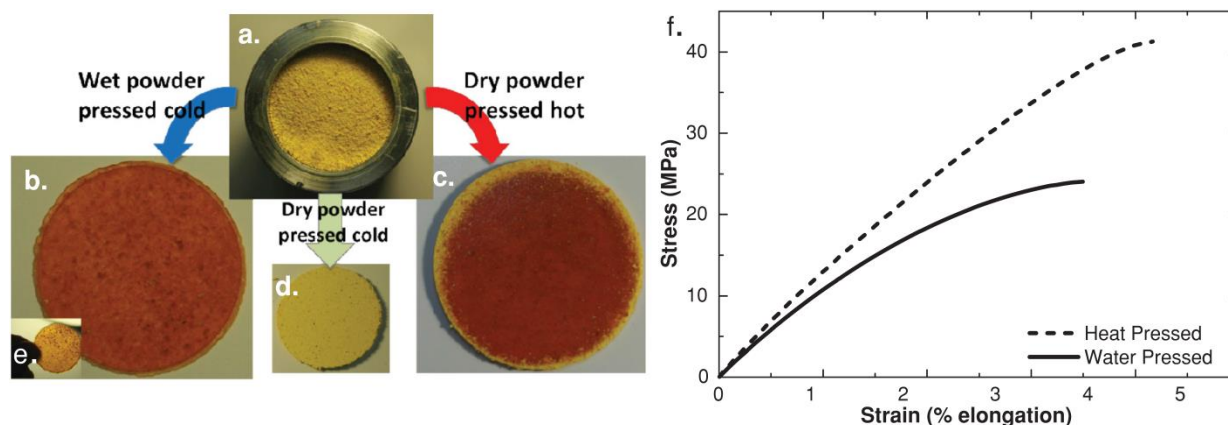


Figure 3.3 Processability summary. **a.** Polyimine powder in aluminum mold. **b.** Polyimine disc formed by pressing the wet powder under 90 kPa at room temperature for 24 h. **c.** Polyimine disc formed by heat pressing the dry powder under 90 kPa at 80 °C for 40 min. **d.** Brittle polyimine disc formed by pressing the dry polyimine powder under 90 kPa for 96 h at room temperature. **e.** The translucent nature of the solid disc in Figure 3.3b. **f.** Stress strain experiments of recycled polymer discs under heat vs. water. The hard resilient polymer disc formed by pressing in water has lower tensile strength and elastic modulus compared to the disc formed by heat pressing of the polyimine powder. **g.** The stress-relaxation behavior of polyimine discs under water vs. heat. The presence of water enables more efficient relaxation than the highest temperature condition.

The use of water to reshape a thermosetting polymer is environmentally friendly, economical, and also highly desirable for applications where it would be impossible to use heat. As a demonstration, a polyimine film was reshaped using water at room temperature. A 0.31 mm thick sample of dry polymer film was submerged in water for 3 h (Figure 3.4a & 3.4b). The wet, newly pliable film was stretched over a round mold (Figure 3.4c), and allowed to dry in a plastic zip bag containing drying agent for 24 h to obtain a dry polymer film which retained its new shape (Figure 3.4d). The dried material exhibits robust mechanical properties. The film could support loads in excess of 190 g without significant flexure (Figure 3.4e). When the object was flattened completely under multi-kg loads, it immediately sprang back to its rounded shape upon removal of the load. These results demonstrate that the polyimine material can be reshaped by simply soaking with water, transforming into a new shape, and drying to set the new shape of the mechanically resilient covalent network polymer.

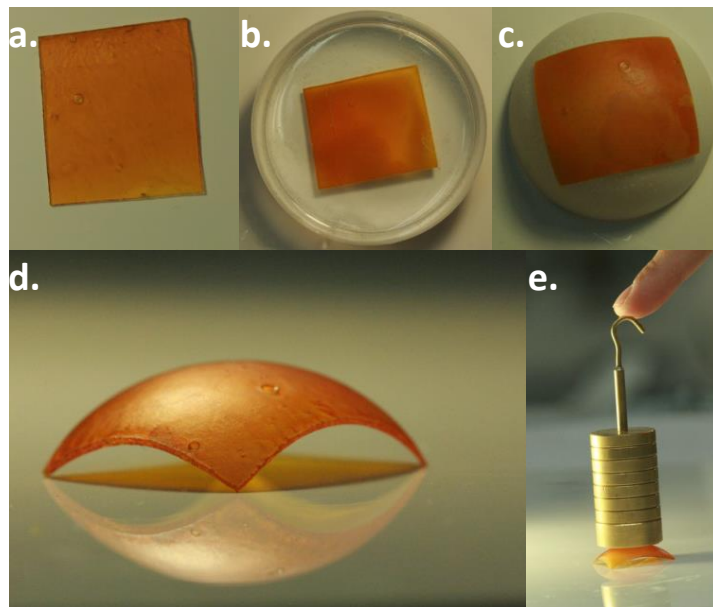


Figure 3.4 Water-induced malleability experiments. **a.** The solid polyimine film which is dry, hard, and glassy. **b.** The film sample after soaking in tap water for 3 h. **c.** The wet film sample is stretched over a round mold made from ping pong ball. **d.** The film sample from figure 3.4c following 24 h in a plastic zip bag with a drying agent. The dried film sample is equally hard and glassy as it was in Figure 3.4a, but retains its rounded shape. **e.** The polymer's ability to retain its new shape is demonstrated by applying a pressure in excess of 190 g without substantial deformation of the solid.

To corroborate the theory that stress relaxation and malleability in the bulk polymer occurs as a result of imine exchange under heat, we studied imine exchange kinetics at various temperatures. Subsequent to the mixing of two parent imine molecules, dibenzylideneethane-1,2-diamine (**aa**), and bis(4-bromobenzylidene)ethane-1,2-diamine (**bb**), the formation of a new imine species (**ab**) was monitored by nuclear magnetic resonance (NMR) spectroscopy at three different temperatures: 35 °C, 45 °C, and 60 °C (Figure 3.8). We observed that the reaction reaches equilibrium most quickly at 60 °C while the reaction at 35 °C takes the longest to equilibrate. Though the bond exchange conditions in the bulk polymer would be different from those of small molecules in solution, the model study demonstrates the feasibility of utilizing imine exchange reactions as a temperature-dependent approach to achieve stress relaxation and malleability of the polymer.

Since the polymer material remains insoluble in water even at high temperatures (96 °C), it is likely that the equilibrium condition involves hydrolysis of only a small proportion of imine linkages. We examined the extent of imine hydrolysis in the equilibrium state by measuring the ratios of imine linkages to aldehyde end groups in the dry and water-saturated polymer using magic angle spinning ^{13}C NMR spectroscopy. The imine to aldehyde ratio in the wet polymer (~40:1) was comparable to that of the dry polymer (~ 60:1) within the error of the measurement (Figure S7), indicating that relatively few imine linkages are hydrolyzed when the polymer is saturated in water. Since the degree of hydrolysis in the polymer is insignificant, hydrolysis alone is not likely the cause of the observed malleable behavior. It should also be noted that several other solvents (*i.e.* toluene, dioxane, and EtOH) tested are unable to reprocess or reshape the polyimine material. It is therefore plausible that water induces hydrolysis and facilitates the subsequent imine/amine exchange reactions, which are responsible for the polymer's capacity to transform from powder to coherent solid when immersed in water.

3.4 Conclusion

We have shown that an inexpensive, catalyst-free network polyimine material exhibits Arrhenius-like malleability in response to heat, leading to >100% recycling efficiency through multiple generations. This malleable covalently cross-linked network polymer can also be recycled and reshaped at ambient temperature using only water, potentially leading to energy-neutral green processing of the material. To the best of our knowledge, this is the first report of water driven malleability in a highly-recyclable covalent network polymer. Starting from either film or powder, simple molds can be used with either heat or water to form strong polymeric structures of any shape. This represents an ideal system for do-it-yourself prototyping of cross-linked polymeric solids, which will retain intrinsic value as the polymer can easily be recycled.

Similar recyclability and solid state processing should be attainable for many functional polyimines, such as conductive polyimines. Furthermore, the use of water for stress-relaxation in polyimines could provide an additional (moisture) trigger for elastomer actuator applications.

3.5 Experimental Details

3.5.1 Differential Scanning Calorimetry

The DSC measurement was performed using a Mettler Toledo DSC823^e. DSC scan was performed from 125 °C to 25 °C at a scan rate of 5 °C/min on a polyimine film sample. The inflection point in the curve is taken to be the glass transition temperature, and is observed near 56 °C.

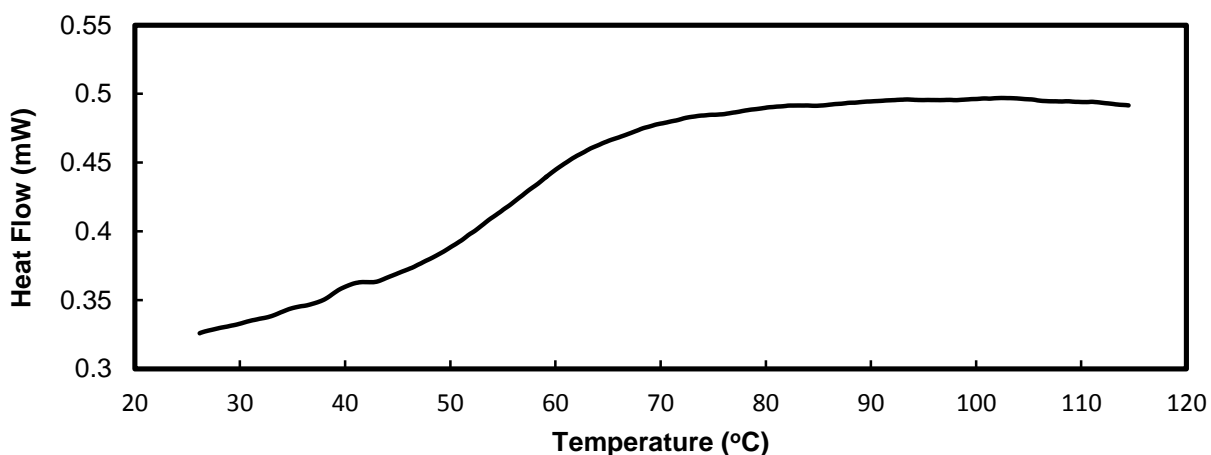
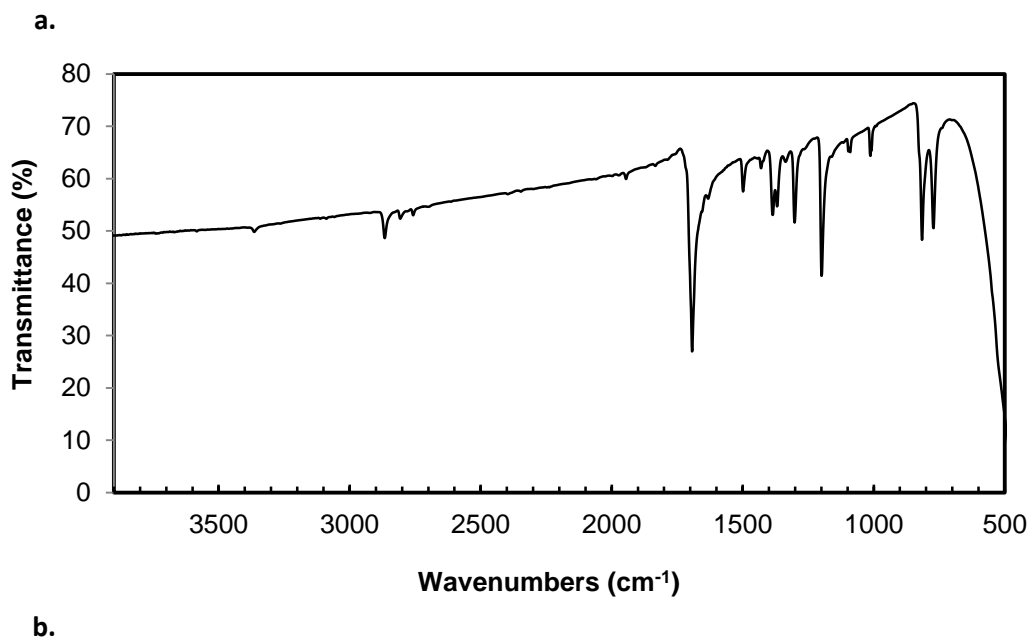


Figure 3.5 Differential Scanning Calorimetry (DSC) experiment to determine the T_g of the polyimine.

3.5.2 IR spectra of polyimine

The samples for FT-IR measurement were prepared as thin films by drop casting CH_2Cl_2 solutions of the analytes onto NaCl plates. The IR spectra were recorded on an Avatar 370. Four scans were averaged for each measurement and the data was analyzed using Omnisec

software. As seen in Figure 3.6a, the terephthalaldehyde linker has a distinctive C=O stretch absorption band at 1693 cm^{-1} . In the IR spectra of the polyimine (Figure 3.6b), the C=O stretch absorption band is barely detectable, while a new absorption band at 1643 cm^{-1} has become prominent. This band corresponds to the C=N stretch of the newly formed imine bond, indicating the consumption of aldehyde groups, and the formation of imine links.



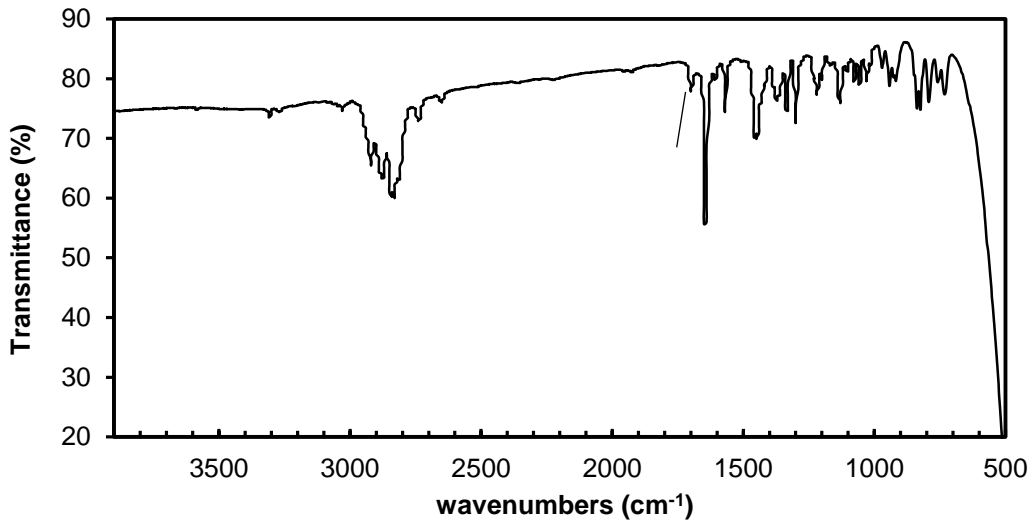


Figure 3.6 a. Infrared spectrum of terephthalaldehyde starting material which has a prominent C=O stretch at 1693 cm^{-1} . **b.** Infrared spectrum of polyimine in which there is a prominent C=N stretch at 1643 cm^{-1} , and the C=O stretch at 1695 cm^{-1} appears as a minor peak.

3.5.3 Mechanical properties of fresh polyimine films

The freshly prepared polymer film sample was characterized by a stress strain experiment (experimental details in 3.5.8). The curve in Figure 3.7 represents the typical stress strain performance for the polyimine: elastic modulus $\sim 1\text{ GPa}$, stress at break $\sim 40\text{ MPa}$, elongation at break between 4 and 7 %.

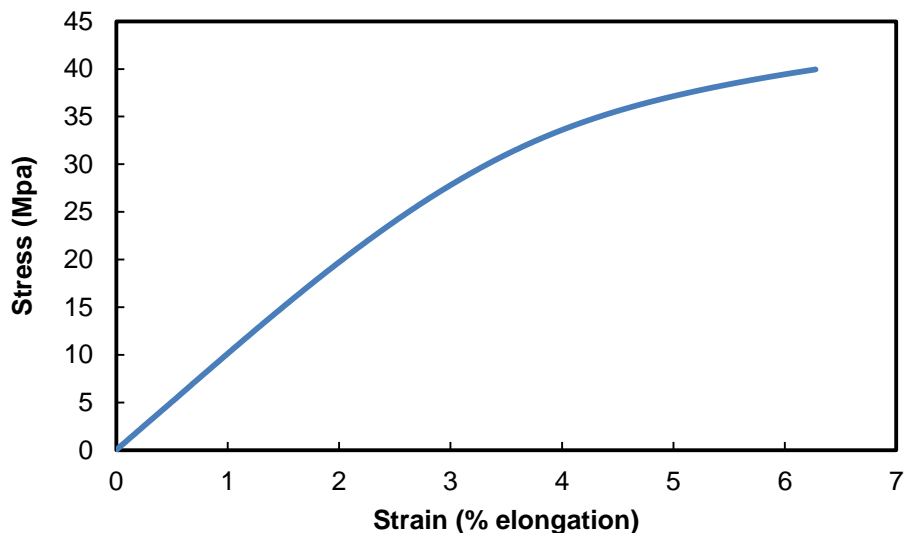
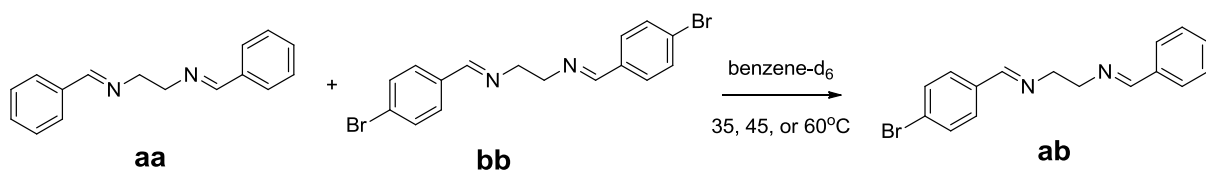


Figure 3.7 Stress v. strain mechanical test of fresh polyimine film sample.

3.5.4 Small molecule model study of a transamination reaction



In order to directly observe the behavior of the imine exchange reaction in a non-equilibrium system, compounds **aa** and **bb** were mixed in deuterated benzene, and the formation of **ab** was monitored by ^1H NMR spectroscopy over time at three different temperatures: 35 °C, 45 °C, and 60 °C. The sample was prepared by mixing 1:1 molar ratio of **aa** and **bb** in benzene- d_6 . The ^1H NMR signal for the methylene groups in **aa** and **bb** appear as singlets at 3.98 ppm and 3.87 ppm, respectively. The methylene signal of **ab** is a multiplet at 3.825 ppm. Figure 3.8a shows the time-dependent NMR spectrum of the sample recorded at 35 °C. We observed the gradual increase of the peak at 3.825 ppm, which corresponds to the methylene group of **ab**. In

Figure 3.8b is given a plot of the ratio of the integration of the methylene peaks of the new imine vs. parent imines over time at various temperatures.

Figure 3.8b clearly shows that the rate of the imine exchange reaction varies with temperature. The 60 °C sample reaches equilibrium most quickly, and the 35 °C sample takes the longest. This model study supports the notion that the temperature-dependent rate of the imine exchange reaction is responsible for the temperature-dependent malleability of the polyimine.

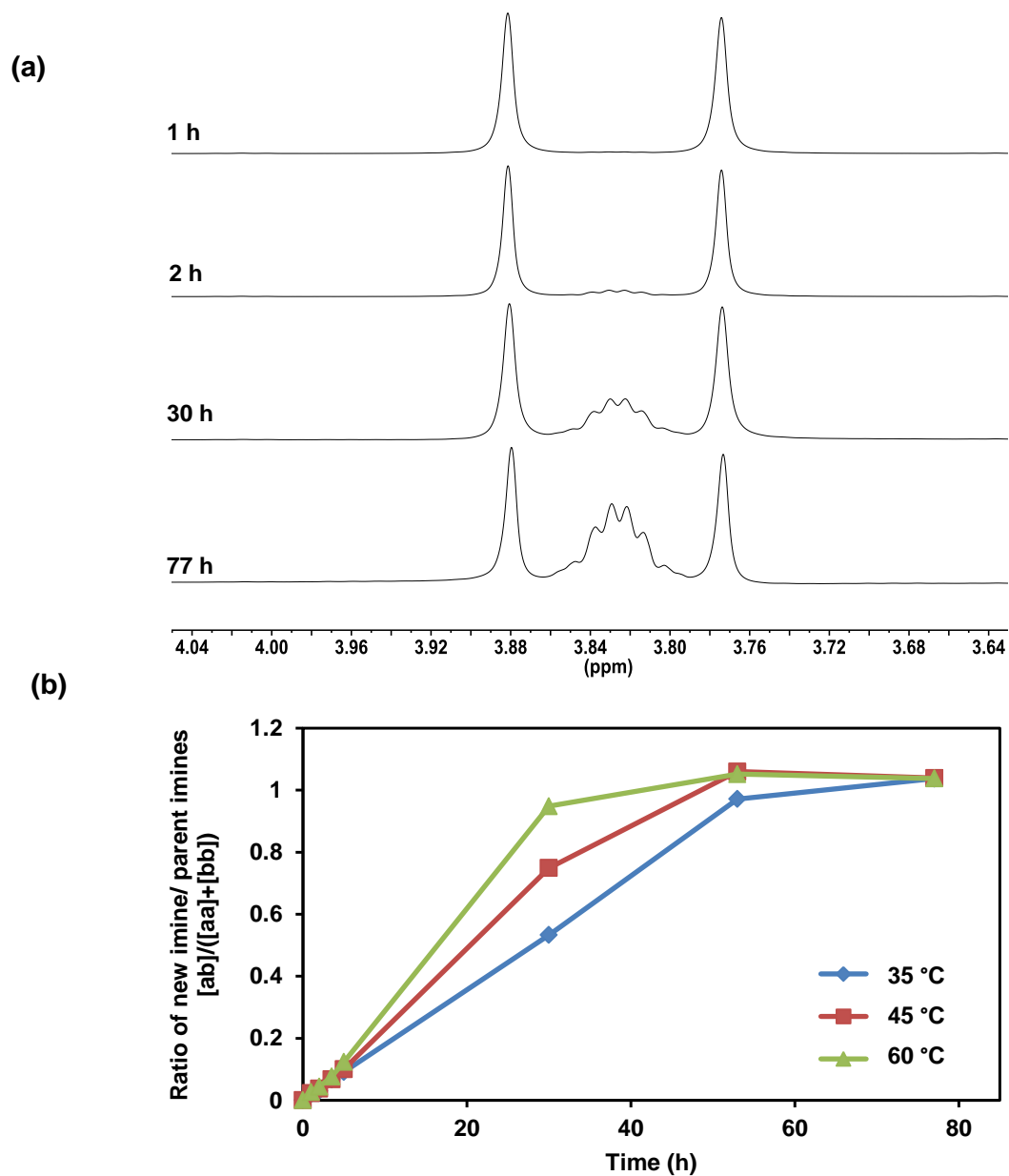


Figure 3.8 a. ^1H NMR spectra of 35 °C sample over time illustrates the growth of the ab methylene peak. **b.** Plot of ratio of concentrations: $\frac{[ab]}{[aa]+[bb]}$ as measured by the integration of the methylene peaks of each species.

Synthesis of model compounds:

Compound **aa**: Ethylene diamine (100 μ L, 1.497 mmol), and benzaldehyde (275 μ L, 2.69 mmol) were added to a Schlenk tube containing a magnetic stirbar, CH_2Cl_2 (15 mL) and 4 Å molecular sieves. The reaction was sealed and stirred at 60 °C in an oil bath for 18 h. The reaction mixture was then allowed to cool to room temperature. The solvent was evaporated, yielding the product with a small excess of unreacted amine groups. The product's ^1H NMR data is in good agreement with previously reported literature values³⁰: ^1H NMR, 500 MHz (CDCl_3) δ 3.98 ppm (s, 4H), δ 7.39 ppm (m, 6H), δ 7.69 ppm (m, 4H), δ 8.29 ppm (s, 2H).

Compound **bb**: The compound was prepared following the similar procedure described for compound **aa**. Using ethylene diamine (100 μ L, 1.497 mmol), 4-bromobenzaldehyde (0.4986 g, 2.69 mmol), and CH_2Cl_2 (15 mL), the product with a small excess of unreacted amine groups was obtained. The product's ^1H NMR data is in good agreement with previously reported literature values³¹: ^1H NMR, 500 MHz (CDCl_3) δ 3.95 ppm (s, 4H), δ 7.53 ppm (dd, 8H, $J_1=15$ Hz, $J_2=5$ Hz), δ 8.21 ppm (s, 2H).

Compound **ab**: Compound **aa** (0.1206 g, 0.51 mmol), and **bb** (0.2 g, 0.51 mmol) were added to a 3 mL vial. Deuterated benzene (1.5 mL) was then added, and the reactants were allowed to dissolve. The vial was then heated in an oil bath at 35 °C, 45 °C, or 60 °C. The reaction was monitored by ^1H NMR. Each sample eventually reached an equilibrium concentration of **ab** approximately equal to the combined concentrations of **aa** & **bb**. The formation of **ab** was confirmed by electrospray ionization mass spectroscopy by direct infusion on a Waters SYNAPT G2 instrument (calculated for $\text{C}_{16}\text{H}_{16}\text{N}_2\text{Br}^+$ [$\text{M} + \text{H}^+$]: 315.1; observed: 315.1). The ^1H NMR spectra of **ab** was not fully characterized as it was not isolated in this experiment.

3.5.5 Swelling/drying study

The polyimine is observed to absorb liquid water and swell to a saturation point. The time required to fully saturate the polymer in water is approximately equal to the time required to fully dry the sample in a plastic zip bag with drying agent (~24 h). Figure 3.9 shows that the material is stable in water and the swelling stays constant beyond the saturation point.

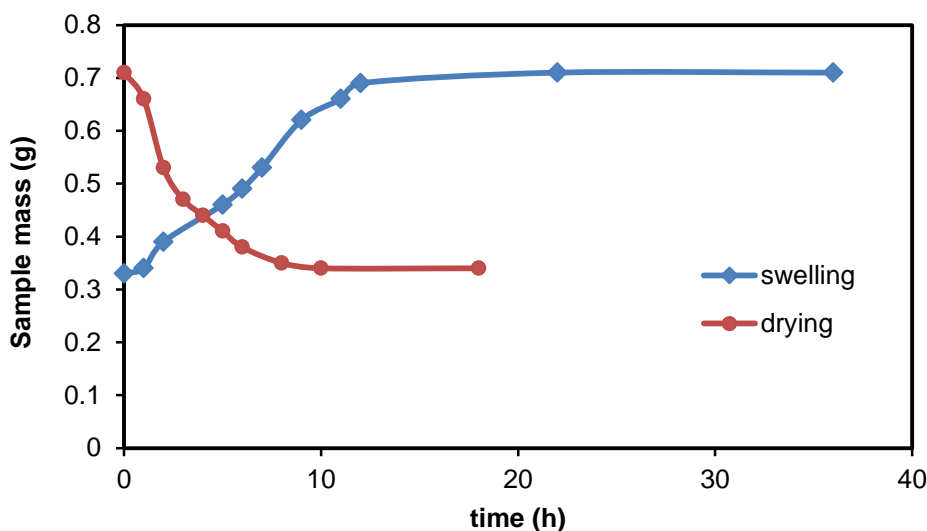


Figure 3.9 Measurement of polymer's mass change with time when immersed in water, and when removed to a dry environment.

3.5.6 Mechanical response to atmospheric humidity

A custom built humidity chamber using an ultrasonic humidifier with two in-line condensing chambers was used for this study. The humidity level was monitored by an AcuRite 613 Indoor Humidity Monitor, which tracked the 24 h high and low humidity readings, confirming that the humidity level was maintained at $\pm 5\%$ of the reported value. All of the experiments were performed at 21 ± 1 °C at an elevation of 1,655 m above sea level. For each humidity level, the polymer film samples were kept at the designated humidity level for 24 h and

each sample was submitted to a stress-strain test on the DMA machine immediately after removal (see 3.5.8 for stress-strain experimental details). The results (Figure 3.10) demonstrate an incremental softening of the material with increasing atmospheric humidity. Thus, like wood, the polyimine material becomes more pliable with increasing atmospheric humidity. Significantly, even at very high humidity levels, the polymer's mechanical properties are drastically different from those of the polymer saturated with water.

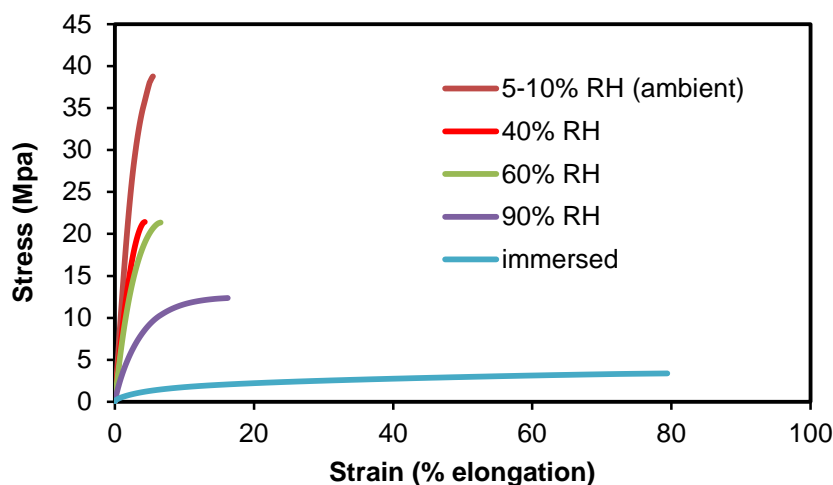


Figure 3.10 Characteristic stress-strain behavior of polyimines at various levels of atmospheric humidity. The stress strain curve of polymer following 12 h of immersion is included for comparison.

3.5.7 Solid state NMR of polyimine when wet and when dry

Solid-State, Cross-Polarization Magic Angle Spinning (CPMAS), ^{13}C NMR spectroscopy was performed using a Varian INOVA-400 (Agilent Technologies, Inc.) spectrometer operating at 100.63 MHz for ^{13}C observation. The probe incorporates a 5mm Magic Angle Spinning module and coil assembly designed and constructed by Revolution NMR, Inc. (Fort Collins, CO), capable of spinning up to 13KHz with Zirconia rotors (also from Revolution NMR, Inc.). Spectra were acquired using cross-polarization spin-lock and decoupling Rf fields of 80.5 KHz,

and TPPM (Time Proportional Phase Modulation) decoupling was applied during signal acquisition. Chemical shifts were referenced using the absolute, calibrated spectrometer configuration frequency and magnetic field offset, such that the methyl carbons of hexamethylbenzene appear at 17.3 ppm. Sample spinning frequencies from 10.5-11.5 KHz were employed with the sample oriented at the *magic angle* (54.736 degrees, relative to the magnetic field axis, calibrated using the ^{79}Br spinning sideband pattern of KBR).

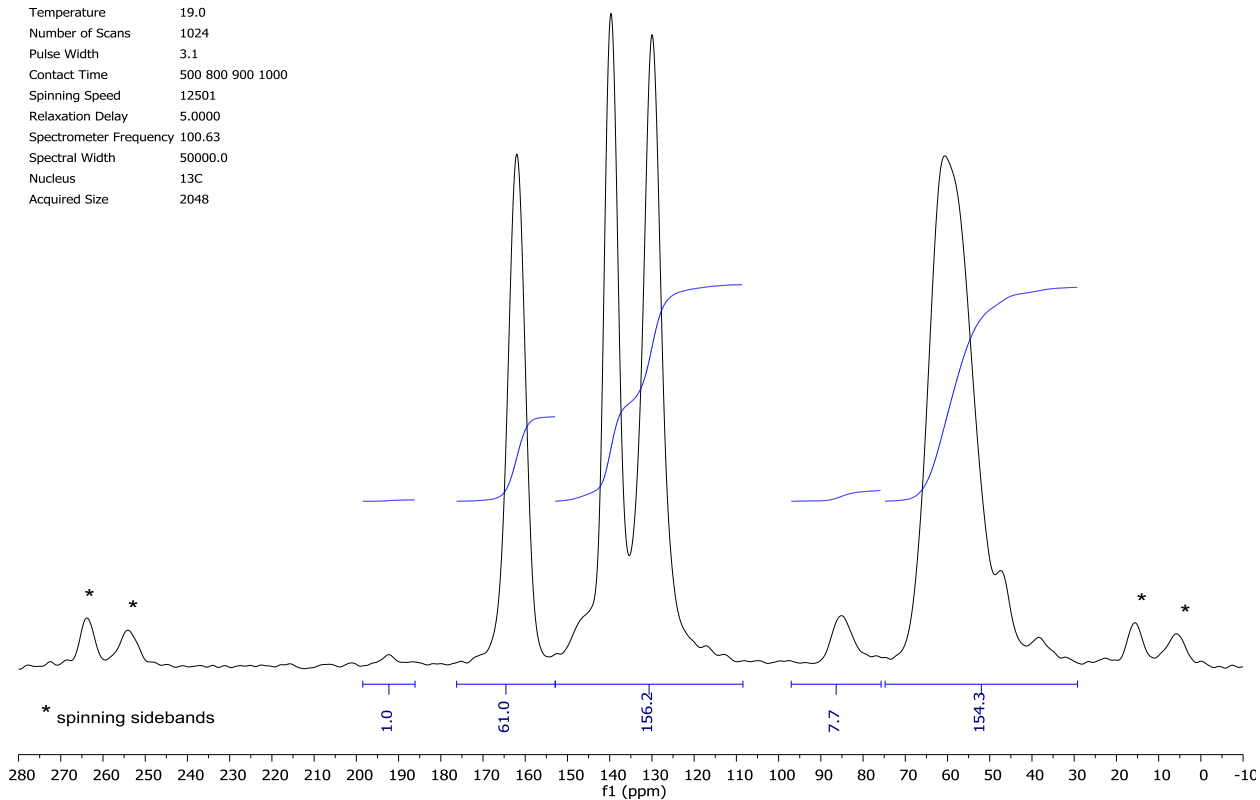
To affect the uniform cross-polarization of ^1H magnetization to all ^{13}C nuclei, spectra were acquired using multiple cross-polarization contact times between 500 and 1000 μsec and these were summed to yield the final spectra. These optimal contact times were determined using variable contact-time experiments and were chosen to obtain uniform excitation across all carbon atoms in the molecules of the dry and hydrated samples. Spectra were the result of between 4,096 and 5,120 scans, yielding adequate signal-to-noise ratios to observe the signal from the terminal aldehyde carbons at ~192 PPM vs. TMS.

Figure 3.10

Parameter	Value
Data File Name	Polyimine-Dry-CPMAS-VariableCT_500-1000us-SUM.fid
Title	PT, 70% Crosslinked polyimine, dry, ^{13}C CPMAS NMR CT(tHX)=500,800,900,1000us:4096 scans total
Pulse Sequence	tancpx

^{13}C NMR (101 MHz, solid) 192.3, 162.0, 139.7, 130.0, 85.1, 60.6.

Temperature	19.0
Number of Scans	1024
Pulse Width	3.1
Contact Time	500 800 900 1000
Spinning Speed	12501
Relaxation Delay	5.0000
Spectrometer Frequency	100.63
Spectral Width	50000.0
Nucleus	^{13}C
Acquired Size	2048

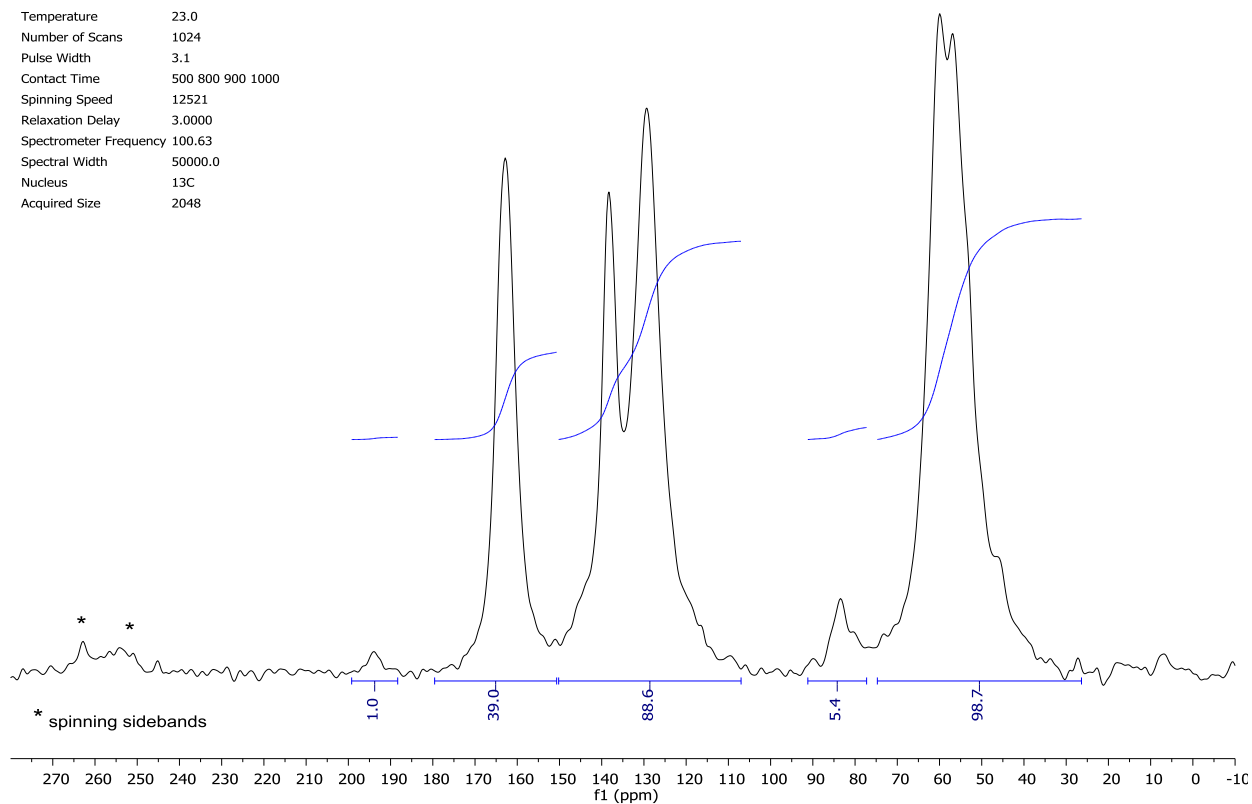


a. Magic angle spinning solid state ^{13}C NMR of dry polyimine powder

Parameter	Value
Data File Name	Polyimine-Wet_ReWet-CPMAS-VariableCT-5120scans.fid/
Title	PT, 70% Crosslinked polyimine, WET, 3x contact times tHX=500,800,900,1000: 5,120 scans total.
Pulse Sequence	tancpx

^{13}C NMR (101 MHz, solid) 193.9, 162.8, 138.3, 129.4, 83.4, 59.9, 56.9.

Temperature	23.0
Number of Scans	1024
Pulse Width	3.1
Contact Time	500 800 900 1000
Spinning Speed	12521
Relaxation Delay	3.0000
Spectrometer Frequency	100.63
Spectral Width	50000.0
Nucleus	^{13}C
Acquired Size	2048



b. Magic angle spinning solid state ^{13}C NMR spectrum of wet polyimine powder.

3.5.8 Mechanical testing

DMA Tension test:

A dynamic mechanical analysis (DMA) machine (Model Q800, TA Instruments, New Castle, DE, USA) was used to carry out tension tests at room temperature (23°C locally). All the samples were trimmed into a uniform size of 12 mm × 3 mm × 1.1 mm, and then stretched under a constant loading rate (2MPa/min) until broken.

DMA Stress Relaxation:

The time and temperature dependent relaxation modulus of the polyimine thermoset was also tested on the DMA machine (Model Q800, TA Instruments, New Castle, DE, USA). During the test, a polymer sample with the same dimension mentioned above was initially preloaded by 1×10^{-3} N force to maintain straightness. After reaching the testing temperature, it was allowed 30 min to reach thermal equilibrium. The specimen was stretched by 1% on the DMA machine and the deformation was maintained throughout the test. The decrease of stress was recorded and the stress relaxation modulus was calculated. Figure 3.1b depicts the results of relaxation tests at 21 different temperatures between 50 °C and 127.5 °C on a double logarithmic plot. Then selecting 80 °C as a reference temperature (T_r), each modulus curve in Figure 3.1a is shifted horizontally to overlap with the next. This produces the master relaxation curve shown in Figure 1c, which spans many decades of modulus (from ~676 MPa to ~0.59 MPa) and represents the actual relaxation behavior of the polymer within a long time scale (1670min, around ~27.9h) at 80 °C. The corresponding shift factors are also plotted against temperature in Figure 3.1c.

The master relaxation curve suggests that the kinetics of the BER induced stress relaxation follows the well-known temperature-time superposition (TTSP) principles. To quantitatively study the relaxation behavior, we used the following definition of relaxation modulus^{2,17,32}:

$$\tau = \frac{1}{k} \exp\left(\frac{E_a}{RT}\right) \quad (3.1)$$

where k is a kinetic coefficient ($k > 0$) R is the gas constant with $R = 8.31446 \text{ J / Kmol}$, and E_a is the activation energy.

The shift factor, namely the ratio between the temperature dependent relaxation time and the relaxation time at a reference temperature T_r , is therefore expressed as:

$$\alpha = \exp\left[\frac{E_a}{R} \left(\frac{1}{T} - \frac{1}{T_r}\right)\right]. \quad (3.2)$$

The predicted shift factors of the relaxation curves are also plotted in Figure 3.1c to compare with the experimental data. An Arrhenius-type dependence on temperature is revealed, which is consistent with what was reported by Leibler et al., where the kinetics was characterized by viscosity. By further examination of Equation 3.2 we found that in the semi-log scale, the energy barrier could be determined by the slope of the shift factor curve. As shown in Figure 3.1c, by measuring the curve slope (18886/K), the energy barrier E_a is calculated to be 157.02 kJ/mol.

MTS for compressing the powder:

An aluminum punch mold was machined on a lathe. Since the rate of imine exchange is thermally sensitive, it is important to precisely control the sample temperature during the tests. In this paper, we adopt the method that was previously developed by the authors. The specially designed aluminum punch mold is shown in Figure 3.3a, where three hollow slots were machined in the platen to improve the thermal convective properties and temperature distribution during heating. After placing polymer powder into the mold (Figure 3.4b), it was then transferred into a customized thermal chamber for heating, while the applied pressure is controlled by a universal material testing machine (MTS, Model Insight 10, Eden Prairie, MN, USA). The temperature in the thermal chamber manufactured by Thermcraft (Model LBO, Winston Salem, NC, USA) is controlled with a Eurotherm controller (Model Euro 2404, N. Chesterfield, VA, USA) where a built-in electrical heater with a fan and an externally attached tank of liquid nitrogen provide the heat and cooling.

3.6 References

- [1] J. Aklonis and W. MacKnight, Introduction to polymer viscoelasticity 2nd ed., New York: Wiley, 1983.
- [2] D. Montarnal, M. Capelot, F. Tournilhac and L. Leibler, "Silica-Like Malleable Materials from Permanent Organic Networks," *Science*, vol. 334, no. November, pp. 965-968, 2011.
- [3] Y. X. Lu, F. Tournilhac, L. Leibler and Z. B. Guan, "Making insoluble polymer networks malleable via olefin metathesis," *Journal of the American Chemical Society*, vol. 134, pp. 8424-8427, 2012.
- [4] P. Zheng and T. McCarthy, "A Surprise from 1954: Siloxane Equilibration Is a Simple, Robust, and Obvious Polymer Self-Healing Mechanism," *J. Am. Chem. Soc.*, vol. 134, pp. 2024-2027, 2012.
- [5] Z. Pei, Y. Yang, Q. Chen, E. M. Terentjev, Y. Wei and Y. Ji, "Mouldable liquid-crystalline elastomer actuators with exchangeable covalent bonds," *Nature Materials*, vol. 13, p. 36, 2014.
- [6] H. H. Jin, K. R. Hart, A. M. Coppola, R. C. Gergely, J. S. Moore, N. R. Sottos and S. R. White, "Self-Healing Epoxies and Their Composites," *Self-Healing Polymers: From Principles to Applications*, pp. 361-380, 2013.
- [7] A. Inglis, L. Nebhani, O. Altintas, F. Schmidt and C. Barner-Kowollik, "Rapid Bonding/Debonding on Demand: Reversibly Cross-Linked Functional Polymers via Diels–Alder Chemistry," *Macromolecules*, vol. 43, no. 13, pp. 5515-5520, 2010.
- [8] C. Kloxin, T. Scott, B. Adzima and C. Bowman, "Covalent Adaptable Networks (CANs): A Unique Paradigm in Cross-Linked Polymers," *Macromolecules*, vol. 43, pp. 2643-2653, 2010.
- [9] K. A. Williams, D. R. Dreyer and C. W. Bielawski, "The underlying chemistry of self-healing materials," *MRS Bulletin*, vol. 33, pp. 759-765, 2008.
- [10] K. A. Williams, A. J. Boydston and C. W. Bielawski, "Towards electrically conductive, self-healing materials," *J. R. Soc. Interface*, vol. 4, p. 359, 2007.
- [11] D. Y. Wu, S. Meure and D. Solomon, "Self-healing polymeric materials: A review of Recent developments," *Progress in Polymer Science*, vol. 33, no. 5, pp. 479-522, 2008.
- [12] A. Rekondo, R. Martin, A. Ruiz de Luzuriaga, G. Cabanero, H. J. Grande and I. Odriozola, "Catalyst-free room-temperature self-healing elastomers based on aromatic disulfide

- metathesis," *Materials Horizons*, p. DOI: 10.1039/C3MH00061C, 2014.
- [13] R. J. Wojtecki, M. A. Meador and S. J. Rowan, "Using the dynamic bond to access macroscopically responsive structurally dynamic polymers," *Nature Materials*, vol. 10, no. 1, pp. 14-27, 2011.
- [14] K. E. Feldman, M. J. Kade, T. F. de Greef, E. W. Meijer, E. J. Kramer and C. J. Hawker, "Polymers with multiple hydrogen-bonded end groups and their blends," *Macromolecules*, vol. 41, pp. 4694-4700, 2008.
- [15] A. Phadke, C. Zhang, B. Arman, C. C. Hsu, R. A. Mashelkar, A. K. Lele, M. J. Tauber, G. Arya and S. Varghese, "Rapid self-healing hydrogels," *Proceedings of the National Academy of Science*, vol. 109, p. 4383, 2012.
- [16] P. Cordier, F. Tournilhac, C. Soulie-Ziakovic and L. Leibler, "Self-healing and thermoreversible rubber from supramolecular assembly," *Nature*, vol. 451, no. 7181, pp. 977-980, 2008.
- [17] M. Capelot, D. Montarnal, F. Tournilhac and L. Leibler, "Metal-catalyzed transesterification for healing and assembling of thermosets," *Journal of the American Chemical Society*, vol. 134, no. 18, pp. 7664-7667, 2012.
- [18] M. E. Belowich and J. F. Stoddart, "Dynamic imine chemistry," *Chemical Society Reviews*, vol. 41, no. 6, pp. 2003-2024, 2012.
- [19] G. Deng, C. Tang, F. Li, H. Jiang and Y. Chen, "Covalent Cross-Linked Polymer Gels with Reversible Sol-Gel Transition and Self-Healing Properties," *Macromolecules*, vol. 43, pp. 1191-1194, 2010.
- [20] C. I. M. G. I. C. I. D. a. A. F. Simionescu, "Chemical synthesis of some Schiff base-type polymers containing pyrrole units.," *Polym. Bull.*, vol. 32, no. 3, pp. 257-264, 1994.
- [21] S. Tripathi, I. Vasudev and A. Ray, "Electrical Conductivity in Polyazomethines: A Novel Mechanism Derived from All Valence MO Calculation and IR Study of Polymer-Dopant Interaction," *Journal of Macromolecular Science, Part B: Physics*, vol. 50, no. 6, pp. 1196-1214, 2011.
- [22] H.-J. Niu, Y.-D. Huang, X.-D. Bai and X. Li, "Novel poly-Schiff bases containing 4,4'-diamino-triphenylamine as hole transport material for organic electronic device," *Mater. Lett.*, vol. 58, no. 24, pp. 2979-2983, 2004.
- [23] P. Gebert, C. Batich, D. Tanner and S. Herr, "Polyaniline via schiff base chemistry," *Synth.*

- Metals*, vol. 29, no. 1, pp. 371-376, 1989.
- [24] W. Skene and J.-M. Lehn, "Dynamers: Polyacylhydrazone reversible covalent polymers, component exchange, and constitutional diversity," *Proc. Natl. Acad. Sci. U.S.A.*, vol. 101, pp. 8270-8275, 2004.
- [25] J. Lehn, "Dynamers: dynamic molecular and supraolecular polymers," *Prog. Polym. Sci.*, vol. 30, no. 8-9, pp. 814-831, 2005.
- [26] Y. Xin and J. Yuan, "Schiff's base as a stimuli-responsive linker in polymer chemistry," *Polym. Chem.*, vol. 3, pp. 3045-3055, 2012.
- [27] H. Saito, A. Hoffman and H. Ogawa, "Delivery of Doxorubicin from Biodegradable PEG Hydrogels Having Schiff Base Linkages," *J. of Bioact. and Compat. Polym.*, vol. 22, no. 6, pp. 589-601, 2007.
- [28] C. Godoy-Alcantar, A. K. Yatsimirsky and J.-M. Lehn, "Structure-stability correlations for imine formation in aqueous solution," *Journal of Physical Organic Chemistry*, vol. 18, pp. 979-985, 2005.
- [29] T. S. M. S. C. A. S. M. W. & C. A. I. Hasell, "Reversible water uptake by a stable imine-based porous organic cage," *Chem. Commun.*, vol. 48, no. 39, pp. 4689-4691, 2012.
- [30] N. Kise, H. Oike, E. Okaxaki, M. Yoshimoto and T. Shono, "Synthesis of nitrogen-containing macrocycles with reductive intramolecular coupling of aromatic diimines," *Journal of Organic Chemistry*, vol. 60, pp. 3980-3992, 1995.
- [31] B. Lee, K. H. Lee, B. W. Lim, J. Cho, W. Nam and N. H. Hur, "Direct Synthesis of Imines via Solid State Reactions of Carbamates with Aldehydes," *Advanced Synthesis and Catalysis*, vol. 355, pp. 389-394, 2013.
- [32] M. Capelot, M. M. Unterlass, F. Tournilhac and L. Leibler, *ACS Macro Lett.*, vol. 1, p. 789, 2012.
- [33] Y. Yang, Z. Pei, Q. Chen, E. M. Terentjev, Y. Wei and Y. Ji, "Mouldable liquid-crystalline elastomer actuators with exchangeable covalent bonds," *Nature Materials*, vol. 13, pp. 26-31, 2014.

CHAPTER 4

Imine-linked malleable thermosets: Influence of Formulation and Moisture on the Bond Exchange Reaction

4.1 Abstract

Polyimine networks have been shown to be a promising class of catalyst-free vitrimers with excellent mechanical properties. It was previously shown that polyimine networks can be stable against hydrolysis, yet liquid water and atmospheric moisture can influence the mechanical properties and malleable properties of the networks. In the present chapter, the effect of various monomer structures-both hydrophilic and hydrophobic- on the mechanical, thermal, and moisture-induced properties of the polymers is investigated. Significantly, simple formulation of inexpensive commercially available diamine linkers enables systematic tuning of the resulting polymers' thermal and mechanical properties. Even highly hydrophilic polyimines, which exhibit greater than 60% moisture swelling by weight, exhibit no detectable hydrolysis, and employment of all-hydrophobic monomers results in polyimines with no detectable response to moisture. The molding temperature, which is related to the activation energy (E_a) of the bond exchange reactions (BER), can be influenced by T_g as well as tautomerization reactions.

4.2 Introduction

Polymers with covalently cross-linked networks are traditionally described as thermosets,¹⁻² obtaining this name from the fact that they cannot flow upon heating and thus

cannot be reshaped and recycled.¹ Very recently, this picture has been changed by incorporating dynamic covalent bonds (DCBs) into polymer networks.³⁻⁶ Such polymers, sometimes referred to as “covalently adaptable networks” by Bowman and his collaborators,³ are still covalently cross-linked, but the dynamic nature of these bonds allows the constant rearrangement of the polymer network through bond exchange reactions (BER) (Figure 4.1), which results in macroscopic stress relaxation and ultimately material flow.^{3,7-10} At equilibrium, the rate of bond dissociation equals that of association and thus the total number of associated bonds is maintained. Because of the stress relaxation enabled by the network rearrangement, this class of polymers exhibits behaviors similar to viscoelasticity, with relaxation time depending on the bond dissociation rate as well as the bond density.⁸

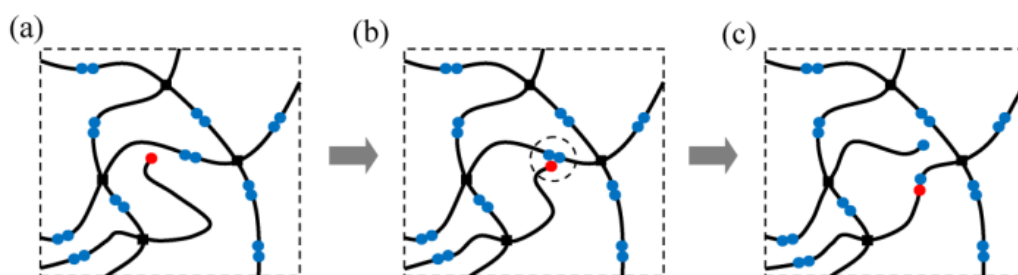


Figure 4.1 Schematic representation of the bond exchange reaction: **a.** before the exchange; **b.** the intermediate state; **c.** after the exchange. The circular symbol represents the exchangeable bonds on the polymer backbone. *Reproduced from [6].*

Network polymers containing DCBs represent an exciting breakthrough in novel polymer development as they open the door to new material processing paradigms for thermosets including thermoforming,⁸ welding,⁹ self-healing,⁴⁻⁵ and recycling.¹¹ Lehn’s early work on polyhydrozones showed creative use of reversible covalent bonds to switch functionalities of a polymer system,¹²⁻¹³ but cross-linked network polymers were not investigated, and high molecular weight is difficult to achieve in conventional linear $aa + bb$ condensation polymers.

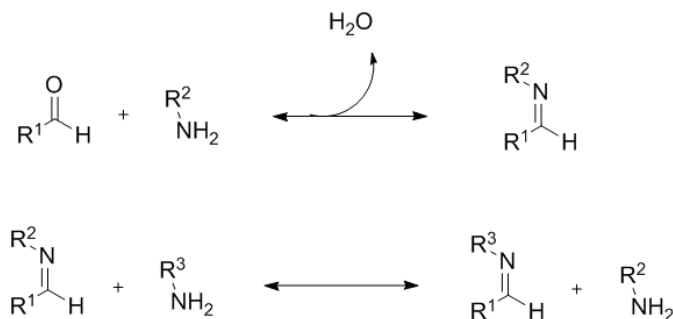


Figure 4.2 Imine formation, and transamination reactions.

Imine-linked polymers represent an attractive potential system for the development of dynamic covalent networks. An imine (also known as a Schiff base) is a carbon-nitrogen double bond typically formed by a condensation reaction between a primary amine and either an aldehyde or ketone, as illustrated in Figure 4.2. Imine condensation and subsequent imine exchange is one of the most frequently employed reactions in dynamic covalent chemistry.¹⁴ Since imine condensation simply requires an amine and an aldehyde or ketone, there is a wide variety of suitable monomers commercially available. Also, although imine condensation and imine exchange have been shown to be catalyzed by both Brønsted and Lewis acids, the reactions can take place at reasonable rates at elevated temperatures even in the absence of a catalyst.¹⁵ Thus polyimine represents a candidate reversible bond with a great potential for developing simple, easily accessible, and inexpensive malleable polymer networks.

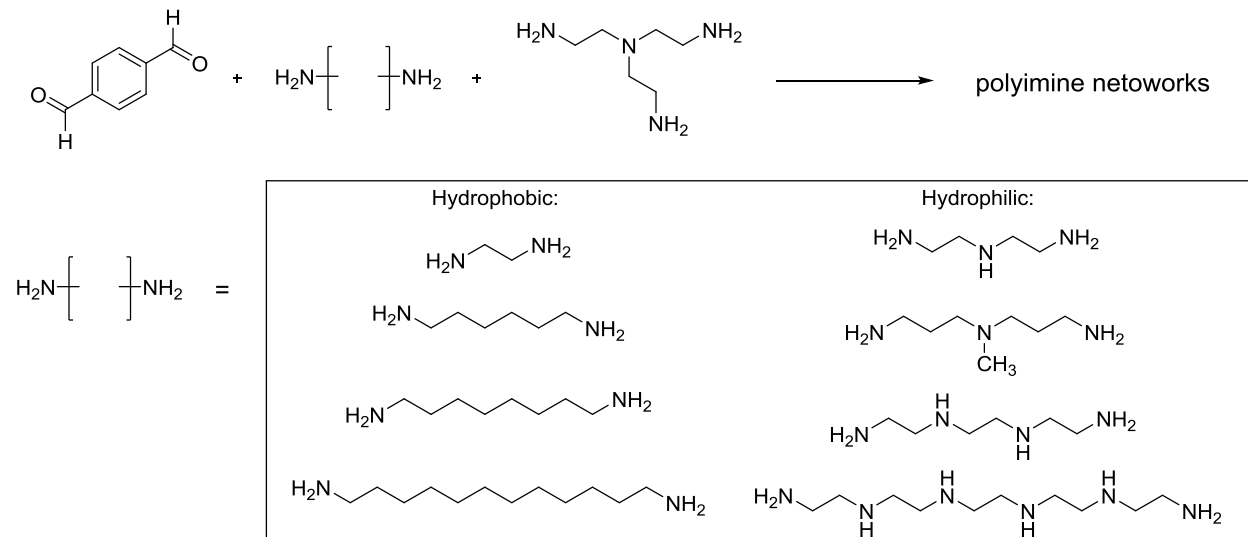
In our preliminary work, we have shown that the imine-linkage can be used to prepare covalent network polymers which do not require catalyst, exhibit thermoset-like behavior at room temperature, and are uniquely water-processable. We showed that water truly catalyzes the bond exchange reaction in the polyimine since in the malleable, wet state, there was no measurable hydrolysis of the polymer network. Polyimines represent a very attractive class of malleable polymers due to their thermoset-like behavior, catalyst-free activity, and moisture-responsive behavior. In the present study we vary the aldehyde- and amine-containing

monomers used to reveal a diversity of mechanical, thermal, and functional properties that can be achieved in malleable polyimine networks.

4.3 Formulating with commercially available diamines

In order to form polyimine networks, diamine and dialdehyde monomers were combined with trialdehyde or triamine crosslinkers. Because of the relative abundance of inexpensive commercially available diamines, we chose to first investigate the impact of changing the functionality of the diamine monomer. A series of diamines were formulated into an otherwise unchanged formulation of terephthalaldehyde and tris(2-aminoethyl)amine (TREN), as shown in Scheme 4.1. The diamine monomers employed essentially consisted of amine-terminated alkyl chains of varying length (the hydrophobic diamines) and amine-terminated ethylene-amine or propylene-amine oligomers of varying length (the hydrophilic diamines). The hydrophobic diamines used were ethylenediamine (ED), 1,6-diaminohexane (C_6), 1,8-diaminooctane (C_8), and 1,12-diaminododecane (C_{12}). The hydrophilic diamines used were diethylene triamine (DETA), 3,3'-Diamino-*N*-methyldipropylamine (N-methyl), triethylene tetramine (TETA), and pentaethylene hexamine (PEHA). In order to form polyimine networks, each of the above diamines was combined with terephthalaldehyde and TREN in a stoichiometric ratio of 0.45:1:0.367 respectively. The resulting polymers can be described as 55% crosslinked since the crosslinking molecule, TREN, constitutes approximately 55% of primary amines in the network. However, the DETA-containing polymers reported were prepared using a 0.3:1:0.467 (DETA:terephthalaldehyde:TREN) ratio for the sake of easy comparison with the properties previously reported.¹⁰

Scheme 4.1 Preparation of polyimine networks by varying the diamine monomer.



Tensile testing of the resulting polymer films revealed a range of mechanical properties of both the hydrophilic and hydrophobic polymers. The ethylene diamine formulation had the highest tensile strength at 65 ± 2 MPa, and a modulus of approximately 1 GPa, similar to the hydrophilic DETA formulation previously reported.¹⁰ The hydrophilic N-methyl formulation had by far the most elastomeric behavior ($162 \pm 22\%$ elongation at break). The hydrophobic C₁₂ formulation also exhibits greater than 100% elongation. A typical tensile trace for each formulation is shown in Figure 4.3.

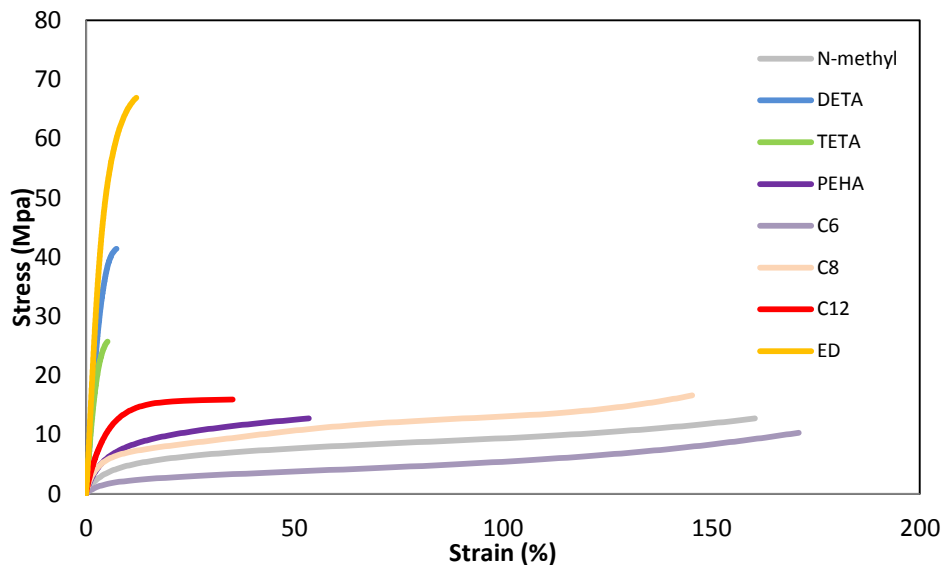


Figure 4.3 Tensile testing of polyimines with varying diamine monomer.

The thermal properties of the polyimines were characterized by differential scanning calorimetry (DSC), thermal gravimetric analysis (TGA), and dynamic mechanical analysis (DMA) stress-relaxation experiments. Catalyst-containing epoxy-acid vitrimers have previously been shown to exhibit a linear relationship between T_g of the bulk polymer and E_a of the BER.¹⁶ In malleable thermosets, the E_a of the BER can be inferred from an Arrhenius plot of the shift factors used to combine the stress-relaxation data collected at different temperatures into a master curve. The DMA stress relaxation data across a range of temperatures was plotted into a master curve for each of the formulations described above. The shift factors were plotted against temperature in order to demonstrate the Arrhenius like behavior and determine the energy barrier of the bond exchange reaction (experimental section, Figure 4.12). In Figure 4.4 the E_a and T_g data for the hydrophilic and hydrophobic series are plotted, since we have previously reported a linear relationship between the E_a and T_g in a series of catalyst-containing malleable epoxy-acid polymers.¹⁶ In the present case however, when the entire data set is examined, there is no apparent correlation between the T_g and E_a , but when the hydrophobic polymers and hydrophilic polymers are examined separately, they each show a general trend of increasing E_a with

increasing T_g (positive slope). Though the data set is very limited, the hydrophilic polymers seem to have higher activation energies for a given glass transition temperature. This could be due to H-bonding interactions, which have been shown to increase the energy barrier for BER in malleable thermosets.¹⁷ Most of the hydrophilic polymers contain H-bond donating and accepting moieties, while the hydrophobic polymers are not expected to have much H-bonding character since only H-bond acceptors are present within the polymer matrix.

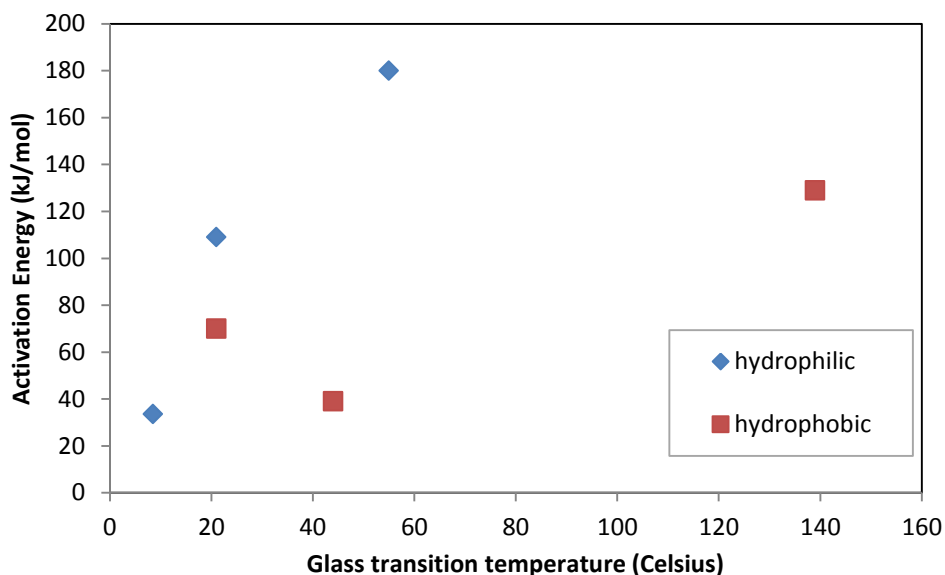


Figure 4.4 Plot of E_a vs. T_g data for some of the polyimines with varying diamine linkers.

Hydrophobic and hydrophobic monomers were selected for the purpose of evaluating the effect of moisture on the behavior of the polymers. We know from our previous work with the DETA formulation that water can have a profound effect on the behavior of a hydrophilic polyimine, even without hydrolyzing the imine links. The DETA formulation have been observed to significantly soften and even gain room-temperature self-healing properties when exposed to water, essentially behaving like a highly plasticized thermoplastic material. We were primarily interested in finding out if the impact of water on the mechanical properties of the polymers could be minimized by inclusion of hydrophobic moieties within the matrix. We also

sought to understand to what extent highly hydrophilic polymers are more susceptible to hydrolysis.

In order to characterize the hydrophilicity of each formulation soaking/swelling and contact angle measurements were made. Each sample was immersed in DI water for 22 h and the weight increase of the fully swelled sample was recorded. The swelling data provides the most relevant insight into the effects of moisture on each formulation, as the weight increase provides a reasonably accurate estimation of the concentration of water molecules within the polymer matrix. The ethylene diamine formulation was observed to have the least swelling of less than 8%, and none of the hydrophobic formulations gained more than 10.5%, and none of the hydrophilic formulations gained less than 28%, and the PEHA formulation gained nearly 60% its original weight in water. The contact angle measurement was performed using a high speed camera, with measurements taken 500 milliseconds after the DI water contacted the surface of the film. Interestingly, no correlation could be found between the swelling and contact angle data (see experimental section). This could be due to an oxidization of the surface of the polymers as they were all formed in open atmosphere, leading to similar surface behavior for most of the films.

Next, the mechanical properties of the films were tested after 24 h immersion in water. The results of the wet tensile testing are shown in Figure 4.5. All of the formulations exhibited a dramatic loss of elastic modulus and tensile strength. The wet ethylene diamine formulation exhibited the least change by far, by retaining 18% of its dry modulus and 54% of its dry tensile strength. While crystallinity was lost by all of the formulations, they all made critical gains in elongation ranging from 150% (ED) to approximately 800% for the C₆ and TETA formulations. Thus considerable toughness was maintained in the wet state. The notable exception was the N-

methyl formulation which essentially lost all mechanical strength, and only retained 45% of its original elongation, and 2% of its initial tensile strength. The N-methyl formulation was shown to be the most elastomeric (Figure 4.3). This is presumably because the N-methyl group prevents efficient packing of the polymer chains, reducing the crystallinity of the polymer and lowering the T_g . It could be that, while water molecules seem to have a plasticizing effect on the more crystalline formulations, the amorphous, hydrophilic nature of the N-methyl formulation causes the polymer to become weaker and more brittle when saturated with water, just as an inflated balloon is easier to break.

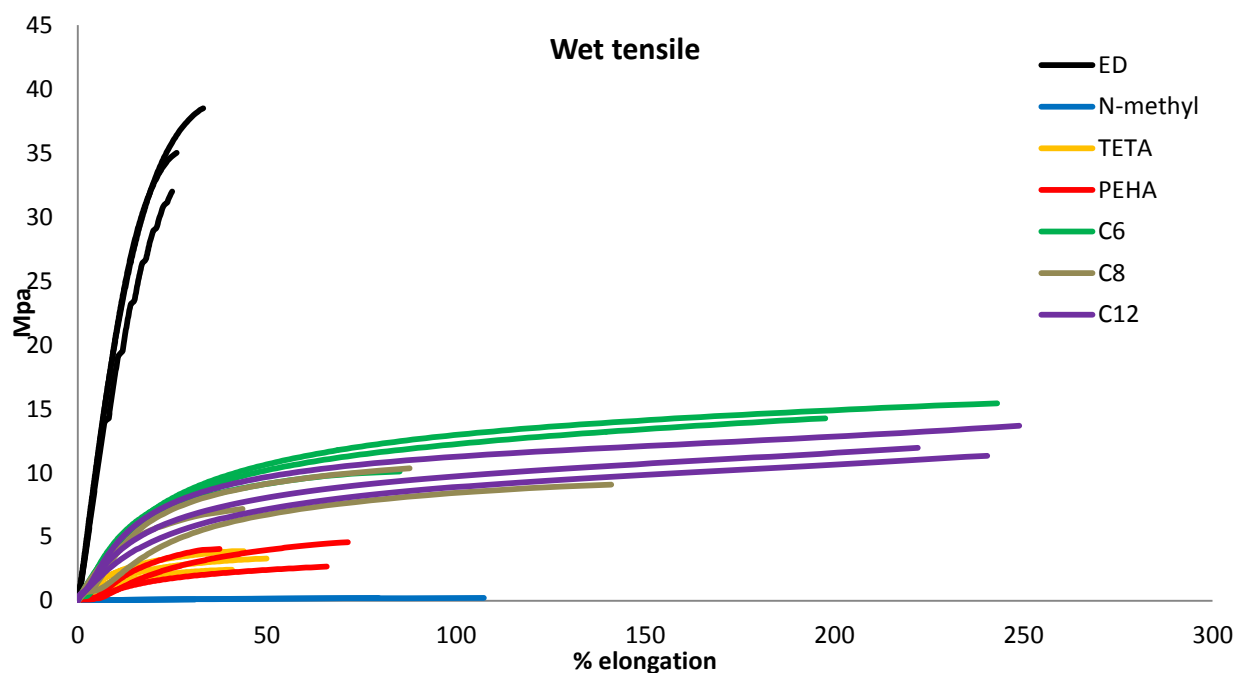


Figure 4.5 Tensile testing of polyimine formulations with varying diamine monomers after 24 h immersion in water.

In order to gauge the impact of hydrophilicity on the hydrolytic stability of the polymers, the solid-state ^{13}C -NMR spectra of the hydrophilic PEHA formulation and the hydrophobic C_{12} formulation were measured in the wet and dry state, in order to observe any change in the ratio of imine to aldehyde peaks, which would correspond to hydrolysis of imine bonds in the polymer matrix. As can be seen in the spectra (experimental section), there is no observable decrease in

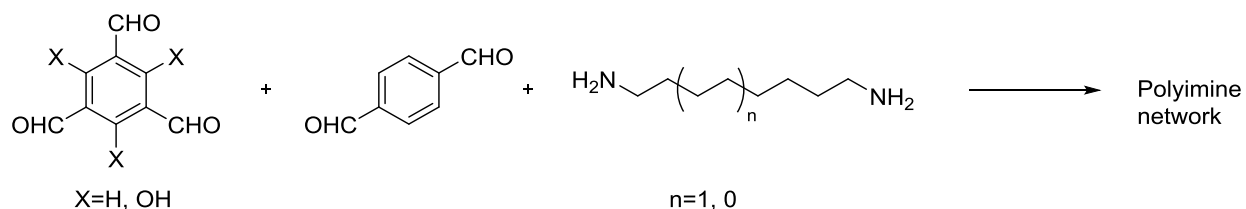
the intensity of the imine peak when either of the polymers are completely immersed and soaked in water. This means that even the most hydrophilic polyimine formulation, which readily absorbs nearly 70% of its weight in water, does not exhibit any measureable hydrolysis in the swollen state.

Overall the impact of the diamine monomer on the moisture-resistance of the polymer matrix is limited when it is combined with a hydrophilic crosslinker such as TREN. This is why even the “hydrophobic” formulations which exhibited less than 10% swelling were significantly plasticized by water and essentially lost their rigidity when exposed to moisture. In order to generate more truly hydrophobic polyimines, a different (trialdehyde rather than triamine) crosslinking monomer was used.

4.4 Formulating with trialdehyde monomers

Two different trialdehyde monomers were prepared in order to make polyimine networks. 1,3,5-benzenetricarboxaldehyde (“benzene trialdehyde”) was prepared in 2 steps from mesitylene, and 1,3,5-benzenetricarboxaldehyde, 2,4,6-trihydroxy- (“trialdehyde-triol”) was prepared in a single step from phloroglucinol. 1,3,5-benzenetricarboxaldehyde was combined with terephthalaldehyde and 1,8-diaminooctane in a stoichiometric ratio of 0.467:0.3:1 respectively. In this way 70% of the aldehyde moieties in the polymer matrix are attributed to the trialdehyde crosslinker and the polymer can thus be considered 70% crosslinked.

Scheme 4.2 Preparation of polyimine networks using trialdehyde monomers.



The mechanical properties of the polymers were characterized by tensile testing, and a data from a single tensile sample of each is shown in Figure 4.6. Though the two materials have similar modulus of elasticity, the benzene trialdehyde formulation exhibits greater elongation and tensile strength than the trialdehyde-triol formulation.

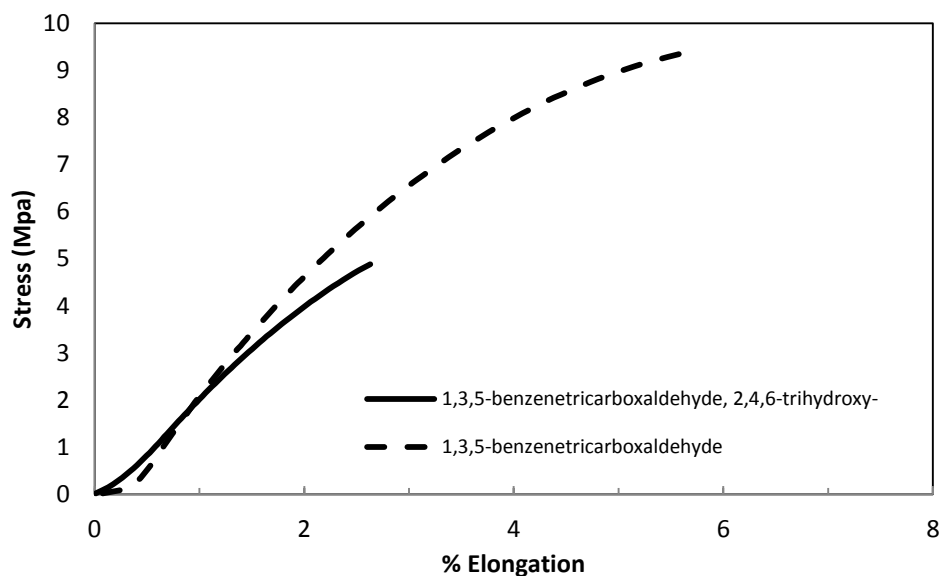


Figure 4.6 Tensile testing of polyimine formulations using trialdhehyde monomers and 1,8-diaminooctane.

In contrast to their similar mechanical behavior, the DMA stress relaxation showed a marked difference between the two trialdhehyde formulations. Figure 4.7 shows that the benzene trialdhehyde formulation relaxes stress more efficiently at 50 °C than the trialdhehyde-triol formulation can at 100 °C. This could be due to H-bonding between the imines and the hydroxyl groups and/or tautomerization to the quinone form (Figure 4.8), which is well-known in the literature.¹⁸ Other workers have also proposed the tautomerization of similar imines in aliphatic systems, and describe vinylogous urethanes as the only structural contribution, making no mention of the imine form, which is likely involved in the BER reaction.¹⁹ The sluggishness of the BER in the case of the trialdhehyde-triol formulation raised the question of whether the tautomerized form was capable of BER, since it is possible that all of the observed stress-relaxation behavior could have occurred through BER of the terephthalaldehyde moieties within the polymer matrix. A small molecule model imine-exchange reaction revealed that the imine links formed from the trialdhehyde-triol monomer are readily reversible in solution (see experimental section).

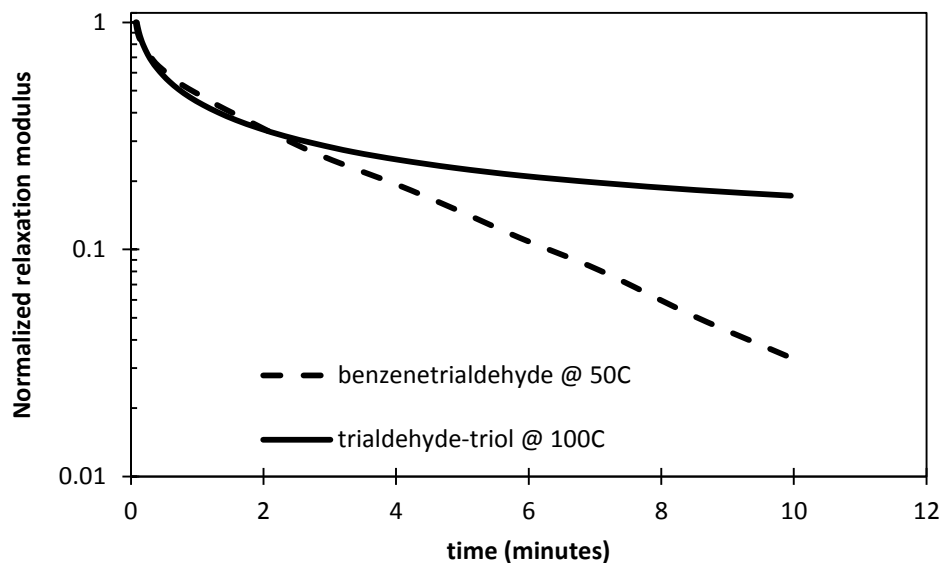


Figure 4.7 Stress relaxation experiment of the benzenetrialddehyde formulation at 50 °C and the trialdehyde-triol formulation at 100 °C.

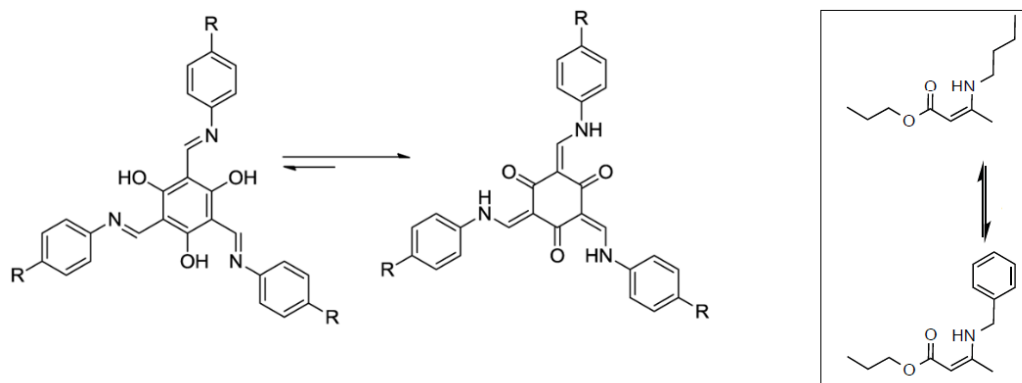


Figure 4.8 Tautomerization of trimine-triol to the quinone form (*reproduced from* [18]). In box: model study of BER of vinylogous urethane vitrimers (*reproduced from* [19]).

In order to characterize the effect of moisture on the stress-relaxation behavior of the hydrophobic benzene trialdehyde formulation, a room temperature DMA stress-relaxation experiment was performed on samples which had been immersed in water for 24 h, and the results compared with dry samples. Figure 4.9 shows that the difference in relaxation behavior of the wet vs. dry polymer is within the experimental error, and essentially no mechanical impact is detected.

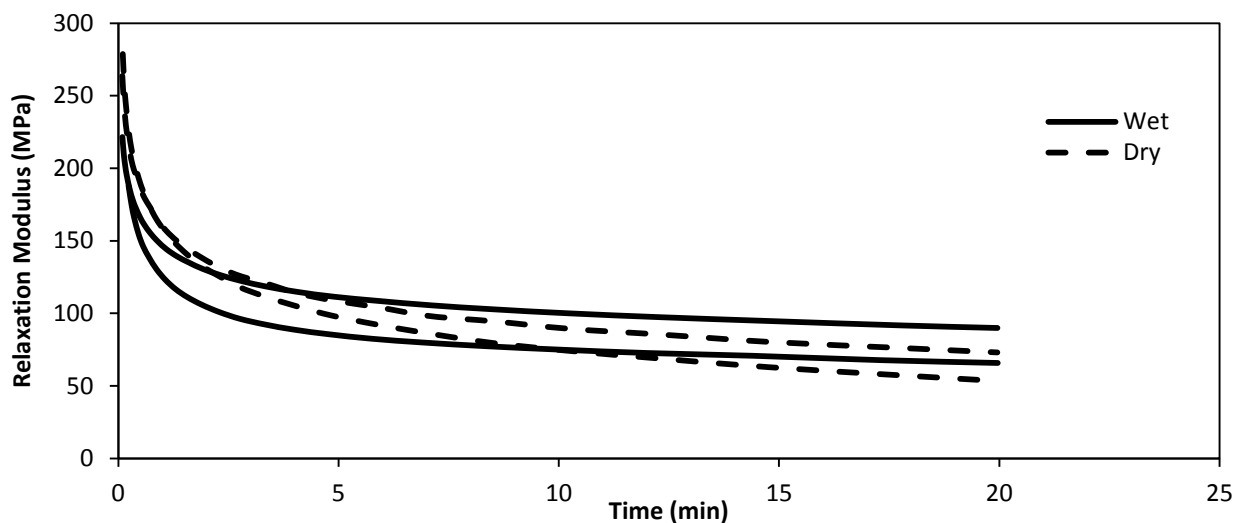


Figure 4.9 Stress relaxation of benzene trialdehyde formulation when wet and when dry.

4.5 Conclusions

We have demonstrated that simple formulation among commercially available dialdehydes can be used to prepare malleable polyimine networks with a wide range of thermal, mechanical, and moisture-induced properties. Semicrystalline polymers with high strength and thermal stability, and tough elastomeric materials with low temperature malleability. The moisture-sensitivity of the networks can be nearly turned off by using hydrophobic trialdehyde crosslinkers in place of the hydrophilic TREN monomer. Further, the E_a of the BER and the functional malleability of the polymers can be altered independent of the T_g and mechanical properties through inclusion of a trialdehyde-triol monomer which contains strong H-bonds and stable tautomers which effectively slow the BER without affecting greater crystallinity in the polymer matrix. With easy means of tuning the mechanical, thermal, and moisture-induced properties, polyimine vitrimers are a catalyst-free malleable thermoset with great potential to be adapted to a large number of potential applications.

4.6 Experimental section

4.6.1 Experimental procedures for preparation of polymer films

General procedure for preparation of hydrophilic polyimine films

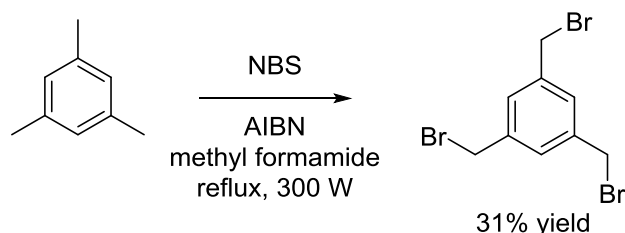
Terephthaldehyde (1 g, 7.45 mmol) was added to a 25 mL screw cap vial followed by ethanol (15 mL) and the solution was stirred for 10 minutes. Diamine monomer (3.36 mmol) was added dropwise while stirring. The solution becomes translucent and yellow-to-orange in color. To a tray made from silicone-coated release paper (with approximate dimensions 5 cm x 5 cm x 3 cm) was added tris(2-aminoethyl)amine (0.398 g, 2.72 mmol), followed by ethanol (~5 mL or enough to cover most of the surface area of the bottom of the tray). The terephthaldehyde and diamine solution was poured into the tray with gentle mixing. The solution was allowed to evaporate in a fume hood for 24 h. The resulting uncured elastomeric film was first heat pressed for 3 h at 78 °C, followed by 1 h at 95 °C, and finally 1 h at 105 °C using a top platen-heated hand-operated heat press under nominal pressure.

General procedure for preparation of hydrophobic polyimine films

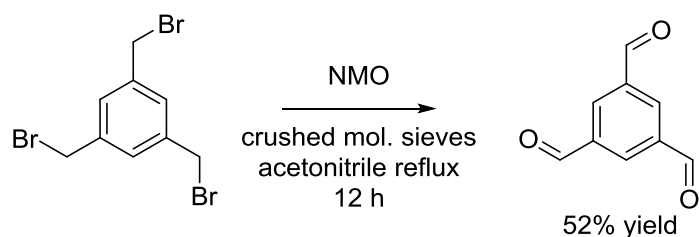
Terephthaldehyde (1 g, 7.45 mmol) was added to a 25 mL screw cap vial followed by ethanol (5 mL) and dichloromethane (8 mL). The solution was stirred for 10 minutes. Diamine monomer (3.36 mmol) was added, and DI water (5 mL) was added dropwise while stirring until the solution became homogeneous. The solution becomes translucent and yellow-to-orange in color. To a tray made from silicone-coated release paper (with approximate dimensions 5 cm x 5 cm x 3 cm) was added tris(2-aminoethyl)amine (0.398 g, 2.72 mmol), followed by dichloromethane (~5 mL or enough to cover most of the surface area of the bottom of the tray). The terephthaldehyde and diamine solution was poured into the tray with gentle mixing. The solution was allowed to evaporate in a fume hood for 24 h. The resulting uncured elastomeric

film was first heat pressed for 3 h at 78 °C, followed by 1 h at 95 °C, and finally 1 h at 105 °C using a top platen-heated hand-operated heat press under nominal pressure.

4.6.2 Synthetic procedures

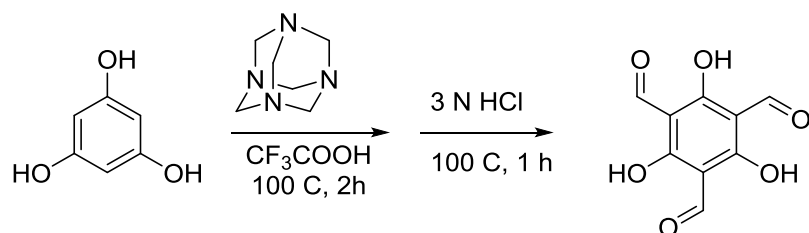


Mesitylene (6.936 mL, 49.9 mmol), N-bromosuccinimide (35.54 g, 199.7 mmol), AIBN (80mg) and methyl formamide (250 mL) were stirred together in a 500mL round bottom flask. After adding a reflux condenser, the flask was lowered into a 40°C oil bath, and the system was left under reflux, under 300W irradiation for 12 h. The resulting red homogeneous solution was washed with sodium carbonate solution then the organic layer was concentrated. The oil was dissolved in cyclohexane (80 °C, stirring), passed through a paper filter and then recrystallized. ~5.5 g pure product was obtained. 31% yield. ¹H-NMR (CdCl₃, 500 MHz) δ 7.34 ppm (s, 3H), δ 4.44 ppm (s, 6H). The NMR data are consistent with the literature reported.²⁰



1,3,5-tribromomethylbenzene (2 g, 5.6 mmol), was added to a 500 mL round bottom flask along with 200 mL of anhydrous acetonitrile. Next N-Methylmorpholine Oxide (4 g, 34.1 mmol) and crushed molecular sieves (40 g) were added and the slurry was refluxed overnight. After cooling to rt, the slurry was filtered through a pad of silica and the filter was washed thoroughly with ethyl acetate. Solvent was then removed and silica gel added. A short column was run with a

50:50 hexane/ethyl acetate eluent. 0.4683 g pure product obtained. 52% yield. $^1\text{H-NMR}$ (CdCl_3 , 500 MHz) δ 10.21 ppm (s, 3H), δ 8.64 ppm (s, 3H). The NMR data are consistent with the literature reported.²¹

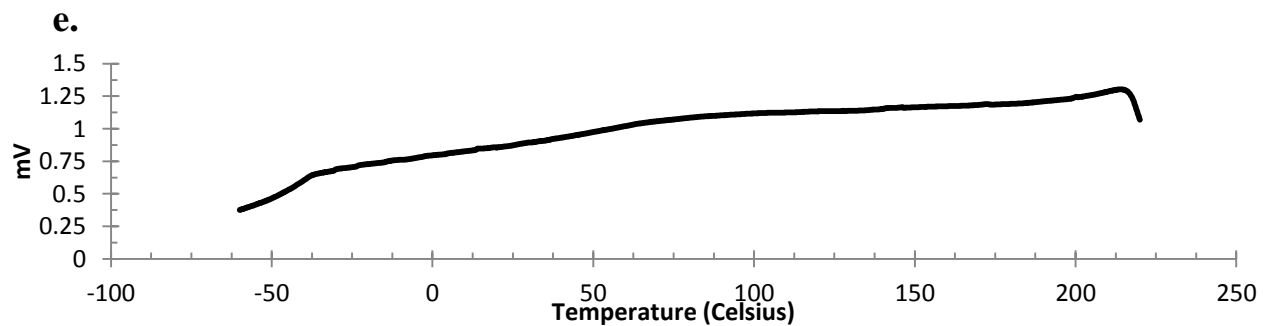
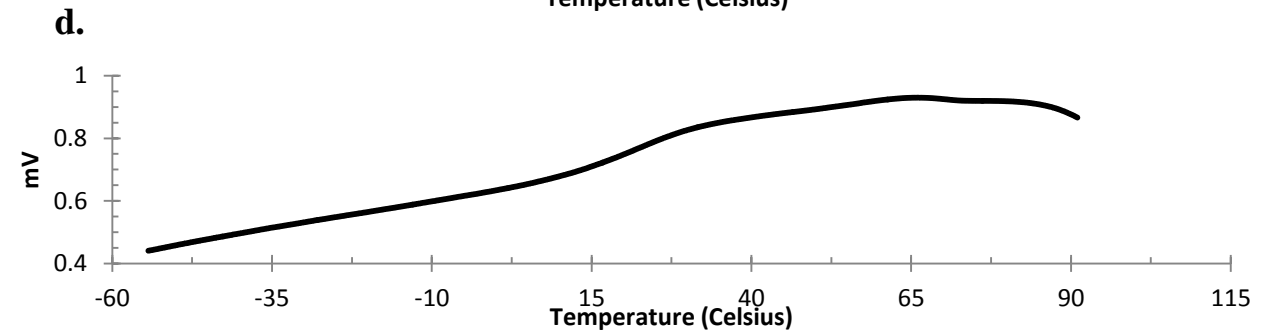
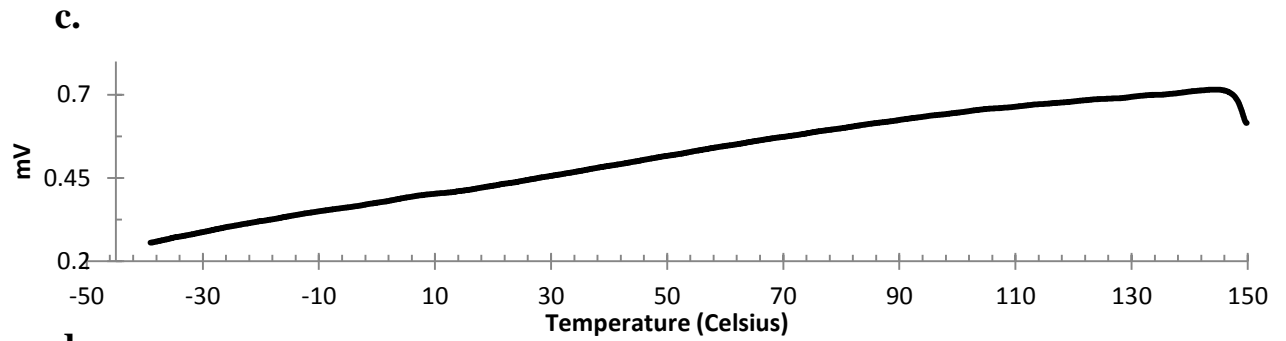
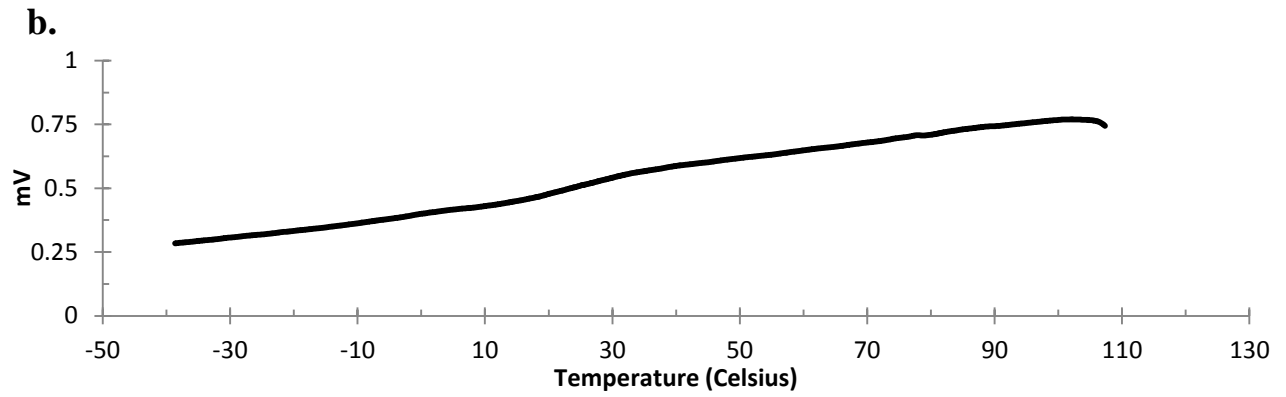
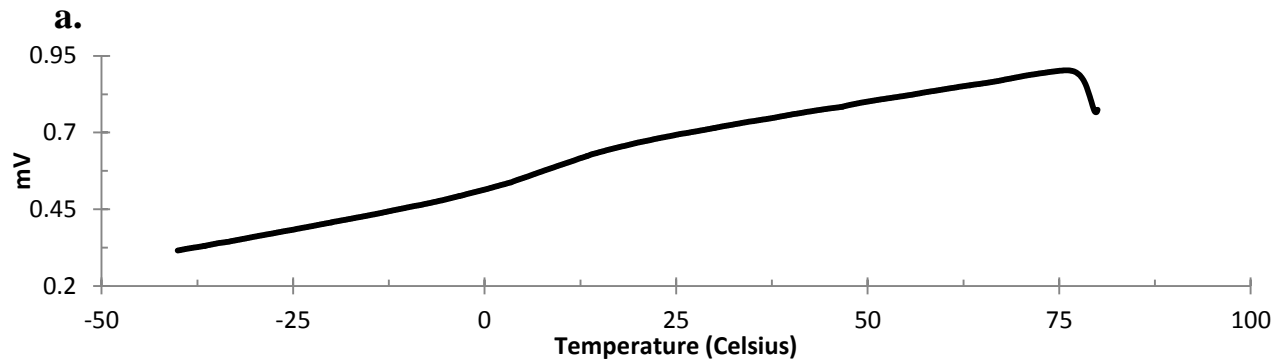


Phloroglucinol (3 g, 23.79 mmol), and hexamethylenetetramine (7.4 g, 52.79 mmol) were added to a 250 mL Schlenk tube. The tube was degassed, and trifluoroacetic acid (45 mL) was added. The tube was sealed and heated at 100 °C for 2 h. 150 mL 3N HCl was added, and the tube was resealed and heated for a further 1 h at 100 °C. The mixture was quickly filtered through celite and extracted with dichloromethane. The dichloromethane was evaporated and the solid was washed with ethanol. 475 mg obtained. 9.5% yield. $^1\text{H-NMR}$ (500 MHz) δ 14.14 ppm (s, 3H), δ 10.17 ppm (s, 3H). The NMR data are consistent with the literature reported.¹⁸

4.6.3 Characterization of thermal properties of polymers

Differential Scanning Calorimetry

The DSC measurement was performed using a Mettler Toledo DSC823e. DSC scan was performed at a scan rate of 5 °C/min on a film sample of each formulation. The inflection point in the curve was taken to be the glass transition temperature (T_g). The DSC curves of each polymer is shown in Figure 4.10. The T_g of the various formulations is reported in Table 4.1.



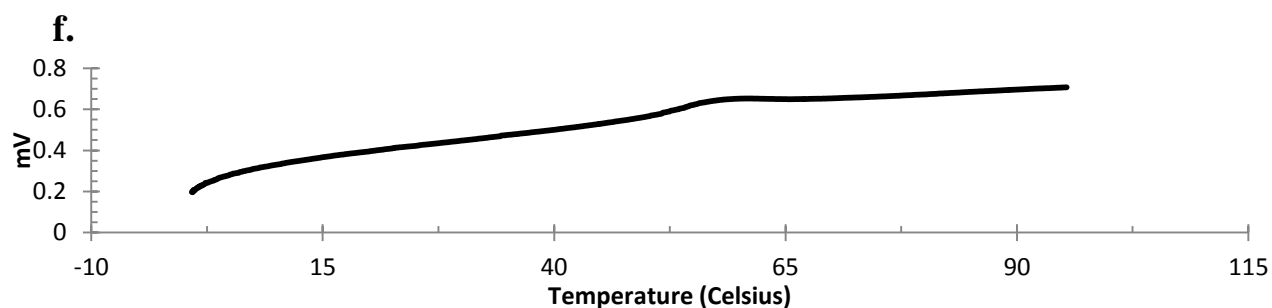


Figure 4.10 The DSC scans of each of the polyimine formulations. Scan rate = 5 °C/min. **a.** N-methyl. **b.** Pentaethylene Hexamine. **c.** Ethylene Diamine. **d.** 1,8-diaminooctane. **e.** 1,12-diaminododecane. **f.** Benzenetrialddehyde formulation.

Thermal Gravimetric Analysis

Samples were run on a TA Instruments Q-500 series thermal gravimetric analyzer with samples held in a platinum pan under nitrogen atmosphere. A 10 K min⁻¹ ramp rate was used. The results are shown below in Figure 4.11.

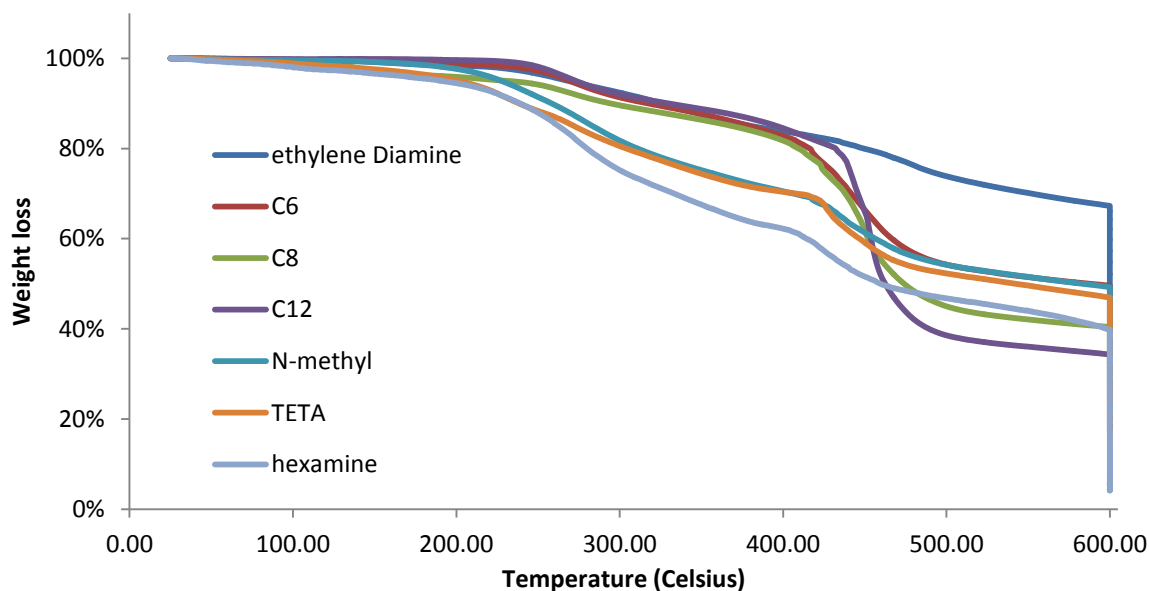


Figure 4.11 TGA plot for polyimine polymers. Scan rate is 5 °C/min.

Dynamic Mechanical Analysis- Stress Relaxation

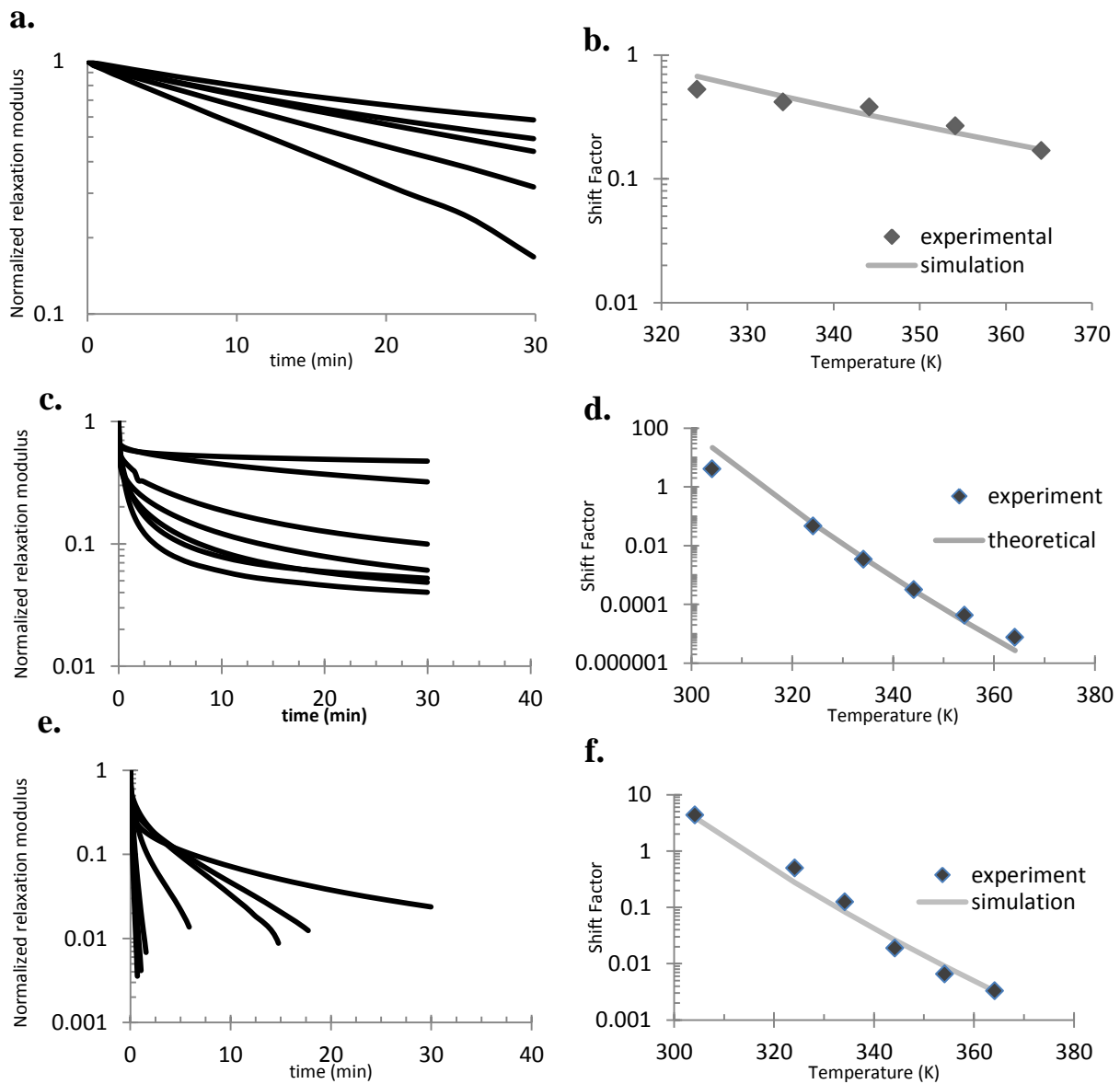
The time and temperature dependent relaxation modulus of the polyimine thermoset was also tested on the DMA machine (Model Q800, TA Instruments, New Castle, DE, USA). During the test, a polymer sample with the same dimension mentioned above was initially preloaded by 1×10^{-3} N force to maintain straightness. After reaching the testing temperature, the sample was allowed 30 min to reach thermal equilibrium. The specimen was stretched by 1% on the DMA machine and the deformation was maintained throughout the test. The decrease of stress was recorded and the stress relaxation modulus was calculated. Figure 4.12 depicts the results of relaxation tests at 4-9 different temperatures between 30 °C and 110 °C for the polyimine formulations. Then selecting 40 °C as a reference temperature (T_r), each modulus curve in the left side of Figure 4.12 was shifted horizontally to overlap with the next. This produced the master relaxation curve (not shown), which can span many decades of modulus and represent the actual relaxation behavior of the polymer within a long time scale at 40 °C. The corresponding shift factors were plotted against temperature in the right side of Figure 4.12. The master relaxation curve suggests that the kinetics of the bond exchange reaction-induced stress relaxation follows the well-known temperature-time superposition (TTSP) principles. To quantitatively study the relaxation behavior, we used the following definition of relaxation Modulus:

$$\tau = \frac{1}{k} \exp\left(\frac{E_a}{RT}\right) \quad (4.1)$$

where k was a kinetic coefficient ($k > 0$) R was the gas constant with $R = 8.31446 \text{ J / Kmol}$, and E_a is the activation energy. The shift factor, namely the ratio between the temperature-dependent relaxation time and the relaxation time at a reference temperature T_r , was therefore expressed as:

$$\alpha = \exp\left[\frac{E_a}{R} \left(\frac{1}{T} - \frac{1}{T_r}\right)\right] \quad (4.2)$$

The predicted shift factors of the relaxation curves were plotted in Figure 4.12 to compare with the experimental data. An Arrhenius-type dependence on temperature was revealed, which was consistent with what was previously reported for the DETA formulation. By further examination of Equation 4.2 we found that in the semi-log scale, the energy barrier could be determined by the slope of the shift factor curve. As shown in Figure 4.12, by measuring the curve slope, the energy barrier E_a was calculated for each formulation.



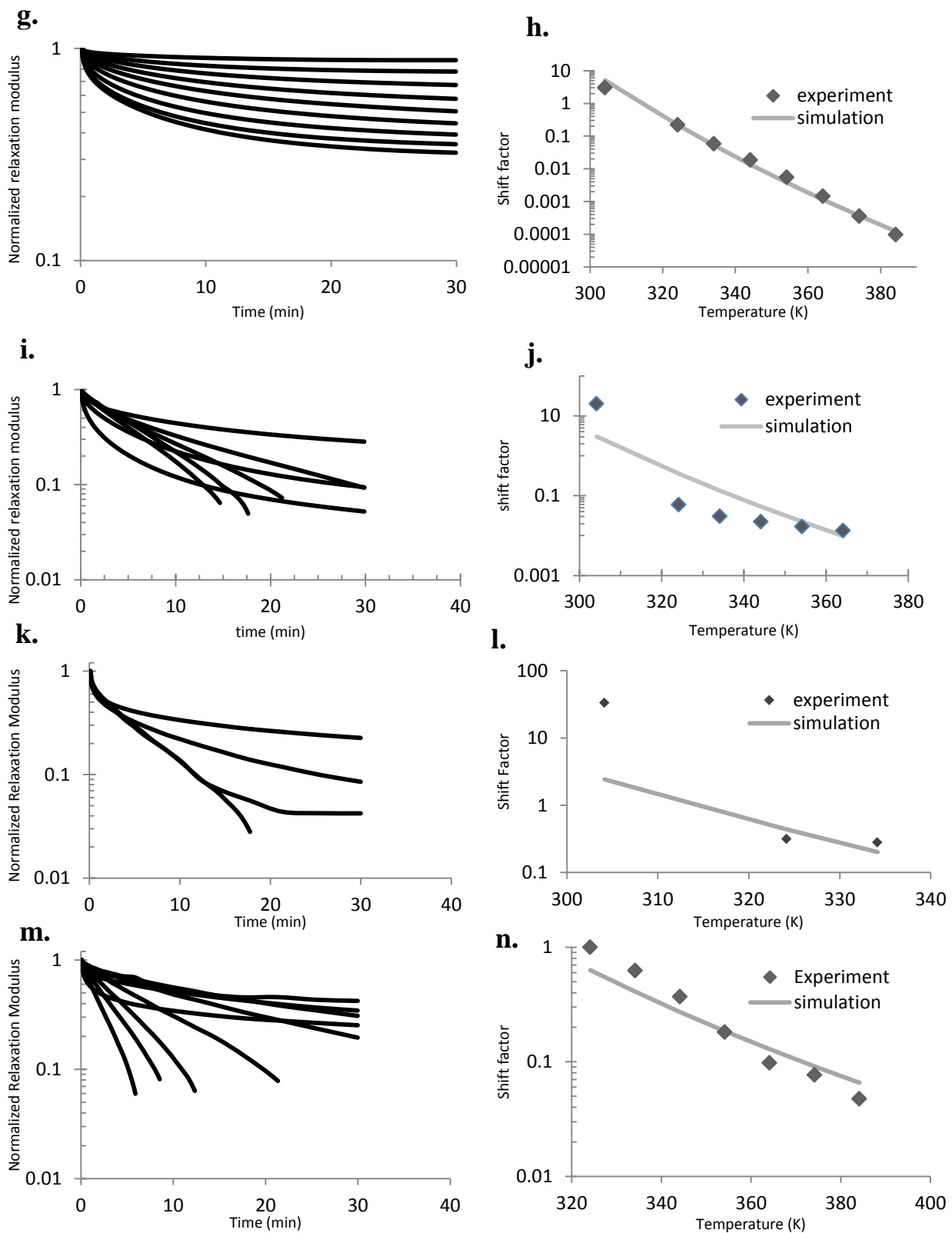


Figure 4.12 Stress-relaxation data for polyimine formulations. The plot of log of shift factors vs temperature most closely matches the arrhenius plot of an activation energy E_a which is listed in Table 4.1 for each formulation. **a.-b.** N-methyl elastomer formulation. **c.-d.** Triethylenetetramine formulation. **e.-f.** Pentaethylene hexamine formulation. **g.-h.** Ethylene diamine formulation. **i.-j.**

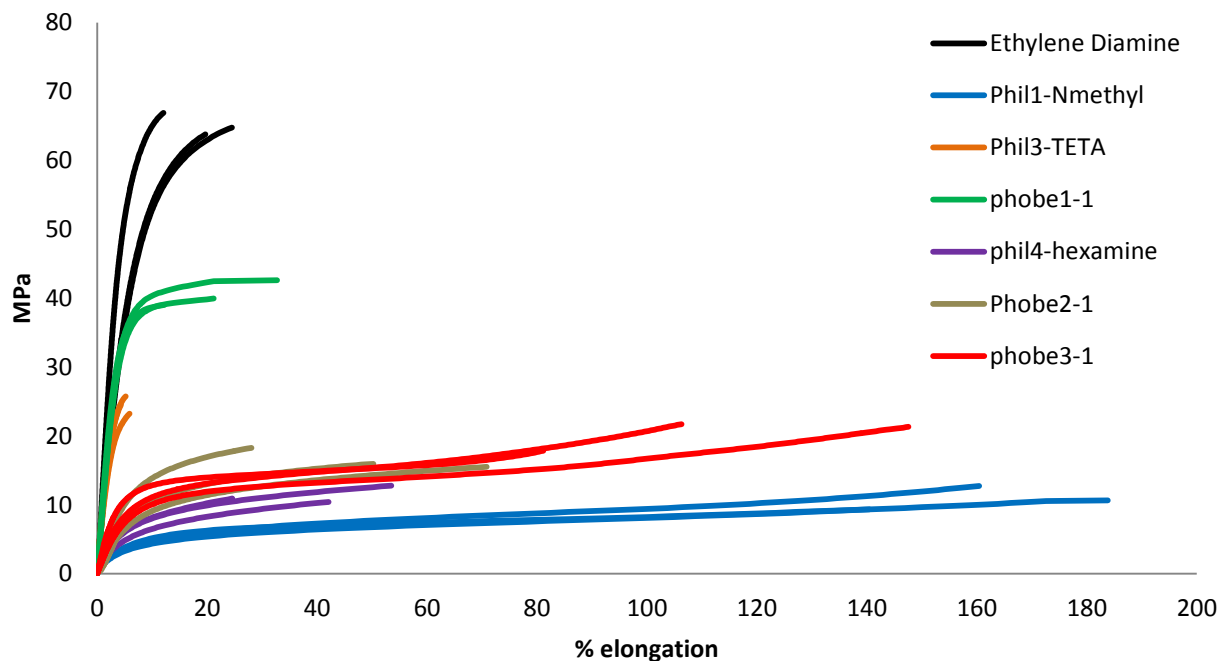
1,6-diamino hexane formulation. **k.-l.** 1,8-diamino octane formulation. **m.-n.** 1,12-diamino dodecane formulation.

4.6.4 Mechanical testing of polymer films

DMA Tension tests

A dynamic mechanical analysis (DMA) machine (Model Q800, TA Instruments, New Castle, DE, USA) was used to carry out tension tests at room temperature (26 °C locally). All the samples were trimmed into a uniform size of 12 mm × 3 mm × 1.1 mm, and then stretched under a constant loading rate (2 MPa/min) until broken. Figure 4.13 shows the result of the tension tests for the new polymer formulations.

For the wet tensile measurements, pre-cut samples were immersed in DI water for 24 h. After being removed from the water, each sample was blotted dry, loaded into the DMA instrument, and tested within 2 minutes to minimize the ambient drying of the films.



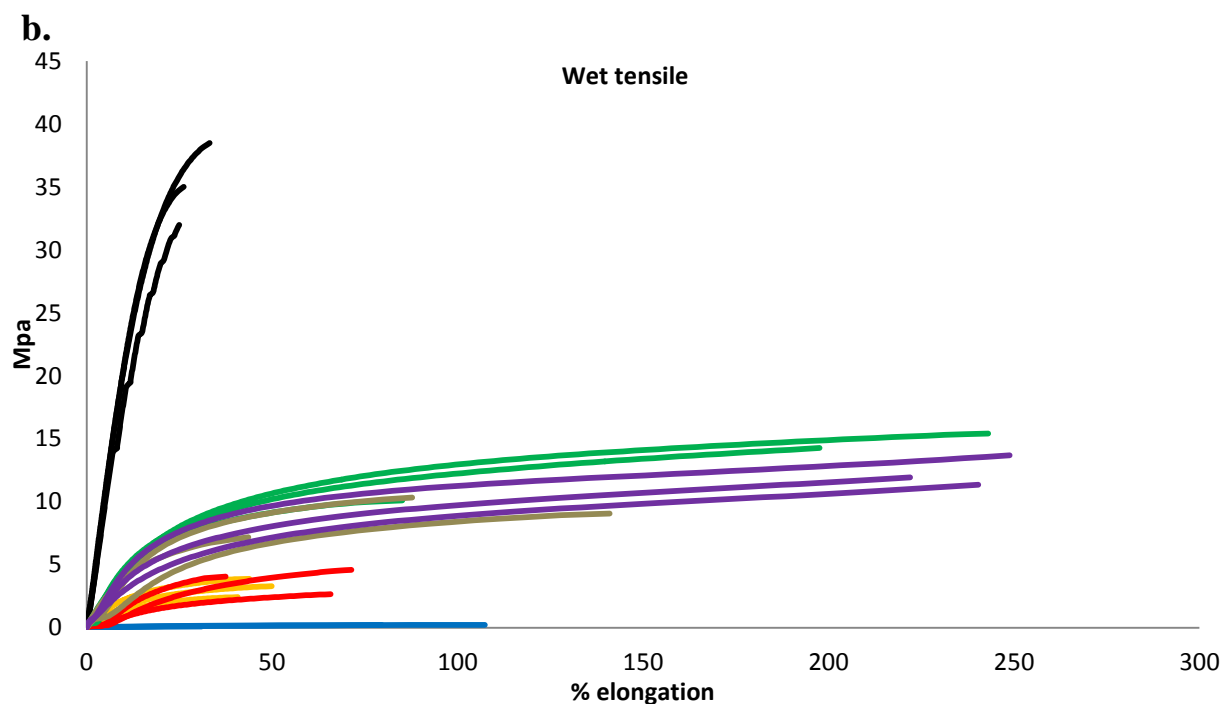


Figure 4.13 Tensile testing of each polymer formulation. **a.** when dry. **b.** after 24 h swelling.

The results of the wet and dry tensile tests are summarized in Table 4.1.

Table 4.1 Summary of results from mechanical testing of each formulation

Dry	modulus (Gpa)		Tensile (Mpa)		Elongation (%)	
	avg	stdev	avg	stdev	avg	Stdev
	ethyleneDiamine	1.05	0.19	65.1	1.6	18.7%
N-methyl	0.013	0.001	10.8	1.6	162.0%	22.0%
TETA	0.93	0.07	24.5	1.3	5.1%	0.8%
Hexamine	0.21	0.025	11.4	1.3	40.1%	14.6%
C6	1.01	0.06	40.5	1.9	22.0%	10.3%
C8	0.014	0.003	16.5	1.46	49.5%	21.0%
C12	0.027	0.007	20.3	2.1	111.7%	33.6%
Wet	modulus (Gpa)		Tensile (Mpa)		Elongation (%)	
	Avg	stdev	avg	stdev	avg	Stdev
	ethyleneDiamine	0.185	0.013	35.2	3.25	28.0%
N-methyl	0.00006	0.00001	0.19	0.08	72.6%	38.7%
TETA	0.0003	0.0001	3.2	0.7	44.8%	4.7%
Hexamine	0.0002	0.00001	3.8	1	58.2%	18.0%
C6	0.0005	0.0001	13.3	2.8	175.2%	81.3%
C8	0.0003	0.0001	8.9	1.6	90.9%	48.8%

C12	0.0005	0.00001	12.3	1.2	237.1%	13.8%
-----	--------	---------	------	-----	--------	-------

4.6.5 Characterizing the interaction of the polymer films with moisture

Pristine polyimine films were prepared in the manner described above, except that they were cured in an oven rather than a heat press to prevent contamination of the film surface. Contact angle measurements were performed using an Olympus i-speed high speed camera at 200 fps shutter rate. The contact angle of a single drop of water was recorded 300 ms after the first contact of the drop to the film surface. The average of at least 3 contact angle measurements per film is reported in Table 4.2.

The swelling study was performed by placing a pre-tared sample (approx. 1 cm x 1 cm) of each formulation in a 25 mL screw cap vial filled with DI water. Upon removal of the sample from the water, the samples were blotted dry and massed on a digital balance (with 0.0001 g resolution) within 1 minute to minimize the ambient drying of the swollen polymer films.

Table 4.2 Summary of moisture effects on each polyimine formulation

	22 h Swelling	contact angle
ethyleneDiamine	-	49
N-methyl	29%	67
DETA	39%	67
TETA	45%	43
Hexamine	58%	50
C6	10%	68
C8	10%	50
C12	8%	56

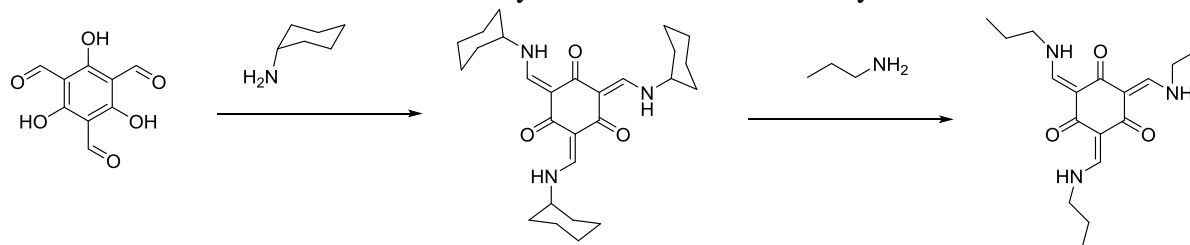
4.6.6 NMR spectra

NMR spectra were taken on Inova 400 and Inova 500 spectrometers. Solid-state cross polarization magic angle spinning (CP/MAS) NMR spectra were recorded on an Inova 400 NMR spectrometer.

H-NMR Spectra: model study of BER in trialdehyde-triol monomers.

The dramatic difference in the stress-relaxation behavior of the benzene trialdehyde formulation and the trialdehyde-triol formulation caused us to wonder whether the keto-ene-amine moieties were undergoing amine-exchange at all. To test this, we performed a model study of amine exchange in triimines formed from the trialdehyde-triol monomer. The chemical transformations are illustrated in Scheme 4.3.

Scheme 4.3 Small molecule model study of imine BER in trialdehyde-triol formulation



1,3,5-Benzenecarboxaldehyde, 2,4,6-trihydroxy- was combined with cyclohexylamine in dichloromethane solvent. After stirring for 1 h over 3Å molecular sieves, the solution was decanted, and rotovaped in order to isolate the first keto-ene-amine shown in Scheme 4.3, and characterized by $^1\text{H-NMR}$ (Figure 4.14). The product was then dissolved in propylamine and stirred for 2 h at room temperature. After this time, the transformation to the 2nd keto-ene-amine was again isolated by evaporating the solvent, and characterized by $^1\text{H-NMR}$ (Figure 4.14). The transformation was verified by the expected doubling of the integration of the methylene protons (labeled H_a in Figure 4.14) at 3.4 ppm in the $^1\text{H-NMR}$ spectrum of the molecule (Figure 4.14). This model study verifies that the keto-ene-amine readily undergoes bond exchange with primary amines in solution.

Figure 4.14 ^1H -NMR spectra of the keto-ene-amine species in model study confirming facile bond exchange with primary amines in solution at room temperature.

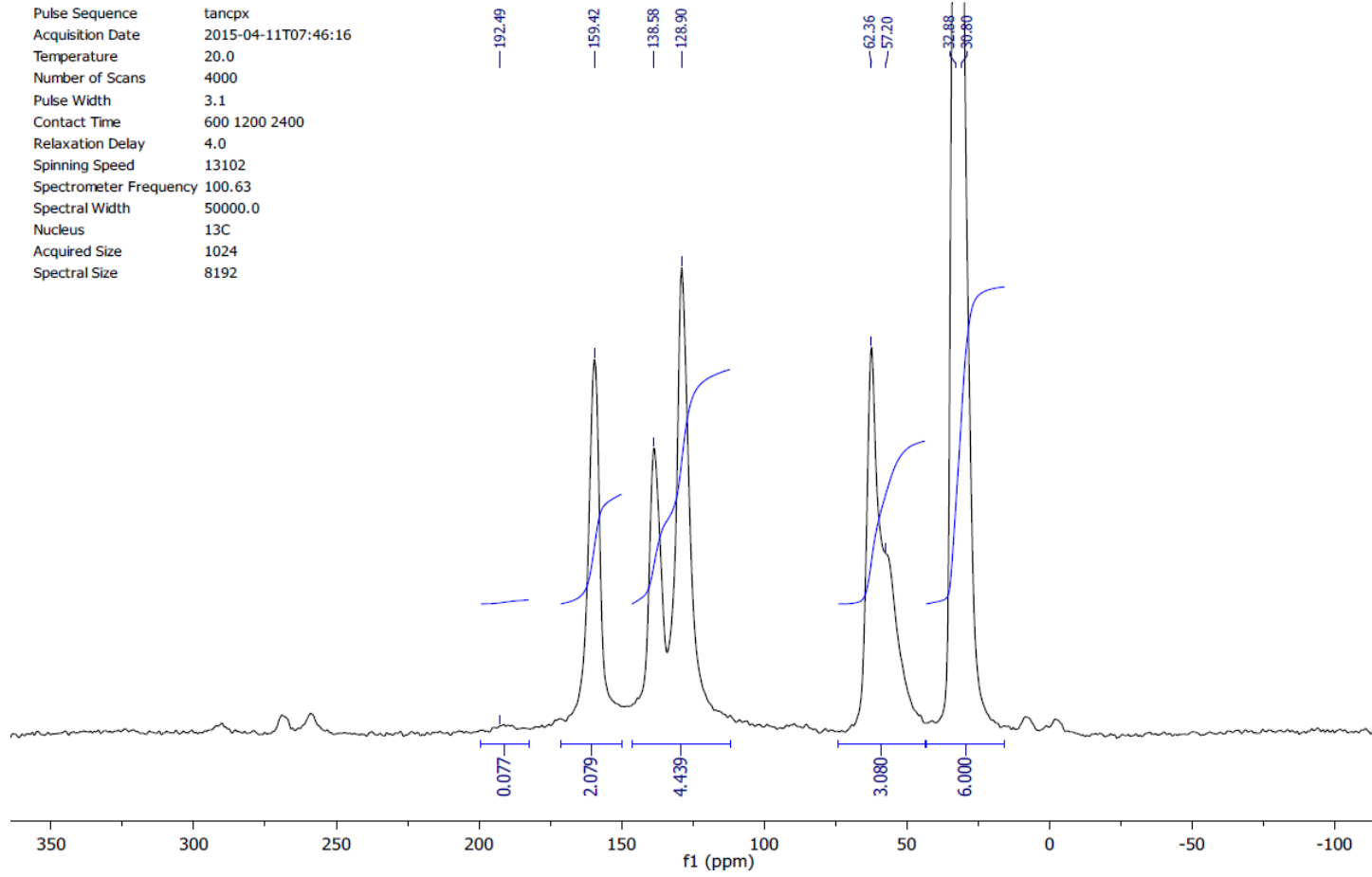
C-NMR Spectra

Solid-State, Cross-Polarization Magic Angle Spinning (CPMAS), ^{13}C NMR spectroscopy was performed using a Varian INOVA-400 (Agilent Technologies, Inc.) spectrometer operating at 100.63 MHz for ^{13}C observation. The probe incorporates a 5mm Magic Angle spinning module and coil assembly designed and constructed by Revolution NMR, Inc. (Fort Collins, CO), capable of spinning up to 13KHz with Zirconia rotors (also from Revolution NMR, Inc.). Spectra were acquired using cross-polarization spin-lock and decoupling R_f fields of 80.5 KHz, and TPPM (Time Proportional Phase Modulation) decoupling was applied during signal acquisition. Chemical shifts were referenced using the absolute, calibrated spectrometer configuration frequency and magnetic field offset, such that the methyl carbons of hexamethylbenzene appear at 17.3 ppm. Sample spinning frequencies from 10.5-11.57 KHz were employed with the sample oriented at the *magic angle* (54.736 degrees, relative to the magnetic field axis, calibrated using the ^{79}Br spinning sideband pattern of KBR). To effect the uniform cross-polarization of ^1H magnetization to all ^{13}C nuclei, spectra were acquired using multiple cross-polarization contact times between 500 and 1000 μsec and these were summed to yield the final spectra. These optimal contact times were determined using variable contact-time experiments and were chosen to obtain uniform excitation across all carbon atoms in the molecules of the dry and hydrated samples. Spectra were the result of between 2,016 and 5,600 scans, yielding adequate signal-to-noise ratios. The spectra are shown in Figure 4.15 below.

Dry C₁₂ formulation:

Parameter	Value
Data File Name	Hydrophobic-3-Dry-13C-CPMAS-20150410-OvntSUM.fid/
Title	Hydrophobic, #3 (Dry). 13C CPMAS 4mmrev., tHX=1200,2400,4800 (interleaved) - SUM

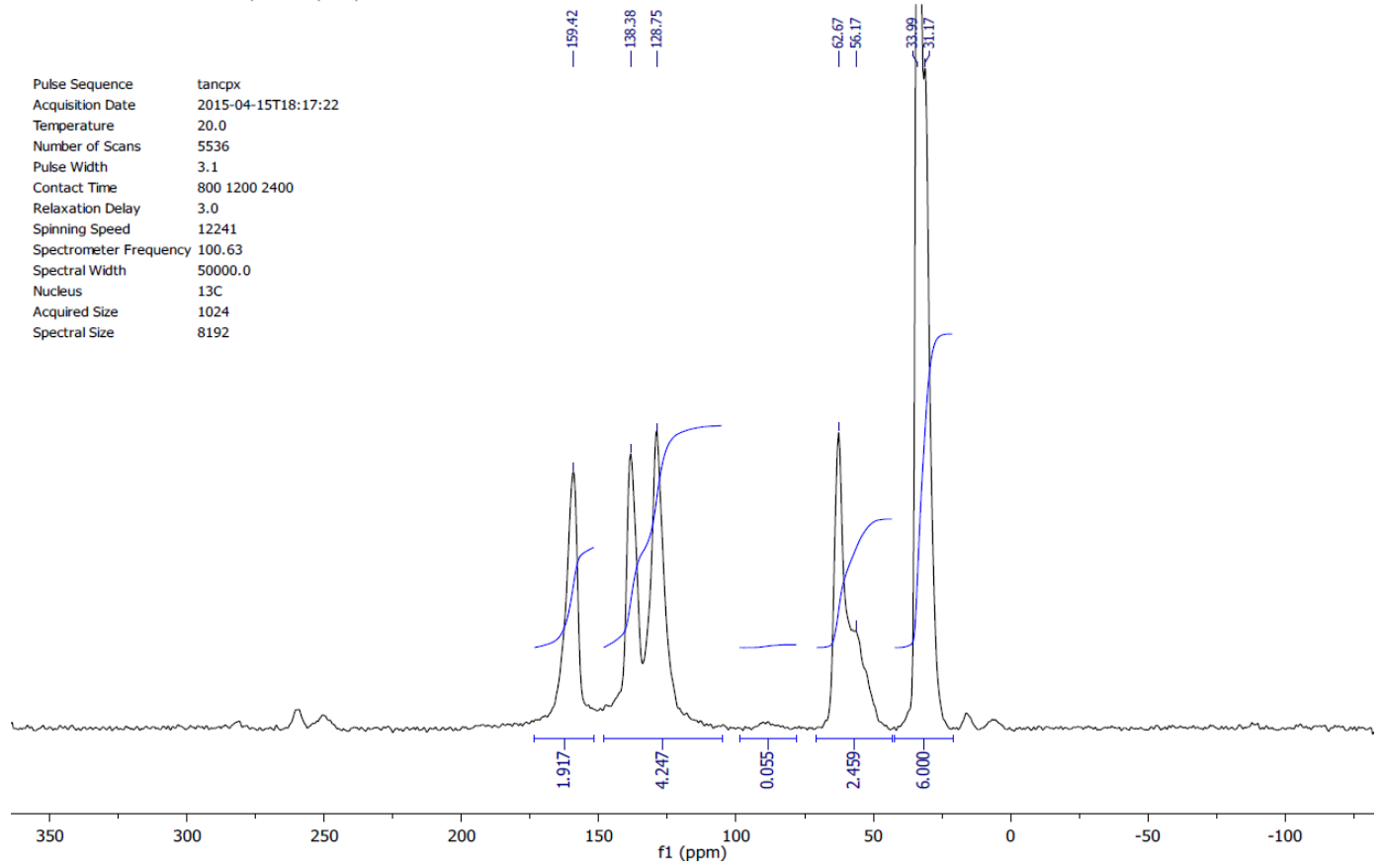
Re-referenced using setref



Wet C₁₂ formulation:

Parameter	Value
Data File Name	Hydrophobic-3-WET-13C-CPMAS-20150415-3cts-Ovnt-SUM.fid/
Title	Hydrophobic, #3 (Wet/ Hydrated), 13C CPMAS 4mmrev., tHX=800,1200,2400 SUM of all 3

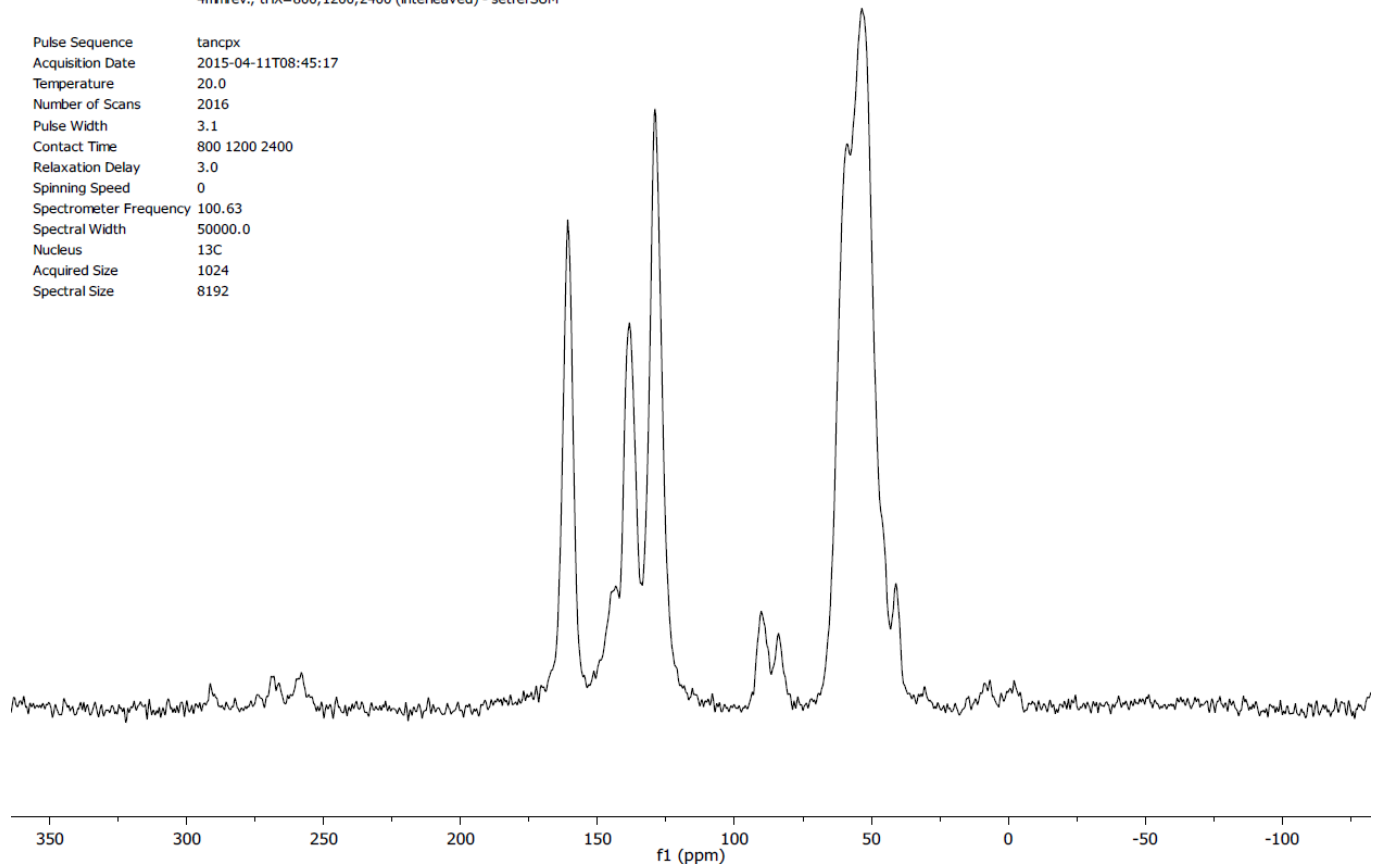
Pulse Sequence	tancpx
Acquisition Date	2015-04-15T18:17:22
Temperature	20.0
Number of Scans	5536
Pulse Width	3.1
Contact Time	800 1200 2400
Relaxation Delay	3.0
Spinning Speed	12241
Spectrometer Frequency	100.63
Spectral Width	50000.0
Nucleus	13C
Acquired Size	1024
Spectral Size	8192



Dry PEHA formulation:

Parameter	Value
Data File Name	Hydrophilic-4-Dry-13C-CPMAS-20150411-SUM.fid/
Title	Hydrophilic_ #4 (Dry), 13C CPMAS 4mmrev., tHX=800,1200,2400 (interleaved) - setrefSUM

Pulse Sequence	tanpdx
Acquisition Date	2015-04-11T08:45:17
Temperature	20.0
Number of Scans	2016
Pulse Width	3.1
Contact Time	800 1200 2400
Relaxation Delay	3.0
Spinning Speed	0
Spectrometer Frequency	100.63
Spectral Width	50000.0
Nucleus	13C
Acquired Size	1024
Spectral Size	8192



Wet PEHA formulation:

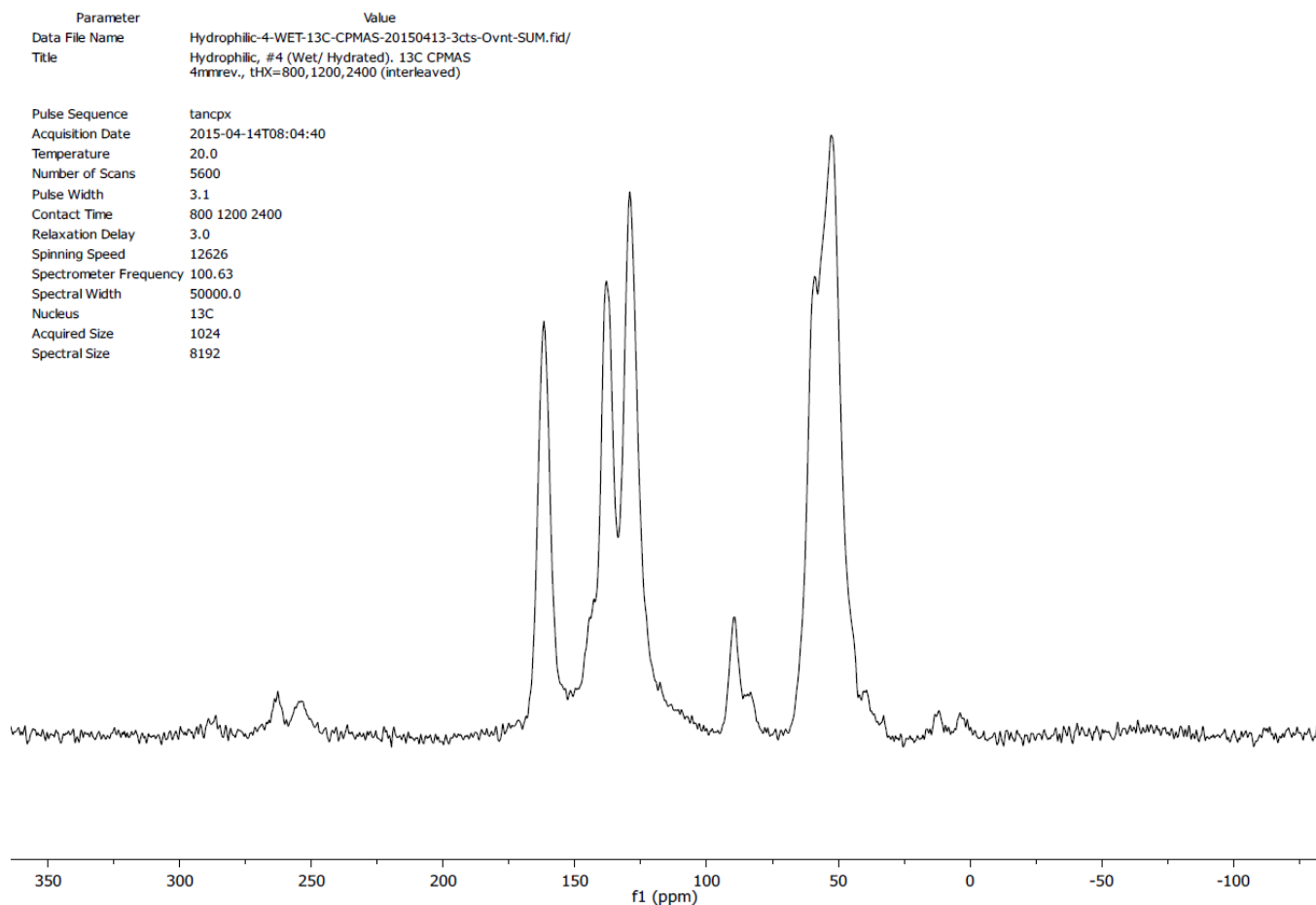


Figure 4.15 Magic angle spinning solid state ¹³C-NMR of C₁₂ formulation powder and PEHA formulation powder in the wet and dry states.

4.7 References

- [1] M. Doi, Introduction to polymer physics, Oxford: Oxford University Press, 1996.
- [2] J. J. Alkonis and W. J. MacKnight, Introduction to polymer viscoelasticity 2nd Ed., New York: Wiley, 1983.
- [3] C. Kloxin, T. Scott, B. Adzima and C. Bowman, "Covalent Adaptable Networks (CANs): A Unique Paradigm in Cross-Linked Polymers," *Macromolecules*, vol. 43, pp. 2643-2653,

- 2010.
- [4] Y. Zhang, A. A. Broekhuis and F. Picchioni, "Thermally Self-Healing Polymeric Materials: The Next Step to Recycling Thermoset Polymers?," *Macromolecules*, vol. 42, no. 6, pp. 1906-1912, 2009.
 - [5] X. X. Chen, M. A. Dam, K. Ono, H. B. Shen, S. R. Nutt, K. Sheran and F. Wudl, "A Thermally Re-mendable Cross-Linked Polymeric Material," *Science*, vol. 295, pp. 1698-1702, 2002.
 - [6] M. Capelot, D. Montarnal, F. Tournilhac and L. Leibler, "Metal-Catalyzed Transesterification for Healing and Assembling of Thermosets," *J. Am. Chem. Soc.*, vol. 134, pp. 7664-7667, 2012.
 - [7] M. Capelot, M. Unterlass, F. Tournilhac and L. Leibler, "Catalytic Control of the Vitrimers Glass Transition," *ACS Macro Lett.*, vol. 1, pp. 789-792, 2012.
 - [8] D. Montarnal, M. Capelot, F. Tournilhac and L. Leibler, "Silica-Like Malleable Materials from Permanent Organic Networks," *Science*, vol. 334, no. November, pp. 965-968, 2011.
 - [9] M. Capelot, D. Montarnal, F. Tournilhac and L. Leibler, "Metal-catalyzed transesterification for healing and assembling of thermosets," *Journal of the American Chemical Society*, vol. 134, no. 18, pp. 7664-7667, 2012.
 - [10] P. Taynton, K. Yu, R. Shoemaker, Y. Jin, H. J. Qi and W. Zhang, "Heat- or Water-Driven Malleability in a Highly Recyclable Covalent Network Polymer," *Advanced Materials*, vol. 26, no. 23, pp. 3938-3942, 2014.
 - [11] K. Yu, P. Taynton, W. Zhang, M. Dunn and H. J. Qi, "Reprocessing and recycling of thermosetting polymers based on bond exchange reactions," *RSC Advances*, vol. 4, no. 20, pp. 10108-10117, 2014.
 - [12] W. Skene and J.-M. Lehn, "Dynamers: Polyacylhydrazone reversible covalent polymers, component exchange, and constitutional diversity," *Proc. Natl. Acad. Sci. U.S.A.*, vol. 101, pp. 8270-8275, 2004.
 - [13] J. Lehn, "Dynamers: dynamic molecular and supraolecular polymers," *Prog. Polym. Sci.*, vol. 30, no. 8-9, pp. 814-831, 2005.
 - [14] Y. Jin, C. Yu, R. J. Denman and W. Zhang, "Recent Advances in Dynamic Covalent Chemistry," *Chem. Soc. Rev.*, vol. 42, pp. 6634-6654, 2013.

- [15] T. Ono, T. Nobori and J. Lehn, "Dynamic polymer blends - component recombination between neat dynamic covalent polymers at room temperature," *Chemical Communications*, vol. 12, pp. 1522-1524, 2005.
- [16] K. Yu, P. Taynton, W. Zhang, M. Dunn and H. J. Qi, "Influence of Stoichiometry on the Glass Transition and Bond Exchange Reactions in Epoxy Thermoset Polymers," *RSC Advance*, vol. 4, pp. 48682-48690, 2014.
- [17] R. Martin, A. Rekondo, A. Ruiz De Luzuriaga, G. Cabanero, H. Grande and I. Odriozola, "The processability of a poly (urea-urethane) elastomer reversibly crosslinked with aromatic disulfide bridges," *Journal of Materials Chemistry A*, vol. 2, no. 16, pp. 5710-5715, 2014.
- [18] Y. Zhu, H. Long and W. Zhang, "Imine-Linked Porous Polymer Frameworks with High Small Gas (H₂, CO₂, CH₄, C₂H₂) Uptake and CO₂/N₂ Selectivity," *Chemistry of Materials*, vol. 25, pp. 1630-1635, 2013.
- [19] W. Denissen, G. Rivero, R. Nicolay, L. Leibler, J. M. Winne and F. E. Du Prez, "Vinylogous Urethane Vitrimers," *Advanced Functional Materials*, vol. 25, no. 16, pp. 2451-2457, 2015.
- [20] E. Diez-Barra, J. C. Garcia-Martinez, S. Merino, R. del Rey, J. Rodriguez-Lopez, P. Sanchez-Verdu and J. Tejada, "Synthesis, characterization, and optical response of dipolar and non-dipolar poly(phenylenevinylene) dendrimers," *The Journal of Organic Chemistry*, vol. 66, no. 17, pp. 5664-5670, 2001.
- [21] P. Pandey, A. P. Katsoulidis, I. Eryazici, Y. Wu, M. G. Kanatzidis and S. Nguyen, "Imine-linked microporous polymer organic frameworks," *Chemistry of Materials*, vol. 22, no. 17, pp. 4974-4979, 2010.
- [22] Y. X. Lu, F. Tournilhac, L. Leibler and Z. B. Guan, "Making insoluble polymer networks malleable via olefin metathesis," *Journal of the American Chemical Society*, vol. 134, pp. 8424-8427, 2012.
- [23] P. Zheng and T. McCarthy, "A Surprise from 1954: Siloxane Equilibration Is a Simple, Robust, and Obvious Polymer Self-Healing Mechanism," *J. Am. Chem. Soc.*, vol. 134, pp. 2024-2027, 2012.

CHAPTER 5

Repairable Woven Carbon Fiber Composites with Full Recyclability Enabled by Malleable Thermosets

(Manuscript submitted under the same title to *Advanced Materials*. Coauthored with Ni, H.; Loob, S.; Li, H.; Qi, H.J.; Zhang, W.)

5.1 Abstract

Carbon-fiber reinforced composites (CFRC's) are the premier lightweight structural materials, yet are difficult to repair and recycle. In the present work, novel CFRC's, which are easily and efficiently repairable with 100% recovery of flexural strength, are prepared using catalyst-free malleable thermoset polyimine networks as binders. An energy neutral closed-loop recycling process has been developed, enabling recovery of 100% of the imine components and carbon fibers in their original form. Polyimine films made using >21% recycled content exhibit no loss of mechanical performance, therefore indicating all of the thermoset composite material can be recycled and reused for the same purpose. Moreover, the polyimine CFRCs exhibit moldability and weldability, which could lead to enhanced manufacturing efficiencies.

5.2 Introduction

Carbon fiber is a light weight graphitic material with a higher tensile strength than steel and a lower density than aluminum.¹ Woven and non-woven carbon fiber materials are combined with polymeric binder materials to form carbon fiber reinforced composites (CFRC's). Due to their excellent strength-to-weight ratios and durability, CFRC's have seen increasing demand in a large number of applications from aerospace to ground transportation to sporting

goods.²⁻³ Typically carbon fibers are combined with epoxy thermosets for their high stiffness. The resulting CFRC's are brittle, and cannot generally be repaired or recycled. With increasing production of CFRC's, the environmental impact of this traditionally non-recyclable material is of great concern. CFRC recycling has been the focus of a growing body of research over the last two decades.⁴⁻⁶ Many mechanical, and thermochemical approaches have been applied, mostly with the aim of recovering the valuable carbon fibers, with preservation of fiber length a key objective, and the thermoset resins are not generally re-used. Some have managed to recover epoxy resins as fine powders (for reuse as fillers),⁵⁻⁷ downgraded chemical feedstocks, or downgraded thermoplastic materials,⁸ but these processes either involve the use of novel synthetic monomers⁸ or energy-intensive processes (such as use of supercritical solvents) which would be difficult to scale economically.⁹ The recycling difficulty comes from the irreversible nature of the epoxy thermoset resins in CFRC's. To the best of our knowledge, the recyclable binder material that can be reused as thermoset resin with comparable mechanical behavior to the virgin material has rarely been reported.

Repairability and recyclability of CFRC's could be enabled by introduction of dynamic covalent bonds in the thermoset binder material. Dynamic covalent chemistry has previously been demonstrated as a promising route to recyclable covalent network composites,¹⁰ but the work has largely focused on reversible chemical links based on Diels-Alder reaction. Such reaction results in a gel-to-sol transition at high temperatures,¹¹ which is undesirable for the majority of structural applications. Recently malleable thermosets, also called vitrimers,¹² have been utilized as polymer binders. These materials incorporate dynamically exchangeable covalent bonds into the polymer networks. The rate of the bond exchange reactions exhibits an Arrhenius-like temperature-dependence, and enables molding, welding, and complete recycling

of the pure polymeric materials, while maintaining the crosslink density of the thermoset.¹³⁻¹⁵ However, this recycling is typically achieved through a mechanical process of abrasive grinding, followed by compression molding the powdered binder above the vitrimeric transition temperature (T_v) of the material.¹⁶ In a fiber-reinforced composite, such a grinding action would result in complete reduction of fiber length, and thus limit the material's potential for re-use to a cheap composite filler, rather than a replacement for virgin fibers.

We have previously reported the development of network polyimines which are stable against hydrolysis, and exhibit robust mechanical properties combined with low molding temperatures.¹⁷ Herein we report the preparation of novel CFRC's from woven carbon fiber sheets and polyimine thermoset. A closed loop recycling of CFRC's is achieved through dissolution of the malleable thermoset binder via dynamic covalent bond exchange with an excess of monomer, resulting in recovery of full-length fiber, as well as full recovery and reuse of the binder material. The process reported herein involves minimal energy input (magnetic stirring), and could be easily scaled up.

5.3 Results and Discussion

Woven carbon fiber reinforced polyimines were prepared by mixing ethanol solutions of terephthaldehyde, diethylenetriamine (DETA), and tris(2-aminoethyl)amine (TREN), in a stoichiometric ratio of 3:0.9:1.4.¹⁷ Twill weave carbon fiber cloth was introduced to the solution followed by evaporation of ethanol and curing to remove water (see Figure 5.1). The approximate binder:filler ratio used was 35:65 by weight, as composites prepared with a 50:50 ratio led to poorer mechanical performance (experimental section 5.5.3), and exhibited excessive binder flow during pressing. The resulting composite sheet exhibited a tensile strength of $399 \pm$

85 MPa a Young's modulus of 14 ± 1 GPa, and an elongation at break of $3.3\% \pm 0.6\%$. The tensile strength and modulus are each about double what is measured for self-reinforced polypropylene composites like Milliken's Tegriss[®] material (200 MPa, and 6 GPa respectively),¹⁸ or Propex's Curv[®] material (120 MPa, and 4 GPa respectively),¹⁹ while the elongation falls somewhere between that of Tegriss (5%),¹⁸ and carbon fiber-reinforced epoxies (typically <1%).²⁰

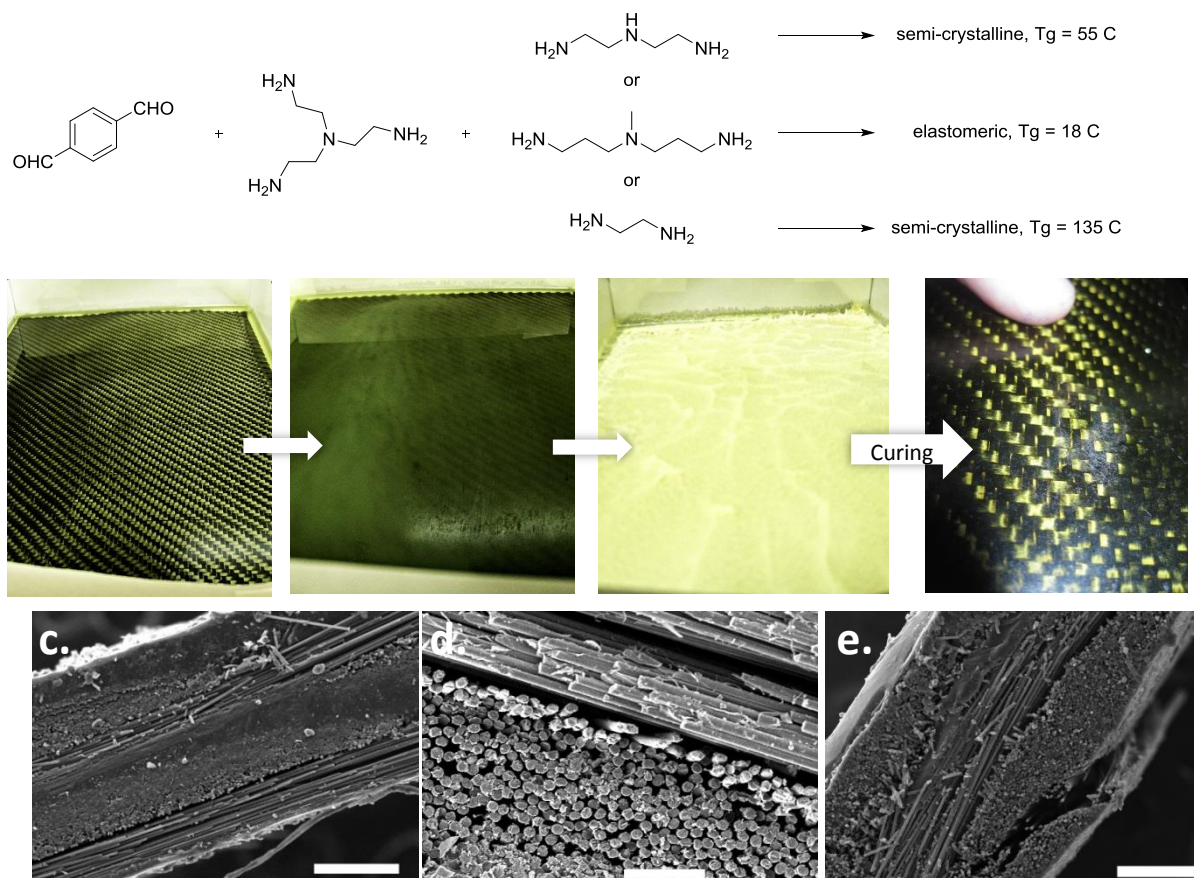


Figure 5.1 Synthesis of polyimide malleable thermosets and carbon fiber reinforced composites (CFRCs), and SEM cross-cut images of multilayer devices. **a.** Monomers used for preparation of polyimide networks. Different diamine monomers resulted in polymers with varying thermomechanical properties. Diethylene triamine (top diamine monomer) is used as a solvent to dissolve and recycle polyimide CFRC. **b.** Process of forming prototypical single ply polyimide CFRC materials used in this study. **c.** 2ply device with a total of four tows of carbon visible (two running in plane, and two tangential to the plane of this page). Running between the bottom woven layer and the top woven layer is the amorphous gray binder layer, which resulted from the binder material from each one-ply device being perfectly welded into a coherent device, scale bar = 200 μm . **d.** close-up to show fiber direction, scale bar = 50 μm . **e.** 2 layer composite after flexural failure, scale bar = 200 μm .

Given the malleability of the polyimine binder enabled by the dynamic nature of the imine bonds, we envision multi-layer CRFCs can also be obtained by simply pressing multiple single layer sheets together. As a proof-of-concept, two layers of the composite sheet were combined by simple heat pressing at 121 °C, 45 MPa, 60 s. Shorter (~30s), or longer pressing times (2-5 minutes), as well as higher temperature led to a loss in mechanical performance (see experimental section 5.5.3). Cross-cut SEM of the two-layer pressed samples (Figure 5.1c) reveals that there is no discernable interface in the binder layer sandwiched between the two woven fiber layers- indicating very efficient crosslink exchange across the interface. The mechanical properties of the two-layer samples were investigated by 3 point flexural testing, revealing a flexural strength of up to 255 ± 56 MPa, (at $1 \pm 0.2\%$ flexural strain) and a flexural modulus of 32 ± 3 GPa. The initial mechanical analysis of this system reveals that it is on-par with commercial composite materials with applications in lightweight structural components and impact-absorbing solutions for vehicles²² and ballistics protection.²³

Commercial epoxy thermosets typically require a heated curing step which is critical to forming the permanent tough covalent network. However, such step significantly slows production cycle times. The heated welding of malleable thermoset composites described above could be disruptive to traditional notions of thermoset curing. Essentially the curing step is eliminated, as the polyimine CFRC sheets are cured prior to forming multilayer devices from the single layer sheets. Because of this, the multilayer composites were formed in ~1 minute, which is the target cycle time for widespread application of carbon fiber-reinforced thermoset composite materials in the automotive industry.²⁴ In addition to the ability to weld multiple

layers of CFRC, the fully cured malleable thermoset binder can also enable reshaping and remolding of the flat woven composite sheet into 3-D curved shapes.

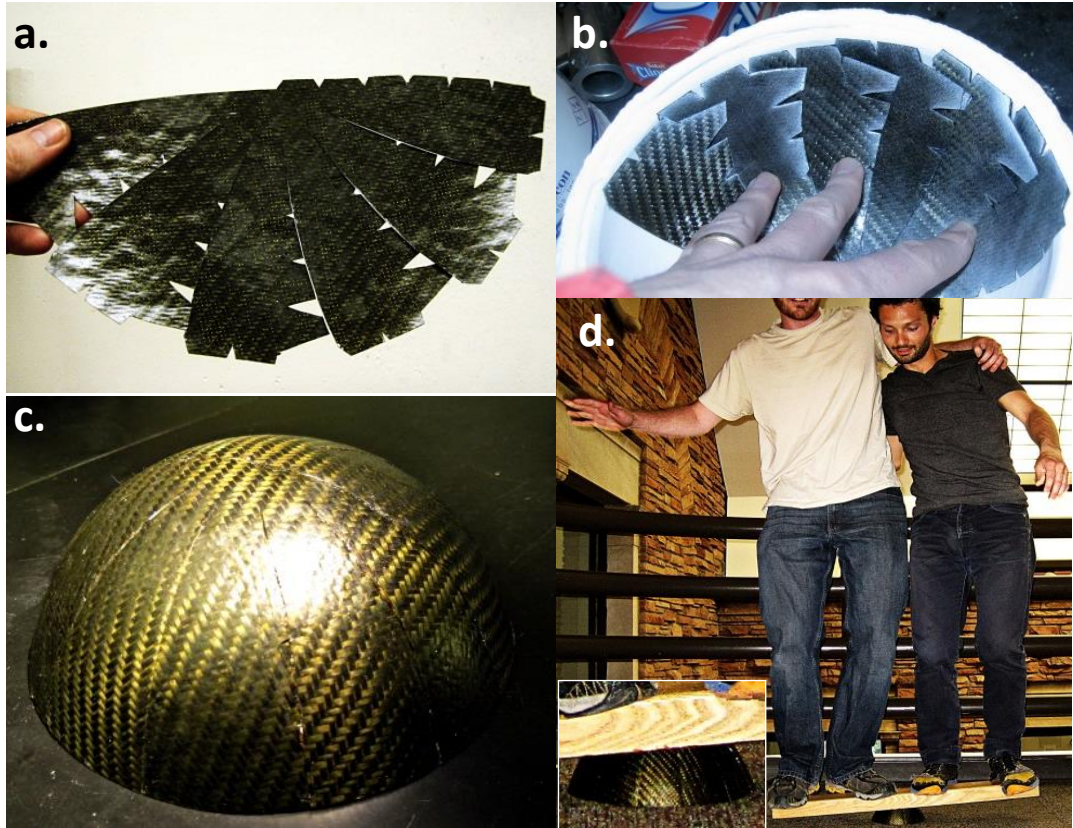


Figure 5.2 Molding of the CFRC sheet stock. **a.** Flat 50 weight % polyimine CFRC sheet is cut into pattern. **b.** Sheet is pressed into hot (1100 C) porcelain mold via vacuum molding. **c.** The process is repeated to form a hemisphere which is 3 layers thick. **d.** Molded sample from Figure 2c) is loaded with ~150 kg. Insert is close-up of CFRC hemisphere shown in Figure 2d.

For the purpose of demonstrating the moldable nature of the composite material, a dome shape was constructed from flat woven polyimine CFRC sheets. First a pattern was cut into the composite sheet to enable overlapping reinforcements. Multiple layers were combined and pressed in a hot (110 °C) porcelain mold. A vacuum bagging process was used. However, vacuum bagging only provides a maximum of 1 atm (<0.1 MPa) of pressure, which is not sufficient pressure for welding of the DETA-containing binder formulation. Therefore, another

formulation of the polyimine network, which makes use of 3,3'-diamino-*N*-methyldipropylamine in place of DETA, was developed and its thermal and mechanical properties were characterized by dynamic mechanical analysis (DMA) and differential scanning calorimetry (DSC) (experimental section 5.5.1). This polyimine exhibits a T_g of 18 °C, and shows malleable flow under low pressures. A ~0.5mm thick film of this elastomeric (180 % elongation at break) polyimine formulation was added as adhesive interlayer between each layer of composite sheet, and enabled welding of a dome shape using a hot porcelain mold and vacuum bag. Figure 5.2 shows the process as well as the resulting 3-layer (3 CFRC layers plus 2 elastomeric interlayers) hemispheric structure which exhibits smooth 3D curvature. 3-Point flexural testing showed that 2-layer composites formed using such an elastomeric interlayer have a flexural strength of 95 ± 11 MPa, and modulus of 7.3 ± 0.5 GPa, which is strong enough to bear the weight of two adults (~150 kg, see Figure 5.2 d). Even better mechanical properties can be achieved when the composite sheets are welded directly at higher pressures. The demonstrated moldable nature of the DETA-containing binder composite sheets and their effective welding condition suggest that industrial compression molding of complex curved multilayer CFRC shapes is possible with short cycle times, on the order of 1 minute.

Within a polyimine network with near-perfect stoichiometric balance among aldehyde and amine units, bond exchange reactions enable stress relaxation of the material, leading to their malleable character. Preliminary observations showed that this stoichiometric balance can be upset by introduction of an excess of free primary amine groups (e.g. excess diamine monomer). Trans-amination reactions among the excess diamine monomers and the imine-linked network can result in the introduction of end groups within the matrix, reducing the molecular weight and

solubilizing the network. We envisioned that this mechanism could enable efficient recycling of composite materials.

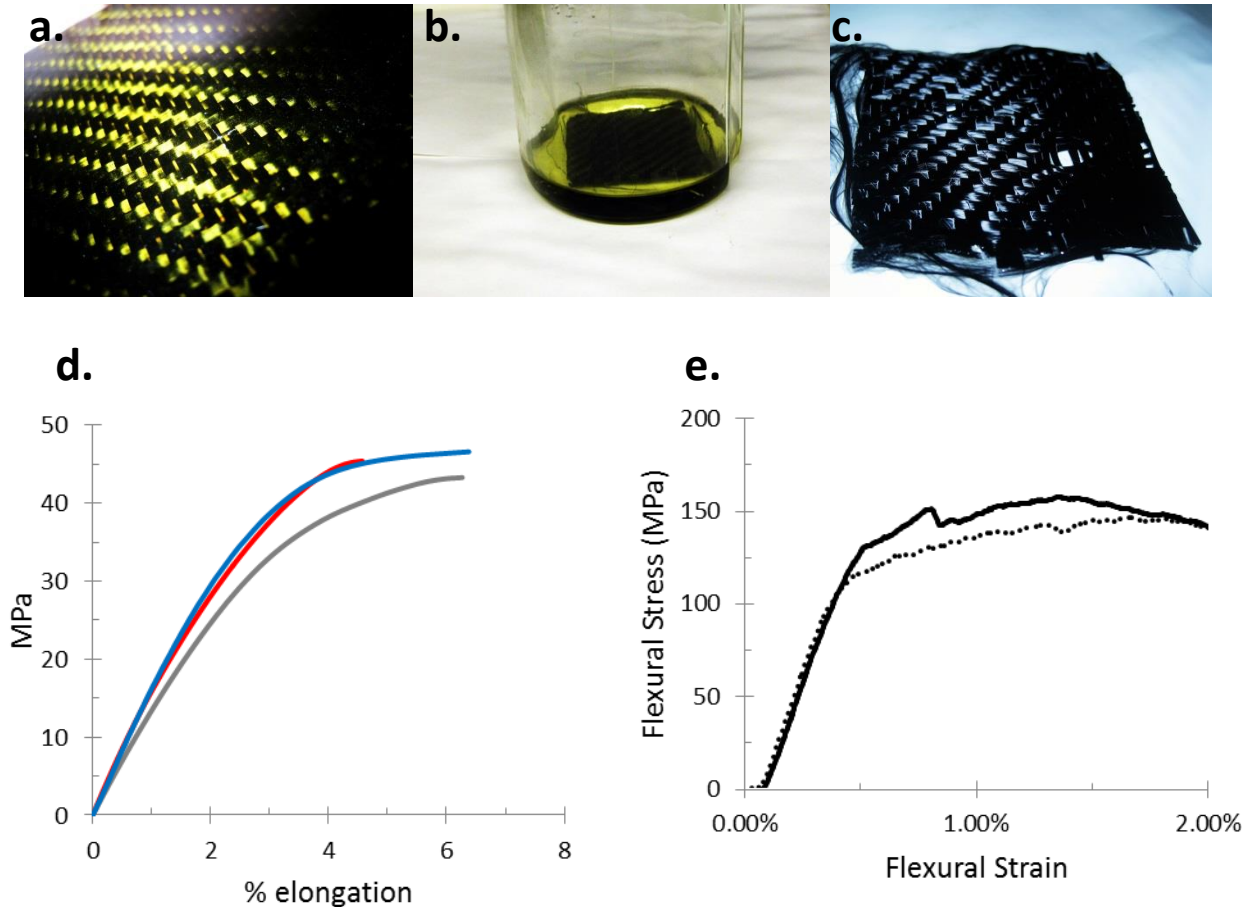


Figure 5.3 Composite recycling process. **a.** Pristine CFRC sheet containing 50 weight % network polyimine binder. **b.** CFRC immersed in neat DETA for ~24 h. Yellow color comes from dissolved polyimine oligomers. **c.** Woven carbon fiber material removed from DETA bath. **d.** Tensile testing of polyimine films: Pristine polyimine film (red line), polyimine film from neat DETA process (gray line), 33% recycled solution, 22% actual recycled content polyimine film from DETA/ethanol process. **e.** Repairing CFRC's: flexural stress vs. flexural strain of pristine 2-layer composite device (dotted line), and the same broken sample after subsequent heat-press processing (solid line).

In order to recycle the polyimine CFRC materials, we found that simply immersing composite samples in neat DETA monomer led to complete dissolution of the polyimine binder.

In this case, loose carbon fiber material could be recovered by decanting and rinsing away the

remaining binder residue with ethanol. As shown in Figure 4, in addition to preserving the fiber length, it is possible to preserve the weave of woven carbon fiber. Thus dissolving in neat monomer enables 100% of the polyimine CFRC material to be recovered and recycled without consuming chemicals or energy. We also found that less DETA was required to dissolve the binder of the CFRC when ethanol was used as a co-solvent. The solution was stirred in a screw-cap bottle following a quick flush of nitrogen gas. In this case, the ethanol-containing recycled solution was directly combined with the complementary solutions of terephthaldehyde and TREN in ethanol. In this way, recycled polymeric materials were prepared that contained greater than 33% material from the recycled monomer solution, which included some fresh DETA as solvent, and greater than 21% truly recycled content (see experimental section 5.5.4). The recycled binder shows no loss of mechanical performance compared to the freshly-prepared binder of the same formulation, as shown in Figure 5.3d.

In addition to the difficulty in recycling of traditional CFRC's, they are challenging to repair. Often, composite parts must be completely replaced when damaged as they cannot be adequately repaired. In our 3 point flexural testing, the failure mode was delamination among the binder and fiber materials (Figure 5.1e). We found that by repeating the heat pressing of the broken test samples, greater than 100% recovery of mechanical performance is achieved (Figure 5.3e). This represents a convenient mechanism for repairing damaged composite materials. Depending on the initial welding and subsequent healing conditions, the recovery of both flexural strength and modulus ranged from 85% to 107% (see experimental section 5.5.5). Broken tensile samples could not be repaired as easily as broken flexural samples, since binder flow cannot heal broken fibers (see experimental section 5.5.5).

One additional potential advantage of using malleable thermosets as the binders for advanced composite materials is the ability to control the processing temperature for a given material. Because the malleability of vitrimers is a function of reaction rate, as opposed to a melting transition (thermoplastics case), there can be greater flexibility in the processing temperatures employed. In catalyst-containing vitrimeric networks, catalyst choice and concentration can greatly affect the T_v of the materials.¹⁴ Alternatively, formulation can achieve the same end. By employing a different formulation which used ethylene diamine as the diamine linker, and a slightly different ratio of monomers, a stronger polyimine network with higher tensile strength of 64 MPa and similar Young's modulus of 0.95 GPa was developed (experimental section 5.5.2). Significantly, this material shows a higher T_g (135 °C) than the original formulation, which has a T_g of 56 °C. Use of this ethylene diamine containing binder led to composites with comparable mechanical properties (see experimental section 5.5.3), yet a 50 °C higher processing temperature (heat-press welding conditions: 45 MPa, 177 °C, 60 seconds). Such tunability in CFRC processing temperature would be highly desired for the composite fabrication targeting various applications.

5.4 Conclusion

We have demonstrated that the use of malleable polyimine networks as the binder component of woven carbon fiber composites enables an efficient closed-loop recycling process, in which all of the fiber and binder materials are recovered and can be directly reused. Further, the malleable nature of the binder enables moldable and weldable woven composite materials. We have demonstrated that fully cured flat CFRC sheets can be molded into shapes with 3 dimensional curvature, and that multilayer devices can be built up through a simple heat-pressing process which results in perfect welding of the binder across the interface. Delamination damage can be

perfectly repaired through heat-pressing. Malleable thermoset composite materials are possibly the greenest potential approach to truly recyclable thermoset composites. Further, malleable thermoset composites enable easy repair, and can remove the time-consuming curing step from manufacture of discrete parts.

5.5 Experimental Details

5.5.1 Preparation of composite materials

Diethylene triamine (DETA) formulation:

To prepare a composite sheet containing ~ 35 weight% binder, terephthaldehyde (9.5176 g, 70.9 mmol) was added to a 500 mL erlenmeyer flask followed by 400 mL ethanol and stirred for 10 minutes. Diethylene triamine (2.1967 g, 21.3 mmol) was added dropwise while stirring. The solution became translucent and yellow-to-orange in color. To a tray prepared from silicone-coated release paper (with approximate dimensions 43 cm x 25.5 cm x 2 cm) was added tris(2-aminoethyl)amine (4.8426 g, 33.1 mmol), followed by ~150 mL ethanol, or enough to cover most of the surface area of the bottom of the tray. The terephthaldehyde+DETA solution was poured into tray with gentle mixing. A single piece of twill-weave carbon fiber which was cut to fit snugly in the tray was added to the tray, and the solution allowed to evaporate in a fume hood for 24 h. The resulting uncured composite film was first heat pressed for 3 h at 78^o C, followed by 1 h at 95^o C, and finally 1 h at 105^o C using a top platen-heated hand-operated heat press under nominal pressure.

Ethylene diamine (ED) formulation:

To prepare a composite sheet containing ~ 35 weight% binder, terephthaldehyde (10.5055 g, 78.3mmol) was added to a 500 mL erlenmeyer flask followed by 400 mL ethanol and stirred for 10 minutes. Ethylene diamine (2.35 mL, 35.2 mmol) was added dropwise while stirring. The

solution became translucent and yellow-to-orange in color. To a tray prepared from silicone-coated release paper (with approximate dimensions 43 cm x 25.5 cm x 2 cm) was added tris(2-aminoethyl)amine (4.1996 g, 28.7 mmol), followed by ~150 mL ethanol, or enough to cover most of the surface area of the bottom of the tray. The terephthaldehyde+ED solution was poured into tray with gentle mixing. A single piece of twill-weave carbon fiber which was cut to fit snugly in the tray was added to the tray, and the solution allowed to evaporate in a fume hood for 24 h. The resulting uncured composite film was first heat pressed for 3 h at 78^o C, followed by 1 h at 95^o C, and finally 1 h at 105^o C using a top platen-heated hand-operated heat press under nominal pressure.

3,3'-Diamino-N-methyldipropylamine (Elastomer) formulation:

Terephthaldehyde (24.7484 g, 184 mmol) was added to a 1000 mL erlenmeyer flask followed by 800 mL ethanol and stirred for 10 minutes. 3,3'-diamino-N-methyldipropylamine (12.060 g, 83 mmol) was added dropwise while stirring. The solution became translucent and yellow-to-orange in color. To a tray prepared from silicone-coated release paper (with approximate dimensions 43 cm x 25.5 cm x 2 cm) was added tris(2-aminoethyl)amine (9.8374 g, 67 mmol), followed by ~150 mL ethanol, or enough to cover most of the surface area of the bottom of the tray. The terephthaldehyde+diamino-N-methyldipropylamine solution was poured into tray with gentle mixing. The solution was allowed to evaporate in a fume hood for 24 h. The resulting uncured elastomeric film was first heat pressed for 3 h at 78^o C, followed by 1 h at 95^o C, and finally 1 h at 105^o C using a top platen-heated hand-operated heat press under nominal pressure.

5.5.2 Characterization of polyimine films

DMA Tension test:

A dynamic mechanical analysis (DMA) machine (Model Q800, TA Instruments, New Castle, DE, USA) was used to carry out tension tests at room temperature (26^o C locally). All the samples were trimmed into a uniform size of 12 mm × 3 mm × 1.1 mm, and then stretched under a constant loading rate (2 MPa/min) until broken. Figure 5.4 gives the result of the tension tests for the two new polymer formulations reported in this work, while the stress-strain of the DETA formulation was given in Figure 4 of the main text (and was previously reported).¹⁶

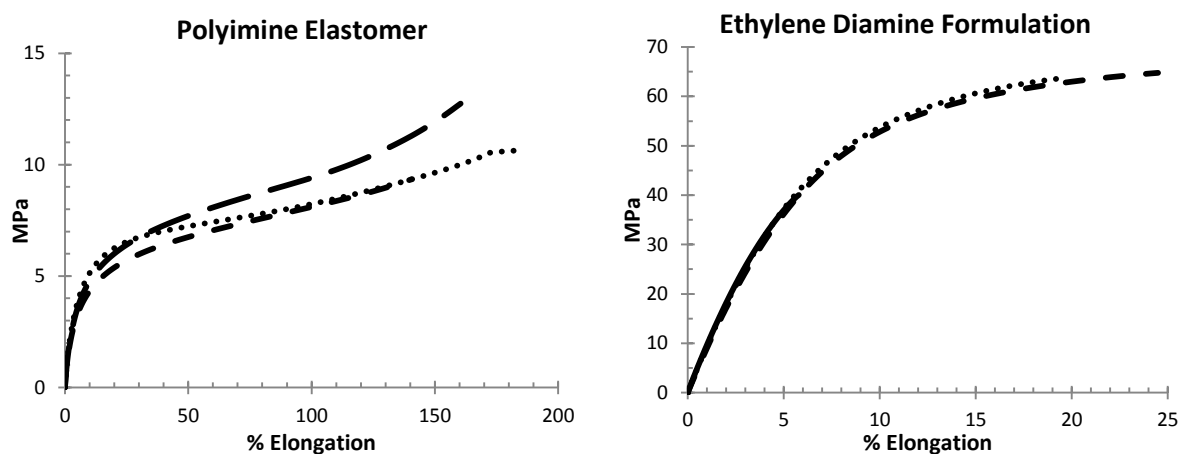


Figure 5.4 Tensile testing results for the polyimine elastomer film, and a film of the ethylene diamine formulation. 3 fresh samples of each were used for the measurement. The elastomer consistently achieved ~150% elongation at break with a final tensile strength ~10 MPa. The ethylene diamine formulation was semicrystalline with a tensile strength ~64 MPa, and an elastic modulus ~0.96 GPa.

Differential Scanning Calorimetry:

The DSC measurement was performed using a Mettler Toledo DSC823e. DSC scan was performed from 150 °C to -25 °C at a scan rate of 5 °C/min on an ED formulation film sample. The inflection point in the curve was taken to be the glass transition temperature (T_g), and was observed near 145 °C. For the elastomer formulation, the DSC scan was performed from 80 °C to -4 °C at a scan rate of 5 °C per minute. The T_g was near 10 °C. The T_g of the DETA formulation was previously reported to be ~56 °C.¹⁷

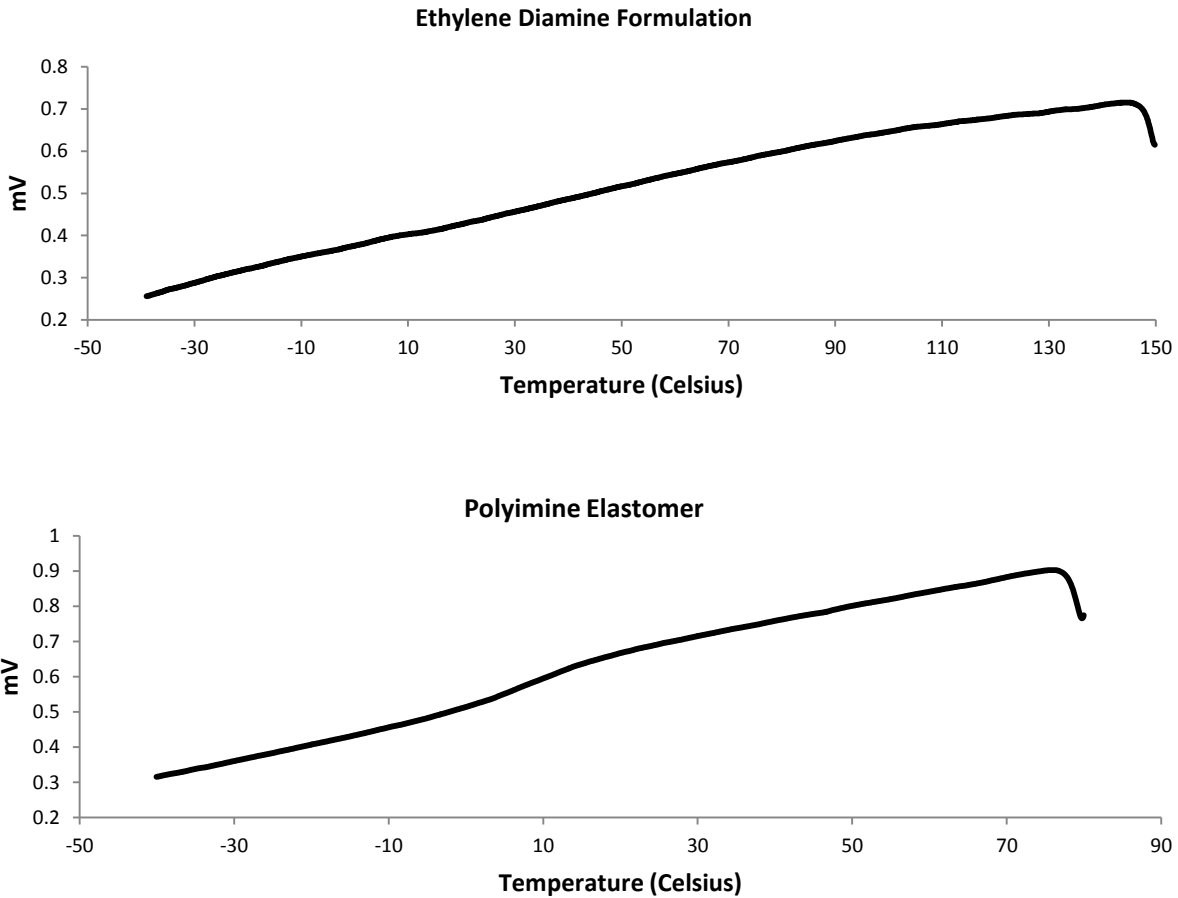


Figure 5.5 The DSC scans of the ED formulation and the elastomer formulation. Scan rate= 5 °C per minute.

DMA Stress Relaxation:

The time and temperature dependent relaxation modulus of the polyimine thermoset was also tested on the DMA machine (Model Q800, TA Instruments, New Castle, DE, USA). During the test, a polymer sample with the same dimension mentioned above was initially preloaded by 1×10^{-3} N force to maintain straightness. After reaching the testing temperature, it was allowed 30 min to reach thermal equilibrium. The specimen was stretched by 1% on the DMA machine and the deformation was maintained throughout the test. The decrease of stress was recorded and the stress relaxation modulus was calculated. Figure 5.6 depicts the results of relaxation tests at 5

different temperatures between 50 °C and 90 °C for the polyimine elastomer, and 9 different temperatures between 50 °C and 110 °C on a logarithmic plot. Then selecting 40 °C as a reference temperature (T_r), each modulus curve in the top half of Figure 5.6 was shifted horizontally to overlap with the next. This produces the master relaxation curve (not shown), which can span many decades of modulus and represents the actual relaxation behavior of the polymer within a long time scale at 40 °C. The corresponding shift factors were plotted against temperature in the bottom half of Figure 5.6. The master relaxation curve suggests that the kinetics of the bond exchange reaction-induced stress relaxation follows the well-known temperature-time superposition (TTSP) principles. To quantitatively study the relaxation behavior, we used the following definition of relaxation

Modulus:^{12-14,25}

$$\tau = \frac{1}{k} \exp\left(\frac{E_a}{RT}\right) \quad (5.1)$$

where k was a kinetic coefficient ($k > 0$) R was the gas constant with $R = 8.31446 \text{ J / Kmol}$, and E_a is the activation energy.

The shift factor, namely the ratio between the temperature-dependent relaxation time and the relaxation time at a reference temperature T_r , was therefore expressed as:

$$\alpha = \exp\left[\frac{E_a}{R} \left(\frac{1}{T} - \frac{1}{T_r}\right)\right] \quad (5.2)$$

The predicted shift factors of the relaxation curves were plotted in Figure 5.6 to compare with the experimental data. An Arrhenius-type dependence on temperature was revealed, which was consistent with what was previously reported for the DETA formulation. By further examination of Equation 5.2 we found that in the semi-log scale, the energy barrier could be determined by

the slope of the shift factor curve. As shown in Figure 5.6, by measuring the curve slope, the energy barrier E_a was calculated to be 33.5 kJ/mol for the polyimine elastomer, and 129 kJ/mol for the ethylene diamine formulation.

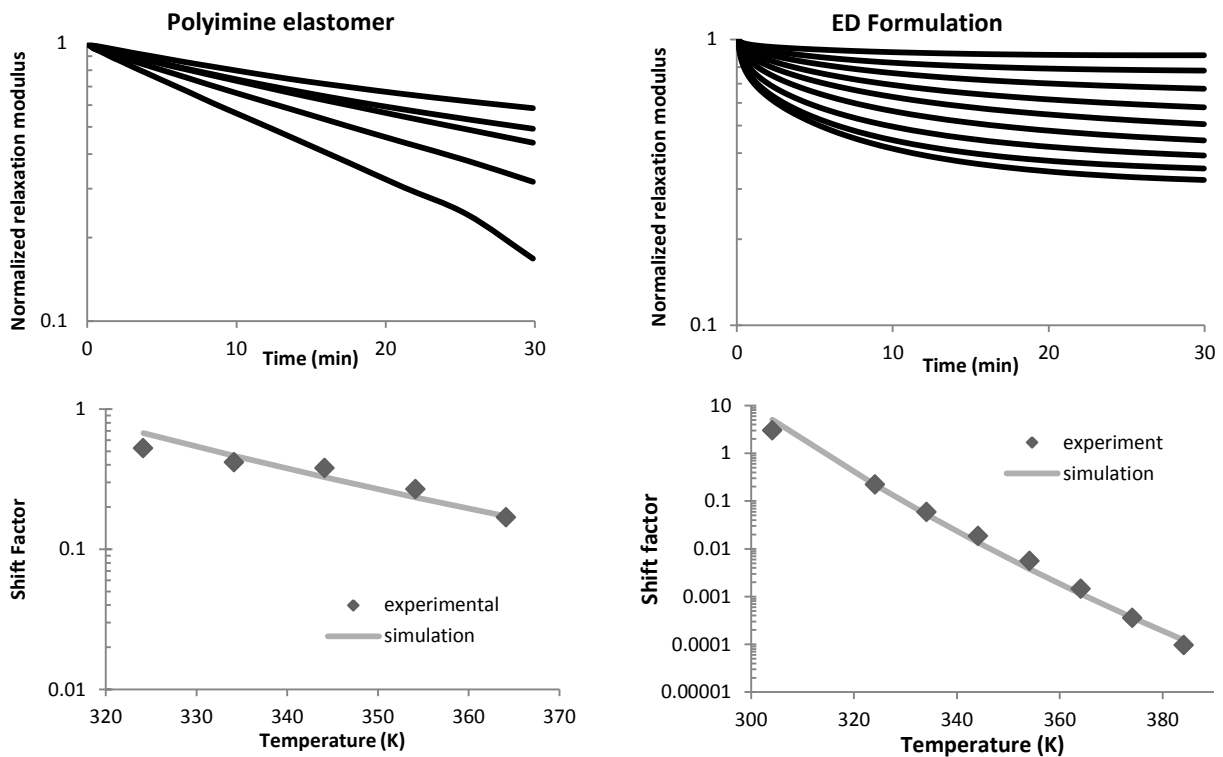


Figure 5.6 Stress-relaxation data for polyimine elastomer and ethylene diamine formulations. The plot of log of shift factors vs temperature most closely matches the arrhenius plot of an activation energy $E_a= 33.5$ kcal/mol for the elastomer, and 129 kcal/mol for the ethylene diamine formulation.

5.5.3 Mechanical testing of composite materials

Flexural and tensile testing of composite materials was performed on an Instron 5800 twin screw mechanical testing instrument with an *Inston 5869* static load cell ± 50 kN and data collected using bluehill 2 software.

3 pt. flexural testing of composite materials:

During the test, samples were prepared by heat-pressing 2 pieces of single-ply polyimine-CFRC material using a PHI (City of Industry, CA) model: Q240H-X6 hand-operated hydraulic heat press for 1 minute at 121 °C and 45 MPa. The sample size was 25 mm x 10 cm. The thickness of each sample was measured using a digital caliper with .01 mm precision. The support span

was 50.8 mm. The rate of crosshead motion was determined individually for each sample according to Equation 5.3 below (ASTM, D790-10, 2010):

$$R=ZL^2/6d \quad (5.3)$$

where R was the rate of crosshead motion in mm/min, Z was equal to 0.01, L was the support span in mm, and d was the thickness of the sample in mm. Flexural stress was calculated from force and position data according to Equation 5.4 below:

$$\sigma_f=(3FL)/(2bd^2) \quad (5.4)$$

where σ_f was flexural stress in MPa, F was force in N, and b was width of beam in mm.

Flexural strain was calculated from force and position data according to Equation 5.5 below:

$$\varepsilon_f=(6Dd)/(L^2) \quad (5.5)$$

where ε_f was flexural strain, and D was deformation in mm. Flexural modulus was calculated using Equation 5.6 below:

$$E_f=(L^3m)/(4bd^3) \quad (5.6)$$

Where E_f was the flexural modulus in MPa, and m was the initial slope in N/mm.

Flexural testing results were summarized below in Figure 5.7 below.

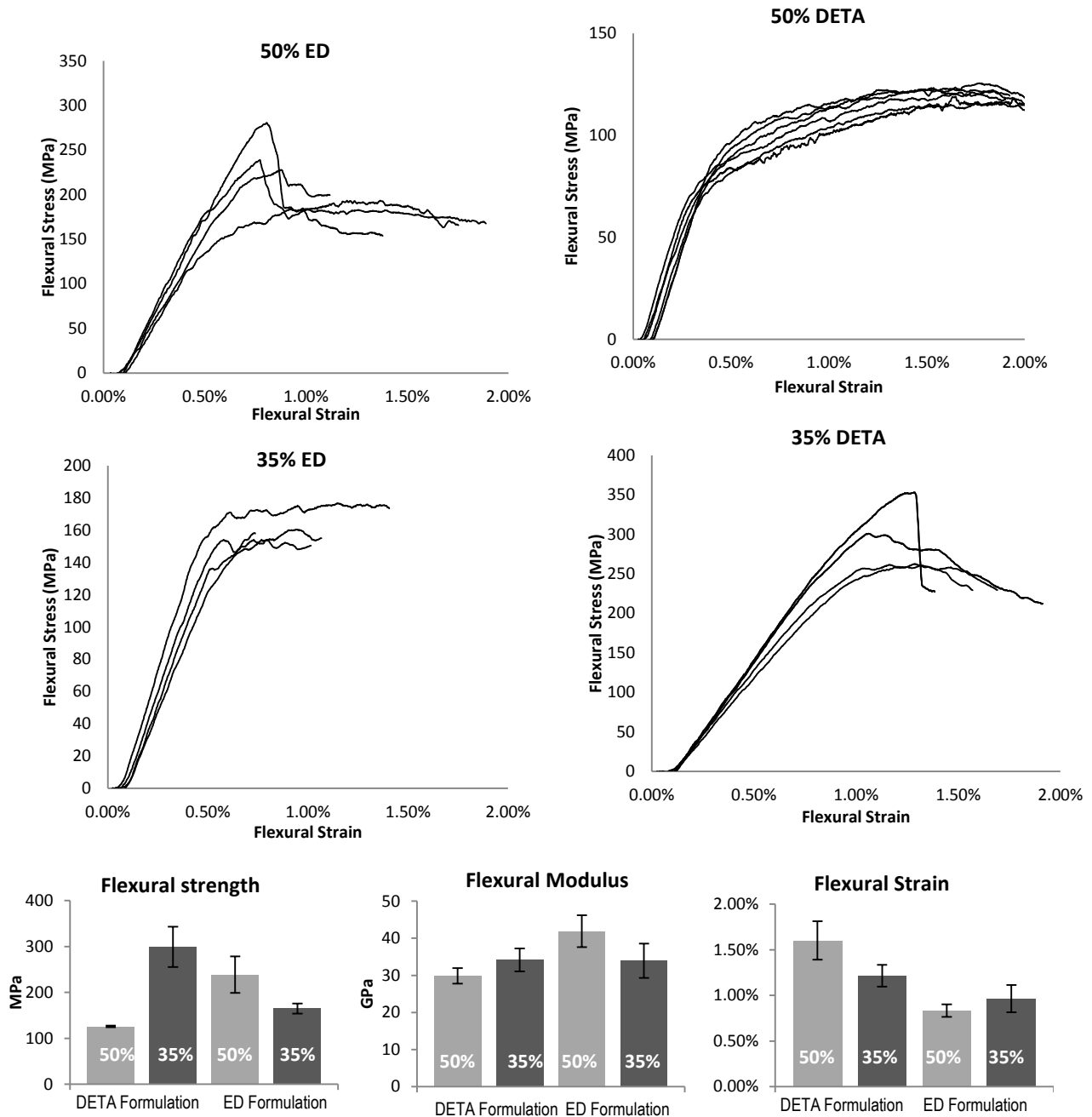


Figure 5.7 The 3-point flexural testing results were displayed as raw data above, and summarized in the three charts below. *Flexural strength*: DETA 50/50 binder-to-filler ratio= 142 ± 39 MPa; 35/65 binder-to-filler ratio= 255 ± 56 MPa; ED 50/50 binder-to-filler ratio= 184 ± 54 MPa; 35/65 binder-to-filler ratio= 147 ± 18 MPa. *Flexural modulus*: DETA 50/50 binder-to-filler ratio= 35 ± 14 GPa; 35/65 binder-to-filler ratio= 32.4 ± 3.7 GPa; ED 50/50 binder-to-filler ratio= 38.1 ± 5.1 GPa; 35/65 binder-to-filler ratio= 32.5 ± 4.4 GPa. *Flexural strain*: DETA 50/50 binder-to-filler ratio= $1.6\% \pm 0.2\%$; 35/65 binder-to-filler ratio= $1.0 \pm 0.2\%$; ED 50/50 binder-to-filler ratio= $0.9\% \pm 0.3\%$; 35/65 binder-to-filler ratio= $0.9 \pm 0.3\%$.

Tensile testing of the composite materials:

Flexural and tensile testing of composite materials was performed on an Instron 5800 twin screw mechanical testing instrument with a 5869 static load cell (± 50 kN) and data collected using bluehill software. Both one- and two-ply composite samples were tested. The two-ply samples were prepared by pressing as previously described. The sample size for the tensile tests was 12 mm x 100 mm, and the thickness of each sample was measured using a digital caliper as mentioned above. The rate of crosshead motion for the tensile testing was 5 mm/min and the gauge length was 30 mm. The results of the tensile testing were summarized in Figure 5.8 below.

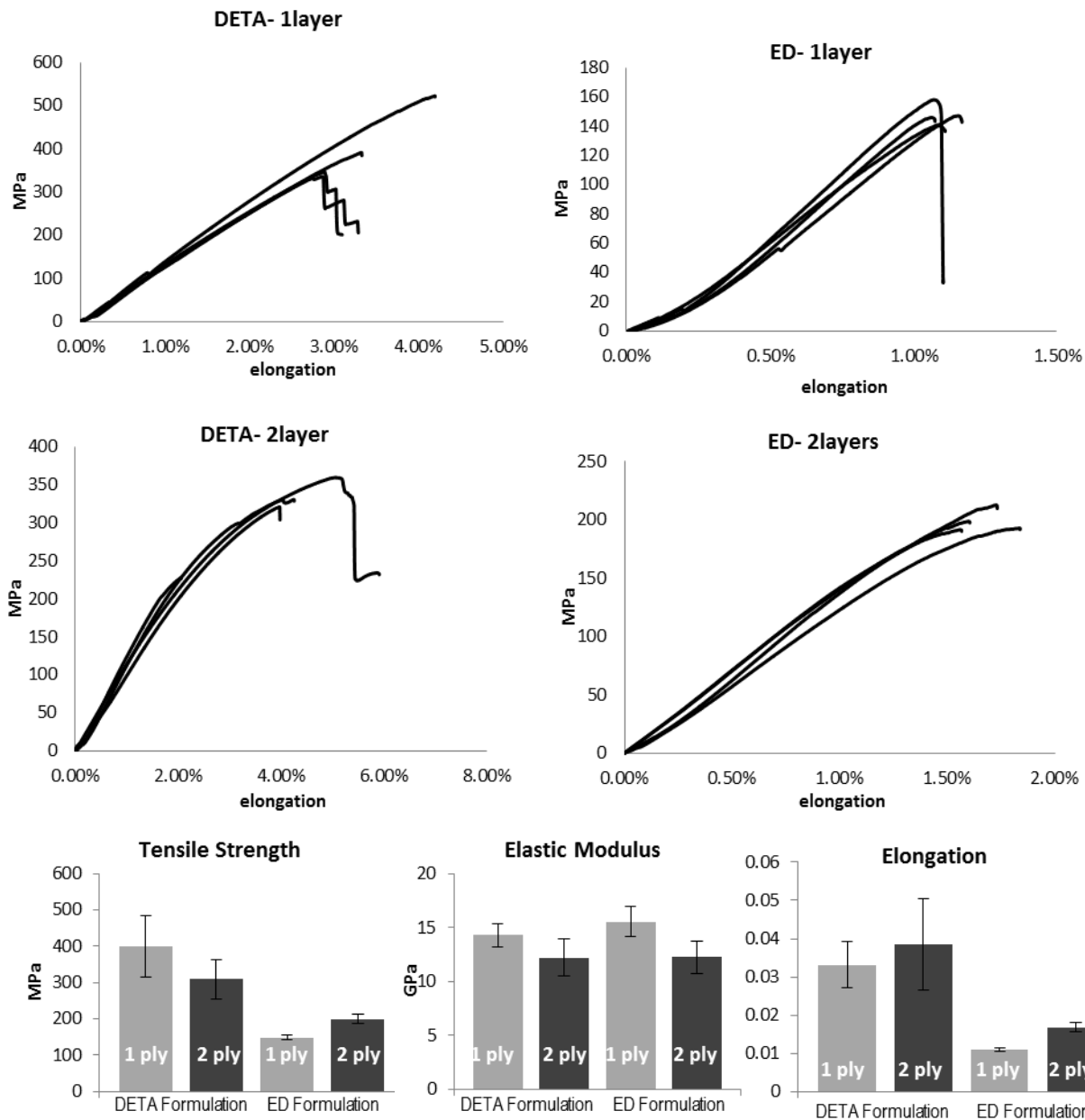


Figure 5.8 The tensile testing results were displayed as raw data above, and summarized in the three charts below. *Tensile strength*: DETA 1 ply = 399 ± 85 MPa; 2 ply = 309 ± 57 MPa; ED 1 ply = 148 ± 7 MPa; 2 ply = 198 ± 9 MPa. *Elastic modulus*: DETA 1 ply = 14.2 ± 1.1 GPa; 2 ply = 12.2 ± 1.7 GPa; ED 1 ply = 15.5 ± 1.4 GPa; 2 ply = 12.2 ± 1.5 GPa. *Elongation at break*: DETA 1 ply = 3.3% ± 0.6%; 2 ply = 3.8 ± 1.2%; ED 1 ply = 1.0% ± 0.04%; 2 ply = 1.6 ± 0.1%.

5.5.4 Recycling of composite materials

NEAT recycling:

As a proof of concept, initially n-propyl amine was added to a sample of 50% binder content DETA formulation CFRC sheet. Within 1 hr, the fibers were floating loosely in the solution as

all of the polyimine binder material had been dissolved. Next, DETA (6.49 g 62.9 mmol) was added to 50 wt% polyimine CFRC (1.298 g) in a 20 mL screw-cap glass vial, and the cap was tightened. After 24 h under ambient conditions, the fiber materials were floating loosely in a homogeneous solution (similar to Figure 2b of the main text). The monomer solution was decanted, and collected in another 20 mL vial. To prepare a recycled polyimine film, the above solution containing monomer (1 g solution, approximate content: DETA ~0.923g, 9 mmol; terephthaldehyde ~0.062 g, 0.6 mmol; TREN ~.031g, 0.2 mmol) was added dropwise to a vial containing terephthaldehyde (3.939 g, 29.3 mmol), and ethanol (~15 mL), while stirring. To a silicone-lined paper tray measuring ~ 10 cm x 10 cm x 2 cm was added TREN (2.004 g, 13.7 mmol) followed by the solution of terephthaldehyde, and recycled monomers in ethanol. After mixing, the solution was left to evaporate overnight followed by curing as described above. The resulting film was submitted to tensile testing using the DMA instrument as described above, and the result was shown in Figure 3 of the main text. The total weight of the cured film was 5.5 g. Approximately 18 % (at least 0.964 g of the 5.5 g, assuming complete curing of the film) of the composition of the final film would have come from the recycled monomer solution, yet only 1.7% (~0.091 g of the 5.5g) came from binder material in the original composite.

Recycling with ethanol as co-solvent:

CFRC material (2.807 g) containing 50% binder DETA formulation was added to a glass jar with a plastic screw lid. DETA (0.741 g, 7.17 mmol) was added followed by degassed ethanol (50 mL), and a magnetic stirbar. The jar was flushed with a stream of nitrogen gas, and the lid was closed and sealed with parafilm. The mixture was stirred for 24 h at 300 rpm, and the solution decanted. The fibers were wrung out and rinsed with ethanol- which was collected and added to the recycled solution. The fibers were dried under vacuum at 150⁰ C for 30 min and weighed to

be 1.505 g. The approximate volume of the recycled solution was measured to be 35.5 mL by pouring the solution into a 100 mL graduated cylinder. The concentrations of terephthaldehyde, TREN and DETA in the recycled solution were determined to be 186 mM, 87 mM, and 258 mM respectively. A portion of the recycled solution (20 mL, approximate content: DETA~ 0.52 g, 5.2 mmol; terephthaldehyde~ 0.38 g, 3.7 mmol; TREN~ 0.24 g, 1.7 mmol) was added to a suspension of terephthaldehyde (1.808 g, 13.5 mmol) in ethanol (~ 15 mL) while stirring. To a silicone-lined paper tray (~ 10 cm x 10 cm x 2 cm) was added TREN (0.92 g, 6.3 mmol) followed by the above solution of terephthaldehyde and recycled monomers in ethanol. After mixing, the solution was left to evaporate overnight followed by curing as described above. The resulting film was submitted to tensile testing using the DMA instrument as described above, and the result was shown in Figure 3 of the main text. The total weight of the cured film was 3.406 g. Approximately 33 % (at least 1.133 g of the 3.406 g assuming complete curing of the film) of the composition of the final film would have come from the recycled monomer solution and 21% (~0.732 g of the 3.406 g) of the composition of the final film would have come from material in the original composite binder.

5.5.5 Repairing of composite materials

Repairing after flexural failure:

In order to test the reparability of the polyimine CFRC materials subsequent to delamination damage, 2-ply samples (prepared as above from 35% binder polyimine CFRC sheets) were first submitted to flexural testing until broken, and subsequently repressed according to their original pressing conditions. For this study, two temperatures and 3 times were chosen, and 3 samples were tested under each condition. The results were summarized in Figure 5.9 below. As can be

seen, the initial mechanical properties were best when pressed for 1 minute at 121^o C (45 MPa). Longer times and higher temperature conditions resulted in lower initial flexural strength and modulus, but a greater recovery of properties upon re-press.

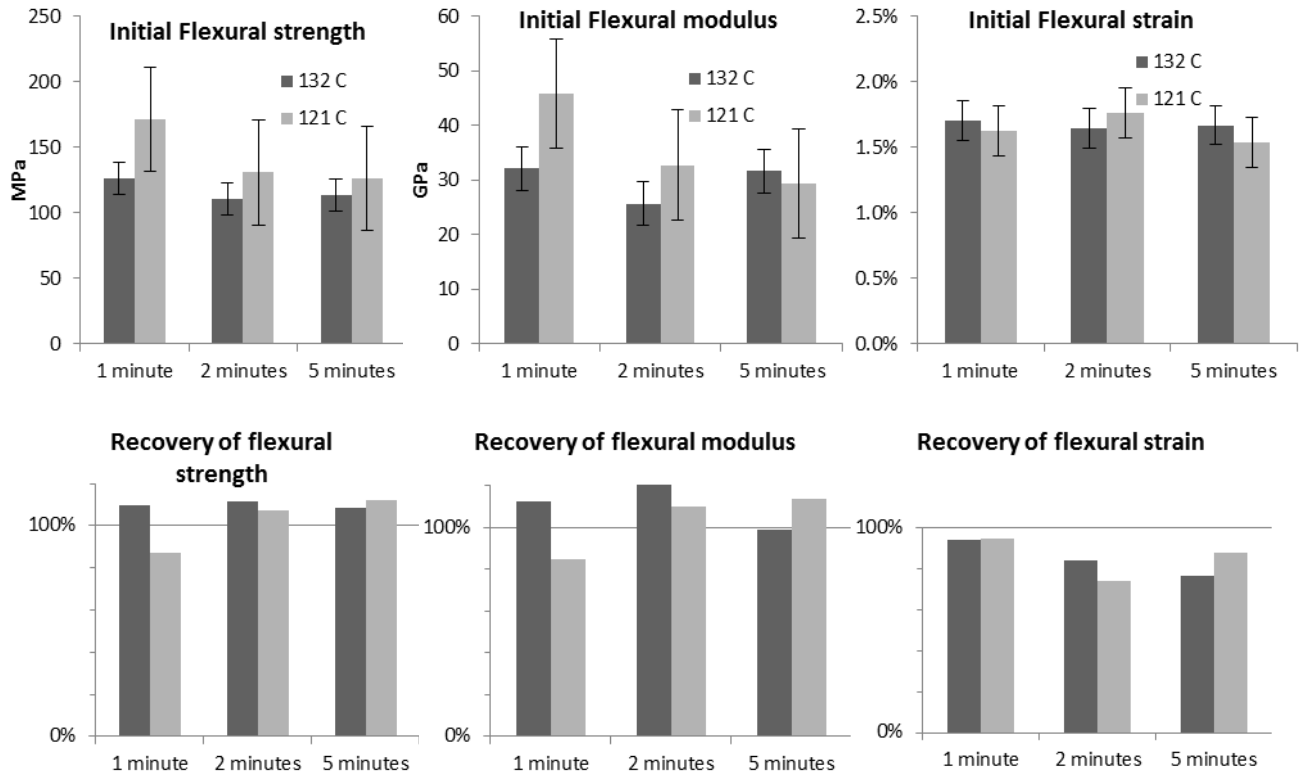


Figure 5.9 Flexural properties as a function of pressing conditions, and the recovery of those properties upon re-pressing. Samples pressed at 132 °C were shown in dark-gray, and samples pressed at 121 °C were shown in light-gray.

Repairing after tensile failure:

Similarly 2-layer tensile samples were re-pressed after testing according to their original condition of 121 °C, 1 minute, 27 metric tons. After subsequent tensile testing, a “patch” was used to repair the material by pressing a piece of 1 ply CFRC sheet (measuring 12 mm x 25 mm) over the broken area of the sample. The statistical data was summarized below in Figure 5.10.

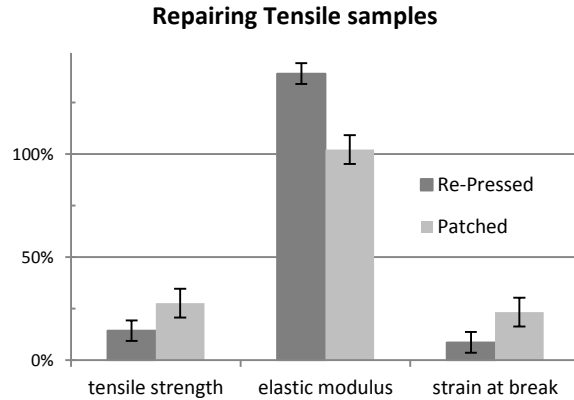


Figure 5.10 Summary of the attempts at repairing the samples broken during tensile testing both through heat pressing, and patching. Four samples of each type were tested. The % recovery was calculated for each sample individually, and the average and standard deviation were shown. For the re-pressed samples, $14\% \pm 6\%$ of tensile strength, $139\% \pm 17\%$ of elastic modulus, and $8\% \pm 4\%$ of strain at break were recovered. For the patched samples, $27\% \pm 7\%$ of tensile strength, $102\% \pm 25\%$ of elastic modulus, and $23\% \pm 3\%$ of strain at break were recovered.

5.5.6 Vacuum forming polyimine CFRC sheets into 3D curvature:

A negative hemispheric porcelain mold with an approximate inner diameter of 16.5 cm was prepared by slip casting over a plaster of Paris positive. The mold was fired to $\Delta 6$ to ensure thermal dimensional stability during molding. 2 semicircular patterns (as shown in Figure 2a) were stenciled onto and then cut from 50/50 DETA CFRC sheet. The pattern was photocopied at 98% and 95% its original size to form new stencils which were each cut from 50/50 DETA CFRC sheets. To the two larger sets of patterned sheets, a layer of polyimine elastomer was bonded by heat pressing under nominal pressure at $100\text{ }^\circ\text{C}$ for 1 minute. Each individual patterned sheet was pre-shaped into the heated mold using hand pressure for 3 minutes as illustrated in Figure 2b. For the pre-shaping and the final molding, the porcelain mold was heated in an oven at $110\text{ }^\circ\text{C}$ for 1 hour before being removed for molding. The two largest patterned sheets were placed CFRC-side down into the hot mold such that all overlapping flaps were facing the surface. A piece of cotton fabric was placed loosely over the assembly and then

moved into a Space-saver™ vacuum bag (purchased from Target™). Vacuum was applied for 30 seconds then the seal was closed for 10 minutes. This process was repeated to add the other two CFRC sandwich layers to the molded shape. The final object was removed from the mold, and the edge was trimmed using a dremmel tool with a diamond blade to give the object pictured in Figure 2c-d. Inclusion of the elastomer layers separating the composite sheets allowed for lower temperature and pressure welding conditions, but results in different mechanical properties than the multilayer composite material. To characterize the properties of the sandwich composite, flexural testing was performed.

3 pt. flexural characterization of elastomer sandwich composites:

3 point flexural samples of elastomer sandwich composites were prepared by pressing 2 samples of 50/50 DETA formulation composite on either side of a sample of polyimine elastomer film. The pressing conditions were 100 °C, 1 minute, 45 MPa. The sample dimensions were 25 mm x 100 mm, and the thickness of each sample was carefully measured using a digital caliper. The flexural testing was conducted in the manner described above, and the results were summarized in Figure 5.11 below.

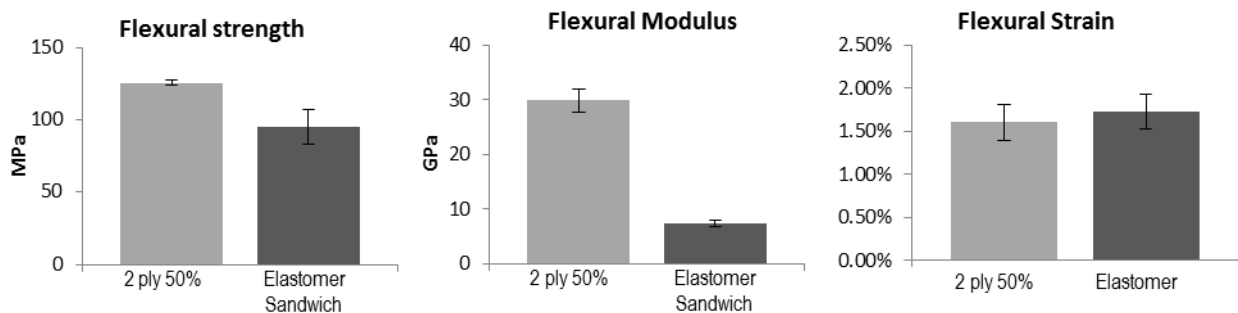


Figure 5.11 The flexural testing revealed that the elastomer sandwich design resulted in a much lower flexural modulus while the flexural strength, and strain values were similar to the case of no elastomer layer. Elastomer sandwich composite: flexural strength = 95 ± 11 MPa, flexural modulus = 7.3 ± 0.5 GPa, flexural strain = $1.7\% \pm 0.3\%$.

5.6 References

- [1] P. Naik, A. O. Surendranathan and N. V. Londe, "A study on carbon fiber reinforced carbon composites for structural applications," *International Journal of Engineering Science and Technology*, vol. 3, no. 5, pp. 3670-3675, 2011.
- [2] C. Red, "Market Outlook: Carbon fiber in sporting goods," *High Performance Composites*, 1 January 2008.
- [3] R. Miel, "Carbon fiber continues its auto growth," *Plastics News*, 17 January 2014.
[Online]. Available:
<http://www.plasticsnews.com/article/20140117/NEWS/140119938/carbon-fiber-continues-its-auto-growth>. [Accessed 15 July 2015].
- [4] G. Oliveux, L. O. Dandy and G. A. Leeke, "Current status of recycling of fibre reinforced polymers: Review of technologies, reuse and resulting properties," *Progress in Materials Science*, vol. 72, pp. 61-99, 2015.
- [5] S. J. Pickering, "Recycling technologies for thermoset composite materials- current status," *Composites Part A: Applied Science and Manufacturing*, vol. 37, no. 8, pp. 1206-1215, 2006.
- [6] S. Pimenta and S. Pinho, "Recycling carbon fibre reinforced polymers for structural applications: technology review and market outlook," *Waste management*, vol. 31, no. 2, pp. 378-392, 2011.
- [7] J. Palmer, O. R. Ghita, L. Savage and K. E. Evans, "Successful closed-loop recycling of thermoset composites," *Composites Part A: Applied Science and Manufacturing*, vol. 40, no. 4, pp. 490-498, 2009.
- [8] S. Pastine, "Can epoxy composites be made 100% recyclable?," *Reinforced Plastics*, vol. 56, no. 5, pp. 26-28, 2012.
- [9] C. Morin, A. Loppinet-Serani, F. Cansell and C. Aymonier, "Near- and supercritical solvolysis of carbon fibre reinforced polymers (CFRPs) for recycling carbon fibres as a valuable resource: state of the art," *Journal of Supercritical Fluids*, vol. 66, pp. 232-240,

2012.

- [10] J. S. Park, T. Darlington, A. F. Starr, K. Takahashi, J. Riendeau and H. T. Hahn, "Multiple healing effect of thermally activated self-healing composites based on Diels-Alder reaction," *Composites Science and Technology*, vol. 70, no. 15, pp. 2154-2159, 2010.
- [11] M. Q. Zhang and M. Z. Rong, "Intrinsic self-healing of covalent polymers through bond reconnection towards strength restoration," *Polymer Chemistry*, vol. 4, pp. 4878-4884, 2013.
- [12] M. Capelot, M. Unterlass, F. Tournilhac and L. Leibler, "Catalytic Control of the vitrimer glass transition," *ACS Macro Letters*, vol. 1, no. 7, pp. 789-792, 2012.
- [13] D. Montarnal, M. Capelot, F. Tournilhac and L. Leibler, "Silica-like malleable materials from permanent organic networks," *Science*, vol. 334, no. 6058, pp. 965-968, 2011.
- [14] M. Capelot, D. Montarnal, F. Tournilhac and L. Leibler, "Metal-catalyzed transesterification for healing and assembling of thermosets," *Journal of the American Chemical Society*, vol. 134, no. 18, pp. 7664-7667, 2012.
- [15] K. Yu, P. Taynton, W. Zhang, M. Dunn and H. J. Qi, "Reprocessing and recycling of thermosetting polymers based on bond exchange reactions," *RSC Advances*, vol. 4, no. 20, pp. 10108-10117, 2014.
- [16] C. Bowman and C. Kloxin, "Covalent Adaptable Networks: Reversible Bond Structures Incorporated in Polymer Networks," *Angewandte Chemie International Edition*, vol. 51, no. 18, pp. 4272-4274, 2012.
- [17] P. Taynton, K. Yu, R. Shoemaker, Y. Jin, H. J. Qi and W. Zhang, "Heat- or Water-Driven Malleability in a Highly Recyclable Covalent Network Polymer," *Advanced Materials*, vol. 26, no. 23, pp. 3938-3942, 2014.
- [18] S. Valluri, S. Sankaran and P. Mallick, "Tensile and Fatigue Performance of a Self-Reinforced Polypropylene," in *Society of Plastics Engineers- Automotive Composites Conference and Exhibition*, Troy, MI, 2010.
- [19] Propex Inc., "Curv technical analysis," Propex Inc., [Online]. Available: www.curvonline.com/products/analysis.html. [Accessed 15 July 2015].
- [20] G. Kretsis, "A review of the tensile, compressive, flexural and shear properties of hybrid fibre-reinforced plastics," *Composites*, vol. 18, no. 1, pp. 13-23, 1987.

- [21] A. Kmetty, T. Barany and J. Karger-Kocsis, "Self-reinforced polymeric materials: A review," *Progress in Polymer Science*, vol. 35, no. 10, pp. 1288-1310, 2010.
- [22] H. Hayes, "Self-Reinforced Polypropylene Composites - A New Class of Material for the Motorsports Industry," *SAE Technical Paper 2008-01-2947*, Vols. doi:10.4271/2008-01-2947.
- [23] Milliken & Co., "Introducing: Tegril/Aramid hybrid Fabric," [Online]. Available: http://tegril.milliken.com/en-us/technology/Documents/Tegril_Aramid_Hybrid_Fabric.pdf. [Accessed 12 July 2014].
- [24] J. Sloan, "Auto composites quest: One-minute cycle time?," *Composites Technology*, 2012 August 2012.
- [25] R. H. Long, H.J. Qi and M. L. Dunn, "Modeling the mechanics of covalently adaptable polymer networks with temperature-dependent bond exchange reactions." *Soft Matter*, vol. 9, p. 4083, 2013.

CHAPTER 6

Ultrathin solid-state Li-ion electrolyte membrane facilitated by a self-healing polymer matrix

(Manuscript recommended for publication under same title in *Advanced Materials*. Coauthored with: Whitely, J.; Zhang, W.; Lee, S.H.)

6.1 Abstract

Emergent technologies are driving iterations of the lithium-ion battery to exhibit enhanced safety and higher temperature capabilities.¹ The commercial lithium-ion battery remains relatively unchanged since its inception in 1991. As such, it would be challenging to adopt the current liquid electrolyte system of LiPF₆ dissolved in EC/DEC solvents for safety concern due to flammability.² Batteries encompassing inorganic solid electrolytes, known as solid-state batteries, have attracted significant attention in recent years due to lithium ion conductivities matching liquids yet still maintaining a lithium transference number of unity.³⁻⁴ With commercial deployment rapidly approaching, most solid-state research focuses on electrode compositions or electrolyte chemistries.^{5,6} Few reports emphasize the engineering issues in the design of an all-solid-state battery, often reworking the solid system to mimic processing of a liquid-based system.⁷ However, solids present vastly different mechanical and fundamental properties. Novel processes and approaches must be employed if solid electrolyte batteries are to be advanced to commercial viability.

6.2 Introduction

Liquid electrolyte systems have the inherent advantage of maintaining intimate contact with electrode materials. A successful solid electrolyte must likewise conform its surface to establish close contact with electrode surfaces.⁸ There are two main classes of inorganic, solid, lithium electrolytes: oxides and sulfides. Oxide electrolytes, while maintaining stability in air, suffer from a lack of compatibility with standard electrode materials, require sintering at elevated temperatures, and possess high charge transfer resistances due to poor electrolyte-electrode contact.⁹ Oxide electrolytes tend to exhibit shear moduli of greater than 50 GPa. Intimate contact with battery materials is therefore precluded due to the lack of plastic deformation under stress.¹⁰ On the other hand, the sulfide family of solid electrolytes, such as $\text{Li}_{10}\text{MP}_2\text{S}_{12}$ crystals and $\text{Li}_2\text{S-P}_2\text{S}_5$ glass-ceramics, have lithium ion conductivities comparable to liquid electrolytes, can be simply processed by cold-compacting the powders, and exhibit ductile-like mechanical properties.^{3,11-12]} Thus, the present study makes use of the sulfide family of solid electrolytes, namely the “a77.5” $77.5\text{Li}_2\text{S} - 22.5\text{P}_2\text{S}_5$ glass-ceramic.

Assembly of laboratory bulk solid-state cells occurs by applying high pressures to the powder forms of the cathode, electrolyte, and anode thus forming a tri-layer pellet.¹³ Due to the brittle nature of the materials being used, if the separator layer is less than approximately 1 mm, cracking tends to develop through the pellet, rendering the cell useless.¹⁴ Limited research has focused on reducing this layer thickness while maintaining a bulk configuration (non-thin film battery). PLD and CVD have been used to deposit thin solid films demonstrating excellent cycling performance;¹⁵ high vacuum deposition techniques, however, are extremely expensive and do not present a scalable process for commercial development of the solid-state battery. A few studies were identified introducing the classic process of a polymeric binder to the inorganic solid.¹⁶ In doing so, the polymer acts to coat the electrolyte particles impeding interparticle

contact, requires a substrate to coat on negating free-standing applications, and doesn't allow absolute density which hinders electrode performance.

Therefore, an optimal method of processing a solid-state battery would encompass a cheap, scalable process, one that doesn't impede the conduction capabilities, and the materials used should be mechanically pliant to suppress cracking. In this work we report a new method of developing a solid electrolyte-in-polymer matrix (SEPM) to form our electrolyte layer. This method takes advantage of the fact that the solid electrolyte pellet is about 15% porous in the green body state.¹⁷ By filling empty voids with an organic polymer, we can create a cross-linked polymer matrix *in situ* to provide mechanical robustness while preserving lithium ion transport pathways in between solid electrolyte particles. Using a newly derived malleable thermoset polymer paired with a $\text{Li}_2\text{S-P}_2\text{S}_5$ inorganic electrolyte, we produce a stand-alone membrane of 64 μm in thickness, high active material loading (80%), and near theoretical density. The membrane performs on par with traditionally prepared solid-state batteries yet has increased the gravimetric and volumetric cell energy densities by an order of magnitude. The processing of our SEPM is completely dry representing not only a new method of processing for batteries, but a technique to form other composites such as high mass-loading mixed matrix membranes.

6.3 Results/discussion

Membranes based on the traditional thermoplastic polymers suffer from active material agglomeration and sedimentation.¹⁸ Additionally, the melt-flow behavior of thermoplastic polymers leads to highly resistive surface coatings that inhibit interparticle conductive contact. Thermoset materials, which must be cured *in situ*, exhibit the same drawbacks as the thermoplastic. Recent advances in polymer chemistry have led to the development of malleable covalent network polymers, often called vitrimers. Vitrimers are capable of stress-relaxation and

flow due to dynamic covalent bonding of reversible crosslinks within the network. Network polyimines were used in this study: they are simple to prepare (one step from commercially available monomers), and contain no metal catalysts, which could demonstrate undesired redox activity.¹⁹ Figure 6.1a represents the SEPM concept. Starting in a bulk powder form, and taking advantage of the malleable properties of the polyimine, our hot iso-static press will theoretically form a continuous cross-linked network interspersed between the voids of the glass-ceramic solid electrolyte. The malleability of polyimines allows for material flow to increase the density of the composite, and instill mechanical toughness, with a minimal impact on the ionic conductivity of the electrolyte. This process does not preclude interparticle contact of the solid electrolyte particles as only a few domains of polymer are introduced. This stands in stark contrast to polymeric binders used in solution processes; these act to coat all surfaces of each individual solid electrolyte particle. Figure 1b is an image of a prepared SEPM membrane approximately 100 μm in thickness with 80% mass loading solid electrolyte.

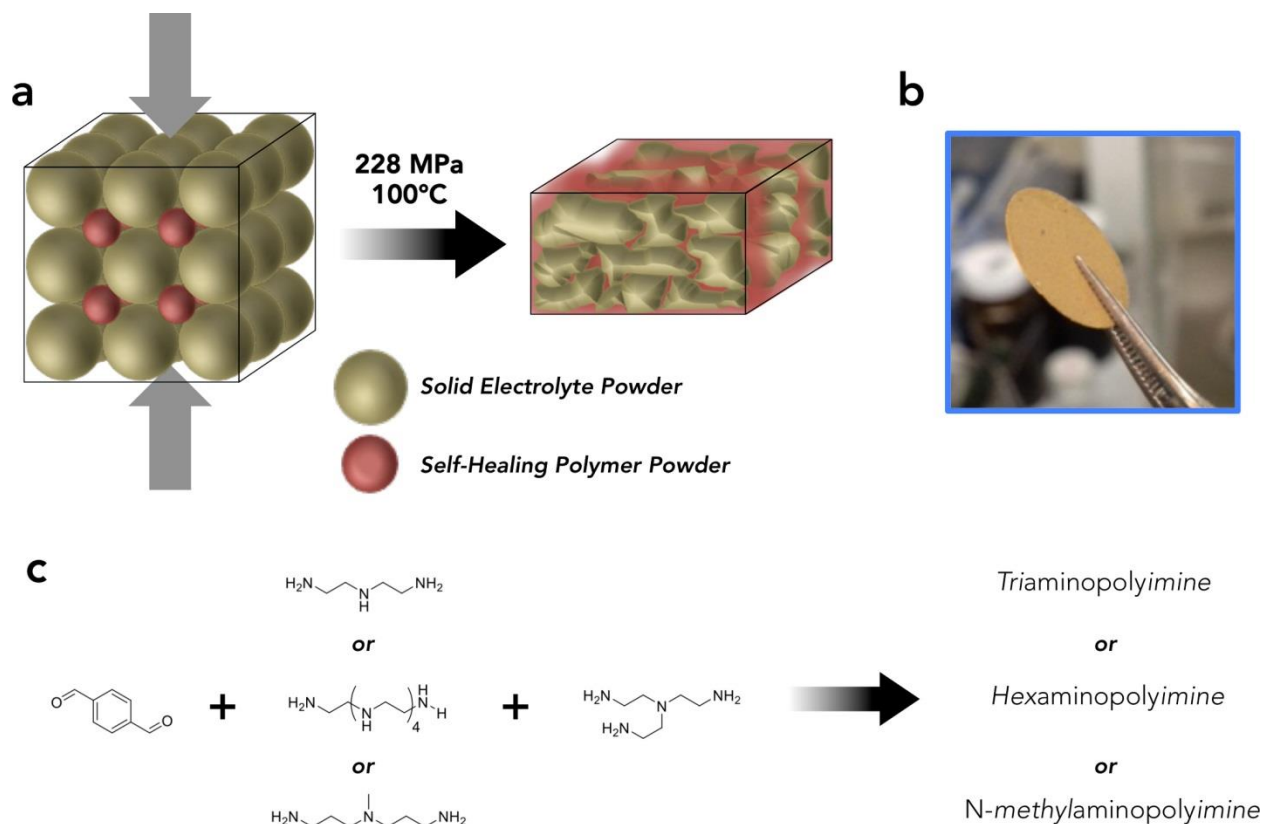


Figure 6.1 a. Schematic for forming the solid electrolyte in polymer matrix membrane. Through the application of heat and pressure, malleability is achieved in the polyimine forming a continuous network without sacrificing solid electrolyte particle contact. **b.** Free-standing solid electrolyte separators thinner than 100 μm can thus be made. **c.** The synthesis process for creating the polyimine formulations: tri-imine, hexa-imine, methyl-imine.

The original polyimine synthesis was reported previously.¹⁹ In this work, new variations of the polyimine were developed by replacing the monomer diethylene triamine with pentaethylene hexamine or 3,3'-diaminodipropyl-N-methylamine. The structures of the monomers are given in Figure 1c along with nomenclature used for the rest of this study: tri-imine, hexa-imine, methyl-imine. Increased elasticity is achieved by either creating a more open framework (hexa-imine) or reducing the degree of hydrogen bonding (methyl-imine). Figure 6.5 presents tensile test results for the new polymers, temperature-dependent stress relaxation, and bond exchange energy. All three formulations exhibit malleable character but hexa-imine and

methyl-imine achieve this characteristic at lower temperatures relating to their reduced glass transition temperature.

Table 1. Summary of SEPM composite membrane properties. All composites consist of 80% solid electrolyte by weight.

Material	Theoretical Density [g cm ⁻³]	Composite Relative Density	Composite $\sigma_{25^\circ\text{C}}$ [mS cm ⁻¹]	Composite Activation Energy [kJ mol ⁻¹]
a77.5	1.75 ^{a)}	0.85 ± 0.01	0.54	34.7
Methyl-imine	1.07 ± 0.02	0.97 ± 0.02	0.092	34.8
Hexa-imine	0.93 ± 0.02	0.94 ± 0.02	0.056	34.5
Tri-imine	1.00 ± 0.02	0.92 ± 0.02	0.015	33.3

^{a)} Density tabulated using tie line between Li₂S and P₂S₅ theoretical densities. Value is in good agreement with literature(reference needed).

To compare membrane properties, all the formulations as well as pure solid electrolyte were prepared into pellets approximately 1 mm thick. Table 1 presents the densities, room temperature ionic conductivity, and activation energies of the SEPMs. The measured experimental densities of the SEPMs as a function of the theoretical density are displayed in Figure 6.2a. The pure a77.5 pellet measures a relative density of 0.85 or about 15% porous. The most elastomeric polyimine, methyl-imine, forms an SEPM with a relative density of about 0.97. This is an excellent result as full density improves solid electrolyte contact. Although addition of the polyimine does reduce overall conductivity, methyl-imine SEPM achieves a room temperature conductivity of $\sim 1 \times 10^{-4}$ S cm⁻¹. This is on the same order of magnitude as the bulk electrolyte. It is important to determine if there is any impact of the polyimine on conductive abilities of a77.5; this can be seen in the Arrhenius plots for the SEPMs (Figure 6.2b). It is clear

that for each polyimine, no change in activation energy occurs. Activation energy is a fundamental material property for ionic motion that defines the energy barrier to ion hopping, and it can therefore be concluded that any decrease in conductivity from a pure a77.5 separator by the addition of polyimine is simply due to the inclusion of resistive domains. This is supported by the trend of decreasing ionic conductivity with decreasing elasticity of the polyimine.

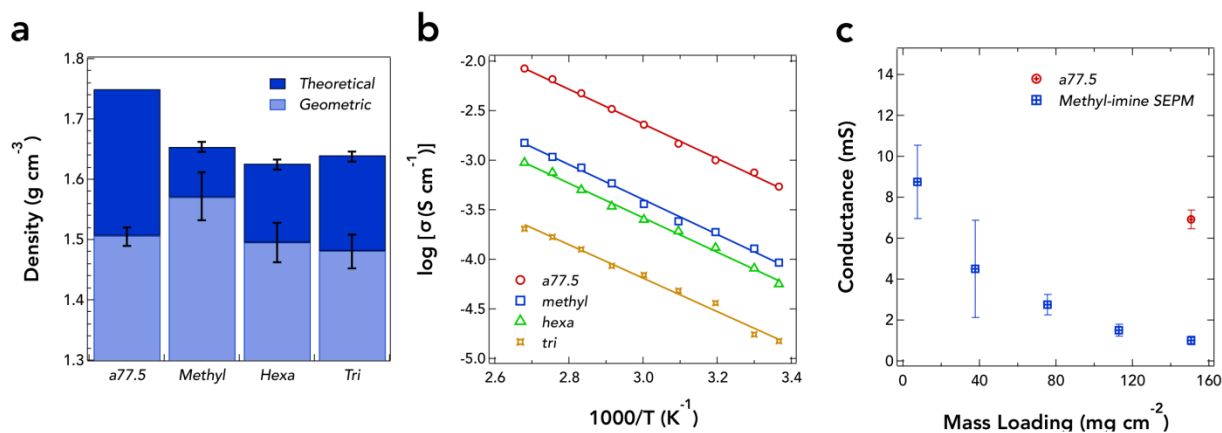


Figure 6.2 a. Theoretical and geometric densities of SEPM membranes consisting of 80% a77.5 and 20% polyimine. The most elastomeric polyimine formulation, methyl-imine, achieves a relative density approximately 0.97 indicating a microstructure without voids is created. **b.** Arrhenius plot of SEPMs. **c.** Conductance of electrolyte membranes as a function of mass loading (thickness). The methyl-imine based SEPM achieves a conductance greater than a pure a77.5 separator at a mass loading of 7.5 mg cm⁻² which corresponds to a thickness of 63.7 μm.

The overarching goal is to achieve a membrane with thickness less than 100 μm with a greater conductance than a pure a77.5 separator. The methyl-imine SEPM is pursued due to its high bulk conductivity. The thickness of the methyl-imine SEPM is reduced and its conductance value is measured rather than conductivity, more reflective of battery performance. The mass loading of the separator is normalized to area to account for any variations in thickness between the samples. Results are displayed in Figure 6.2c. It should be noted that although these SEPMs

were processed at elevated temperature, these same structures could also be formed at room temperature as methyl-imine demonstrates malleable properties at ambient conditions. However, in order to speed up this process, increased temperature is applied. A clear inverse trend is evident, meaning a linear resistance decrease is present with decreasing SEPM thickness. At a mass loading of 7.5 mg cm^{-2} , the SEPM achieves a greater conductance than a pure solid electrolyte membrane. This could be extrapolated for any solid electrolyte used, so that one should always be able to achieve a greater conductance than the solid electrolyte counterpart at this thickness level. Increased amount of error occurred at the thinner levels due to variations in the Ag-blocking electrode areas.

To confirm the hypothesized structure of self-healing polymer dispersed throughout a densified solid electrolyte, SEM is used to image the top and cross-sectioned view of the 7.5 mg cm^{-2} methyl-imine SEPM, Figure 6.3a and 6.3c, respectively. Methyl-imine is observed to be well-dispersed with domain sizes on the order of a few microns. Figure 3b is an enhanced view of the interface between polyimine and a77.5. The interface appears to be continuous, demonstrating the ability of the methyl-imine to flow through the electrolyte pore-space. This confirms the idealized structural mechanism of filling the voids of the solid electrolyte with polymer. The cross-section of SEPM methyl-imine reveals a thickness of $63.7 \text{ }\mu\text{m}$. To track dispersion and interconnectedness of polyimine, EDS is used to distinguish between polyimine and a77.5. Figure 6.3d, EDS map of C K signal, represents the polyimine and Figure 6.3e and 6.3f, EDS maps of P K and S K respectively, represents the a77.5. It is clear that the polyimine is well-dispersed and the domains appear connected.

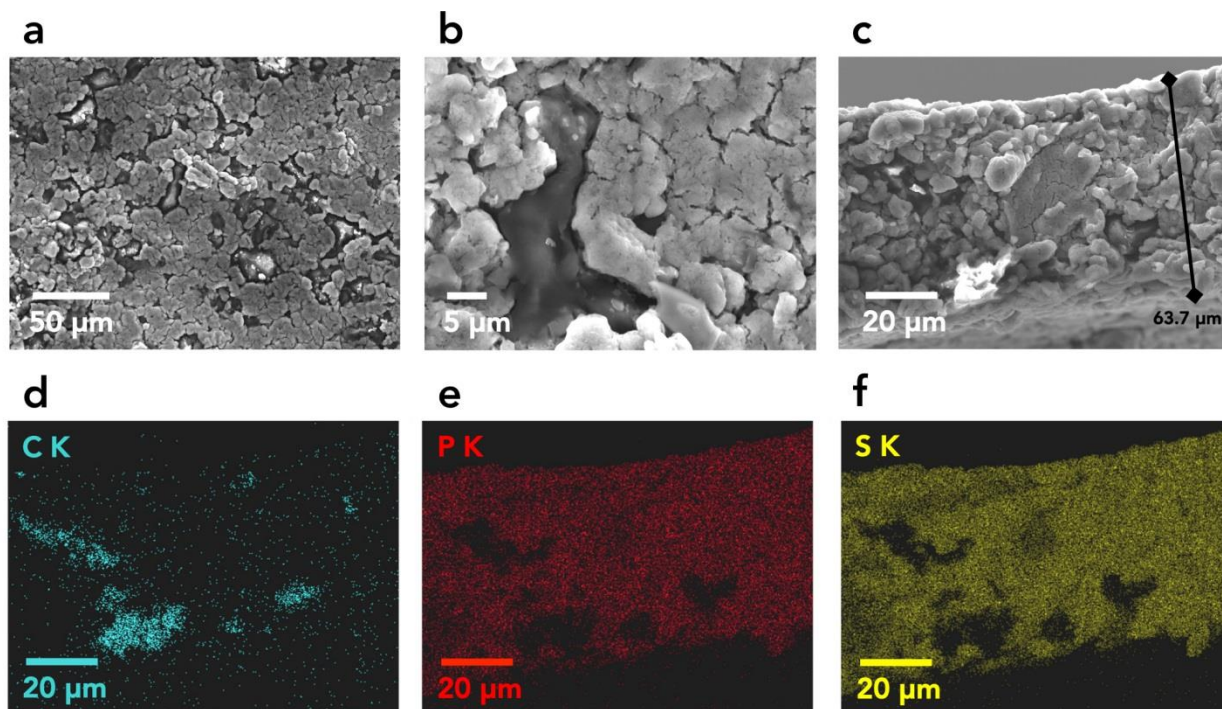


Figure 6.3 **a.** SEM of 7.5 mg cm^{-2} methyl-imine SEPM top. **b.** Zoomed in interface of polyimine and electrolyte. **c.** Cross-section. **d.** EDS map of C-K. **e.** P-K. **f.** S-K. in cross-section. The polyimine, registered as carbon, penetrates the voids between the solid electrolyte.

To demonstrate its application, the methyl-imine SEPM is investigated as a functional separator in an all solid-state lithium ion battery. A cathode containing 45% weight FeS_2 is mounted on an SEPM of mass loading 7.5 mg cm^{-2} using uni-axial compression.⁵ Figure 6.4a displays a symmetric rate study comparing discharge performance of the SEPM cell to a standard a77.5 construction. Associated voltage profiles are shown in Figure 6.9. At cycle 5, the cell achieves a specific capacity of around 450 mAh g^{-1} (mass normalized with respect to the full electrode). This corresponds to a FeS_2 specific capacity of 1000 mAh g^{-1} . Greater than theoretical capacity can be achieved through electrochemical activation of the sulfide components of the electrolyte.²⁰ The SEPM shows enhanced rate capability due to the greater conductance value of the separator manifesting in a smaller ohmic overpotential. The identical capacity retention of both cells results from identical FeS_2 reaction kinetics, inherent to the cathode itself. Figure 4b

shows long-term cycling at a rate of C/5. Over 100 cycles, the SEPM-based battery retains 82% capacity constituting one of the longest-lasting bulk FeS₂ cells reported to date.^{11,20-21]} Evolution of the voltage profile in this region is displayed in Figure 6.9. By measuring out the cathode tap density, we report on the volumetric and gravimetric cell-based energy density values. By replacing the thick a77.5 separator with the methyl-imine SEPM, the cell-level energy density values are increased by an order of magnitude and rapidly approach commercial lithium-ion battery values.²² Additional work to improve cathode capacity can further enhance this value.

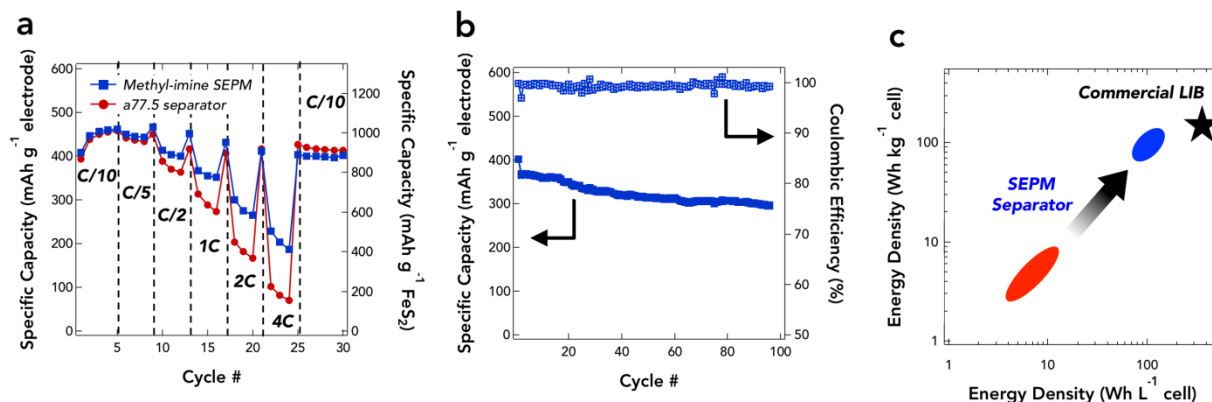


Figure 6.4 a. Rate study of an FeS₂ cell using a standard a77.5 separator and a methyl-imine SEPM separator. Greater capacity values are attributed to greater conductance and thus less ohmic overpotential. **b.** Long-term cycling of cell at C/5. 82% capacity retention is achieved after the 100th cycle. **c.** Enhancement in gravimetric and volumetric energy densities by moving to a SEPM configuration.

6.4 Conclusion

We have presented a new processing technique of forming a thin electrolyte membrane by creating a solid electrolyte-in-polymer matrix. An in-situ derived polymer matrix can be formed by penetrating the void space of an inorganic solid, green compacted through reversible cross-links of the self-healing polymer. Essentially a mixed-matrix is formed with a high mass loading of 80% solid electrolyte by weight. This constitutes an order of magnitude improvement

in thickness from a 1 mm to a 64 μm separator, achieving a greater conductance, and increasing relative density to 97%. The desired structure is confirmed with SEM and EDS. The SEPM, when used as a separator in an all-solid-state battery with a FeS_2 -based cathode, achieves excellent rate capability and stable cycling for over 100 cycles. This is the first report of a self-healing material being used to create a solid membrane and first application in a solid-state battery. Processing in the dry condition could represent a paradigm shift for incorporating high active material mass loadings into mixed-matrix membranes.

6.5 Experimental section

6.5.1 General procedures for membrane preparation

All processes occurred in an argon environment. The $77.5\text{Li}_2\text{S}-22.5\text{P}_2\text{S}_5$ solid electrolyte (denoted as a77.5) and original polyimine syntheses are reported elsewhere.^{11,19} A77.5 and polyimine powders were measured in a 4 to 1 weight ratio into an agate jar with 50 x 6 mm agate balls; the powders were mixed through planetary ball-milling for 30 minutes.

Free-standing pellets (referred to as SEPM) of the resultant powder were developed with the following procedure: the composite was pressed at 38 MPa in a stainless steel die ($\phi = 1.3$ cm) while the temperature was raised to 100°C at 5°C min^{-1} ; the pressure was held for another 15 minutes before increasing pressure to 228 MPa; the composite was held at this temperature and pressure for 1 hour, periodically reapplying pressure lost due to shrinkage.

Densities were determined using a micron-resolution caliper to measure thickness (Mitutoyo, 547-400) and accurate mass of the samples. 3 samples were prepared for each formulation to get a standard error. Theoretical density for a77.5 is tough to accurately measure due to the nature of glass-ceramics. 1.75 g cm^{-3} is chosen using a tie line between densities of the

precursors: Li_2S and P_2S_5 . This value matches closely with what others have reported for similar near full-dense variations.¹⁷ Theoretical densities of polyimine materials were measured by pressing polyimine powders into translucent films using the method outlined previously.

For ionic conductivity tests, silver paint (SPI) was used as blocking electrodes and allowed to cure at 120 °C under ambient pressure. AC Impedance measurements were taken using a Solartron 1260 with a 100 mV amplitude between 1MHz to 1Hz on a heating process, equilibrating the temperature for 1 hour between tests. Typical equivalent circuits for ion blocking electrodes fit to the data in conjuncture with equation 6.1 to back out resistance and thus conductivity values.²³ Activation energy is determined from the slope of the Arrhenius plot.

$$\sigma = \frac{l}{R \cdot A} \quad (6.1)$$

A reinforced cell die is used for all cycling tests.²⁰ A pyrite based cathode is prepared by hand-mixing FeS_2 (Washington Mills, SULFEX Red), a77.5, and C65 (Timcal) in a 5:5:1 weight ratio. A large enough batch is prepared to mount on both the standard and SEPM separators. 5 mg of cathode is pressed onto aluminum foil at 38 MPa. 10 mg of prepared a77.5:polyimine powder is then pressed onto the cathode at 76 MPa. The whole stack then undergoes the same HT procedure as before. Finally, an indium-lithium alloy ($\text{In} + \text{Li}_x\text{In}$, $0 < x < 1$) is pressed onto the prepared cell at 76 MPa. Galvanostatic cycling of cells occur on an Arbin B2000 Battery Testing Station. A rate of C/10 refers to an aerial current density of 0.15 mA cm^{-2}). Volumetric energy densities are calculated by measuring the tap density of the prepared cathode powder pressed into discs at 228 MPa.

6.5.2 Preparation and characterization of neat malleable polyimine films and powders

Figure 6.5 below reveals the room temperature mechanical performance, as well as temperature-dependent stress-relaxation of 3 formulations of network polyimine. The polymers were prepared by mixing the ethanolic solutions of the monomers in molar ratios of 1:0.45:0.367 (terephthalaldehyde to diamino linker to tris(2-aminoethyl)amine). The mixture was added to a tray of silicone-coated paper, and the ethanol was allowed to evaporate. After curing the films in a heat press (1 hr 100 °C), the solid polymers were ground to powder using sand paper. The self-healing behavior of the methyl-imine formulation is due to its room temperature malleability, and the powders and films of this formulation are observed to heal into coherent solids when left under gentle pressures at room temperature. Full characterization of the self-healing behavior and healing efficiencies is forthcoming.

DMA Tension test:

A dynamic mechanical analysis (DMA) machine (Model Q800, TA Instruments, New Castle, DE, USA) was used to carry out tension tests at room temperature (23 °C locally). All the samples were trimmed into a uniform size of 12 mm × 3 mm × 1.1 mm, and then stretched under a constant loading rate (2MPa/min) until broken.

DMA Stress Relaxation:

The time and temperature dependent relaxation modulus of the polyimine thermoset was also tested on the DMA machine (Model Q800, TA Instruments, New Castle, DE, USA). During the test, a polymer sample with the same dimension mentioned above was initially preloaded by 1×10^{-3} N force to maintain straightness. After reaching the testing temperature, it was allowed 30 min to reach thermal equilibrium. The specimen was stretched by 1% on the DMA machine and the deformation was maintained throughout the test. The decrease of stress was recorded and the

stress relaxation modulus was calculated. Figure 6.5 d-f depicts the results of relaxation tests at 5 different temperatures between 50 °C and 90 °C on a double logarithmic plot. Then selecting 40 °C as a reference temperature (T_r), each modulus curve in Figure 6.5 d-f is shifted horizontally to overlap with the next. This produces the master relaxation curve, which spans many decades of modulus and represents the actual relaxation behavior of the polymer within a long timescale 40 °C. The corresponding shift factors are plotted against temperature in Figure 6.5 g-i.

The master relaxation curve suggests that the kinetics of the BER induced stress relaxation follows the well-known temperature-time superposition (TTSP) principles. To quantitatively study the relaxation behavior, we used the following definition of relaxation modulus:

$$\tau = \frac{1}{k} \exp\left(\frac{E_a}{RT}\right) \quad (6.2)$$

where k is a kinetic coefficient ($k > 0$) R is the gas constant with $R = 8.31446 \text{ J / Kmol}$, and E_a is the activation energy.

The shift factor, namely the ratio between the temperature dependent relaxation time and the relaxation time at a reference temperature T_r , is therefore expressed as:

$$\alpha = \exp\left[\frac{E_a}{R} \left(\frac{1}{T} - \frac{1}{T_r}\right)\right]. \quad (6.3)$$

The predicted shift factors of the relaxation curves are also plotted in Figure 6.1c to compare with the experimental data. An Arrhenius-type dependence on temperature is revealed, which is consistent with what we previously reported for the tri-imine. By further examination of Equation 6.3 we found that in the semi-log scale, the energy barrier could be determined by the

slope of the shift factor curve. As shown in Figure 6.5 g-i, by measuring the curve slope, the energy barrier E_a is calculated for each formulation.

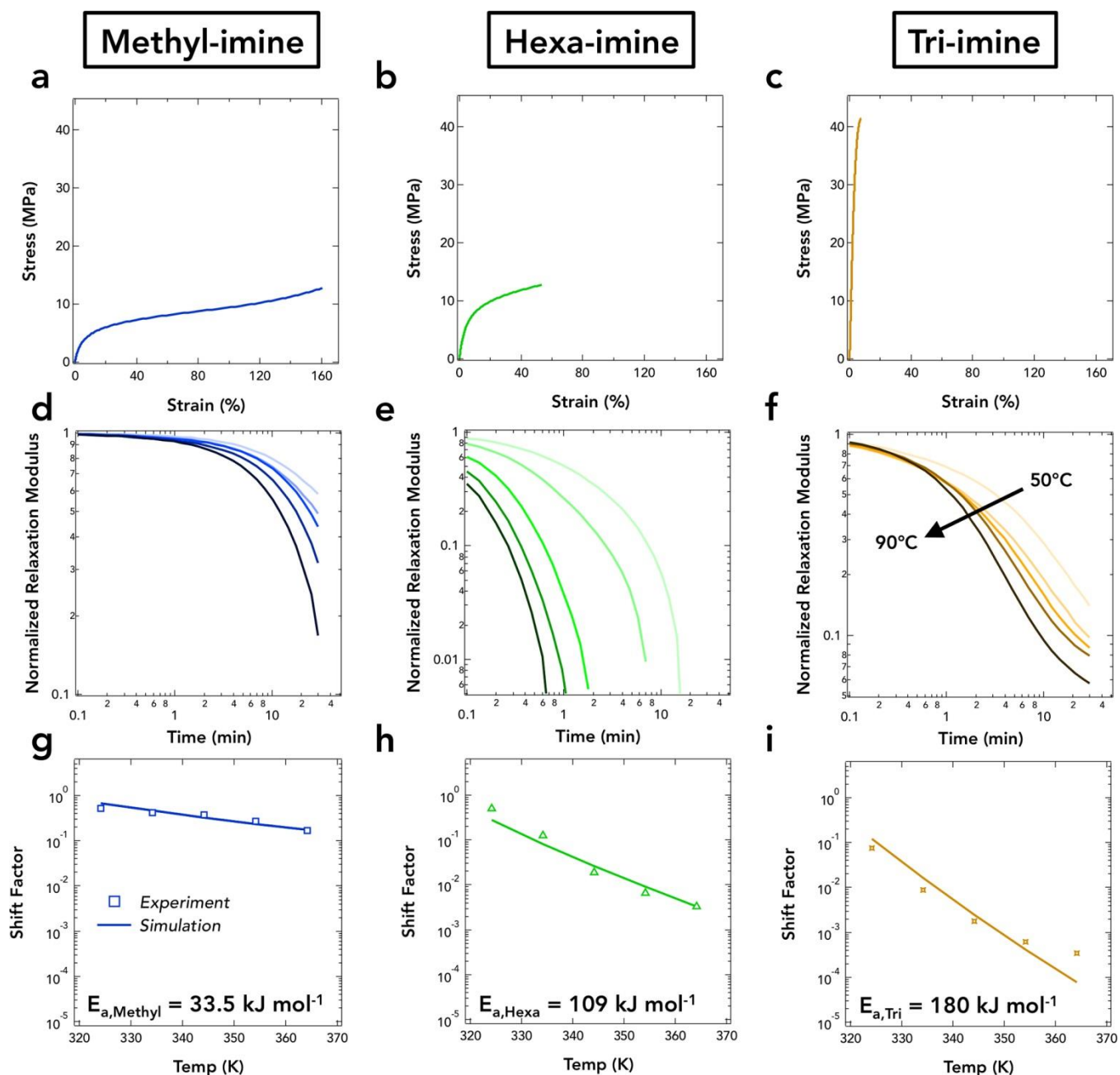


Figure 6.5 a.-c. Stress-strain curve of each formulation at room temperature. **d.-f.** Stress relaxation curves for each formulation of polyimine at 30 °C- 90 °C over a 30 minute period. **g.-i.** Arrhenius plot of polyimine temperature dependent relaxation time to extract bond exchange activation energy.

6.5.3 Electrochemical Characterization of Composite Membranes

Figure 6.6a-d displays the AC impedance results of a77.5 and the three SEPMs. A steep tail at low frequencies indicates good contact was made between the Ag-blocking electrodes and electrolyte layer.

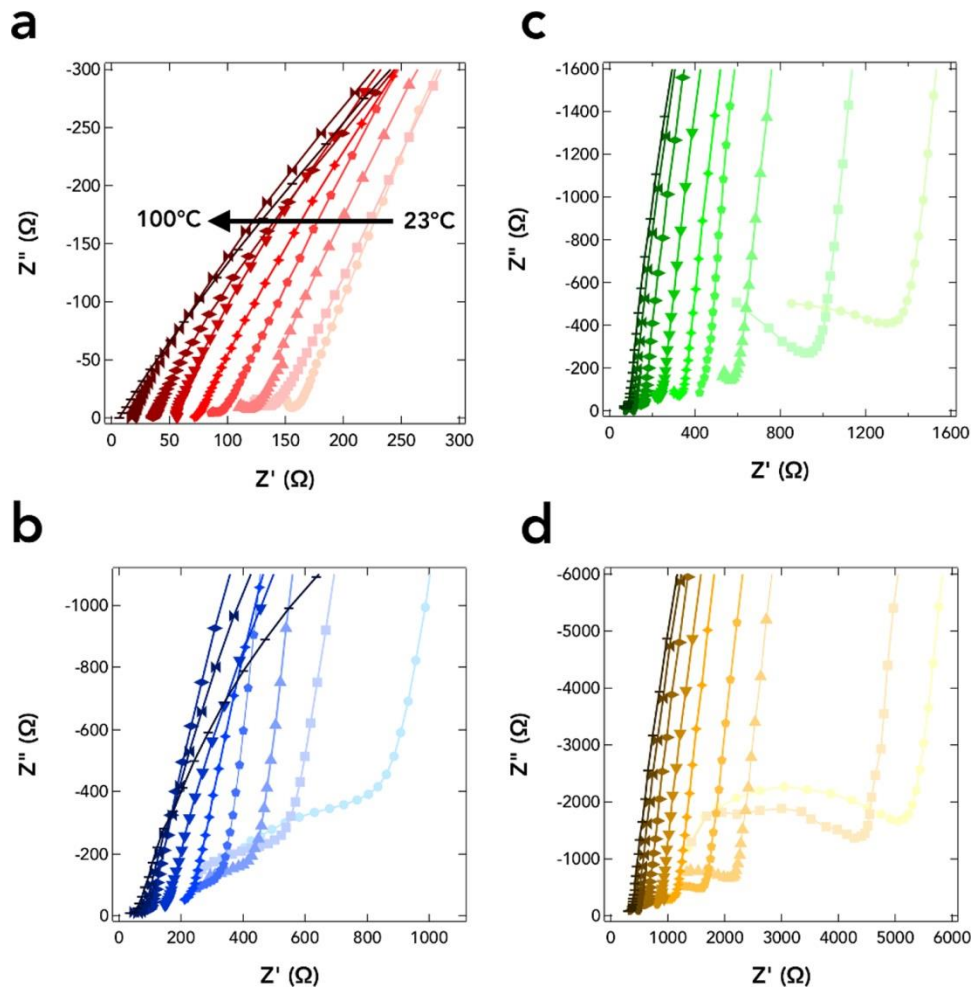


Figure 6.6 Nyquist plot as determined by AC Impedance for the temperature range between 23 °C to 100 °C for a77.5 **a.** Methyl-imine composite. **b.** Hexa-imine composite. **c.** Tri-imine composite. **d.** Pure a77.5.

To measure long-term interaction between polyimine and electrolyte, i.e. decomposition of material, we can use a DC pulse technique to measure internal resistance of SEPMs. DC pulse resistance measurements are taken on symmetric lithium cells (lithium/SEPM/lithium) using a 0.1 mA pulse applied every 5 minutes.

Figure 6.7 displays this measurement on un-heat-treated composites in contact with lithium metal at 60 °C to exacerbate any possible interactions. This serves the dual purpose of also measuring long-term stability with lithium and polyimine. As it can be seen, there are no general increases across any samples. a77.5 is already known to be stable in contact with lithium metal. A few fluxuations occur across the 10 days in the polyimine samples. As they occur at the same times, it can be concluded that this is directly due to temperature changes in the oven (opening the oven door).

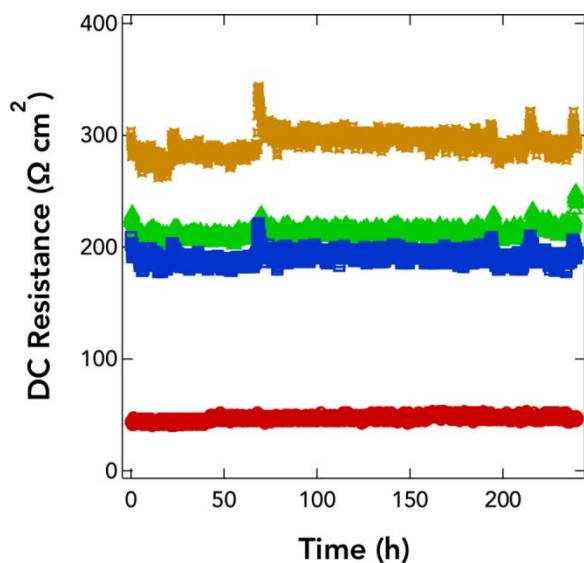


Figure 6.7 Long-term DC resistance of SEPMs in contact with lithium metal electrodes at 60 °C; fluxuations are due to changes in oven temperature.

We wanted to further probe the electrochemical characteristics of the polyimine material. First, it is worth seeing if the polyimine is lithium active. Electrochemical stability (Figure 6.8a) is tested using linear sweep voltammetry (LSV) with a lithium/a77.5/polyimine/titanium construction at a scan rate of 1 mV s⁻¹. LSVs are performed from OCV up to 5V and down to 0.1V corresponding to anodic and cathodic sweeps, respectively. Anodic and cathodic sweeps yielded no response meaning no interaction between the two. This is expected as methyl-imine is neither electrically or ionically conductive, a necessity to have some conduction of lithium ions. Second, in order to see if there are any mobile species within methyl-imine, we tested lithium ion transference number in both pure a77.5 and the methyl SEPM (Figure 6.8b). Lithium ion transference number is calculated using the Bruce-Vincent-Evans (BVE) technique as in equation 6.2.²⁴ SEPMs are constructed into a symmetric lithium cells (lithium/SEPM/lithium); lithium is scraped prior to use to remove any native layer. BVE requires the measurement of initial and steady state current, I₀ and I_s, respectively, for a given DC polarization, ΔV. Initial and steady state resistance values, R₀ and R_s, are determined through AC Impedance using the same test as before. Steady state is determined once less than a 1% change in current occurred in a 10-minute period.

$$t_{Li^+} = \frac{I_s(\Delta V - I_0 R_0)}{I_0(\Delta V - I_s R_s)} \quad (6.4)$$

Solid superionic conductors are well known for having transference values of unity meaning the only mobile species are lithium ions hopping between vacancies. In the SEPM, we see the same value showing no negative interactions caused by the addition of polyimine. Figure 6.8c displays the initial and steady-state impedance sweeps used to calculate transference number.

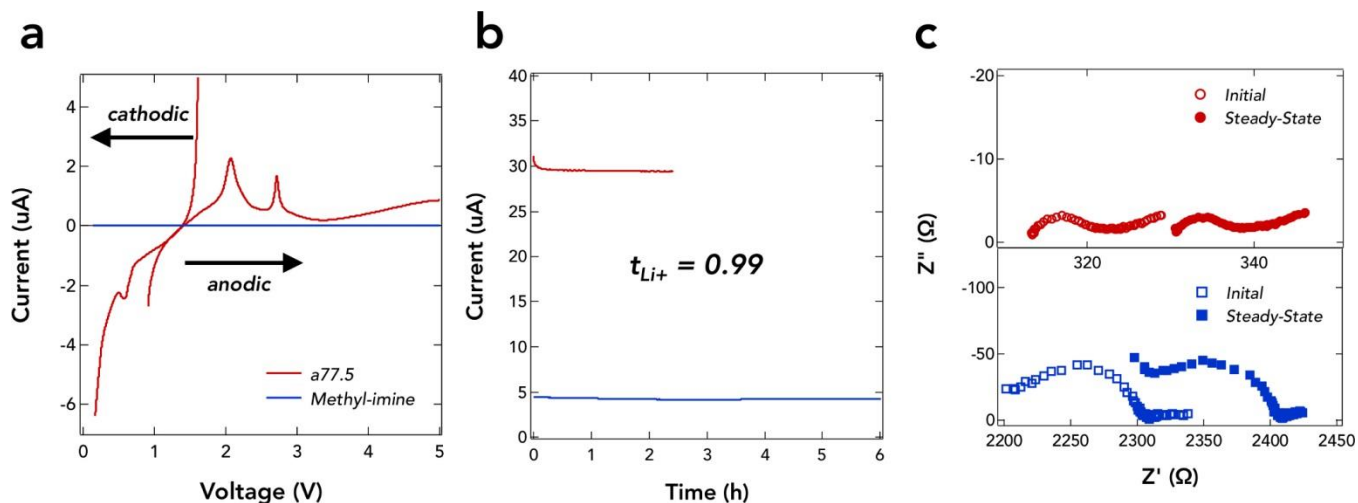


Figure 6.8 **a.** Cathodic and anodic Linear sweep voltammetry of pure a77.5 and methyl-imine. Peaks in the anodic a77.5 sweep are attributed to excess Li_2S in the electrolyte. Methyl-imine appears to be electrochemically inert to lithium in the range of 0 – 5V. **b.** Transference number of pure a77.5 separator and methyl-imine SEPM. Both cases exhibit a lithium ion transference number of 0.99 indicating methyl-imine does not contain any mobile species and does not affect conductive abilities of the solid electrolyte. **c.** Initial and steady-state impedance sweeps required to calculate transference number values.

6.5.4 Rechargeable Lithium ion Electrochemical Cell Cycling study

Figure 6.9 reveals the voltage profiles associated with the cycling tests displayed in Figure 6.4. Figure S5a and S5b are the discharge profiles of the methyl-imine SEPM and a77.5 separator cells, respectively. It can be seen that the main difference between the two cells is the larger ohmic overpotential associated with the a77.5 separator leading to lower capacity. Figure 6.9c is the evolution of voltage profiles for the methyl-imine SEPM cell run at C/5 for extended cycling. The loss in capacity is attributed to a shortening of the lower plateau due to the slower kinetics in the conversion reaction. While capacity is lost during this period of cycling, the energy density does not degrade nearly as much as the high voltage region remains relatively intact.

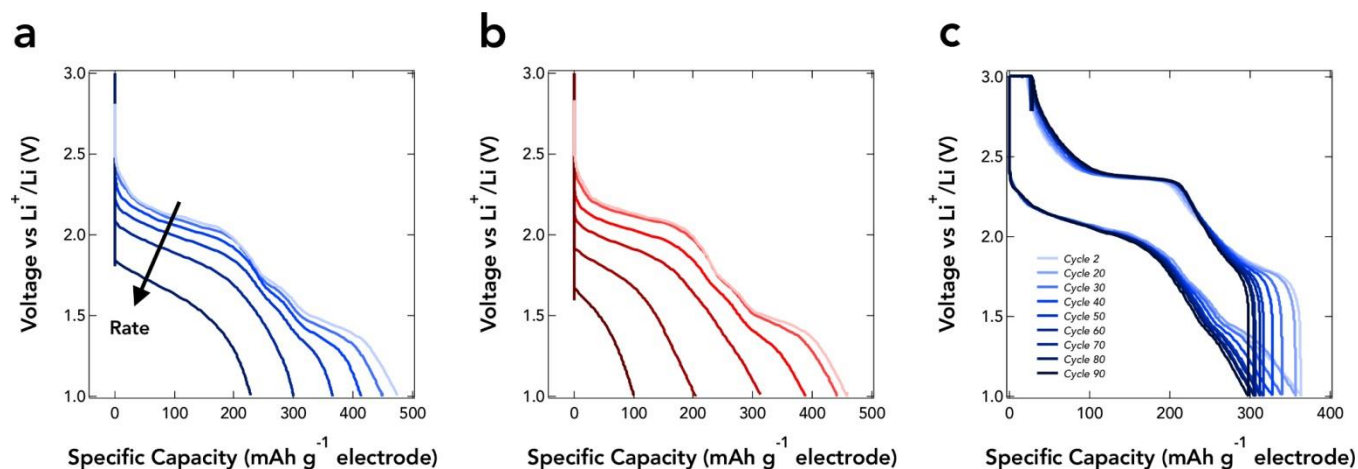


Figure 6.9 a. Voltage profiles of rate study using methyl-imine SEPM. b. Voltage profiles of rate study using a77.5 separator. c. long-term cycling voltage profile evolution of methyl-imine SEPM cell.

6.6 References

- [1] J. M. Tarascon, M. Armand, *Nature* 2001, 414, 359; J. B. Goodenough, Y. Kim, *Chemistry of Materials* 2010, 22, 587.
- [2] J. R. Dahn, E. W. Fuller, M. Obrovac, U. Vonsacken, *Solid State Ionics* 1994, 69, 265.
- [3] N. Kamaya, K. Homma, Y. Yamakawa, M. Hirayama, R. Kanno, M. Yonemura, T. Kamiyama, Y. Kato, S. Hama, K. Kawamoto, A. Mitsui, *Nature Materials* 2011, 10, 682.
- [4] Y. Seino, T. Ota, K. Takada, A. Hayashi, M. Tatsumisago, *Energy & Environmental Science* 2014, 7, 627; J. M. Whiteley, J. H. Woo, E. Hu, K.-W. Nam, S.-H. Lee, *Journal of the Electrochemical Society* 2014, 161, A1812.
- [5] J. M. Whiteley, J. W. Kim, C. S. Kang, J. S. Cho, K. H. Oh, S.-H. Lee, *Journal of the Electrochemical Society* 2015, 162, A711.

- [6] E. Rangasamy, Z. C. Liu, M. Gobet, K. Pilar, G. Sahu, W. Zhou, H. Wu, S. Greenbaum, C. D. Liang, *Journal of the American Chemical Society* 2015, 137, 1384; Z. Lin, Z. C. Liu, N. J. Dudney, C. D. Liang, *Acs Nano* 2013, 7, 2829.
- [7] S. Teragawa, K. Aso, K. Tadanaga, A. Hayashi, M. Tatsumisago, *Journal of Power Sources* 2014, 248, 939.
- [8] A. Hayashi, S. Hama, H. Morimoto, M. Tatsumisago, T. Minami, *Journal of the American Ceramic Society* 2001, 84, 477; A. Sakuda, A. Hayashi, Y. Takigawa, K. Higashi, M. Tatsumisago, *Journal of the Ceramic Society of Japan* 2013, 121, 946.
- [9] M. Kotobuki, H. Munakata, K. Kanamura, Y. Sato, T. Yoshida, *Journal of the Electrochemical Society* 2010, 157, A1076; P. Knauth, *Solid State Ionics* 2009, 180, 911.
- [10] J. E. Ni, E. D. Case, J. S. Sakamoto, E. Rangasamy, J. B. Wolfenstine, *Journal of Materials Science* 2012, 47, 7978.
- [11] T. A. Yersak, H. A. Macpherson, S. C. Kim, V. D. Le, C. S. Kang, S. B. Son, Y. H. Kim, J. E. Trevey, K. H. Oh, C. Stoldt, S. H. Lee, *Advanced Energy Materials* 2013, 3, 120.
- [12] A. Sakuda, A. Hayashi, M. Tatsumisago, *Scientific Reports* 2013, 3.
- [13] F. Mizuno, S. Hama, A. Hayashi, K. Tadanaga, T. Minami, M. Tatsumisago, *Chemistry Letters* 2002, 1244.
- [14] T. Inada, K. Takada, A. Kajiyama, M. Kouguchi, H. Sasaki, S. Kondo, M. Watanabe, M. Murayama, R. Kanno, *Solid State Ionics* 2003, 158, 275.
- [15] A. Sakuda, A. Hayashi, T. Ohtomo, S. Hama, M. Tatsumisago, *Journal of Power Sources* 2011, 196, 6735; M. Ogawa, R. Kanda, K. Yoshida, T. Uemura, K. Harada, *Journal of Power Sources* 2012, 205, 487; T. Uemura, K. Goto, M. Ogawa, K. Harada, *Journal of Power Sources* 2013, 240, 510.

- [16] T. Inada, K. Takada, A. Kajiyama, H. Sasaki, S. Kondo, M. Watanabe, M. Murayama, R. Kanno, *Journal of Power Sources* 2003, 119, 948; Y. M. Wang, Z. Q. Liu, X. L. Zhu, Y. F. Tang, F. Q. Huang, *Journal of Power Sources* 2013, 224, 225.
- [17] S. S. Berbano, M. Mirsaneh, M. T. Lanagan, C. A. Randall, *International Journal of Applied Glass Science* 2013, 4, 414.
- [18] G. Dong, H. Li, V. Chen, *Journal of Materials Chemistry A* 2013, 1, 4610.
- [19] P. Taynton, K. Yu, R. K. Shoemaker, Y. Jin, H. J. Qi, W. Zhang, *Advanced Materials* 2014, 26, 3938.
- [20] T. A. Yersak, C. Stoldt, S. H. Lee, *Journal of the Electrochemical Society* 2013, 160, A1009.
- [21] T. A. Yersak, T. Evans, J. M. Whiteley, S. B. Son, B. Francisco, K. H. Oh, S. H. Lee, *Journal of the Electrochemical Society* 2014, 161, A663; T. Evans, D. M. Piper, S. C. Kim, S. S. Han, V. Bhat, K. H. Oh, S.-H. Lee, *Advanced Materials* 2014, 26, 7386; S. B. Son, T. A. Yersak, D. M. Piper, S. C. Kim, C. S. Kang, J. S. Cho, S. S. Suh, Y. U. Kim, K. H. Oh, S. H. Lee, *Advanced Energy Materials* 2014, 4.
- [22] D. M. Piper, T. A. Yersak, S. B. Son, S. C. Kim, C. S. Kang, K. H. Oh, C. M. Ban, A. C. Dillon, S. H. Lee, *Advanced Energy Materials* 2013, 3, 697.
- [23] R. A. Huggins, *Ionics* 2002, 8, 300.
- [24] J. Evans, C. A. Vincent, P. G. Bruce, *Polymer* 1987, 28, 2324.

Chapter 7

Conclusions and Future Work

7.1 Overview of objectives

The objectives of this research project were to develop robust malleable thermoset materials which take advantage of the dynamic imine linkage. Such polymer networks were developed, and surprisingly did not require a catalyst, and exhibit a fascinating water-activated malleability. Further exploration revealed the tunable nature of the mechanical, thermal and moisture-responsive properties. Bond exchange reactions with monomers lead to dissolution of the malleable resins, enabling completely recyclable high performance composite materials. Finally collaborative exploration led to development of solid state lithium ion batteries, whose brittle separator membrane was critically strengthened by inclusion of malleable polyimine, allowing for a ten-fold decrease in thickness, and four-fold increase in energy density. In each of these applications, only proof-of-concept level work has been done, and further developments are needed. In order for polyimines to lead to resins which could serve as replacements for non-recyclable epoxy materials, formulations must be developed which have much higher elastic modulus. Also, though we've developed solid state lithium ion batteries, the ultimate goal is solid state lithium metal batteries, and malleable thermosets may hold the key to blocking lithium dendrite growth, which is the major technical challenge for lithium metal batteries. Beyond this, the technology holds promise for cheap, solid state processing and production of

mixed matrix membranes for gas separation. In principle, such membranes should be able to be prepared in a similar fashion to the composite electrolyte membranes described in Chapter 6. The moisture-responsive behaviors of polyimines could lead to functional or self-healing cross-linked hydrogels for biomimetic and other applications.

7.2 Advanced composite materials

In Chapter 5 we reported the development of carbon fiber composite materials which exhibit unique processing and re-processing abilities which are enabled by the reversible and exchangeable nature of imine chemistry. This proof-of-concept work demonstrated the potential utility of developing imine-linked polymer resins for advanced composite materials. The reported material matches or exceeds the performance of current commercial thermoplastic composites, but the best use of a recyclable thermoset is to replace a non-recyclable thermoset, such as the epoxy resin/amine hardener systems used in many lightweight structural composite applications. In order to do this, harder formulations need to be developed. Such resins typically have elastic moduli of higher than 3 GPa.¹

In order to reach the next level of mechanical performance, two approaches will be tried. One approach is to systematically continue to explore imine networks through introduction of new monomers, and formulation to vary crosslink density, as well as varying the formulation with combinations of diamines. Alternatively, imine links can be incorporated into existing epoxy resin systems, and further formulated to achieve the desired combination of strength and processability. This could be simply achieved by use of amine-terminated imine-linked oligomers in place of traditional small molecule diamine hardeners in the epoxy resin systems. The imine-as-hardener approach also has the advantage of being a plug-and-play type solution

which can be easily adapted to current industrial processes.

The materials described in chapter 5 may have immediate appeal for deployable structures.² The mechanical performance of these materials at very low temperatures has not yet been evaluated, but is a critical metric for such applications. Therefore formulation and development toward optimizing the low temperature mechanical performance of fiber-reinforced polyimine composites could lead development of uniquely reprocessable and reusable deployable structural materials, which may be useful for future lunar or planetary missions.³

7.3 Lithium metal batteries

Batteries which use pure lithium metal as an electrode material would have the highest possible energy density. One major hurdle to the development of rechargeable lithium metal batteries is the growth of lithium dendrites during the charge/discharge cycling of the cells. As lithium ions reduce onto the surface of lithium metal, they tend to form dendritic structures which grow closer to the opposite electrode. Unless the dendritic growth is suppressed, the dendrites will reach the counter electrode, shorting out the battery and potentially releasing massive amounts of heat energy. It has recently been shown that highly crosslinked network polymers can effectively suppress such dendrite growth.⁴ Unfortunately, both linear and crosslinked polymer electrolytes typically require a minimum amount of plasticizing organic solvents in order to enable lithium ion conductivities on the order of 10^{-4} Scm^{-1} . The use of organic solvents greatly increases the safety concerns of liquid electrolyte lithium ion batteries, due to their thermal instability. This safety concern is dramatically increased when lithium metal is introduced.

The solid-state composite electrolyte materials reported in chapter 6 represent a very

attractive potential separator material for solid state lithium metal batteries. While preliminary experiments applying the current electrolyte system to lithium metal have failed, a more systematic approach will be needed to develop the desired materials.

First polymer formulations, including ionic liquid polyimines, will be developed and subsequently tested for their neat ionic conductivity, and dendrite blocking capabilities. Subsequently, various formulations will be doped with lithium salts to understand the impact of doping on the conductivity and barrier properties of the polyimines. Following proper optimization, solid state lithium metal batteries with composite electrolyte membranes will be prepared and tested.

7.4 Mixed Matrix Membranes

Mixed matrix membranes are based on solid–solid system comprised of inorganic dispersed phase inserted in a polymer matrix.⁵ Compared to neat polymer membranes, mixed matrix membranes have the potential to achieve higher selectivity, permeability, or both due to the addition of the inorganic particles with their inherent superior separation characteristics.⁶⁻⁸ Work in mixed matrix membranes is a natural extension of our work developing solid state composite electrolytes, and in our future work we look to develop permeable, highly selective mixed matrix membranes which can be prepared through simple solid-state mixing of powders followed by treatment with heat and pressure. Our preliminary results have shown that this approach can generate membranes with any desired mass loading of zeolite without nucleation and precipitation of the zeolite content which is a common challenge to the solution-processing approach.

7.5 References

- [1] T. P. Skourlis and R. L. McCullough, "An experimental investigation of the effect of prepolymer molecular weight and stoichiometry on thermal and tensile properties of epoxy resins," *Journal of applied polymer science*, vol. 62, no. 3, pp. 481-490, 1996.
- [2] Hanaor and Levy, "Evaluation of deployable structures for space enclosures," *International Journal of Space Structures*, vol. 16, no. 4, pp. 211-229, 2001.
- [3] D. Cadogan, J. Stein and M. Grahne, "Inflatable composite habitat structures for lunar and mars exploration," *Acta Astronautica*, vol. 44, no. 7, pp. 399-406, 1999.
- [4] R. Khurana, J. L. Schaefer, L. A. Archer and G. W. Coates, "Suppression of Lithium Dendrite Growth Using Cross-Linked polyethylene/poly (ethylene oxide) electrolytes: a new approach for practical lithium-metal polymer batteries," *Journal of the American Chemical Society*, vol. 136, no. 20, pp. 7395-7402, 2014.
- [5] D. Bastani, N. Esmaili and M. Asadollahi, "Polymeric mixed matrix membranes containing zeolites as a filler for gas separation applications: A review," *Journal of Industrial and Engineering Chemistry*, vol. 19, no. 2, pp. 375-393, 2013.
- [6] D. Shekhawat, D. R. Luebke and H. W. Pennline, "A review of carbon dioxide selective membranes, A Topical Report," *National Energy Technology Laboratory United States Department of Energy*, vol. December 1st, 2003.
- [7] C. M. Zimmerman, A. Singh and W. J. Koros, "Tailoring mixed matrix composite membranes for gas separations," *Journal of Membrane Science*, vol. 137, p. 145, 1997.
- [8] R. D. Noble, "Perspectives on Mixed Matrix Membranes," *Journal of Membrane Science*, vol. 378, p. 393, 2011.

Bibliography

- B. J. Adzima, H. A. Aguirre, C. J. Kloxin, T. F. Scott and C. N. Bowman, "Rheological and Chemical Analysis of Reverse Gelation in a Covalently Cross-Linked Diels-Alder Polymer Network," *Macromolecules*, vol. 41, no. 23, pp. 9112-9117, 2008.
- C. N. Albano, N. Camacho, J. Reyes, J. L. Feliu and M. Hernandez, "Influence of scrap rubber Portland I concrete composites: destructive and non-destructive testing," *Composite Structures*, vol. 77, pp. 439-446, 2005.
- J. J. Alkonis and W. J. MacKnight, *Introduction to polymer viscoelasticity* 2nd Ed., New York: Wiley, 1996.
- F. I. Altuna, V. Pettarin and R. J. Williams, "Self-healable polymer networks based on the crosslinking of epoxidised soybean oil by an aqueous citric acid solution," *Green Chemistry*, vol. 15, pp. 3360-3366, 2013.
- A. A. Askadskii, "Influence of crosslinking density on the properties of polymer networks," *Physics of Chemistry U.S.S.R.*, vol. 32, no. 10, pp. 2061-2069, 1990.
- J. P. Brutman, P. A. Delgado and M. A. Hillmyer, "Polylactide Vitrimers," *ACS Macro Letters*, vol. 5, pp. 607-610, 2014.
- A. A. Barber, V. A. Bhagavati, L. Ukkonen, A. Z. Elsherbeni, P. Kallio and L. Sydanheimo, "Fabrication and characterization of high-permittivity ceramic-polymer composite as a substrate for UHF RFID tag antennas," *International Journal of Antennas and Propagation*, pp. 1-8, 2012.
- D. Bastani, N. Esmaili and M. Asadollahi, "Polymeric mixed matrix membranes containing zeolite filler for gas separation applications: A review," *Journal of Industrial and Engineering Chemistry*, vol. 23, no. 2, pp. 375-393, 2013.
- M. E. Belowich and J. F. Stoddart, "Dynamic imine chemistry," *Chemical Society Reviews*, vol. 41, pp. 2003-2024, 2012.
- A. S. Benjamin, M. Ahart, S. A. Gramsch, L. L. Stevens, E. B. Orler, D. M. Dattelbaum and R. A. Creswell, "Acoustic properties of Kel F-800 copolymer up to 85 GPa," *The Journal of Chemical Physics*, vol. 136, no. 1, p. 014514, 2012.
- C. L. Beyler and M. M. Hirschler, "Thermal Decomposition of Polymers," in *SFPE Handbook of Fire Protection Engineering*, 3rd ed., Quincy, NFPA, 2001.

H. F. Brinson and C. L. Brinson, *Polymer engineering science and viscoelasticity: an introduction*, 2007.

D. Cadogan, J. Stein and M. Grahne, "Inflatable composite habitat structures for lunar and mars exploration," *Acta Astronautica*, vol. 44, no. 7, pp. 399-406, 1999.

M. Capelot, D. Montarnal, F. Tournilhac and L. Leibler, "Metal-Catalyzed Transesterification for the Assembling of Thermosets," *J. Am. Chem. Soc.*, vol. 134, pp. 7664-7667, 2012.

M. Capelot, M. Unterlass, F. Tournilhac and L. Leibler, "Catalytic Control of the Vitrimer Glass Transition," *ACS Macro Lett.*, vol. 1, pp. 789-792, 2012.

X. X. Chen, M. A. Dam, K. Ono, H. B. Shen, S. R. Nutt, K. Sheran and F. Wudl, "A Thermally Reversible Cross-Linked Polymeric Material," *Science*, vol. 295, pp. 1698-1702, 2002.

P. Cordier, F. Tournilhac, C. Soulie-Ziakovic and L. Leibler, "Self-healing and thermoreversible cross-linking from supramolecular assembly," *Nature*, vol. 451, no. 7181, pp. 977-980, 2008.

O. R. Cromwell, J. Chung and Z. Guan, "Malleable and self-healing covalent polymer networks with tunable dynamic boronic ester bonds," *Journal of the American Chemical Society*, vol. 137, pp. 1200-1205, 2015.

E. Diez-Barra, J. C. Garcia-Martinez, S. Merino, R. del Rey, J. Rodriguez-Lopez, P. Sanchez-Vizcaino and J. Tejada, "Synthesis, characterization, and optical response of dipolar and non-dipolar poly(phenylenevinylene) dendrimers," *The Journal of Organic Chemistry*, vol. 66, no. 17, pp. 5600-5605, 2001.

G. Deng, C. Tang, F. Li, H. Jiang and Y. Chen, "Covalent Cross-Linked Polymer Gels with Reversible Sol-Gel Transition and Self-Healing Properties," *Macromolecules*, vol. 43, pp. 1191-1194, 2010.

W. Denissen, G. Rivero, R. Nicolay, L. Leibler, J. M. Winne and F. E. Du Prez, "Vinylogous Urethane Cross-Linked Vitrimers," *Advanced Functional Materials*, vol. 25, no. 16, pp. 2451-2457, 2015.

M. Doi, *Introduction to polymer physics*, Oxford: Oxford University Press, 1996.

Z. A. Dreger, J. Zhou, N. C. Dang and Y. M. Gupta, "Effect of high pressure on acoustic properties of several polymers: Use of impulsive stimulated light scattering method," *Journal of Applied Physics*, vol. 97, no. 11, pp. 114301-114305, 2005.

109, no. 8, p. 083507, 2011.

F. R. Eirich, in *Science and technology of rubber 3rd edition*, Amsterdam, Elsevier, 2005, p. 70

K. E. Feldman, M. J. Kade, T. F. de Greef, E. W. Meijer, E. J. Kramer and C. J. Hawker, "Poly multiple hydrogen-bonded end groups and their blends," *Macromolecules*, vol. 41, pp. 4694-4700, 2008.

P. Gebert, C. Batich, D. Tanner and S. Herr, "Polyaniline via schiff base chemistry," *Synth. Met.* no. 1, pp. 371-376, 1989.

A. N. Gent, "Relaxation processes in vulcanized rubber II: Secondary relaxation due to network breakdown," *Journal of Applied Polymer Science*, vol. 6, pp. 442-448, 1962.

G. Ghosh and M. W. Urban, "Self-Repairing Oxetane-Substituted Chitosan Polyurethane Networks," *Science*, vol. 323, no. 5920, pp. 1458-1460, 2009.

G. Godin, B. Legrand, A. Trachsel, J.-M. Lehn and A. Herrmann, "Dynamic polymer blends--recombination between neat dynamic covalent polymers at room temperature," *Chemical Communications*, vol. 46, pp. 3125-3127, 2010.

C. Godoy-Alcantar, A. K. Yatsimirsky and J.-M. Lehn, "Structure-stability correlations for imine networks in aqueous solution," *Journal of Physical Organic Chemistry*, vol. 18, pp. 979-985, 2005.

M. S. Green and A. V. Tobolsky, "A New Approach to the Theory of Relaxing Polymeric Media," *Journal of Applied Physics*, vol. 17, no. 5, p. 407, 1946.

J. J. Griebel, N. A. Nguyen, A. V. Astashkin, R. S. Glass, M. E. Mackay, K. Char and J. Pyun, "Synthesis of Dynamic Covalent polymers via Inverse Vulcanization of Elemental Sulfur," *ACS Macro Letters*, vol. 5, pp. 1258-1261, 2014.

Hanaor and Levy, "Evaluation of deployable structures for space enclosures," *International Journal of Structures*, vol. 16, no. 4, pp. 211-229, 2001.

T. S. M. S. C. A. S. M. W. & C. A. I. Hasell, "Reversible water uptake by a stable imine-based organic cage," *Chem. Commun.*, vol. 48, no. 39, pp. 4689-4691, 2012.

S. A. Hayes, F. R. Jones, K. Marshiya and W. Zhang, "A self-healing thermosetting composite," *Composites Part A: Applied Science and Manufacturing*, vol. 38, no. 4, pp. 1116-1120, 2007.

F. Hernandez-Olivares, G. Barluenga, M. Bollati and B. Witoszek, "Static and dynamic behavior of recycled tyre rubber-filled concrete," *Cement and concrete research*, vol. 32, no. 10, pp. 1578-1584, 2002.

K. Imato, M. Nishihara, T. Kanehara, Y. Amamoto, A. Takahara and H. Otsuka, "Self-Healing Gels Cross-Linked by Diarylbibenzofuranone-Based Trigger-Free Dynamic Covalent Bonds at Temperature," *Angewandte Chemie International Edition*, vol. 51, no. 5, pp. 1138-1142, 2012.

L. Imbernon, E. K. Oikonomou, S. Norvez and L. Leibler, "Chemically crosslinked yet reproducible epoxidized natural rubber via thermo-activated disulfide rearrangements," *Polymer Chemistry* 4271-4278, 2015.

A. Inglis, L. Nebhani, O. Altintas, F. Schmidt and C. Barner-Kowollik, "Rapid Bonding/Debonding Demand: Reversibly Cross-Linked Functional Polymers via Diels–Alder Chemistry," *Macromolecules* 43, no. 13, pp. 5515-5520, 2010.

H. H. Jin, K. R. Hart, A. M. Coppola, R. C. Gergely, J. S. Moore, N. R. Sottos and S. R. White, "Self-Healing Epoxies and Their Composites," *Self-Healing Polymers: From Principles to Applications* 380, 2013.

Y. Jin, Q. Wang, P. Taynton and W. Zhang, "Dynamic Covalent Chemistry Approaches Toward Self-Healing Macrocycles, Molecular Cages, and Polymers," *Accounts of Chemical Research*, vol. 47, pp. 1-11, 2014.

Y. Jin, C. Yu, R. J. Denman and W. Zhang, "Recent Advances in Dynamic Covalent Chemistry," *Soc. Rev.*, vol. 42, pp. 6634-6654, 2013.

D. M. Joseph and R. B. Prime, *Thermal Analysis of Polymers: Fundamentals and Applications* & Sons, 2009.

R. Khurana, J. L. Schaefer, L. A. Archer and G. W. Coates, "Suppression of Lithium Dendrite Growth in Cross-Linked polyethylene/poly (ethylene oxide) electrolytes: a new approach for practical lithium polymer batteries," *Journal of the American Chemical Society*, vol. 136, no. 20, pp. 7395-7402, 2014.

J. I. Kim, S. H. Ryu and Y. W. Chang, "Mechanical and dynamic mechanical properties of wood powder/HDPE composite," *Journal of Applied Polymer Science*, vol. 77, no. 12, pp. 2595-2603, 2000.

N. Kise, H. Oike, E. Okazaki, M. Yoshimoto and T. Shono, "Synthesis of nitrogen-containing polymers with reductive intramolecular coupling of aromatic diimines," *Journal of Organic Chemistry*, vol. 60, pp. 3980-3992, 1995.

C. Kloxin, T. Scott, B. Adzima and C. Bowman, "Covalent Adaptable Networks (CANs): A Universal Paradigm in Cross-Linked Polymers," *Macromolecules*, vol. 43, pp. 2643-2653, 2010.

B. Lee, K. H. Lee, B. W. Lim, J. Cho, W. Nam and N. H. Hur, "Direct Synthesis of Imines via Reactions of Carbamates with Aldehydes," *Advanced Synthesis and Catalysis*, vol. 355, pp. 38

J. Lehn, "Dynamers: dynamic molecular and supraolecular polymers," *Prog. Polym. Sci.*, vol. 30, pp. 814-831, 2005.

Z. Q. Lei, H. P. Xiang, Y. J. Yuan, M. Z. Rong and M. Q. Zhang, "Room-temperature self-heal remoldable cross-linked polymer based on the dynamic exchange of disulfide bonds.," *Chemical Materials*, vol. 26, no. 6, pp. 2038-2046, 2014.

L. Leibler, M. Rubinstein and R. H. Colby, "Dynamics of Telechelic Ionomers - Can Polymers Large Distances without Relaxing Stress," *Journal of Physics II*, vol. 3, no. 10, pp. 1581-1590,

G. Li, M. A. Stubblefield, G. Garrick, J. Eggers, C. Abadie and B. Huang, "Development of water modified concrete," *Cement and Concrete Research*, vol. 34, no. 12, pp. 2283-2289, 2004.

R. H. Long, H. Qi and M. L. Dunn, "Modeling the mechanics of covalently-adaptable polymer with temperature-dependent bond exchange reactions," *Soft Matter*, vol. 9, no. 15, pp. 4083-40

Y. X. Lu, F. Tournilhac, L. Leibler and Z. B. Guan, "Making insoluble polymer networks malleable via olefin metathesis," *Journal of the American Chemical Society*, vol. 134, pp. 8424-8427, 2012.

X. Luo, R. Ou, D. E. Eberly, A. Singhal, W. Viratyaporn and P. T. Mather, "A Thermoplastic/Thermoset Blend Exhibiting Thermal Mending and Reversible Adhesion," *ACS applied materials & interfaces*, no. 3, pp. 612-620, 2009.

T. Maeda, H. Otsuka and A. Takahara, "Dynamic covalent polymers: Reorganizable polymers with dynamic covalent bonds," *Progress in Polymer Science*, vol. 34, no. 7, pp. 581-604, 2009.

R. Martin, A. Rekondo, A. Ruiz De Luzuriaga, G. Cabanero, H. Grande and I. Odriozola, "The processability of a poly (urea-urethane) elastomer reversibly crosslinked with aromatic disulfide bonds," *Journal of Materials Chemistry A*, vol. 2, no. 16, pp. 5710-5715, 2014.

D. Montarnal, M. Capelot, F. Tournilhac and L. Leibler, "Silica-Like Malleable Materials from Organic Networks," *Science*, vol. 334, no. November, pp. 965-968, 2011.

J. A. Neal, D. Mozhdzhi and Z. Guan, "Enhancing Mechanical Performance of a Covalent Self-Healing Material by Sacrificial Noncovalent Bonds," *Journal of the American Chemical Society*, vol. 137, pp. 4846-4850, 2015.

R. Nicolay, J. Kamada, A. Van Wassen and K. Matyjaszewski, "Responsive Gels Based on a Covalent Trithiocarbonate Cross-Linker," *Macromolecules*, vol. 43, no. 9, pp. 4355-4361, 2010.

H.-J. Niu, Y.-D. Huang, X.-D. Bai and X. Li, "Novel poly-Schiff bases containing 4,4'-diaminotriphenylamine as hole transport material for organic electronic device," *Mater. Lett.*, vol. 58, pp. 2979-2983, 2004.

R. D. Noble, "Perspectives on Mixed Matrix Membranes," *Journal of Membrane Science*, vol. 2011.

M. M. Obadia, B. P. Mudraboyina, A. Serghei, D. Montarnal and E. Drockenmuller, "Reprocessing: Recycling of Highly Cross-linked Ion-Conducting Networks through Transalkylation Exchange Bonds," *Journal of the American Chemical Society*, vol. 137, no. 18, pp. 6078-6083, 2015.

G. G. Odian, *Principles of polymerization* 4th Ed., Hoboken, NJ: Wiley, 2003.

C. Ohm, M. Brehmer and R. Zentel, "Liquid crystalline elastomers as actuators and sensors," *Advanced Materials*, vol. 22, pp. 3366-3387, 2010.

H. Otsuka, K. Aotani, Y. Higaki and A. Takahara, "Polymer scrambling: Macromolecular radical reaction between the main chains of alkoxyamine-based dynamic covalent polymers," *Journal of the American Chemical Society*, vol. 125, no. 14, pp. 4064-4065, 2003.

J. O. Outwater and D. J. Gerry, "On Fracture Energy, Rehealing Velocity and Refracture Energy of Epoxy Resin," *Journal of Adhesion*, vol. 1, pp. 290-298, 1969.

P. Pandey, A. P. Katsoulidis, I. Eryazici, Y. Wu, M. G. Kanatzidis and S. Nguyen, "Imine-linked microporous polymer organic frameworks," *Chemistry of Materials*, vol. 22, no. 17, pp. 4974-4980, 2010.

J. S. Park, T. Darlington, A. F. Starr, K. Takahashi, J. Riendeau and H. T. Hahn, "Multiple heat thermally activated self-healing composites based on Diels-Alder reaction," *Composites Science and Technology*, vol. 70, no. 15, pp. 2154-2159, 2010.

Z. Pei, Y. Yang, Q. Chen, E. M. Terentjev, Y. Wei and Y. Ji, "Mouldable liquid-crystalline elastomers with exchangeable covalent bonds," *Nature Materials*, vol. 13, p. 36, 2014.

M. Pepels, I. Filot, B. Klumperman and H. Goossens, "Self-healing systems based on disulfide exchange reactions," *Polymer Chemistry*, vol. 4, no. 18, pp. 4955-4965, 2013.

A. M. Peterson, H. Kotthapalli, M. A. M. Rahmathullah and G. R. Palmese, "Investigation of interpenetrating polymer networks for self-healing applications," *Composites Science and Technol* 72, no. 2, pp. 330-336, 2012.

A. Phadke, C. Zhang, B. Arman, C. C. Hsu, R. A. Mashelkar, A. K. Lele, M. J. Tauber, G. Ary Varghese, "Rapid self-healing hydrogels," *Proceedings of the National Academy of Science*, vol. 109, no. 19, pp. 4383, 2012.

M. A. Rahmathullah and G. R. Palmese, "Crack-Healing Behavior of Epoxy-Amine Thermosets," *Applied Polymer Science*, vol. 113, no. 4, pp. 2191-2201, 2009.

A. Rekondo, R. Martin, A. Ruiz de Luzuriaga, G. Cabanero, H. J. Grande and I. Odriozola, "Cyclization of room-temperature self-healing elastomers based on aromatic disulfide metathesis," *Materials Letters* 137, pp. 103-106, 2014. DOI: 10.1039/C3MH00061C, 2014.

S. J. Rowan, S. J. Cantrill, G. R. Cousins, J. K. Sanders and J. F. Stoddart, "Dynamic covalent chemistry," *Angewandte Chemie International Edition*, vol. 41, no. 6, pp. 898-952, 2002.

M. Rubinstein and A. N. Semenov, "Thermoreversible gelation in solutions of associating polymers," *Linear dynamics*, *Macromolecules*, vol. 31, no. 4, pp. 1386-1397, 1998.

H. Saito, A. Hoffman and H. Ogawa, "Delivery of Doxorubicin from Biodegradable PEG Hydrogels via Schiff Base Linkages," *J. of Bioact. and Compat. Polym.*, vol. 22, no. 6, pp. 589-601, 2007.

J. C. Salamone, *Polymeric Materials Encyclopedia*, Boca Raton: CRC Press, 1996.

M. S. Sanford, M. Ulman and R. H. Grubbs, "New insights into the mechanism of ruthenium-catalyzed olefin metathesis reactions," *Journal of the American Chemical Society*, vol. 123, no. 4, pp. 741-742, 2001.

T. F. Scott, A. D. Schneider, W. D. Cook and C. N. Bowman, "Photoinduced Plasticity in Crosslinked Polymers," *Science*, vol. 308, pp. 1615-1617, 2005.

A. M. Shanmugaraj, J. K. Kim and S. H. Ryu, "Modification of rubber powder with peroxide and its influence on the properties of polypropylene/rubber composites," *Journal of Applied Polymer Science*, vol. 104, pp. 2237-2243, 2007.

A. M. Shanmugaraj, J. K. Kim and S. H. Ryu, "UV surface modification of waste tire powder and its influence on the properties of polypropylene/waste powder composites," *Journal of Applied Polymer Science*, vol. 24, no. 6, pp. 739-745, 2005.

D. Shekhawat, D. R. Luebke and H. W. Pennline, "A review of carbon dioxide selective membrane Topical Report," *National Energy Technology Laboratory United States Department of Energy* December 1st, 2003.

R. Siddique and T. R. Naik, "Properties of concrete containing scrap-tire rubber - an overview," *Management*, vol. 24, no. 6, pp. 563-569, 2004.

C. I. M. G. I. C. I. D. a. A. F. Simionescu, "Chemical synthesis of some Schiff base-type polymer containing pyrrole units.," *Polym. Bull.*, vol. 32, no. 3, pp. 257-264, 1994.

W. G. Skene and J.-M. Lehn, "Dynamers: Polyhydrazone reversible covalent polymers, complex exchange, and constitutional diversity," *Proceedings of the National Academy of Science*, vol. 8275, 2004.

L. L. Stevens, E. B. Orler, D. M. Dattelbaum, M. Ahart and R. J. Hemley, "Brillouin-scattering determination of the acoustic properties and their pressure dependence for three polymeric elastomers," *Journal of Chemical Physics*, vol. 127, no. 10, p. 104906, 2007.

E. B. Stukalin, L.-H. Cai, N. A. Kumar, L. Leibler and M. Rubinstein, "Self-Healing of Unentangled Polymer Networks with Reversible Bonds," *Macromolecules*, vol. 46, no. 18, pp. 7525-7541, 2013.

P. J. Taynton, K. Yu, R. K. Shoemaker, Y. Jin, H. J. Qi and W. Zhang, "Heat- or Water-Driven Self-Healing in a Highly Recyclable Covalent Network Polymer," *Adv. Mater.*, vol. 26, pp. 3938-3942, 2014.

P. Taynton, H. Ni, S. Loob, H. Li, H. J. Qi and W. Zhang, "Fully Recyclable & Repairable Wood Fiber Composites enabled by Malleable Thermosets," *Advanced Materials*, Submitted.

P. Taynton, S. Loob, H. Ni, Li, R. Shoemaker, K. Yu, H. J. Qi and W. Zhang, "polyimine vitrimers: synthesis and preparation."

S. Tripathi, I. Vasudev and A. Ray, "Electrical Conductivity in Polyazomethines: A Novel Mechanism Derived from All Valence MO Calculation and IR Study of Polymer-Dopant Interaction," *Journal of Macromolecular Science, Part B: Physics*, vol. 50, no. 6, pp. 1196-1214, 2011.

G. C. Vougioukalakis and R. H. Grubbs, "Ruthenium-Based Heterocyclic Carbene-Coordinated Metathesis Catalysts," *Chemical Reviews*, vol. 110, no. 3, pp. 1746-1787, 2009.

J. M. Whiteley, P. J. Taynton, W. Zhang and S.-H. Lee, "Ultrathin solid-state Li-ion electrolyte facilitated by a self-healing polymer matrix," *Advanced Materials*, Under Review.

K. K. Westbrook, F. Castro, K. N. Long, A. J. Slifka and H. J. Qi, "Improved testing system for thermomechanical experiments on polymers using uniaxial compression equipment," *Polymer* 29, no. 4, pp. 503-512, 2010.

K. A. Williams, A. J. Boydston and C. W. Bielawski, "Towards electrically conductive, self-healing materials," *J. R. Soc. Interface*, vol. 4, p. 359, 2007.

K. A. Williams, D. R. Dreyer and C. W. Bielawski, "The underlying chemistry of self-healing polymers," *MRS Bulletin*, vol. 33, pp. 759-765, 2008.

M. L. Williams, R. F. Landel and J. D. Ferry, "Temperature Dependence of Relaxation Mechanisms in Amorphous Polymers and Other Glass-Forming Liquids," *Physics Reviews*, vol. 98, no. 5, p. 1099, 1955.

R. J. Wojtecki, M. A. Meador and S. J. Rowan, "Using the dynamic bond to access macroscopically responsive structurally dynamic polymers," *Nature Materials*, vol. 10, no. 1, pp. 14-27, 2011.

D. Y. Wu, S. Meure and D. Solomon, "Self-healing polymeric materials: A review of Recent developments," *Progress in Polymer Science*, vol. 33, no. 5, pp. 479-522, 2008.

Y. Xin and J. Yuan, "Schiff's base as a stimuli-responsive linker in polymer chemistry," *Polymers* 3, pp. 3045-3055, 2012.

M. Yamaguchi, S. Ono and M. Terano, "Self-repairing property of polymer network with dynamic covalent bonds," *Materials Letters*, vol. 61, no. 6, pp. 1396-1399, 2007.

Y. Yang, Z. Pei, Q. Chen, E. M. Terentjev, Y. Wei and Y. Ji, "Mouldable liquid-crystalline elastomers with exchangeable covalent bonds," *Nature Materials*, vol. 13, pp. 26-31, 2014.

Y. Yang, Z. Pei, X. Zhang, L. Tao, Y. Wei and Y. Ji, "Carbon nanotube-vitrimer composite for efficient photo-welding of epoxy," *Chemical Science*, vol. 5, pp. 3486-3492, 2014.

H. Ying, Y. Zhang and J. Cheng, "Dynamic urea bond for the design of reversible and self-healing polymers," *Nature Communications*, vol. doi:10.1038/ncomms4218, p. 3218, 2014.

K. Yu, P. Taynton, W. Zhang, M. Dunn and H. J. Qi, "Influence of Stoichiometry on the Glass Transition and Bond Exchange Reactions in Epoxy Thermoset Polymers," *RSC Advances*, vol. 4, pp. 4868-4875, 2014.

K. Yu, P. Taynton, W. Zhang, M. Dunn and H. J. Qi, "Reprocessing and recycling of thermoset polymers based on bond exchange reactions," *RSC Advances*, vol. 4, no. 20, pp. 10108-10117, 2014.

M. Q. Zhang and M. Z. Rong, "Intrinsic self-healing of covalent polymers through bond reconnection towards strength restoration," *Polymer Chemistry*, vol. 4, pp. 4878-4884, 2013.

Y. Zhang, A. A. Broekhuis and F. Picchioni, "Thermally Self-Healing Polymeric Materials: The Path to Recycling Thermoset Polymers?," *Macromolecules*, vol. 42, no. 6, pp. 1906-1912, 2009.

P. Zheng and T. McCarthy, "A Surprise from 1954: Siloxane Equilibration Is a Simple, Robust Polymer Self-Healing Mechanism," *J. Am. Chem. Soc.*, vol. 134, pp. 2024-2027, 2012.

C. M. Zimmerman, A. Singh and W. J. Koros, "Tailoring mixed matrix composite membranes for gas separations," *Journal of Membrane Science*, vol. 137, p. 145, 1997.

Y. Zhu, H. Long and W. Zhang, "Imine-Linked Porous Polymer Frameworks with High Small Molecule (CH₄, C₂H₂) Uptake and CO₂/N₂ Selectivity," *Chemistry of Materials*, vol. 25, pp. 1630-1635

Vita

Philip Taynton was born in California where he grew up with five siblings and two parents. He attended the University of California, Santa Cruz, where he met his wife Preethi within his first week on campus. As an undergraduate student, he joined Professor Bakthan Singaram's lab as a research assistant, working on the development of indium-mediated asymmetric allylation of ketones. Philip graduated with a B.S. degree in chemistry in June 2008. He subsequently worked at Avery Dennison's Avery Research Center in Pasadena, CA for 3 years. While at Avery Dennison, Philip learned polymer and thin film coatings technology while working to develop breathable heat transfer labels for sports apparel. In July 2011, Philip moved to the Denver metro area where Preethi attended the University of Denver (earning her MSW in 2013). Philip began working as a professional research assistant in Wei Zhang's research group in October 2011, then enrolled in the doctoral program in University of Colorado at Boulder in January 2012. Under the supervision of Professor Wei Zhang, he has been working on developing novel malleable thermoset polymers taking advantage of the reversible dynamic covalent chemistry developed in the Zhang group. After completion of his doctoral studies, he will work full time for Mallinda LLC, the start-up company which Philip co-founded along with Professor Wei Zhang, and Dr. Chris Kaffer. Mallinda LLC was started in 2014 to commercialize the malleable thermoset polymers developed at CU Boulder.